UNIVERSITY OF SOUTHAMPTON

FACULTY OF ENGINEERING AND APPLIED SCIENCE

DEPARTMENT OF CIVIL AND ENVIRONMENTAL ENGINEERING

BEHAVIOUR OF SEMI-RIGID COMPOSITE CONNECTIONS SUBJECT TO WIND LOADS

by

Maged Abdel-Ghaffar Moussa

(B.Sc.,M.Sc.)

A thesis submitted for the degree of

Doctor of Philosophy

in Structural Engineering

OCTOBER 1993

UNIVERSITY OF SOUTHAMPTON

ABSTRACT

FACULTY OF ENGINEERING AND APPLIED SCIENCE

DEPARTMENT OF CIVIL AND ENVIRONMENTAL ENGINEERING

Doctor of Philosophy

BEHAVIOUR OF SEMI-RIGID COMPOSITE CONNECTIONS SUBJECT TO WIND LOADS

by Maged Abdel-Ghaffar Moussa

This thesis describes a numerical study and an experimental investigation of the behaviour of semi-rigid beam-to-column composite connections subject to wind loads. Connections in composite frames are normally designed as pin-jointed connections. Diagonal wind bracing is included in such buildings to resist wind loads. The use of semi-rigid connections in the design of such frames can provide substantial savings in material and erection costs. It also avoids the intrusion of bracing into the useful space within the building.

The connection was studied numerically using a finite element package (ANSYS). The parameters affecting the behaviour of the connection have been used to develop two-dimensional finite element models for the different configurations. A three-dimensional model was also developed to check the accuracy of the two-dimensional analysis. Material properties, geometrical dimensions, boundary conditions and loading were carefully given as input data to represent, as realistically as possible, those of the actual joint. Material nonlinearity was considered for concrete, steel, reinforcing bars and shear connectors. The bolt slip and the construction tolerance were also accounted for. The developed model was then used to determine not only the overall stiffness of the frame but also the stress and deformation distributions within the joint components. Different options for stiffening up the joint laterally were also studied. The models predicted with a very good accuracy the joint lateral stiffness under horizontal loading. Also they provided useful information which could not be obtained experimentally e.g., concrete stresses, tensile stresses in the reinforcing bars.

An experimental investigation was carried out to verify the safe behavioural prediction of this type of connection. Because of the high cost and time consumption required to make the sample, a single and representative connection was selected on which the experimental work was carried out. Modifications were introduced during the tests to increase the lateral stiffness of the original connection.

Finally, the main conclusions based on both the numerical and the experimental parts and recommendations for further work have been given.

CONTENTS

ACKNOWLEDGEMENTS

I would like to express my sincere gratitude to my supervisor Dr. C.K. JOLLY for his knowledgeable and skilful guidance throughout this research programme. His encouragement and keen supervision greatly contributed to the steady progress of the project.

Special thanks are owed to Dr. A.C. LOCK for his kind assistance in computer and finite element related problems.

Thanks are owed to the staff of the Civil Engineering Heavy Structures Laboratory. Their co-operation contributed not only to the motivation of the experimental programme but to making the task a pleasant one.

Thanks are extended to all my friends and colleagues within the Department of Civil Engineering for their help and fruitful discussions.

Finally, I gratefully acknowledge the generosity and encouragement of my parents, my wife, my brother and my sister in law for their unlimited support.

CHAPTER ONE

GENERAL INTRODUCTION AND LITERATURE REVIEW

1.1 Introduction

The recent popularity of composite construction systems has opened further scope for research. One subject of interest to designers is the stiffness of composite joints. In previous use of composite construction, it has been assumed that the flooring system and the supporting frames act independently. In composite construction, the steel beam and the concrete slab are designed to act together in an efficient structural system. Despite that, at beam-to-column connections the composite action is usually ignored and the joints are assumed to behave as pinned ones [1,2,3].

The idea behind semi-rigid composite connection is to improve the performance of a relatively weak steel connection such as the top and seat angle by making use of the composite slab and replacing the top angle by slab reinforcement [4,5]. The non-composite top and seat connection is relatively weak because the top angle yields under a combination of flexural and tensile forces at a load considerably lower than the tensile capacity of either angle leg [6]. The composite system offers increased moment capacity and stiffness for the following reasons [4,5,6]:

(1) The moment arm in a composite connection is longer than that in a non-composite one.

(2) The reinforcing bars resist tensile forces as pure tensile stresses, while the top cleat in a steel connection yields under a combination of tensile and bending stresses.

(3) The yield strength of reinforcing bars is greater than that of the structural steel. The yield stress of reinforcing bars is 460N/mm^2 while that of the structural steel is 275 or 355N/mm^2 for grades 43 and 50 steel, respectively.

Despite that, composite beams are still designed as simply supported with the beam-to-column connections being selected to carry only the design shear loads.

It is therefore the scope of this work to study the overall performance of semi-rigid composite connections resisting lateral loads in a range similar to that of wind loads. The intention is to study this connection numerically by finite element analysis and then experimentally to confirm the numerical results

1.2 The Purpose of this Study

Connections in steel frames supporting composite floors with profiled steel decking are normally designed as simple (pin-jointed) connections. Buildings containing such connections cannot resist any of the lateral forces on the building without the inclusion of diagonal wind bracing or shear walls. The alternative is to use unbraced frames with rigid connections which is an expensive solution. However, the concrete surrounding the steelwork does, in fact, provide some rigidity at the joints to resist these forces.

The use of semi-rigid connections in the design of such frames can provide substantial savings in material and erection costs over the pinned connection design method. It also avoids the intrusion of wind bracing into the useful space within the building. The purpose of this study is to examine the behaviour of semi-rigid composite connections resisting wind loads and to quantify the degree of rigidity achieved.

1.3 Composite Construction

Composite Construction is the general term used to denote the composite action of steel beams and concrete floors. Composite deck slabs are those where profiled steel sheeting (or decking) acts as permanent formwork and as reinforcement to the concrete placed on top. Composite metal deck flooring has now become a common feature in the typical U.K. multi-storey steel frame building [7,8].

1.3.1 Behaviour of Composite Slabs

The cross-sectional area of the sheeting acts as conventional reinforcement in the direction parallel to the sheet profiles [2,3,9]. Tensile forces are developed in the sheeting because of the bond between the steel decking and the concrete. The profile shape appears to have a significant effect on the composite behaviour. Mechanical interlock is usually dependent on local plate bending, and therefore indentations are best situated close to the stiff sections of the profile such as corners or on narrow plate elements [10,11].

The direction in which the deck spans determines both the cross-sectional area of concrete available to resist tensile forces and the ability of the metal deck to contribute to moment resistance. The stiffness of the uncracked slab, based on the second moment of area of concrete, is significantly greater when the deck flutes run parallel to the beam rather than being perpendicular [11,12,13]. The steel decking, which is used as both permanent shuttering and tensile reinforcement to the slab, ranges between 46 and 76mm in depth and between 0.8 and 1.5mm in thickness [7,14]. The common values for previous terms are 50mm and 0.9 to 1.2mm [14,15]. A light reinforcing mesh is supplied to control crack width and to carry the slab in case of fire. Composite action between the slab and the deck is achieved through three shear transfer mechanisms: chemical bonding between the cement paste and the surface of the steel decking, mechanical interaction due to the interlock of the geometrical shape or presence of embossments and frictional interaction [18,19]. Use of a re-entrant profile or by indentations (embossments) in

the sheet is sometimes associated with end anchorage to increase the load carrying capacity of the composite slab [20,21,38]. The indentations also have the advantage of increasing the strength of the sheet through strain hardening effect.

1.3.2 Advantages of Composite Construction

The recent rapid expansion in the use of the system in the U.K. may be a result of the significant advantages that it offers which may be summarised as follows [3,5,9]:

(1) The steel deck acts as permanent shuttering for the in-situ cast concrete slab. This saves the time and cost of erection and removing of forms and falsework.

(2) After the erection of the steel deck there will be a safe platform for other construction stages. Since there is no supporting falsework, finishing trades can operate on the floor immediately below the one being constructed; this accelerates the construction programme.

(3) The steel decking acting as the tensile reinforcement saves the time consumed in placing and fixing the reinforcing bars of the slab.

(4) A reduction of about 30% in the amount of concrete fill can be achieved by the profiled steel deck geometry. This reduction leads to lighter superstructures.

(5) The cellular geometry of the deck permits the formation of ducting cells within the floor so that services can be incorporated and distributed within the floor depth. This may lead to an increase in the clear storey height or a decrease in the building height.

(6) Since the steel decks are formed from thin gauge sheet steel, their light weight facilitates the handling and placing by site workers. For the same reason, the sheeting can be transported to site in a compactly stacked form, thus saving on transport costs.

(7) Metal decked floor systems provide quick, reliable overhead protection.

1.3.3 Disadvantages of Composite Construction

The system has some minor disadvantages which may be listed as follows [3]:

(1) The difficulty in achieving an adequate fire rating which is now largely overcome as further fire test information is available.

(2) Prior to concreting, the surface of the decking must be cleaned of any foreign matter to ensure proper bonding between steel and concrete.

(3) Steel decks are slippery to walk on. This may be dangerous for workers using it as a working platform.

(4) High winds during site construction may disturb laying and fixing of the light decking.

(5) In areas of concentrated traffic or storage, the upper surface of the steel decking must be protected against damage from high local loads.

1.4 Types of Connections

Structural steel connections may be divided according to their use into three categories [21,22] as follows:

(a) Connections required to produce a structural member like those used in trusses and compound members.

(b) Connections used to connect together individual elements e.g., beam-to-column connections.

(c) Connections between the steelwork and supporting concrete or masonry structure. An example of this category is the connection of concrete slabs to steel beams in composite construction.

1.4.1 Types of Beam-to-column Connections

Structural connections may be classified according to their response into three groups [21,22,23]:

(i) Flexible connections (pinned)
(ii) Rigid connections (fixed)
(iii) Semi-rigid connections

Another categorisation has been suggested by A.I.S.C. dividing connections into either fully restrained (FR), or partially restrained (PR), connections.

The web cleat connection is considered a very flexible one while extended end plates and T-stubs are nearly rigid ones. Figure 1.1 shows the moment-rotation, or M-Φ, curves for the most common joints. The non-linearity of the M-Φ curve in most cases arises from softening (yield) in some of the connection constituents.

When the moment applied to a connection is carried as axial tension and compression, it tends to possess high stiffness. This is because axial deformations prior to yield are generally small. However, connections in which the forces are resisted by members in bending, for example the flange cleated joint or endplate to un-stiffened thin column flanges, or those in which the moment is transferred

through a connection to the beam web, are much more flexible [24,25].

1.4.2 Semi-rigid Composite Connections

The semi-rigid nature of most beam-to-column connections in steel frames has been recognised. In fact, most of the connections lie in the grey area of neither rigid nor pinned ones. Despite the obvious economical and structural advantages of semi-rigid connections over rigid and simple ones, their practical application is still limited. This is due to the non-linear nature of its moment-rotation curve which requires an iterative solution for each load step to ensure convergence and equilibrium. This has led to a lack of sufficient data base for the design of frames incorporating semi-rigid composite connections and a limitation in use [26,27,28].

1.5 Methods of Studying Beam-to-column Connections

Most of the previous studies on beam-to-column connections concentrated on the knowledge of the connection moment-rotation (M-Φ) characteristics. Design methods which are based on test data are limited by the availability of good quality, carefully documented test results. The number of connection types tested is still limited compared with the number of possible connection types, and variations within each type [27]. A short description will be presented for different methods used to predict the joint behaviour.

(a) Mathematical Expressions

The idea of this method of prediction is to carry out a mathematical representation for connection M-Φ curve. The semi-rigid connection factor Z is defined as the angle change per unit moment.

Polynomial representations which take into account the curved nature of the M-Φ relationship often use a standardised format to express rotation in terms of moment via several constants. These constants are obtained by a combination of

straightforward least-squares curve fitting for c_i constants and using experimental results to determine k parameters:

$$\Phi = c_1(kM) + c_2(kM)^3 + c_3(kM)^5$$

k depends on the main geometrical parameters of the connection. As an alternative, the polynomial of the previous equation may be replaced by an exponential function that has the advantage of yielding a positive slope for all values.

More mathematical expressions for the M-Φ relationship are explained in reference [27]. Purely empirical methods have the disadvantage of being unable to be extended outside the range of the calibration data.

(b) Simplified Analytical Models

To carry out a simple model of the key components of beam-to-column connections it is essential to have:

(1) Close observation of test behaviour to identify the major sources of deformation in the connection.

(2) Elastic analysis of the initial loading phase, concentrating on the key components to predict initial connection flexibility.

(3) A plastic mechanism analysis for the key components to predict ultimate moment capacity.

(4) Verification of the resulting equations against test data.

(5) Description of connection M-Φ behaviour.

This technique is more suitable for flexible forms of connections and has the disadvantage of being dependent on test data [27].

(c) Prediction by Mechanical Models

In this type of modelling, the connection is considered as a set of rigid and deformable components. Test data and/or analytical models are used to supply inelastic nonlinear laws to different parts.

Although mechanical models are an adequate tool for the study of steel connections, they possess the disadvantage of being dependent for their accuracy on the assumed load-deformation response. A second disadvantage is that they are not easily applicable in cases where the connection includes many different variables, which is the case of semi-rigid composite connections. Further details of this method of prediction are explained in reference [27].

(d) Prediction by the Finite Element Method

The finite element method is the most suitable tool for studying connections. It has been used widely in solving different engineering problems for many years [29,30,45,46]. The number of variables in semi-rigid composite joints make numerical approaches, such as the finite element technique, the most suitable methods for undertaking comprehensive parametric studies.

Although the finite element technique has many advantages over experimental studies regarding cost and time, it should be used carefully to represent the actual problem correctly. Experimental studies are always expensive, time consuming, and are limited to certain connections. Although experimental measures are powerful in studying overall performance of a connection, especially for measuring displacements and rotations, they are very poor in studying local effects such as bolt local deformations, or the extension of contact zones. Moreover, the number of geometrical parameters is limited in experimental studies. An extensive

parametric study is economically possible only by means of numerical modelling [27,28,29].

1.6 Earlier Modelling of the Connection Constituents

Since a rather limited quantity of work has been carried out on semi-rigid composite connections, it was decided to make use of any available research on both steel and composite connections. The techniques used to model different parts of steel connections are reviewed. A review of the previous work on composite connections will also be presented. The number of experimental and numerical studies carried out to study composite connections is very limited.

(a) Modelling of Bolts

Bolts are modelled in finite element analysis by different approaches [27,29,30]. These can be summarised as follows:

(1) Indirect modelling by replacing the bolt by its force or boundary conditions.

(2) By introducing equivalent structural systems having the same mechanical properties as the bolt.

(3) Directly using separate finite elements to represent the bolt.

Maxwell *et al.*, [31] prepared a finite element model to study end plate connections. In this model, bolt positions were described by element numbers. These elements had an effectively zero stiffness but with the area of the bolt hole. A bolt which is subject to moment and tension or compression is represented by four forces symmetrically placed about the bolt centre line and at the nodes of the aforementioned elements. Extension of the bolt material was catered for in the analysis. Bolts which were positioned close to the compression flange have been

ignored.

Lipson & Hague [32] studied the single angle bolted-welded connection shown in Figure 1.2. The connection was modelled by representing the weld as an idealised rigid line support. The bolts were represented by nodal forces. The whole connection was modelled as a rigidly supported elastic-plastic plate. The load criterion was a distributed load simulating the bolt-hole interaction which was determined experimentally.

Richard and his associates [33] studied single web plate connections. The aim of the numerical work was to calibrate a mathematical expression which is suitable for the prediction of the moment-rotation curve. An inelastic finite element was used to model the bolt action. The load-deformation relationship of that bolt was determined by carrying out a series of single bolt, single shear tests.

Patel & Chen [35] introduced an equivalent truss system to simulate bolt action. This was carried out using 3 bar elements as shown in Figure 1.3 (a), in which elements one and two represent pre-tension while the third bar element represents shear forces carried by the bolt. Plane stress isoparametric elements were used to model the beam, column and connection plates. The major disadvantage of this system is that it neglected slip of the bolts.

The previous approach has been improved by Beaulieu & Picard [29] by adding a fourth bar element to represent slip or friction as shown in Figure 1.3 (b). This contact element is coupled with the bar element which simulates shear and can account for slip and contact.

Krishnamurthy [27] developed the finite element model shown in Figure 1.4 to study end plate connections. In this model, the approach of replacing the bolt by the displacements produced after the application of bolt forces was used. The main features of this model are:

(i) An iterative solution to follow the change in the zone of contact between the endplate and the support. This support was considered rigid. The endplate and the support were assumed to be initially in contact.

(ii) The bolt pre-load was accounted for by applying the initial bolt forces, the bolt extension was determined and in the subsequent phases the bolt clamping effect was represented by displacement conditions.

(b) Modelling of Weld

Any two welded plates can be modelled considering them to behave monolithically. A more accurate model can be obtained using springs, the spring constants being determined from experiments on the weld material [10,27]. Beaulieu *et al.*, [36] developed a 15 node 3-D prismatic quadratic element which was used in combination with a 20 node 3-D hexahedric quadratic (brick) element to represent the connected plates. The choice of the most suitable approach depends on the degree of accuracy required. If in the range of loading used no significant effect of the weld will be expected, the first method will be acceptable.

(c) Contact Elements

Contact between two solids can be modelled by a set of nonlinear orthogonal springs calibrated according to the nature of the contact between the surfaces. These elements can represent separation or firm contact between solids, and perfect slip or friction between two surfaces. In order to account for slip and contact in a bolted connection, a contact element is coupled with the bar element which simulates shear as shown in Figure 1.3 (b) [29].

The two-dimensional interface element contained in ANSYS [37] element library was proved to be capable of representing 2-D friction/gap closure. This element represents two parallel surfaces which may or may not maintain contact in the normal direction and may or may not slide relative to each other in the tangential

direction. The element may resist compressive loads only in the normal direction and shear in the tangent direction.

(d) Modelling of Shear Connection

Shear connection has been modelled by means of non-linear springs following constitutive laws which were deduced experimentally. This approach was used by Zandonini *et al.*, [36]. The finite element model and the constitutive laws for the shear connectors are shown in Figure 1.5. Another approach, developed by Lin *et al.*, [40] (Figure 1.6), was carried out to study composite bridges and can be extended to cover all similar cases. In this approach, the composite action between the concrete slab and the steel beam is described by two interactions at the interface: traction and shear due to the presence of studs. The contact mechanisms and mechanical connections are simulated by the use of a bar element with two nodes i and j. The bar element can be seen as two independent linear springs. These springs have a stiffness k_t perpendicular to the longitudinal axis of the bar and k_n parallel to it. The constitutive laws of this element are explained in detail in reference [40]. In this study, a combination of ANSYS interface and spar elements were used to represent the shear connection of studs.

1.7 Previous Work on Composite Beam-to-column Connections

A review of all available test data on composite beam-to-column connections has been reported by Zandonini [5,27]. Although experimental analysis is essential to establish the fundamental background, it has a limited scope.

Different researchers have used the finite element method to study beam-to-column connections in bare steel and in composite constructions. In fact, a steel connection is contained in each composite one. Regarding the steel part of a composite connection, previous techniques used to model weldments, bolts, and contact areas may be used.

An experimental as well as an analytical programme was carried out to study the behaviour of semi-rigid composite connections carrying monotonic and cyclic loading by Leon and his associates [4,41-43].

Van Dalen and Godoy [39] carried out an experimental study of the moment capacity and rotation characteristics of beam-column composite connections. The concrete slab was a solid one with headed shear studs to provide shear connection. Three types of connections were studied, flexible, semi-rigid, and rigid. From the test results, it was concluded that a composite beam-column connection with reinforcement continuing beyond the column centreline has a moment capacity in excess of that of the bare steel connection. The effect of the slip of the seat cleat bolts on the rotation, and consequently on the lateral deflection of the flexible connections was also reported.

Ammerman & Leon [43] developed a comprehensive finite element model for semi-rigid composite connections using the finite element code ADINA. The model requires a two step analysis. Firstly, the connection angles were modelled using a detailed mesh of 3-D solid elements. The behaviour of angle cleat segments subject to either a tension or a compression force acting along one leg was studied. The effect of slip due to bolt-hole clearance was included. Secondly, the results of this analysis were incorporated into a large mesh of the entire connection sub-assemblage in which the angles were replaced by equivalent truss elements.

This procedure is lengthy and requires a large amount of computer time. In this model, the effect of the deformation of bolts and of the column components as well as the shear connectors' flexibility were neglected. Shear connectors were assumed to be rigidly fixed to the steel beam which means a full interaction between the slab and the beam.

The steel beam was modelled using 20-node 3-D elements and the steel column was replaced by a line support. Beam elements were used to model the shear

connectors while truss elements were used to model the reinforcing bars. The concrete slab was not included in this model. The concentration in this model, Figure 1.7, was on the connecting angles more than on the concrete slab.

The aim of the large scale experimental programme carried out by Leon and his associates was to investigate the behaviour of semi-rigid composite structures. Four full-scale semi-rigid specimens were tested. The first two were to modify non-composite connections that had been studied earlier by Radziminski and Azizinimini [27]. In additional to the web and seat cleats and the concrete slab, one had a top angle and the other had not. The major finding of these two tests is that the results showed the advantage of composite connections over the similar non-composite ones.

The third included testing of interior connections under monotonic and cyclic loading as well as lateral loading on a full-scale frame which incorporated the same connections as the first two tests. In the frame tested, the depth of the steel decking used was 51mm and the total depth of the light weight concrete slab was 125mm. Full composite beam action was provided by a pair of headed studs placed in each rib of the metal deck. High strength friction grip bolts A325 were used in the steel connection.

The specimen was subjected to a combination of gravity and lateral loads with the gravity loads representing a reasonable service load level (about 3500N/m^2). The structure was cycled at inter-story drift of a range of 0.1, 0.25, 0.5, 0.75, 1.0, 1.5 and 2.0% which covered a wide range of wind and seismic loads. The fourth sample incorporated a much thicker and wider seat angle.

It was concluded that semi-rigid composite frames offer very large gains in strength and stiffness over bare steel connections. For the service load range, rigidities of these connections may be similar to those of a rigid frame. This is applied for the case where no slip of the seat cleat bolts took place. For the stability limit state, the continuous composite action over the column lines provides

significant additional stiffness which resulted in decreased drifts.

Davison, Lam, and Nethercot [14] investigated the influence of the presence of a composite floor slab on the performance of beam-to-column connections. Two main sets of connections were tested, the first contained bare steel connections and the second was of composite ones. Direct comparisons between the results of both groups showed improvements in moment capacity of the composite connections over bare steel ones by different percentages. All the connections were subjected to gravity loads only and the loads were applied monotonically.

Besides the experimental programme in reference [14], a finite element model was adopted to study the composite connection numerically. The finite element mesh for this model is shown in Figure 1.8. The composite beam was modelled using an equivalent all-steel I-section. The second moment of area of the transformed section was calculated using a modular ratio of 15. The minimum elastic modulus of the transformed section, and the plastic moment capacity of the composite section were also determined. From these values the dimensions of a doubly symmetric I-section was found. The connection was represented using a spring with multilinear M-Φ curve obtained from test data.

In this model, the equivalent I section extended from the mid-span of the beam to a point at a distance =0.35 L where L is the span of the beam. The rest of the half span which is 0.15L was modelled using a Non-composite bare steel section. This means that at the joint zone, the strength of the concrete slab has been neglected. This model may be considered a much simplified one.

The behaviour of concrete is more complicated and needs more care to be studied. The equivalent all-steel I section is not capable of representing cracking or crushing of concrete at any load level.

A set of boundary conditions was applied to this model which is suitable for the case of non-sway frames only because at mid-span of the beam only vertical

deflection was allowed. This is not the case when the frame is subject to lateral loads. At both ends of the column, rotation was allowed, while deflections in the vertical and the horizontal directions were prevented.

Although a good agreement with the experimental results was achieved, the modelling of the connection itself is dependent on the data obtained from the experimental work. Moment-rotation curves were prepared as multilinear versions of the data, which means that any change in the geometry of the connection needs further tests for the continued use of this model. The model was dependent on the experimental data.

The local behaviour of different constituents of the connection could not be studied using this approach. The effect of bolt hole clearance and the erection tolerance also could not be investigated. The effect of partial interaction between steel beam and concrete was not accounted for.

Zandonini *et al.*, [36] prepared a finite element model using the finite element programme ABAQUS. The final model is shown in Figure 1.5. Different components of beam deformations were detected experimentally. The shear connection flexibility in this study was accounted for by non-linear springs.

Xiao, Nethercot and Choo [20,44] carried out three groups of tests on composite beam-column connections with the main objective of assessing the performance of steel and composite connections. The research proved that the behaviour of the different types of connections is influenced by a wide variety of parameters. The results also indicated that composite connections are different from bare-steel ones of similar details in a way which makes it illogical to design them as bare steel joints. The steel components of the composite connections were the partial depth end plate, the flush end plate, and the finplate joints. The study is one of the largest experimental programmes carried out on composite connections. Based on the test results, a simple design for moment and rotation capacity was proposed. The results could be used for comparison purposes to justify numerical models.

This will enlarge the outcome of such costly work.

Although experimental analysis is essential to establish the fundamental background, it has a limited scope because it is limited to the number of parameters involved in the work.

1.8 Summary of the Previous Work

A fairly limited range of conditions and governing factors is actually covered. In most of the research work so far conducted, slab-column interaction was not accounted for and no attention was paid to the bolt-hole relative motion.

Partial interaction was neglected in most of the numerical studies so far conducted. The effect of construction tolerance and of the bolt-hole clearance also was not accounted for.

Although one of the major factors which govern the behaviour of the joint is the slab action, the actual behaviour of the concrete material and its complicated nature has not been accounted for in an accurate way. Numerical models have to be capable of simulating slab action and the slab-column interaction adequately.

In models including profiled steel decking, modelling of the voided concrete layer resulting from the geometrical shape of sheets, was not presented.

Further experimental and numerical studies are still required to cover the large number of variables involved in the formation of composite connections.

1.9 Objectives

This study is concerned with the investigation of semi-rigid composite connections subject to wind loads. The finite element analysis is used to study the major parameters which may affect the behaviour of the connection. It is also used to

examine the different options of increasing the lateral stiffness of the connection.

To check the accuracy of the finite element predictions, a full scale test frame was prepared on which a series of tests were carried out. These tests comprise lateral loading of the bare steel frame, the decked frame and the composite frame. Later, the bearing bolts were replaced by HSFG bolts to minimize the slip. Finally the seat cleat was welded to the steel beam to prevent any relative movement between the two.

The research is described in separate chapters dealing with: finite element modelling of semi-rigid composite connections, 2-D numerical analysis to study the behaviour of the connection concerning the development of the models and its geometries, 2-D numerical results, verification of shear connection modelling, the experimental programme, 3-D numerical study to check the accuracy of the 2-D predictions, and general conclusions and recommendations for future work.

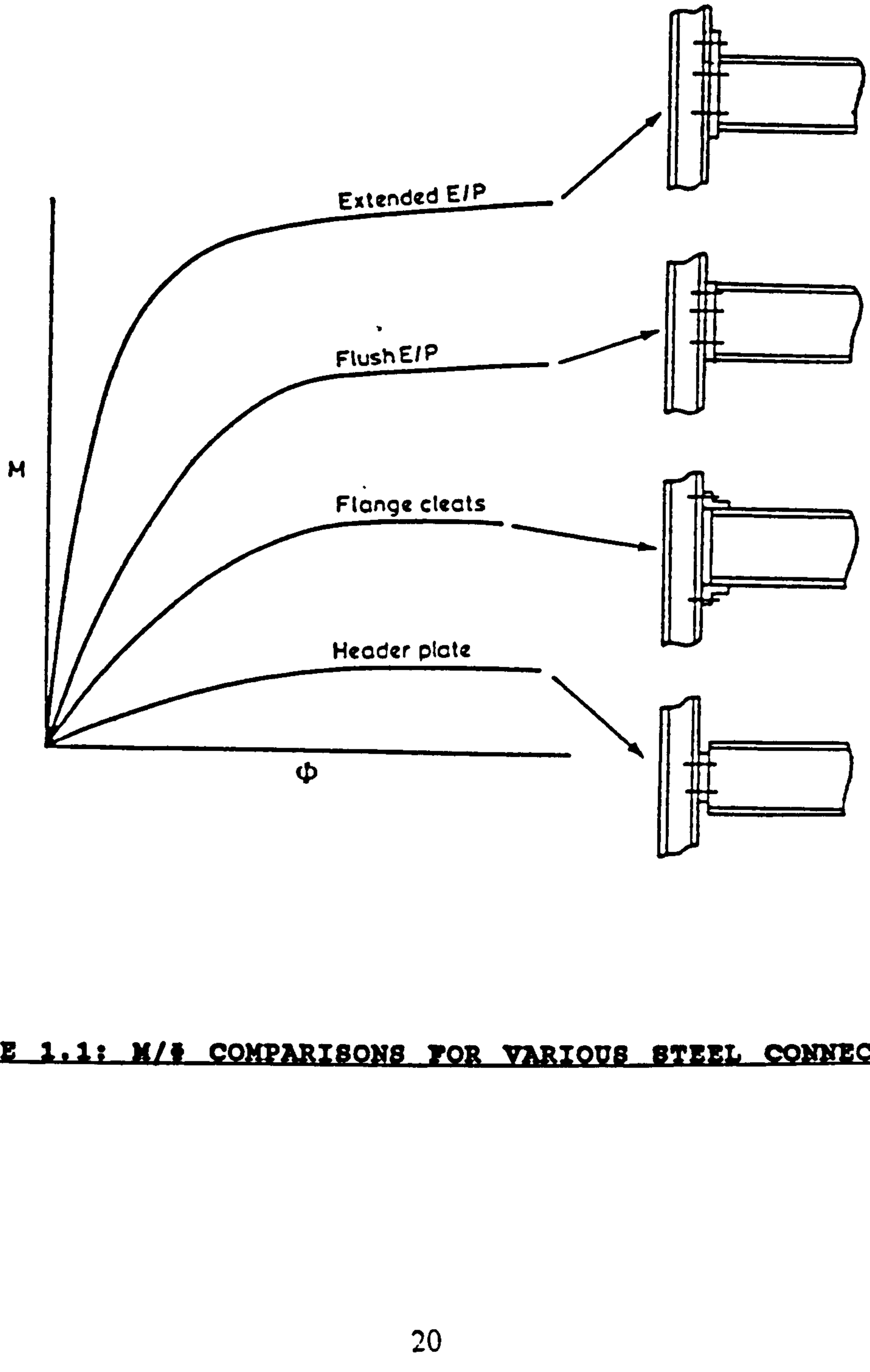

FIGURE 1.1: M/Φ COMPARISONS FOR VARIOUS STEEL CONNECTION TYPES

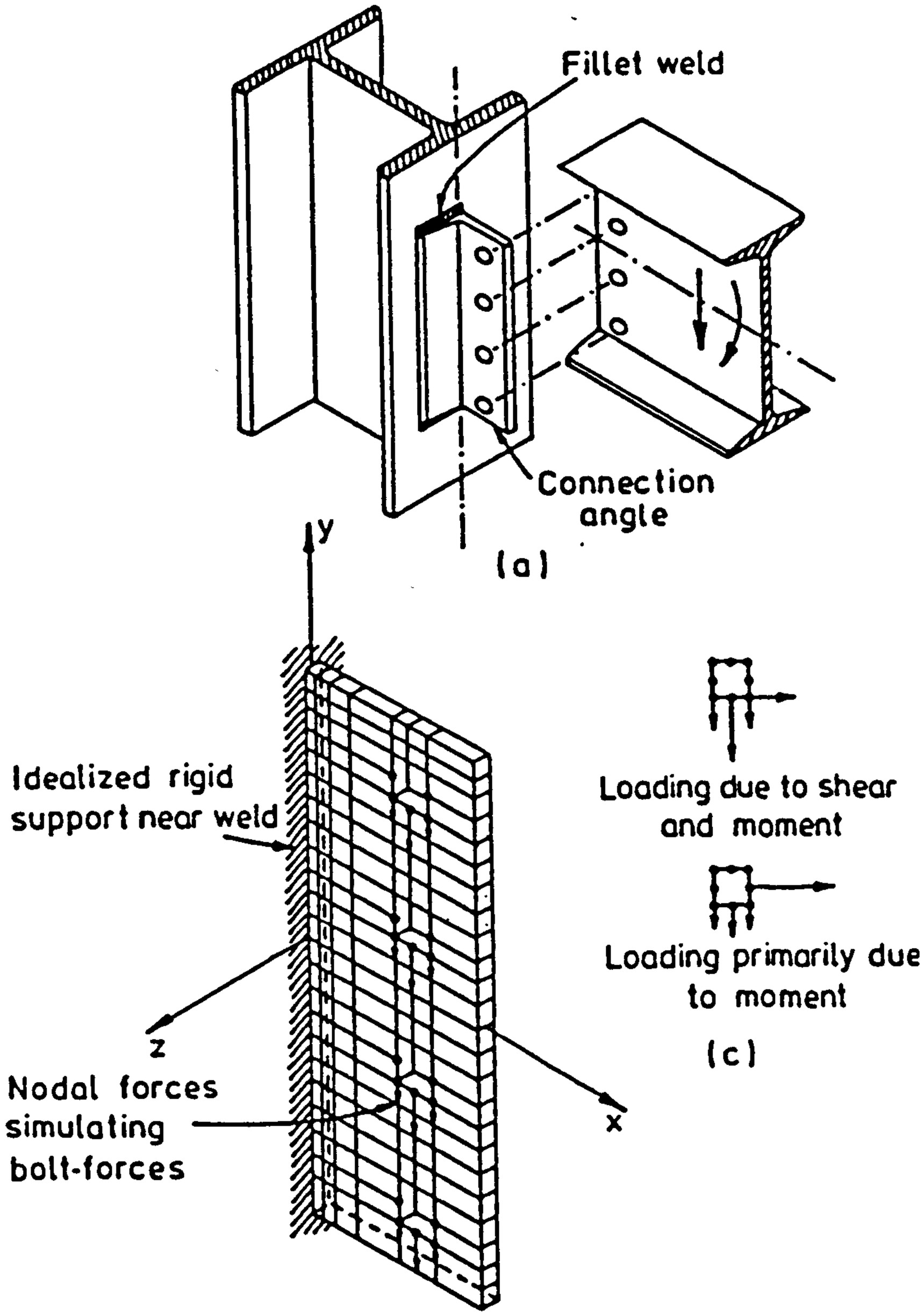

FIGURE 1.2 : FINITE ELEMENT MODELLING OF A SINGLE ANGLE BOLTED-WELDED CONNECTION BY LIPSON AND HAUGE [32]

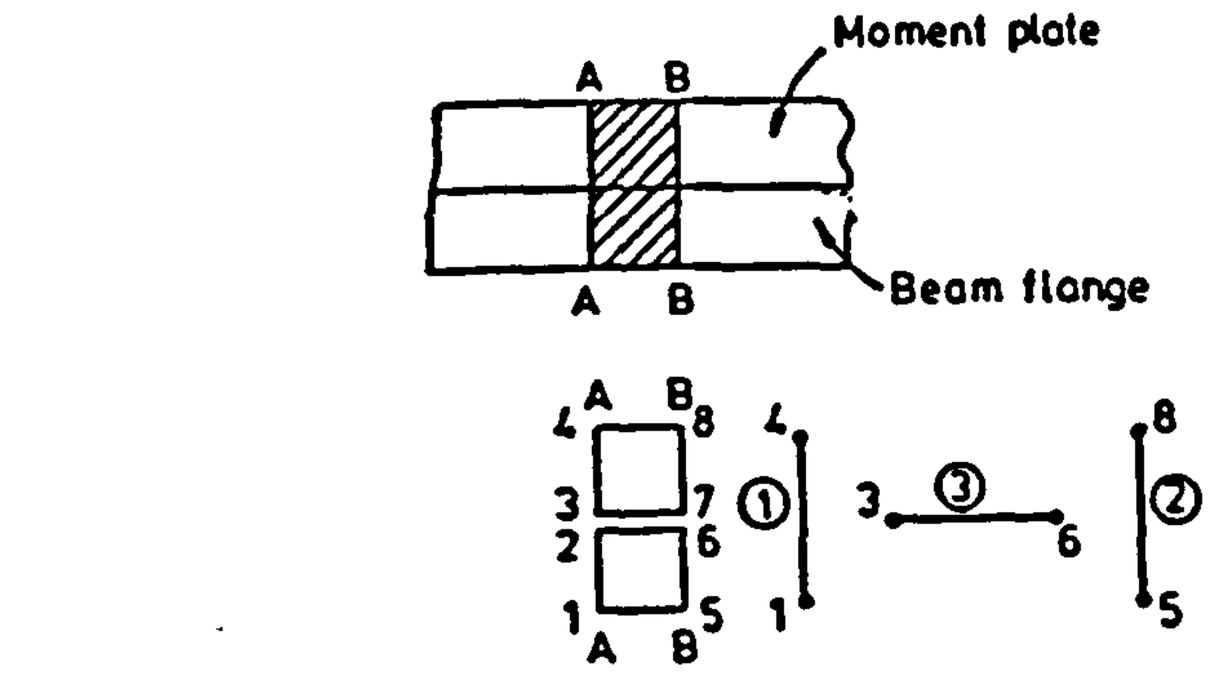

(a) 3 BAR REPRESENTATION

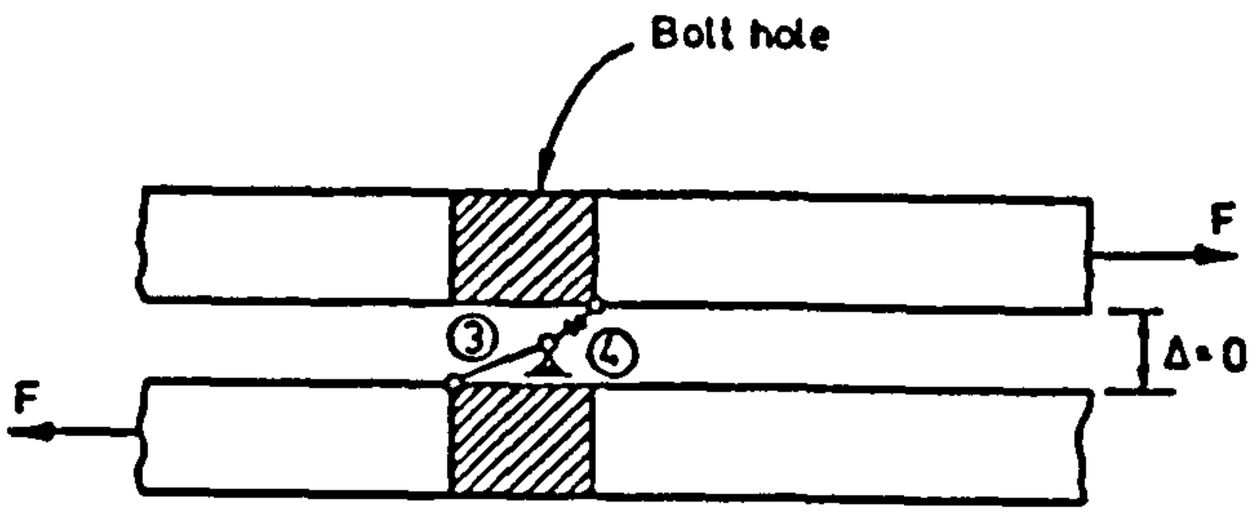

(b) SLIP AND CONTACT SIMULATION

FIGURE 1.3 : BOLT MODELLING TECHNIQUE USED BY BEAULIEU AND PICARD [29]

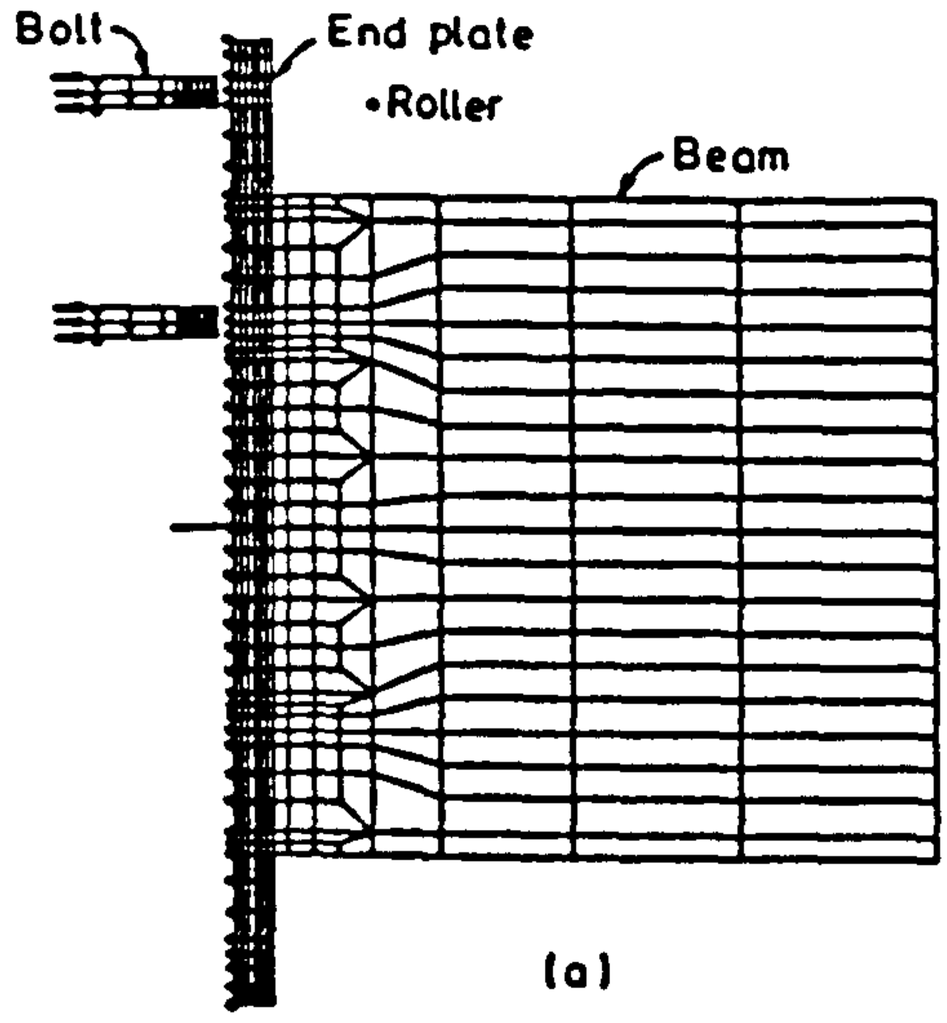

Finite element mesh for the 2-D analysis

FIGURE 1.4 : FINITE ELEMENT MODEL OF EXTENDED END PLATE CONNECTION BY KRISHNAMURTHY ET AL. [27]

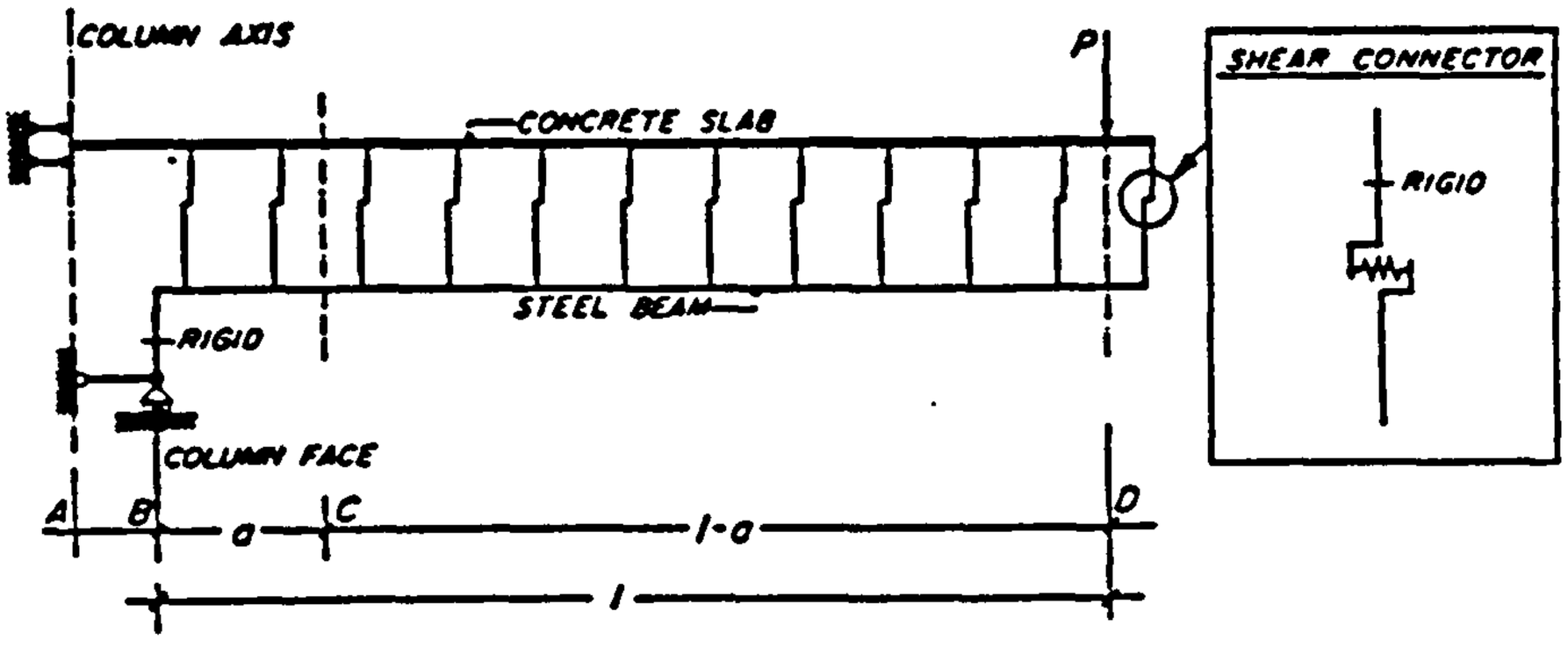

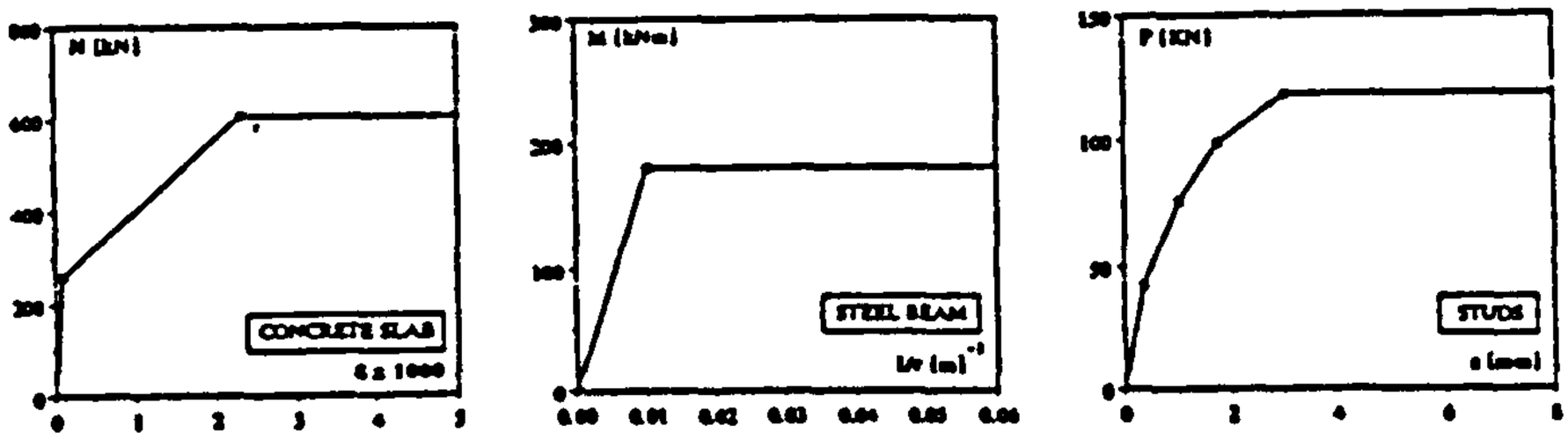

FIGURE 1.5 : FINITE ELEMENT MODEL AND CONSTITUTIVE LAWS OF A BEAM WITH A SEMI-RIGID JOINT BY ZANDONINI ET AL [36]

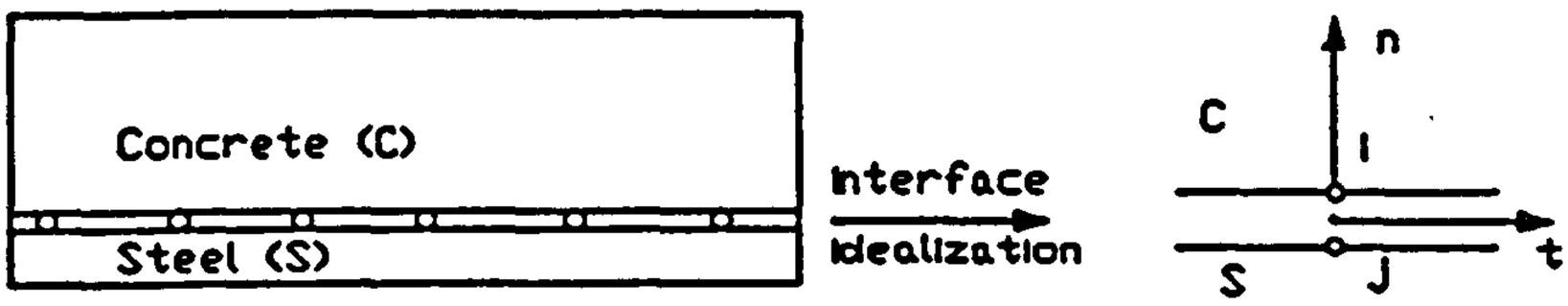

(a) INTERFACE DESCRIPTION

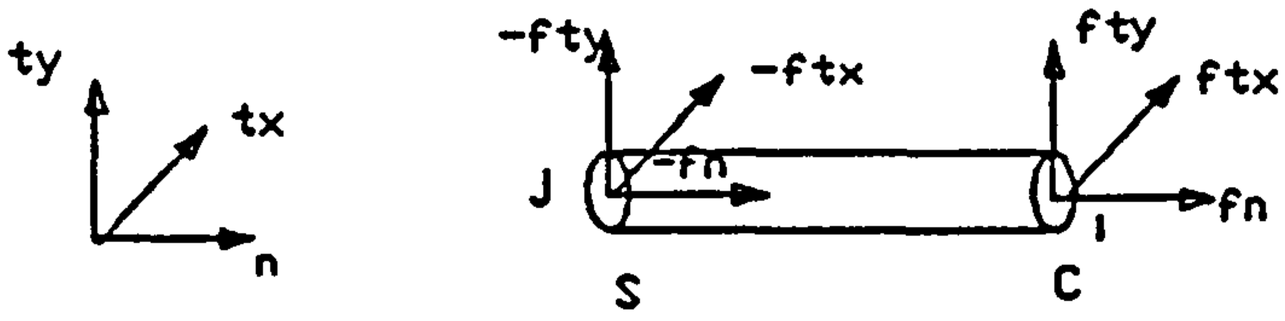

(b) FINITE ELEMENT MODELLING OF THE INTERFACE

zero stiffness element to represent hole

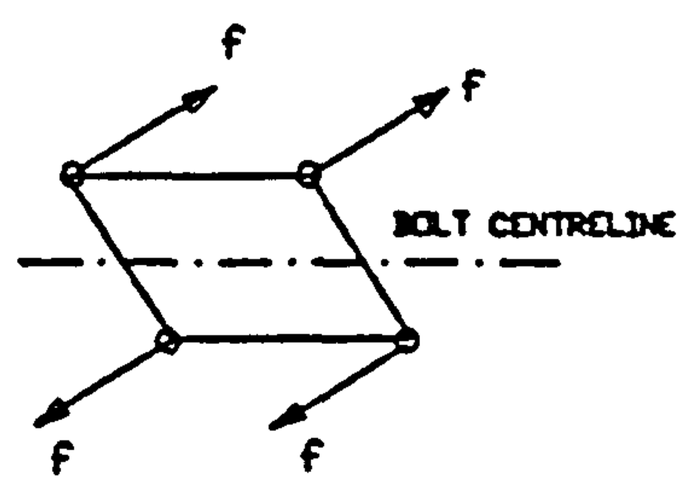

bolt representation by four forces and zero stiffness element

FIGURE 1.6 : MODELLING OF SHEAR CONNECTION BY LIN ET AL. [40]

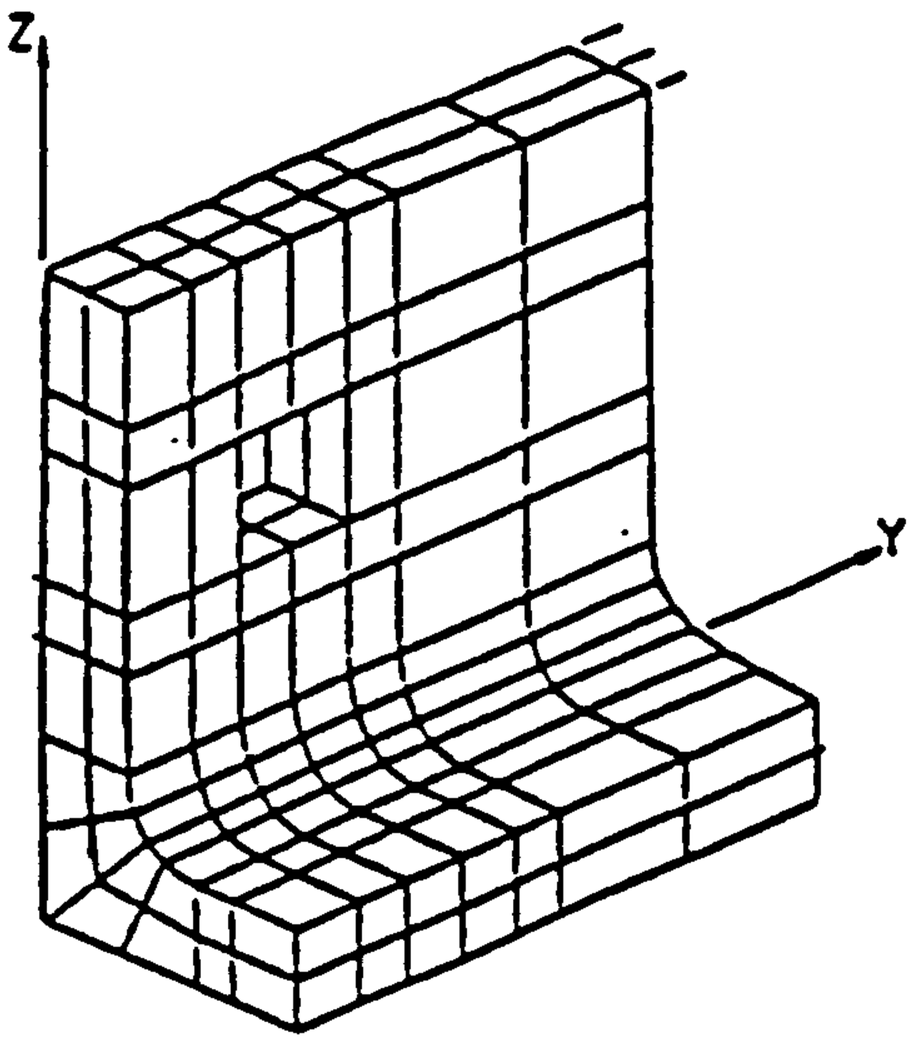

(a) Model of one half of an angle

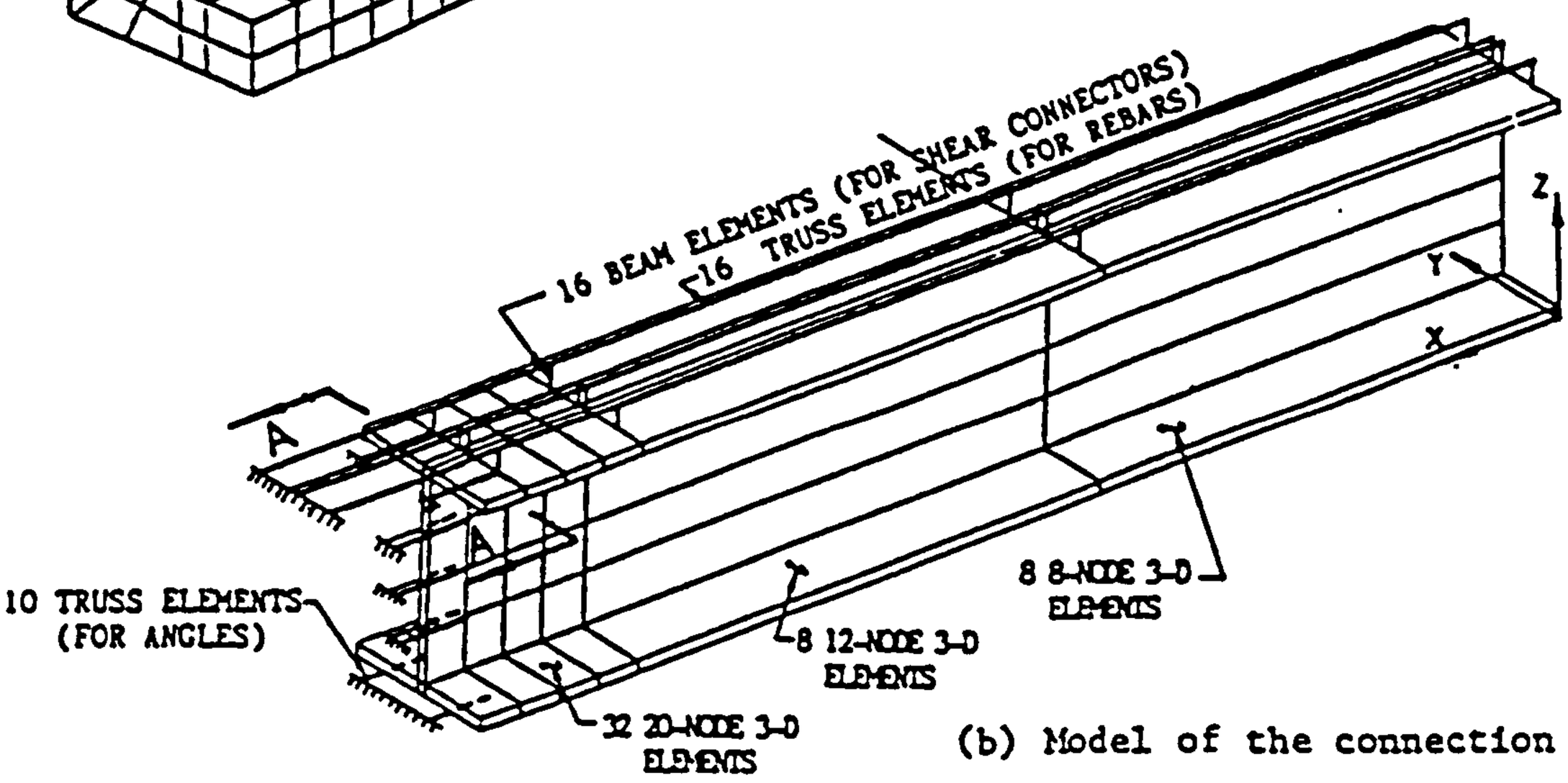

(b) Model of the connection

FIGURE 1.7 : FINITE ELEMENT MODEL BY LEON ET AL [41]

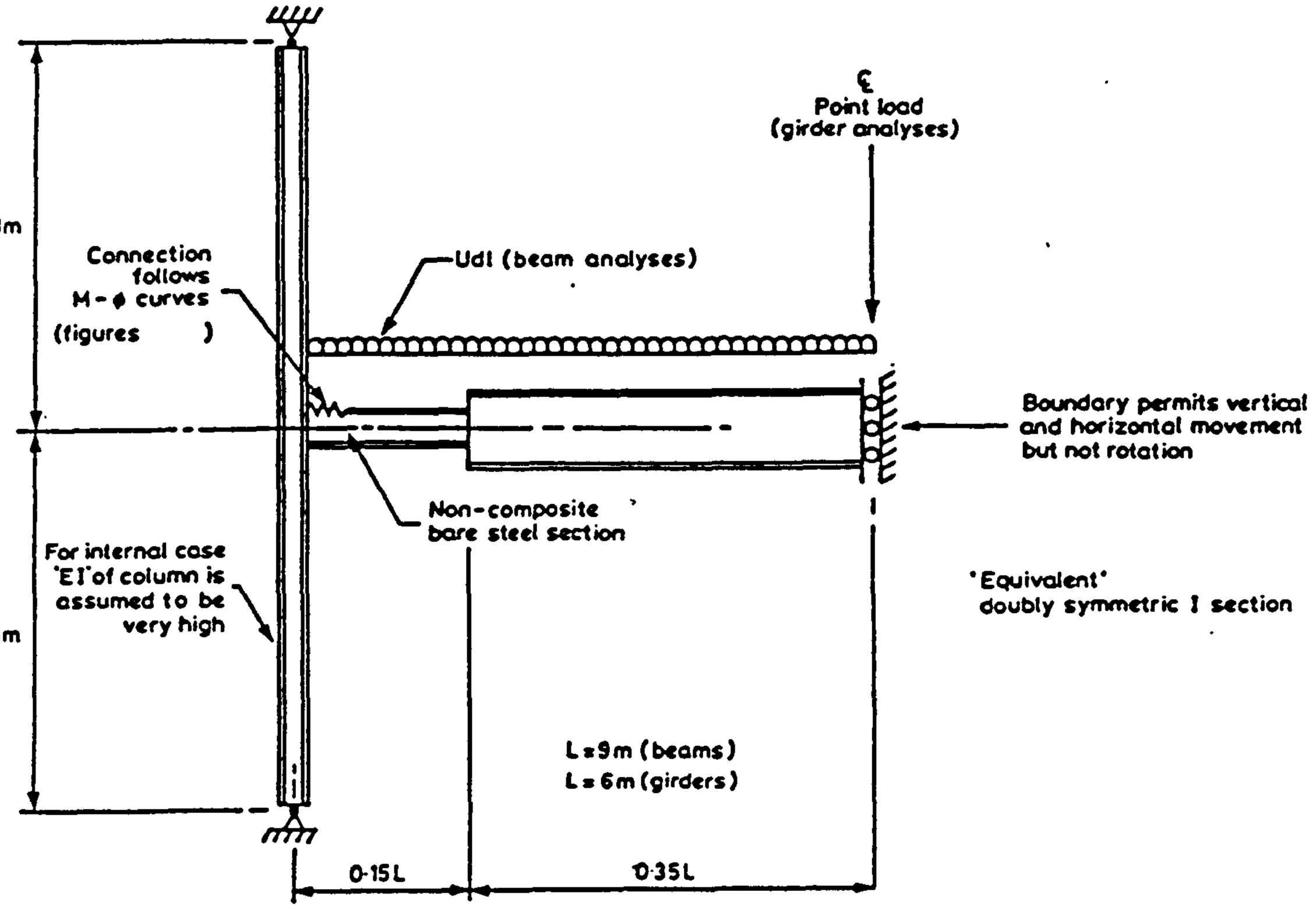

FIGURE 1.8 : FINITE ELEMENT MODEL BY NETHERCOT ET AL. [14]

CHAPTER TWO

FINITE ELEMENT MODELLING OF SEMI-RIGID COMPOSITE CONNECTIONS SUBJECT TO WIND LOADS

2.1 Introduction

In this chapter, the overall behaviour of semi-rigid composite connections was to be studied using the ANSYS finite element software package supplied by SWANSON. The connection was subject to lateral pseudo-static loads due to wind. Direction of loading was either positive or negative to produce closing or opening moment.

It was intended to obtain a model which represents components of the typical building shown in Figure 2.1 and which satisfies the following requirements:

(1) Its geometry represents that of the semi-rigid composite connection.

(2) Wind loads are applicable to the model and have a range of values to represent actual wind loads.

(3) The number of elements and the wave front should be within the computer storage capacity.

(4) Different connection configurations should be modelled to test the sensitivity of the results to various parameters.

Once the above conditions are satisfied, justification of the numerical results should take place.

2.2 Modelling of Beam-to-column Connections

The analysis of steel beam-to-column connections requires the modelling of:

(a) Geometrical and material nonlinearities of the various plate components of the members and of the connection.

(b) Bolt pre-load and its stress strain relationship for different stresses.

(c) Contact between bolt and plates and between bolt head and the nut.

(d) Bolt-hole clearance.

(e) Changing of area of contact by loading.

(f) Stress-strain relationship for weldments.

(g) Possibility of imperfections in the connection fabrication (thermal deformations, lack of fit, etc.).

(h) Compression and friction stresses resulting from bolt re-tensioning.

Composite connections are more complicated because of the presence of the concrete slab. Concrete material properties are themselves more difficult to model with accuracy. Shear connection between concrete and steel is another problem which should be accounted for. Further components and effects to be modelled are:

(i) Non-linearity of concrete material which cracks in tension and crushes in compression.

(j) Reinforcing bars.

(k) Shear connectors.

(l) Interaction between concrete slab and steel beam.

(m) Modelling of profiled steel sheet.

(n) Modelling of the concrete layer which contains voids resulting from the geometrical shape of the steel sheet.

(o) Interaction between concrete and decking.

(p) Accounting for the problems associated with the yielding of the reinforcing bars, growth of cracks in the concrete slab and possibility of local bond failures.

(q) Effect of slip in angles and beams due to the tolerances of bolt holes.

In this study, the joint was represented using different elements to model the steel column, steel beam(s), concrete slab, reinforcing bars, bolts, web and seat cleat, and shear connectors. The construction clearance between the end of the steel beam and the column as well as the tolerance between the bolts and their holes were modelled. Although the purpose of the analytical study was to investigate the overall behaviour of semi-rigid composite connections subject to wind loads, care was taken to enable subsequent detailed study of the local behaviour of each part of the connection.

2.3 Finite Element Modelling Using ANSYS

ANSYS is a finite element multipurpose programme. It is suitable for linear and non-linear problems and for static, dynamic, thermal, and buckling analyses. Its modular structure simplifies the process of preparing the model. It has an element library which contains a good selection of about 99 different elements which can

be used for elastic, elasto-plastic and stiffness analysis of structures. The educational version of ANSYS can solve problems with a wave front up to 800. It has graphics capabilities and input data check options. The programme may be run interactively or non-interactively (batch). ANSYS has also capabilities of dealing with problems which contain large deflections, slip, creep, contact surfaces, and friction. These problems frequently exist in structural connections. Because of these capabilities, ANSYS was chosen as the finite element software package to carry out the numerical study.

2.3.1 Procedures for Preparing a Finite Element Model

Each connection studied was divided into a number of finite elements. Elements are interconnected by nodes. The nodes are located at the corners of a three or two-dimensional element, or at the end of line elements. Nodes may also take different positions at mid-side or centre of surface. Connected nodes should have the same number of degrees of freedom. A system of supports must be applied as boundary conditions to provide equilibrium and compatibility.

2.3.2 Selection of the Analysis Type

There are some considerations which should be taken into account when choosing the analysis type. For a composite structure, the three-dimensional analysis was expected to give the most accurate results. The slender geometry of the members would have led to an increase in the number of elements in the model if the aspect ratio was to be kept within the recommended range of 1 to 3, making it unmanageable with regard to computer storage and run time. On the other hand, the sensitivity analysis was more concerned with the overall behaviour of the structure rather than detailed stress analysis of the components. Moreover, the presence of a rather stiff continuous concrete slab usually allows out-of-plane and torsional deformations of the joint to be neglected. For these reasons, an in-plane analysis was expected to be suitable for studying the overall behaviour of semi-rigid composite connections.

Generalized plane strain analysis may be used with ANSYS by using the special options associated with the three-dimensional solid elements. This procedure could alternatively be done with coupled nodes i.e., by keeping the distance between the two nodes fixed in a certain direction throughout the solution. Hence, the generalized plane strain option was selected because it runs more quickly. The accuracy of the 2-D numerical results will be checked by comparing them with the experimental results and with those obtained from a 3-D numerical analysis.

2.3.3 Generalised Plane Strain Procedure

The presence of a stiff continuous floor slab was expected to permit the out-of-plane and torsional deformations of the joint to be neglected. This enabled the joint behaviour to be described by its in-plane characteristics. The plane strain procedure, which has been used, is carried out by using the special options associated with the three-dimensional solid elements (STIF45 and STIF65). This option is selected by setting KEYOPT(3) =1 for the solid element types being used. The applied loads should be identified in the x-y plane.

Element nodes were created at first bearing in mind that the active nodal plane is the x-y plane. For the composite beam, nodes of the plane at x=0.0 were created at first and then generated along the x-axis. For each element, one plane of nodal points (defined as the active nodal plane) at z=0.0, was considered. An identical plane of nodal points (defined as the parallel nodal plane) at any convenient z>0.0 representing the element thickness was then created.

The 3-D elements defined in this analysis should be oriented such that the nodes are numbered counter-clockwise in the right handed co-ordinate system with the first four nodes defined in the active nodal plane. In-plane nodal forces F_x and F_y have been specified only in the active nodal plane as well.

2.3.4 Static Loading

Solving for displacements, strains, and stresses developed as a result of applying monotonically increasing loads on the structure made the problem a static one. The static analysis is capable of solving problems which include elastic, plastic, creep, swelling, large deflections, stress stiffening, and non-linear elements.

The basic equation for the static analysis of linear problems is:

$$[K]\{u\} = \{F_{app}\} + \{F_{th}\} + \{F_{pr}\} + \{F_{ma}\}$$

For non-linear problems, which use the incremental Newton-Raphson solution procedure, the equation is:

$$[K]\{Du\} = \{F_{app}\} + \{F_{th}\} + \{F_{pr}\} + \{F_{ma}\} - \{F_{el}\}$$

where

[K] = total stiffness matrix (sum of element stiffness matrices)
{u} = nodal displacement vector
{Du} = nodal displacement increment vector
$\{F_{app}\}$ = applied nodal force load vector
$\{F_{th}\}$ = applied element thermal load vector
$\{F_{pr}\}$ = applied element pressure load vector
$\{F_{ma}\}$ = applied element body force load vector
$\{F_{el}\}$ = element elastic load vector

The full Newton-Raphson option was used. This option updates the matrix every iteration and is recommended for large deflection and plasticity problems.

2.3.5 Co-ordinate System and the Finite Element Mesh

The co-ordinate system is shown in Figure 2.2. The active plane was the x-y plane. The origin was selected at the mid-span of the beam and was situated at its bottom flange. The positive x-axis extended along the composite beam. The negative z-direction was the direction of the width of the steel beam and the depth of the steel column.

It is well known that the fineness of a mesh may affect the accuracy of the numerical results. Since the high stress concentrations were expected to occur at the joint zone, the finite element mesh in this region should be a finer one. At the areas away from this zone, which are expected to have small stresses, elements are large. A medium mesh was created to form a transition between these two zones.

For the best numerical conditioning of the stiffness equations, the aspect ratio for an element should preferably be within the range of 1 to 3. This condition was very difficult to be satisfied all over the model without the use of a very fine mesh. This is because of the geometrical shape of the steel sections which are composed of thin plates. On the other hand, a very fine mesh would have led to problems regarding the time and storage capacity of the computer.

2.4 The Element Types Used

The choice of the suitable element for the modelling of different connection parts requires an understanding of the behaviour of each part and its geometrical shape, material properties and connectivity with adjacent elements. ANSYS has an element library which covers different engineering problems.

Modelling of semi-rigid composite connections requires the modelling of their different constituents. Six different elements have been used to model the concrete slab, shear connectors, reinforcing bars, steel columns, steel beams, bolts, seat and web cleats, stiffener plate, construction tolerance bolt-hole clearance and interface between the concrete slab and the steel beam. In this section, a description of the capabilities and the properties of each element is presented to show how the component properties are modelled.

2.4.1 Steel Column

It was required to have an element to represent the I shaped cross-section of the universal beams and columns which can be subject to a shear load with or without

a combined bending moment. The element found to satisfy this condition is the "3-D Isoparametric Solid" contained in the ANSYS element library and known as STIF45.

This element is used for the three-dimensional modelling of solid structures. However, it may be used in the 2-D analysis. The element has eight nodes with three degrees of freedom each: translation in the nodal x, y, and z directions. The element has a 2×2×2 lattice of integration points which is used with the numerical integration procedure and does not coincide with the element nodes. Zero volume elements are not allowed for STIF45. The element may not be twisted such that it has two separate volumes. A prismatic element may be formed by defining duplicate K and L and duplicate O and P node numbers. The generalized plane strain option is available by selecting KEYOPT(3) =1.

As mentioned before, the 2-D analysis needs the element to have only one active plane. This was accounted for by dividing the I-shaped cross-section of both the steel beam and column into a set of elements each with a rectangular cross-section as shown in Figure 2.2. Each element had one of its faces coincident with the active plane. The I shape was transformed to a channel shape in which the two flange plates were kept in their original position while the web plate was moved to have its face coincident with the active plane. This active plane was selected to be the global x-y plane as shown in Figure 2.2.

The finite element mesh of the steel column together with its modelled cross-section are shown in Figure 2.3. The steel column was divided into 10 elements in each horizontal cross-section, two elements for the flanges and eight elements for the web. The dimensions of the elements are changed along the height of the column. The mesh was divided into four regions with a fine region adjoining the beam. The finite element mesh was generated starting at the lowest point of the column.

It is important to point out that in order to keep the number of elements at the lowest possible level, while keeping the overall geometry compatible to that of the actual structure, the finite element mesh contained coarse, medium and fine zones.

The finite element mesh of the steel column was divided into four parts. The first, which started at the column lowest point, was a coarse mesh. Considering the steel column 254×254×73kg/m, the elements had the following x, y, and z dimensions: 14.2, 150.0, and 254.0mm for the flange plate elements. For the web plate, the elements had the following dimensions: 28.2, 150.0, and 8.6mm respectively. In the second part, with the medium mesh, the dimensions were 14.2×50.0×254.0 and 28.2×50.0×8.6mm for flange and web elements respectively. In the fine part of the mesh, element dimensions were: 14.2×25.0×254.0mm and 28.2×25×8.6mm for the flange and the web respectively. In the fourth region, the vertical (y) dimensions of the elements were equal to the (y) dimensions of the steel beam elements. In the fourth region, where higher stress concentrations are expected, the elements' dimensions were controlled by the vertical and horizontal boundaries of the elements of the column and the beam. A summary of the element dimensions is presented in table 2.1.

Table 2.1 Element Dimensions

Component	Element Type	Zone	Part	Element Geometry (mm)		
				x	y	z
Column	STIF45	Coarse	flange	14.2	150	254
			web	28.2	150	8.6
		Medium	flange	14.2	50	254
			web	28.2	50	8.6
		Fine	flange	14.2	25	254
			web	28.2	25	8.6
Steel Beam	STIF45	Coarse	flange	150	8.4	102
			web	150	58.3	6
		Medium	flange	50	8.4	102
			web	50	58.3	6
		Fine	flange	25	8.4	102
			web	25	58.3	6
Concrete Slab	STIF65	Coarse	L1	150	51	1750
			L2	150	54	1750
			L3	150	25	1750
		Medium	L1	50	51	1750
			L2	50	54	1750
			L3	50	25	1750
		Fine	L1	25	51	1750
			L2	25	54	1750
			L3	25	25	1750

L1 Bottom layer of the concrete slab
L2 Intermediate layer of the concrete slab
L3 Top layer of the concrete slab

2.4.2 Steel Beam

The Three Dimensional Isoparametric Solid (STIF45) which was used to model the steel column was also used to model the steel beam. The technique described above to transform the I section to the channel shape, which is suitable for the plane strain analysis, was also used with the steel beam. The steel beam cross-section was divided into six rectangular elements as shown in Figure 2.4. from which it is also clear that the single active plane in the model is the x-y plane.

Both the steel beam and the steel column, which have been modelled using 3-D isoparametric element (STIF45), are divided into a set of elements. For the beam, the upper and the lower flanges are similar. The finite element mesh can be divided into three parts. At the beam end, coarse mesh was used. In the middle of the beam, a medium one and in the connection zone, a fine mesh was created.

In the coarse part of the mesh, and considering the steel beam 250×102×25 UB, the elements had the following x, y, and z dimensions: 150.0×8.4×102.0mm for the flange plate elements and 150×58.3×6mm for the web plate elements. In the second region, the dimensions were 50.0×8.4×102.0 and 50.0×58.3×102.0mm respectively. In the fine part of the mesh, element dimensions were 25.0×8.4×102.0mm and 25.0×58.3×102.0mm for the flange and the web respectively. The finite element mesh of the steel beam is shown in Figure 2.4 and the element dimensions are presented in Table 2.1

2.4.3 Concrete Slab

The Three Dimensional Concrete Element (STIF65) has been used to model the concrete slab. This element has eight nodes and eight integration points. Each node has three translational degrees of freedom. The element has cracking and crushing capabilities as well as compressive and tensile stresses. Although the element has the option of representing the reinforcing bars as smeared elements,

separate elements have been used to model the reinforcing bars. The use of a separate bar element which has the same degrees of freedom at its nodes as the concrete element nodes was considered the most representative method to model the reinforcing bars in the connection undertaken. This is because the position of the reinforcement is known in advance, and its lever arm from the steel beam will affect the moment development within the joint.

The most important aspect of this element is the representation of nonlinear material properties.

(a) Modelling of Voided Concrete

The concrete slab is divided into three layers as shown in Figure 2.5. The bottom layer is the one contained in the profiled steel decking and it contains trapezoidal voids. The modelling of this layer has been carried out by using reduced material properties for this part. This was done by calculating the cross-sectional area of the voids as a percentage of the whole cross-sectional area of the concrete layer and a reduction in the material properties was made equal to this ratio. This simple approach avoids many problems such as the representation of the bond strength between concrete and steel sheet and the modelling of the complicated geometrical shape of the profiled steel decking. Since the ribs are perpendicular to the steel beam, the effect of the cross-section of the profiled steel sheet as reinforcing steel was neglected in the x-direction which is the direction of the applied load.

(b) Modelling of the Concrete within the Column Boundaries

As mentioned before, a single active plane is allowed to exist in the plane strain analysis. In some models, the concrete part within the column was separated from the active plane by the column web. To overcome this problem, overlapping of the concrete and the column web elements took place.

The bond strength between the concrete and the steel column was neglected since a crack was expected to occur between them and no recovery was expected. This was accounted for by using different nodes to create steel and concrete elements even when the two elements are in contact. Forces are transmitted between the concrete slab and the steel beam only through the shear connectors as will be explained later. Full bond strength was assumed to develop between concrete and both the shear connectors and the reinforcement.

(c) Dimensions of Concrete Elements

Concrete elements were arranged in three layers with different aspect ratios. This arrangement was chosen to accommodate the profiled steel sheet, the shear connectors and the anti-crack mesh. The first layer, which is in contact with the upper flange of the steel beam contains prismatic voids representing the shape of the profiled steel sheet. The second and the third layers are solid ones. To facilitate the process of mesh generation, the x dimensions of concrete and steel elements in the composite beam were the same.

The width of the concrete elements varied according to the equation of slab effective width as explained in Appendix II. This means that some of the adjacent concrete elements had different mean widths. The construction of the finite element mesh in the z-direction was carried out in several steps for concrete elements. This was true in the case of a closing moment (i.e. one which causes the angle between beam and column to become acute) where the concrete slab was expected to crack and take a parabolic effective width shape. On the other hand, in the case of an opening moment, (i.e. one which causes the angle between beam and column to become obtuse) the concrete slab width was the same along the steel beam and had a parabolic shape only within the column zone. Cross-section of the composite beam is shown in Figure 2.6.

Owing to the curved shape of the effective width of the concrete slab, some concrete elements had an angle between adjacent sides which was outside the

recommended range. Although warning messages appeared after the checking of input data, these were ignored and the solution satisfactorily obtained. In Table 2.1, dimensions of the concrete elements in x and y directions are shown while the effective width was kept 1750mm as in the case of an unloaded slab or one in which the stresses are laterally distributed.

2.4.4 Reinforcing Bars

Modelling of reinforcing bars was carried out using Two Dimensional Spar Element (STIF1). This element is a uniaxial tension-compression element with two degrees of freedom at each node: translation in the nodal x and y direction. No bending of the element is considered. The element is defined by two nodal points, the cross-sectional area, an initial strain, and the material properties. The initial strain was taken equal to zero. The displacement function for the spar element is assumed to be linear, of the form:

$$u_x(x) = c_1 + c_2 x$$

where the element x-axis is oriented along the length of the element from node I toward node J. A uniform stress along the element is assumed.

Material properties are assumed to be uniform from end to end. The Spar Element is connected to concrete element nodal points applying full bond (no slip) between concrete and reinforcing bars. Thus the linear displacement functions of the surrounding concrete elements are used to distribute the net nodal point forces arising from the reinforcement elements.

2.4.5 Shear Connectors

Two Dimensional Elastic Beam Element (STIF3) has been used for the modelling of shear connectors. This element is a uniaxial one with tension-compression, and bending capabilities. It has three degrees of freedom at each node : translation in

the nodal x and y directions and rotation about the nodal z-axis. The geometry, nodal point locations, and the co-ordinate system for this element are described in [37]. The element is defined by two nodal points, the cross-sectional area, the area moment of inertia, the height, the material properties and the shear deflection factor. Shear connectors were assumed to be rigidly connected to concrete elements and no slip between shear connector and concrete was allowed. This assumption was considered realistic in the range of loading applied. The displacement functions are a first order polynomial in the element axial direction and a cubic polynomial in bending. The functions have the following form:

$$u_x(x) = c_1 + c_2 x$$

$$u_y(x) = c_3 + c_4 x + c_5 x^2 + c_6 x^3$$

The rotational displacement $W_z(x)$ is given by du_y/dx

When full interaction is assumed between concrete and steel, no slip takes place between them. This is not the actual case. The load-slip characteristics of a single shear connector was modelled using a system of ties as will be explained later. In practice, each shear connector is prevented from moving vertically while some horizontal displacement is likely to take place.

2.4.6 Concrete-steel Interface

The vertical motion of shear connectors and concrete slab relative to the steel beam is prevented by two closed gap elements having the same nodal points with reversed order. The purpose of the first gap element is to ensure that penetration of one material into the other will not take place, while the second one was introduced to control separation of the two surfaces. The stiffness of compressive gap elements was calculated as the weakest of the steel beam or concrete elements which are in contact.

The partial interaction between concrete and steel was modelled using two ties in the plane of interface. These ties had a cross-sectional area of 1mm. Each two were connected to a shear connector and the stress-strain curve of its material was half the load-slip curve of a single shear connector. In other words, the traction caused by a shear connector was modelled using tie elements. The two-dimensional spar element (STIF1) was selected to model these tie elements. Verification of the accuracy of this system in modelling shear connection is presented in Chapter Five.

2.4.7 Cross-beam (Perpendicular Beam)

The effect of the cross beam, which extended in z-direction, was accounted for by introducing a shear connector with properties equivalent to the group of connectors within the effective width of the slab at the column centreline (i.e., this beam was assumed to add no torsional resistance to the column, but does give additional shear connection at this point between slab and steel frame). The modulus of elasticity of the material of the new shear connector was calculated as follow:

$$E_g = E_s \times n$$

where

E_g is the modulus of elasticity of the equivalent shear connector used to model a group of n shear connectors.

E_s is the modulus of elasticity of the material of the original shear connector.

n is the number of shear connectors within the slab effective width.

The other material properties were calculated in the same way. A tie element representing the traction of the group of shear connectors was used. The stress-strain relationship of the tie material was calculated using the same method.

2.4.8 Construction Tolerance

In the connection studied, a construction tolerance (Figure 2.7) of nominal width of 6mm is allowed between the end of the steel beam and the column flange to facilitate the construction process. Two-Dimensional Interface or Gap Element (STIF12) has been used to model the construction tolerance between the end of the steel beam and the steel column flange. The element used represents two surfaces which maintain or break physical contact and may slide relative to each other. The introduction of these gap elements was also to ensure that no overlapping of the two surfaces would take place. They also helped in getting accurate information about the start of the contact and its propagation along the beam end.

The element is defined in the x-y plane and operates bilinearly only in the static analysis. The coefficient of friction μ, which is the only material property, was set to zero. The element is defined by two nodal points, an angle to define the interface, a stiffness k, an initial displacement interference, and an initial element status. The geometry, nodal point locations, and the co-ordinate system for the element are explained in reference [37]. The element is nonlinear and an iterative solution is required. Gap elements may have one of three conditions: closed and not sliding, closed and sliding, or open. The element is normally oriented based on the angle between the global x-axis and the element s-axis. Since energy lost in the slide cannot be recovered, the load needs to be applied gradually. When the gap becomes closed, the two nodes are forced to move together. The value of stiffness associated to gap element is calculated from the formula:

$$K = \frac{(E \times A)}{L}$$

where

E is Young's modulus of the adjacent element
A is the area of the adjacent element in the active plane
L is the element thickness

For the upper and lower gap elements, these values were calculated regarding adjacent element dimensions. The dimensions of the steel beam flange element were 14.0×8.9×102.4mm in x, y, and z directions respectively. For the steel column, two adjacent elements were considered, the dimensions of these elements were 14.2×8.9×254.0 and 20.0×14.2×254.0. The stiffness of the beam flange element is calculated as follows:

$$= \frac{2.05 \times 10^5 \times 14.0 \times 8.9}{102.4} = 2.49 \times 10^5$$

The stiffness of the column flange element is calculated by considering the mean value of the areas of the two adjacent elements as follows:

$$= \frac{\frac{2.05 \times 10^5 \times 14.2\ (20.0 + 8.9)}{2}}{254} = 1.65 \times 10^5$$

The associated stiffness with the upper and the lower gap elements, which represent the tolerance between the steel beam and column, was taken as 1.65×10^5. This is the least of the above calculated values. The spring stiffness of other gap elements was calculated in the same way.

The steel beam would have deflected under gravity loads. The end of the beam was assumed to be inclined to the vertical and the gap width would therefore differ from its initial value of 6mm. This means that the distance between the uppermost point and the column would have increased while that of the lowermost point would have decreased.

A one-to-one correspondence mapping of the nodes of the steel beam elements to those on the column flange was used to facilitate the modelling of the contact region by the 2-D Interface Element. The gap elements, as all the 2-D elements, were created in the active plane.

2.4.9 Bolts

Modelling of bolts was carried out by replacing the bolt by an equivalent structural system representing the principal features of the bolt together with the plate connected to it. In the connection studied (Figure 6.2) there are two bolts connecting the web cleat to the web of the steel beam and two bolts connecting the seat cleat to the beam lower flange. Each of these two bolts together with the part of the attached cleat was replaced by a two dimensional beam element rigidly connected to the steel column. Actually, the cleat is welded to the steel column. Material properties of the 2-D beam element were those of the web and flange cleats. This means that the high yield strength of the bolt was not used. This was representative of the actual behaviour of the bolt and the surrounding segments of the cleat since the surrounding steel plate will yield first.

At the other end, a gap element was introduced between the web plate of the steel beam and the bolt to represent bolt-hole clearance.

The stiffness of the gap element was taken to be equal to the average value of the stiffness of the bolt and the steel element connected to it. Because of the uncertainty of the initial gap condition, different gap sizes were used to represent bolt-hole clearance.

For the seat cleat, the same technique was used. The two bolts were replaced together by a single beam element connected to a horizontal and a vertical gap elements.

2.4.10 Bolt-hole Clearance

In this type of connections, 2mm clearance is usually allowed between the bolt and its hole. The purpose of this clearance is to facilitate the construction process. Due to gravity loads, and considering the web cleat, the bolts were assumed to rest at the bottom of their holes. When the frame is subject to lateral loads, the bolt was

assumed to move laterally in the direction of the applied force. An initial slip may then take place, leading to a large lateral deflection in the frame. The force required to cause slip is dependent on the coefficient of friction between the nut and the plate and their geometrical shape.

Theoretically, the area of contact between the two cylindrical bodies of the bolt and its hole is zero. Concentrated stresses will lead to a local deformation. This complicated process was not accounted for because the purpose was to investigate the overall performance of the connection.

Three conditions were considered in the analysis. The first assumption of an initially closed gap element was considered simple and probably the most realistic. The second, which is the worst case from the stiffness point of view, was the one in which the bolt-hole gap was assumed to be initially open with the full tolerance of 2mm. The third assumption was that the bolts of the web cleat under gravity loads rest in the bottom of the hole with maximum gap size of 1mm whichever way it tries to move. The seat cleat bolt was assumed to have its centreline coincident with the hole centreline with a uniform clearance of 1mm around the bolt.

2.4.11 Seat Cleat

The seat cleat angle is modelled using a two-dimensional elastic beam element of the same net area of the upper leg of the angle. The horizontal leg of the angle contains two bolt holes each of diameter 18mm. The vertical leg, which is welded to the column flange was neglected assuming that its stiffness is small compared with the steel column stiffness. A gap element was introduced between the end of the cleat and the beam flange to represent the interface between the bolt and the flange plate. The other end of the seat cleat is rigidly connected to the column to represent welding.

The centrally located stiffener plate, which is welded to the seat cleat, was modelled using the Two Dimensional Isoparametric Solid Element (STIF42). This element is used for 2-D modelling of solid structures. The element can be used either as a biaxial plane element (plane stress or plane strain) or as an axisymmetric element. The element is defined by four nodal points having two degrees of freedom at each node: translation in the nodal x and y directions. The element has plasticity, creep, swelling, stress stiffening, and large deflection capabilities.

The element input data includes four nodal points, the thickness and the orthotropic material properties.

The geometry, nodal point locations, face numbers, loading, and co-ordinate system for this element are explained in [37].

2.4.12 Modelling of Weld

Two welded plates can be modelled considering them to behave monolithically. Although this approach is crude, it is very simple and adequate where the welded parts are not the critical part being studied. In the connection investigation, the overall behaviour of the frame was to be studied. Assuming that failure couldn't take place in the weld at service loads, this method was considered acceptable. Welded parts were constructed using the same nodes.

2.5 Mesh Generation

The finite element mesh of the beam is divided into three regions. The first is a coarse mesh with aspect ratio of 2.56 for the web plate elements and of 18.75 for flange plate. The second part is a medium mesh which has an aspect ratio of 1.17 for the web and 2.77 for the beam flange. The third region is a fine mesh with aspect ratio of 2.34 for web and 3.125 for flanges.

The concrete slab mesh is also divided into three regions. The aspect ratio in each region differs according to the layer. The first region has aspect ratios of 6.00, 2.77, 2.94 for the upper, the middle, and the lower layers respectively. The second one has aspect ratios of 2.00, 1.08, and 1.02. The third region has aspect ratios of 1, 2.16, and 2.04. These aspect ratios are calculated to be the ratio of the x to the y dimensions in the active plane. The finite element mesh of the joint zone is shown in Figure 2.8.

2.6 Boundary Conditions and Load Application

A set of boundary conditions is applied to each model to provide stability to the structural system. These represent boundary supports simulating the actual constraints. In the next chapter, and with each individual model, boundary conditions will be explained.

Wind loads affect the whole area of the building under consideration. In design, wind loads are considered acting at the floor level for each storey i.e., concentrated by the cladding into actions at each floor level. In the finite element analysis, the load application took place at the nodal point which lies on the upper flange of the steel beam where it is in contact with the concrete slab. This point is always close to the centroid of the composite beam, and at midspan, which is assumed to be a point of contraflexure.

2.7 Stability and Solution Convergence

The material properties, which are given as input data, contain nonlinear properties. Plasticity may occur in any stressed material resulting in instantaneous, unrecoverable strains. An iterative solution is required to reach convergence. The main disadvantage of a purely iterative solution is that recording of results is impossible during the solution. The construction of a load-deflection curve needs intermediate values before reaching the maximum load. An incremental solution has been followed and within each load step an iterative solution has been used to

achieve convergence. It was decided to load the frame laterally to 50kN for the ¬ shaped sub-frame. This value is based on wind load calculations as explained in Appendix I. The maximum load was divided into a set of increments. In most cases these were of equal values of 5kN each. In some cases it was realised that the application of small forces is required at first to ensure closure of gaps. In this case, load increments of 0.1kN were used until after the closure of gaps, when larger increments were applied. A sudden increase in load may lead to an unstable structure and convergence will not be reached. A monotonically increasing load should be applied gradually rather than in one step because a sharp increase in load might cause an improper distribution of internal forces since plastic strains cannot be removed after they occur.

For a static analysis, a load step is said to be converged if the changes in plastic strain increments are less than a preset value at all integration points from an iteration to the next one. This value can be interpreted as how far off the stress-strain curve the converged solution will be. This preset data is given as input in the convergence command and was taken equal to 0.10. It should be noted that this value reflects the most erroneous integration point i.e., all other points have the same or less error. Convergence can be affected by other factors such as deflection increment and status of gap elements, or integration points in concrete elements. These can be described in the following points:

(1) Solution is considered unconverged if there is a change in deflection at a particular node between two successive iterations which exceeds a certain limit.

(2) Convergence is incomplete if the status of an integration point in any concrete element changes from one state to another, regardless of the plasticity criterion limit or the deflection.

A preset value for deflection can also be given as an input in the convergence command. This means that the change in the deflection at a certain integration

point should not exceed a certain value between successive iterations. If the structure contains gap elements, like the one undertaken, the gap status should remain unchanged between the first two iterations to reach convergence. In an interactive run, the number of non-converged concrete and bilinear elements appears on the screen after each iteration. This gives a feeling of how far from convergence the solution is. The occurrence of cracks during an iteration also requires at least another iteration to fulfil convergence.

2.8 Wave Front Reduction

ANSYS has a capability for reordering the elements to reduce the wave front by one of two ways. The first is carried out by reordering the elements according to their geometrical locations, sequentially numbering nodes bounding the next nearest element. The second takes place by numbering nodes on a starting surface and then numbering nodes in the next nearest plane. The wave lists are used to start and stop the ordering process. The first method has been used during the analysis.

The generation of elements took place by using a single element across z-direction starting at the face on x-y plane and proceeding anti-clockwise to complete the four nodes of an eight nodes element. The other four nodes are arranged in the same way.

2.9 Summary

The main objective of this part of the study was to develop a representative model for the analysis of semi-rigid composite connections. The model was constructed using 3-D and 2-D elements while the analysis was a plane strain analysis. Eight noded isoparametric elements were used in representing the steel beam and column. 3-D concrete element was used to model the concrete slab. The reinforcing bars were modelled using spar elements. Beam elements were used to represent the shear connectors and the bolts. Gap elements were used to model the

concrete-steel interface, bolt-hole clearance and the construction tolerance. A system of gap and spar elements was used to model partial shear interaction between the concrete slab and the steel beam.

Load was applied as a point nodal horizontal force at the end of the steel beam, with increments of 5 to 10kN. Each load step started after the convergence of the previous one.

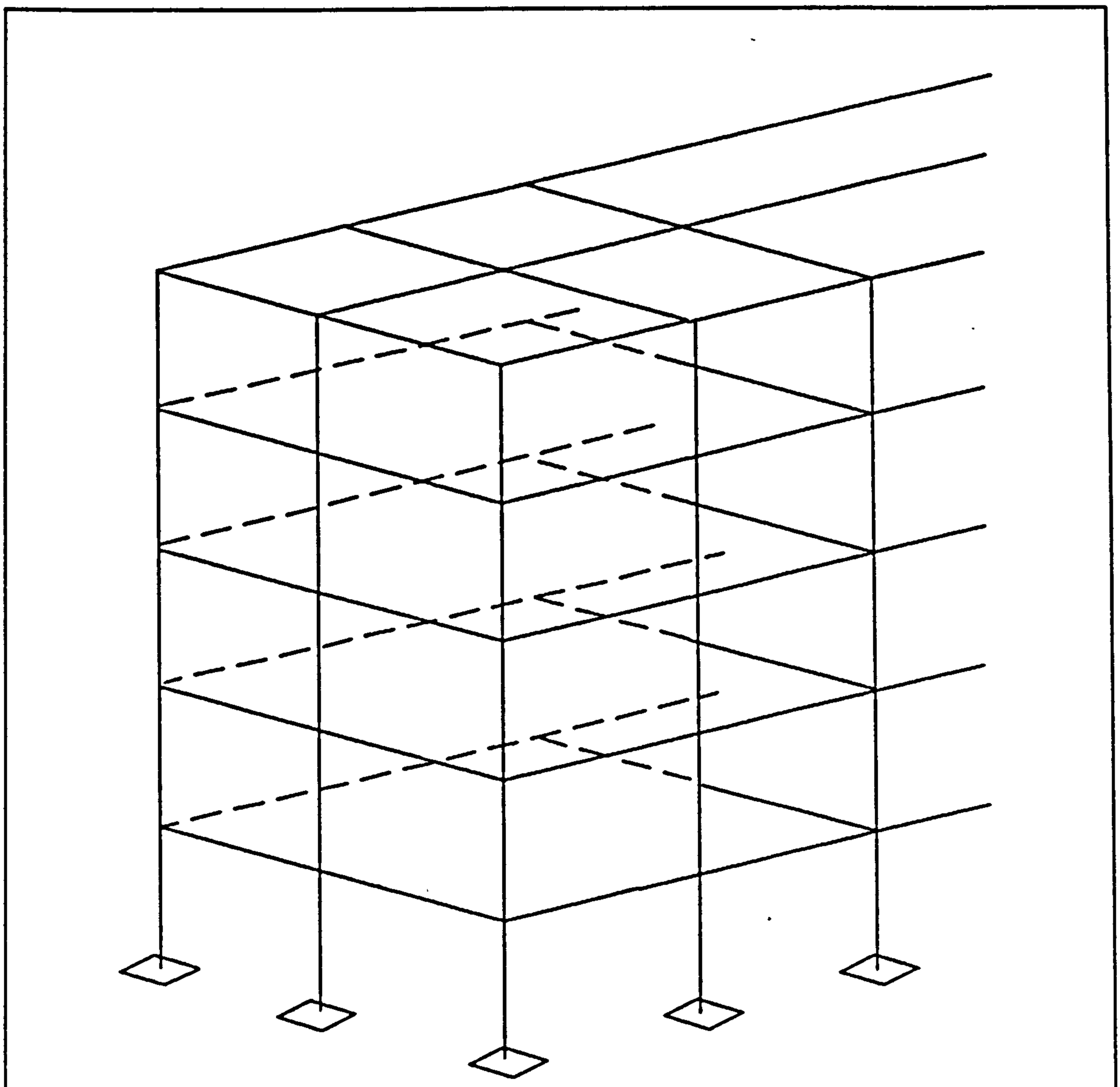

FIGURE 2.1

TYPICAL COMPOSITE BUILDING

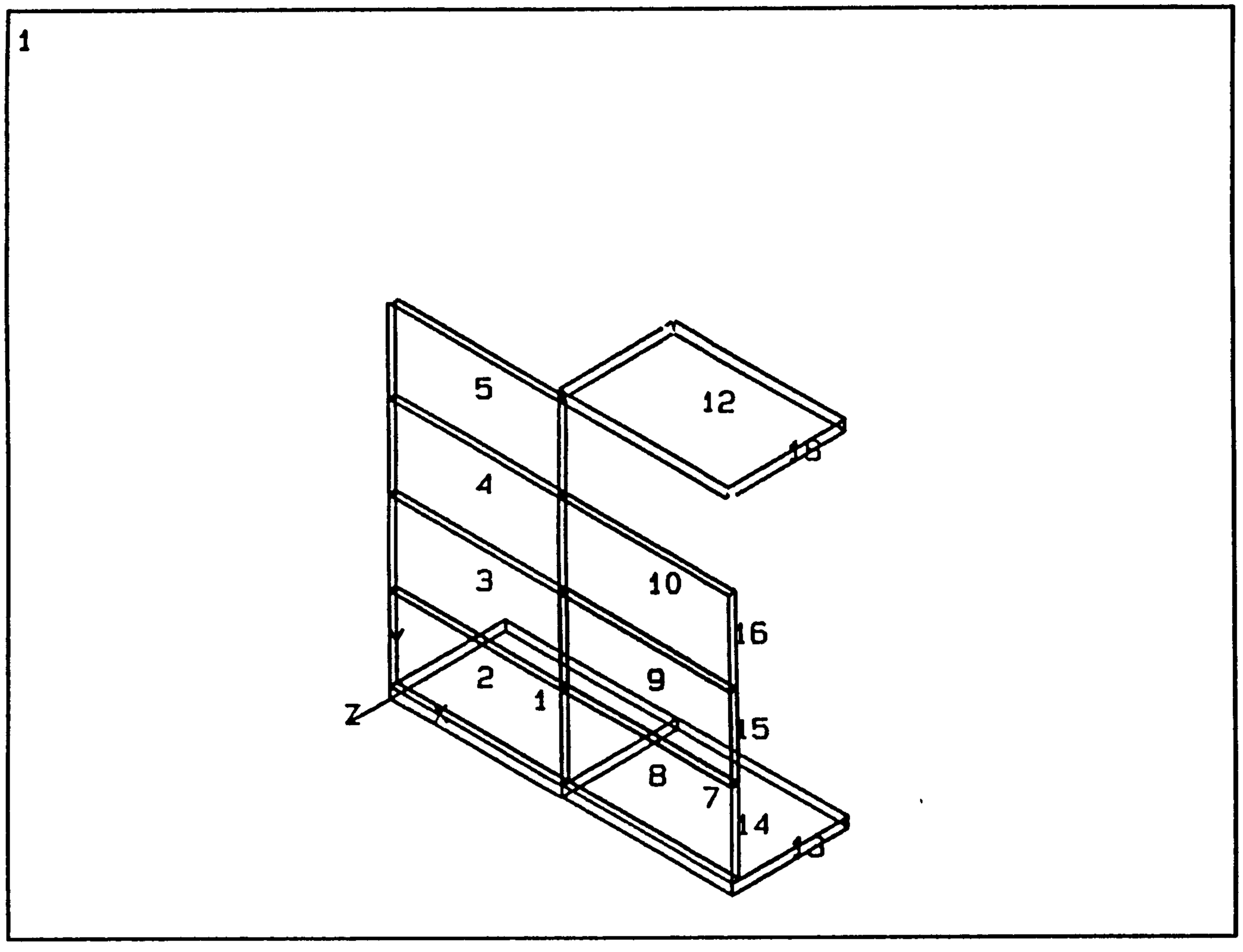

FIG 2.2 CROSS-SECTION OF THE STEEL BEAM

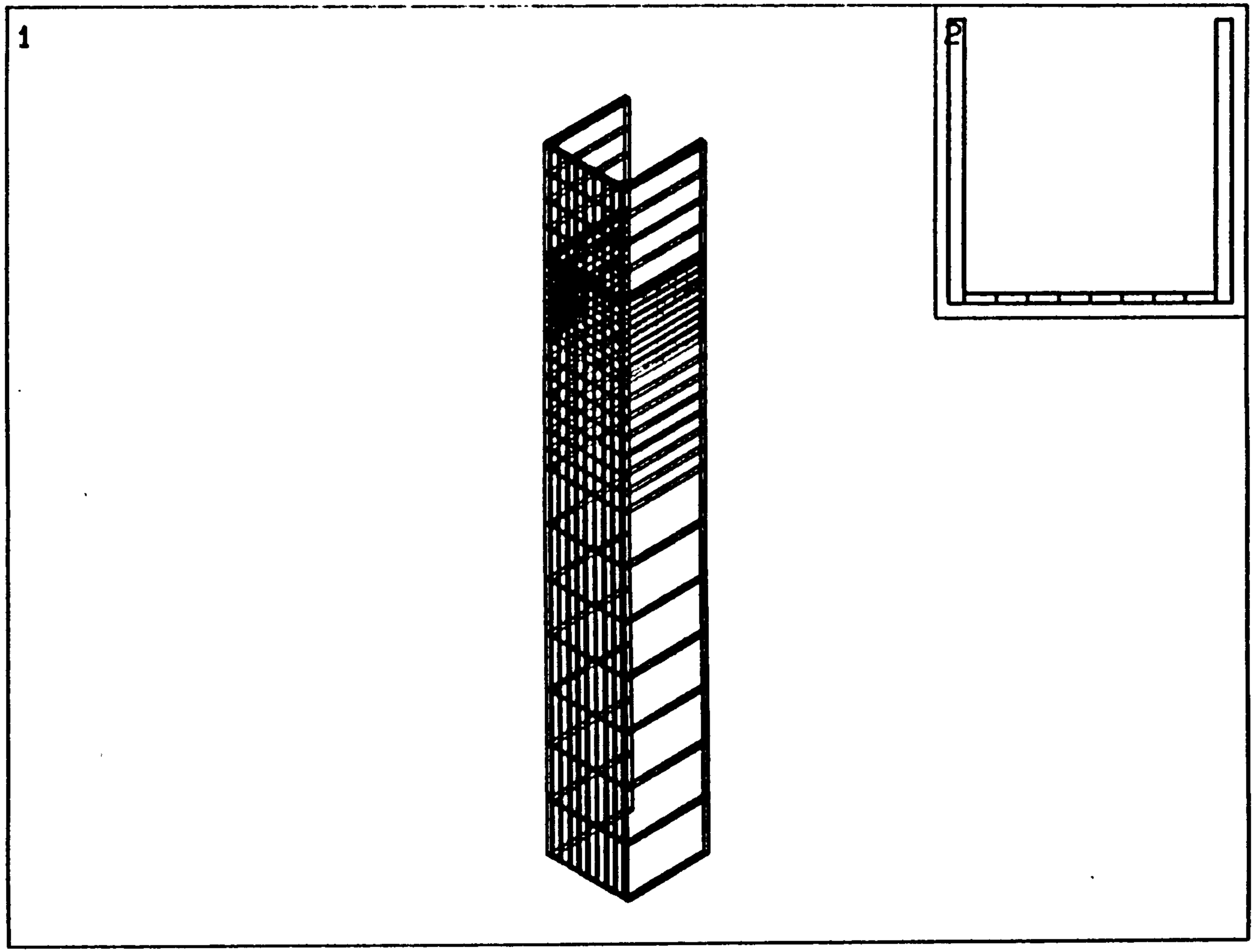

FIG. 2.3 FINITE ELEMENT MESH OF THE COLUMN

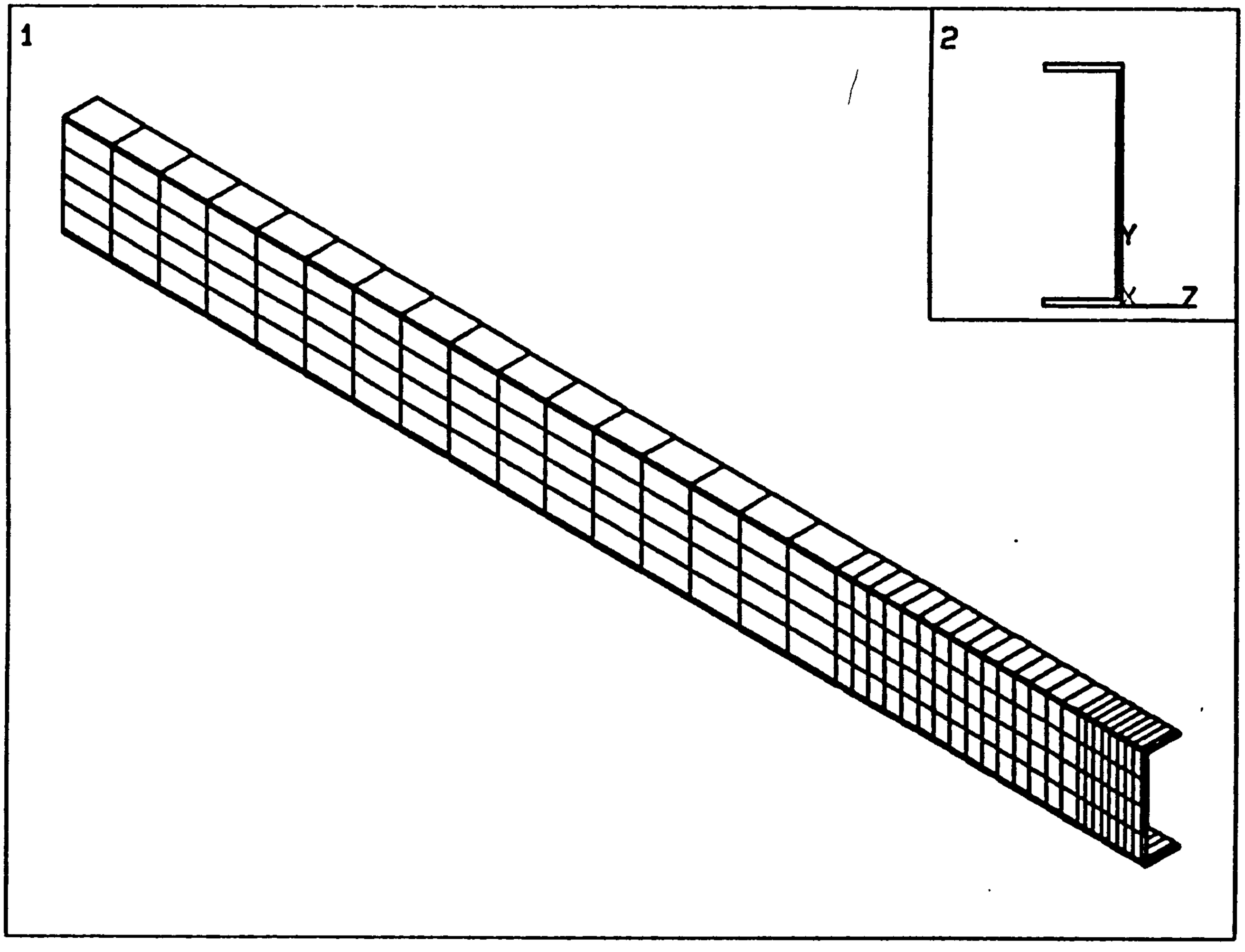

FIG. 2.4 FINITE ELEMENT MESH OF THE STEEL BEAM

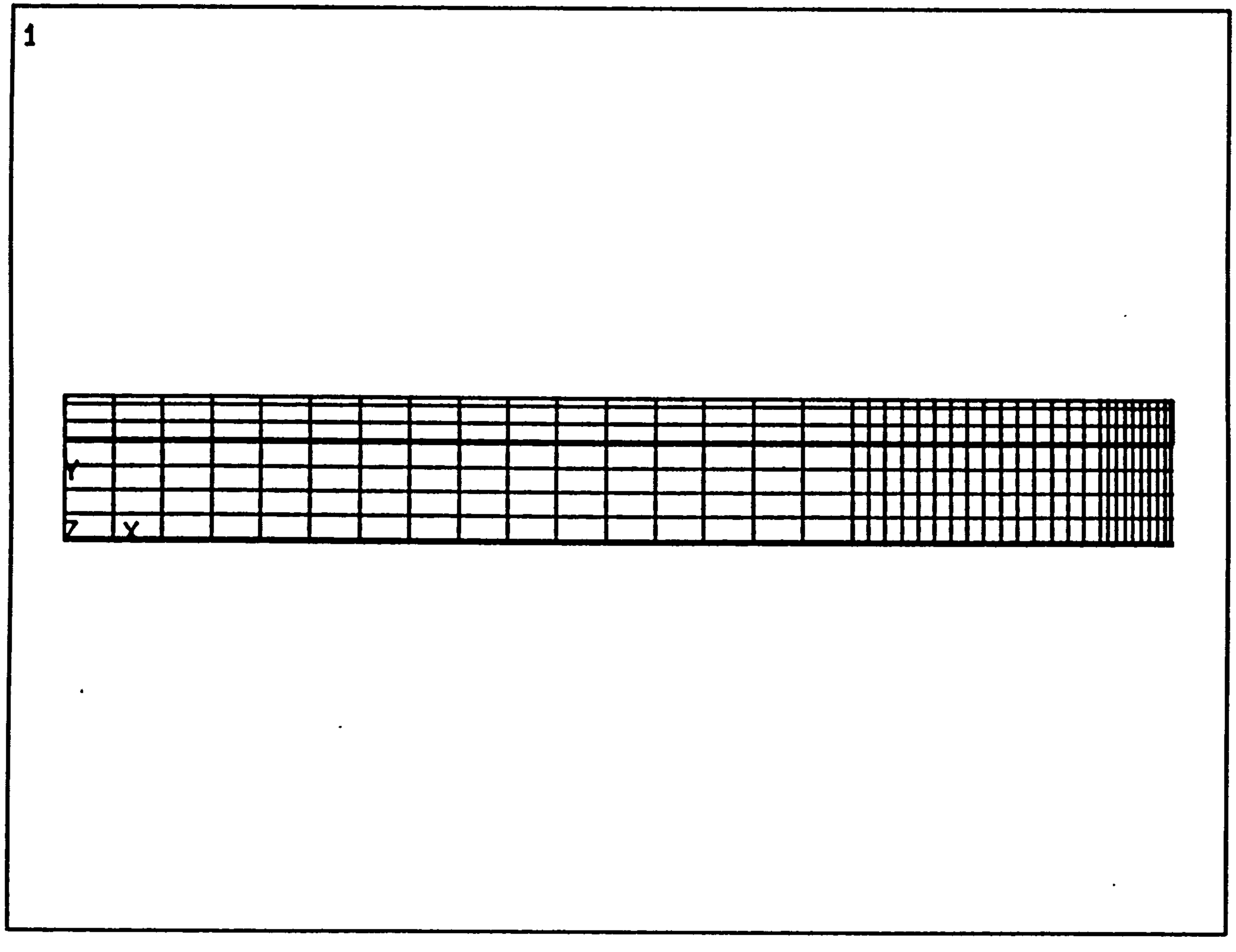

FIG. 2.5 FINITE ELEMENT MESH OF THE COMPOSITE BEAM

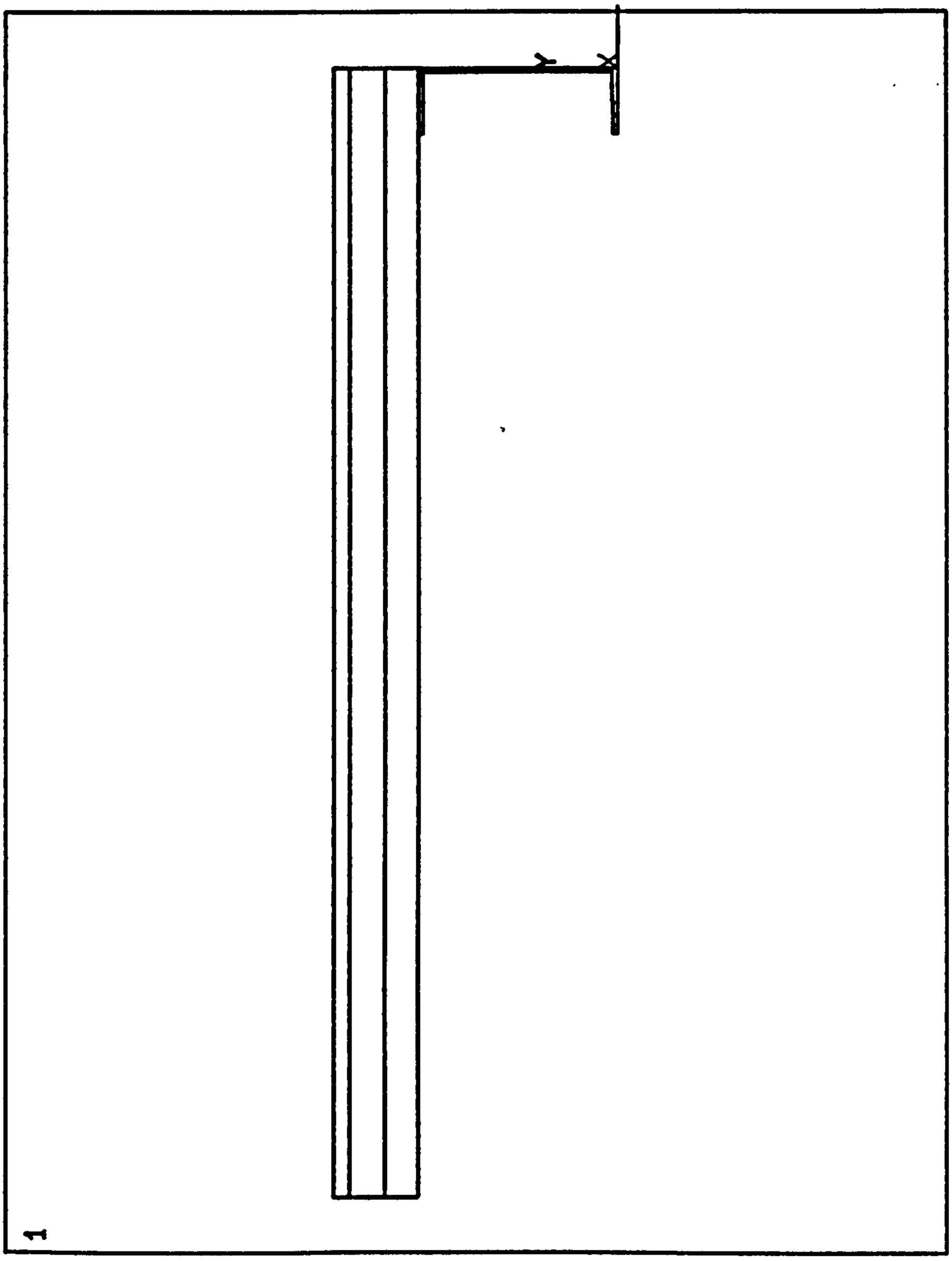

FIG. 2.6 CROSS-SECTION OF THE COMPOSITE BEAM

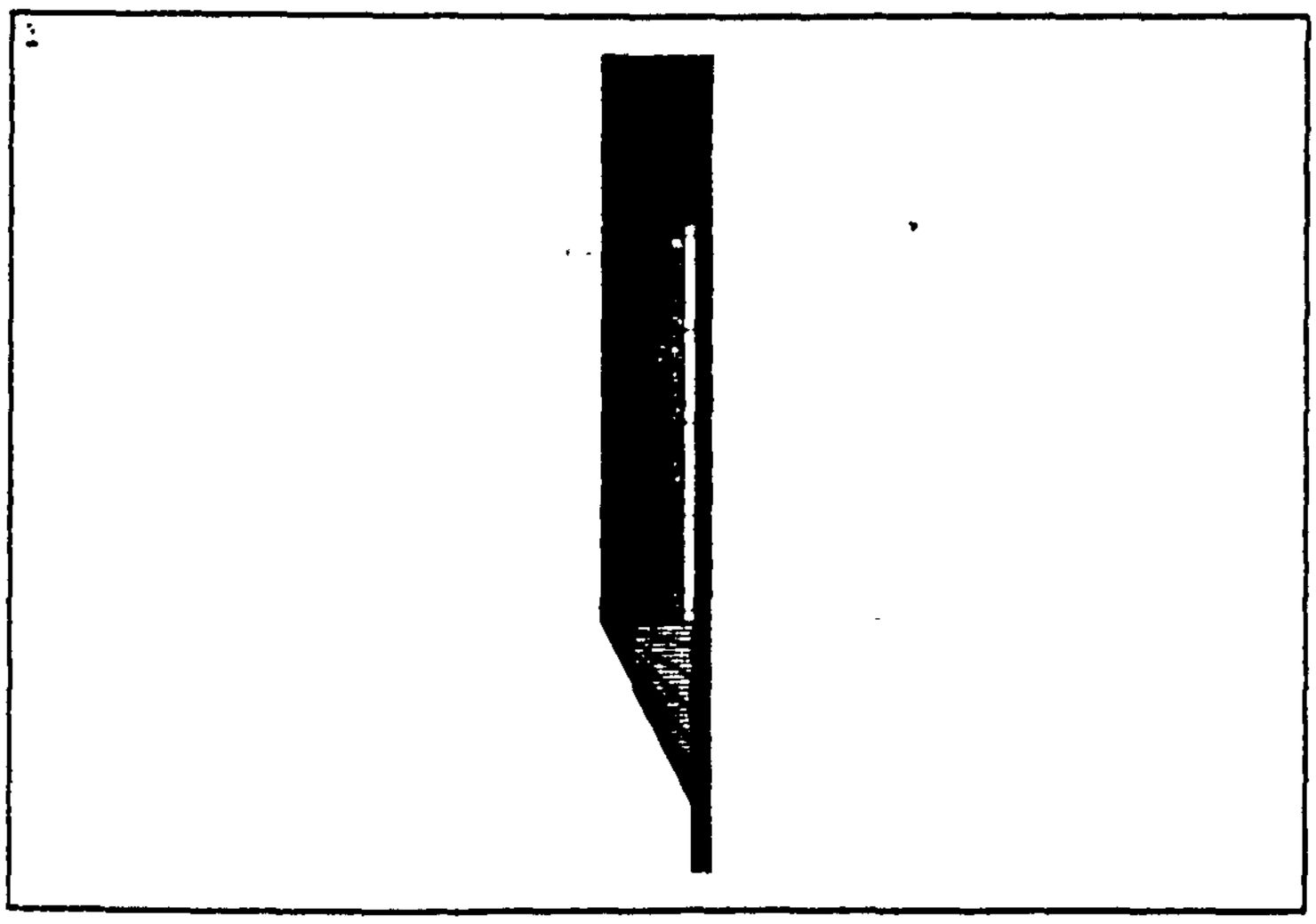

FIG. 2.7: CONSTRUCTION TOLERANCE SHOWN IN THE MESH SURROUNDING THE BEAM TO COLUMN INTERFACE

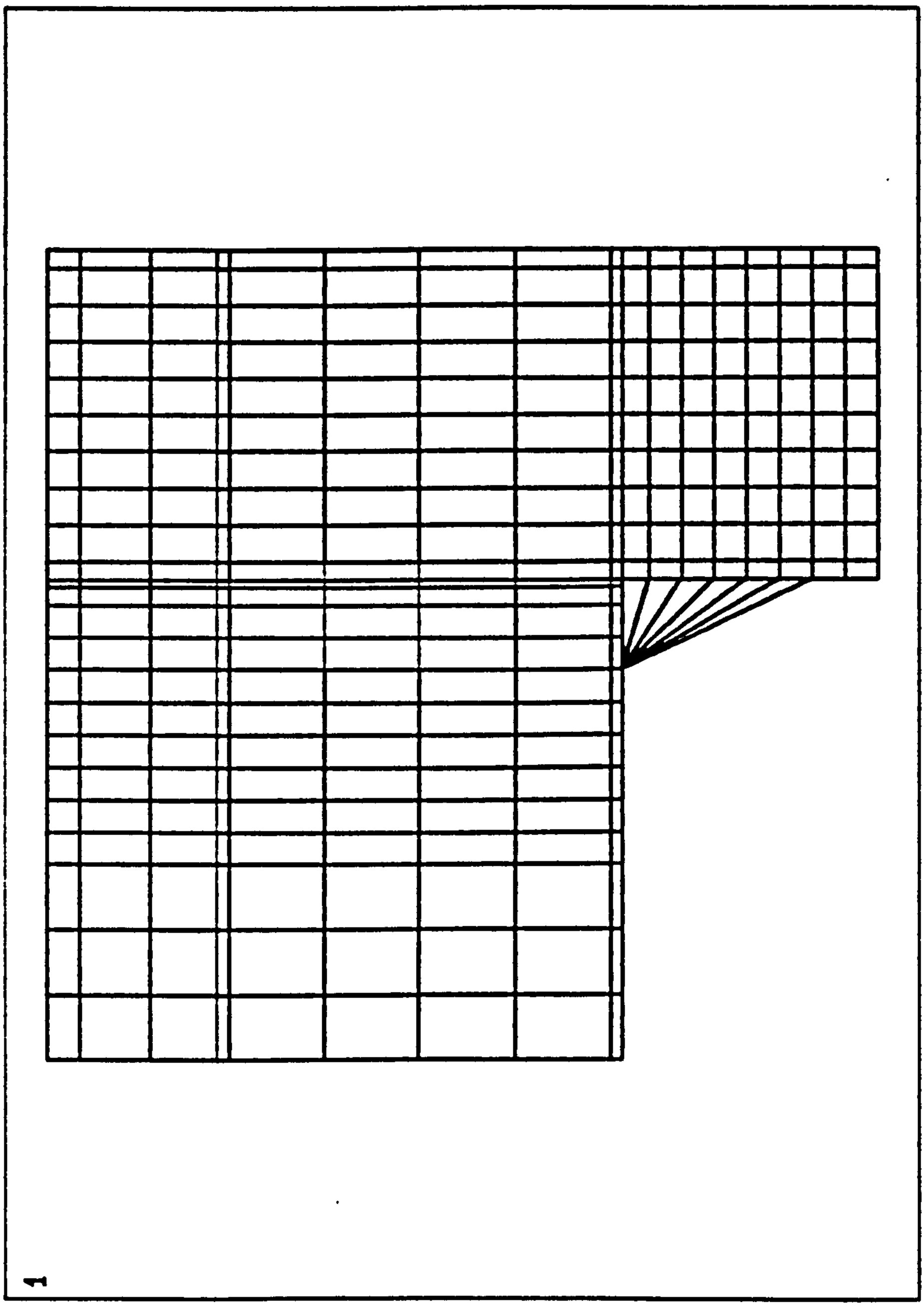

FIG. 2.8 FINITE ELEMENT MESH OF THE JOINT

CHAPTER THREE

2-D MODELS USED IN THE NUMERICAL STUDY

3.1 Introduction

Structural connections are well known for their highly complex nature and the large number of parameters involved in their formation. In a composite connection, the number of variables is greater than in a steel one. It was decided to develop numerical models in which one could vary the parameters involved in the connection. The results obtained from such models lead to the development of better analysis and consequent understanding of the connection behaviour. In this chapter, modelling of semi-rigid composite connections is described.

All connection configurations identified as sub-frames A to E in Figure 3.1 were studied numerically. Each of the sub-frames B to D were expected to be contributing to the stiffness of the building as multiples of the stiffness of sub-frame A. For example, sub-frame B equals sub-frame A' (i.e., A reversed) plus sub-frame A . The computation was to predict the stiffness of each joint from the geometry and material properties.

The first configuration is the ¬ shaped sub-frame, Figure 3.2, which was considered the basic one. The second joint is the ⊣ shaped and is shown in Figure 3.3. While the ⊤ and ┼ shaped ones are shown in Figures 3.4 and 3.5 respectively. These configurations represent the most common shapes of beam-to-column connections. The ¬ shape joint was considered as the reference one and comparisons were carried out to check the ability of this joint to represent the others. For each joint, the loading took place as a positive or negative horizontal force resulting in a closing or an opening moment.

It was decided to make use of the assumption that contraflexure points take place at midpoints of columns and beams. This assumption is one of the assumptions of wind load analysis, which is the area of interest of this study, and is explained in detail in reference [48]. At these points there are effectively zero moments. Consequently, the boundary conditions at these points are easily applied. With the complete structure divided into sub-frames each comprises one joint plus half the length of each adjoining member. Thus the numerical study represented a complete frame by a series of the four fundamental shapes, viz. ¬ , ⊣ , ⊤ and ┼.

The steel beam-to-column connection was a seat cleat plus a single web cleat, being a popular connection detail for use in composite frames due to its economy and simplicity.

In all models, the lateral displacement at the point of load application was taken as a measure of the lateral stiffness of the connection. This point, which was the mid-span of the composite beam, was situated at the top flange of the steel beam since that is the approximate location of the beam neutral axis.

In order to facilitate the modelling of the composite frame, some assumptions were taken into account. These are:

(1) The type of connection to be studied, consisted of web angles to transmit shear, and a seat cleat and composite slab to transmit bending.

(2) For the composite frame, wind loads are applied after the concrete hardens.

(3) The connection frames into the strong axis of the column. This was decided to be the case in the experimental work as well.

(4) Two bearing bolts were used to fix each cleat to the steel beam.

(5) Gravity loads were assumed to have no effect on the lateral stiffness of the

frame.

(6) Since concrete is well known by its low tensile strength, effective width of the concrete slab resisting tensile stresses was assumed to be different from that subject to compression. The effective width calculation method is detailed later in this report.

3.1.1 Material Properties

Material properties were supplied in the input data for each element. The nonlinear analysis which was adopted requires the nonlinear material properties to be provided. Young's modulus E and Poisson's ratio are also given.

For the steel beam and column, Young's modulus was taken as $2.05\times10^5 N/mm^2$ and Poisson's ratio =0.25. The tensile yield stress for hot rolled sections was taken as $275N/mm^2$ for steel grade 43 and $355N/mm^2$ for grade 50. The stress-strain curve consisted of two straight lines connected together at the yield point. The first of these has slope equal to Young's modulus E, and the second part was assumed to have a reduced elastic modulus of 5% E to represent the combined effects of yield and work-hardening.

For the reinforcing bars the values of Young's modulus and Poisson's ratio were taken as $2.05\times10^5 N/mm^2$ and 0.25 respectively. The tensile yield stress was taken as $460N/mm^2$ and the stress-strain curve was again a bilinear one.

The angle cleats were assumed to have material properties similar to those of the steel beam and column.

For concrete elements, the crushing stress was taken as $30N/mm^2$. This value is reasonable for light weight concrete and has been used repeatedly in composite construction since it is comfortably within 25 to $40N/mm^2$ range specified. The concrete tensile stress was taken initially as $3N/mm^2$ which is 1/10 of the crushing

stress to account for the case of wind loading at early stage. Young's modulus of concrete was taken equal to $2.05\times10^4 N/mm^2$. This value was selected according to BS 8110: part 2, table 7.2, [51] modified to represent lightweight concrete. The actual values for materials, measured for the test sample, are used in a later analysis.

The stress-strain curve for concrete is a trilinear one with the first slope equal to Young's modulus. The second and the third parts have lesser slopes in order to satisfy ANSYS requirements in the nonlinear analysis and to represent the actual behaviour of concrete as shown in Appendix V.

3.1.2 Load Application

The loading criterion consisted of wind load applied as horizontal point load at the point of contraflexure of the steel beam. This point is represented by the left support as shown in Figure 3.2. This criterion was the same in all models. An incremental loading took place starting from zero to a load of 50kN. At first, and to achieve convergence, the load was applied gradually with very small increments, to ensure the stability of the connection while bolt gaps were initially open. In connections with initially closed bolt-hole gaps, the load increment was 5 or 10kN.

The loading consisted of a nodal force at the top flange of the steel beam. This represents the wind load acting at the floor level which is another assumption of wind load analysis [48,55,56]. The single-storey sub-frame considered contained three connections, two of which are ¬ or ⊣ shape, and the third is a ⊤ or a ┼ shape joint. The lateral stiffness of the ¬ shape connection was expected to be about one half of that of the ⊤ or ┼ shaped joint. In other words, the lateral force resisted by the ¬ shaped connection was expected to be approximately one quarter of the total lateral force resisted by the frame. The maximum total wind load, as calculated in Appendix I, was 108kN. This is the wind load which was expected to act at the first storey floor. Consequently, the maximum force applied

on the ¬ connection was equal to 108/4=27 kN. It was decided to study the behaviour of each joint to a load of 50kN initially. Wind loads are assumed to be applied at floor levels by cladding. The expected deflected shape of the building is as shown in Figure 3.6.

3.2 Finite Element Models

According to the geometrical shape and the direction of loading, which affected the assumed effective width of the concrete slab, the following numerical models were developed:

3.2.1 Model One (the ¬ Shaped Sub-frame)

The geometry for this model represents that of the ¬ shaped semi-rigid composite connection, as shown in Figure 3.2. 3-D isoparametric elements (STIF45) were used to represent the steel beam and column, 3-D concrete elements (STIF65) were used to represent the concrete slab, spar elements (STIF1) were used to represent the reinforcing bars and beam elements (STIF3) were used to represent the shear connectors. Physical gaps or clearances were modelled using 2-D interface element (STIF12). A more detailed description of these element types is given in chapter 2 and in reference [37].

As mentioned before, slab effective width was assumed to change according to the direction of the applied load. This means that for the same ¬ shape configuration, there are two cases which will be referred to as Model One (a) in the case of an opening moment and Model One (b) in the case of a closing moment.

Partial interaction was assumed to take place between the concrete slab and the steel beam. This interaction was modelled using a system of tie and gap elements as described in chapter two.

In the preliminary runs, the steel beam was a 250×102×28kg/m UB and the steel column was a 254×254×89kg/m UC. The seat cleat was 150×90×10mm without a stiffener plate and the web cleat was a single 80×60×8mm cleat. These sections were changed to be 305×102×28kg/m UB, 254×254×73kg/m UC, 150×90×10 stiffened cleat and 80×60×8 angle cleat for the steel beam, column, seat and web cleats respectively.

The only reinforcement was the A 193 anti-crack fabric. The reinforcing bars were rigidly connected to the concrete, therefore assuming that there is no slip between concrete and reinforcing bars. Shear connectors were 19mm diameter and were arranged with a constant spacing of 150mm centres.

Material properties for this model are as mentioned in section 3.1.1

A set of boundary conditions was used to represent the actual frame. The nodal point at the column point of contraflexure was allowed only to rotate while translation was prevented in both x and y directions. In other words, a hinged support was assumed to take place on the axis of the steel column at its lowest point. The point of contraflexure at the mid span of the beam was allowed to move horizontally and to rotate in plane and no vertical deflection was allowed at this point. In the model this point is the point of load application and is shown as a support in Figure 3.2.

(a) Model One (a)(the ¬ Shaped Sub-frame Resisting Opening Moments

The geometry of this model is that of the ¬ shaped joint resisting opening moment. The finite element mesh is shown in Figure 3.2 and the boundary conditions and material properties are as mentioned above. The effective width of the slab was taken as the least of the two values:

(i) One half of the distance between centrelines of frames which was 6000/2=3000mm

(ii) One quarter of the total span of the beam =7000/4=1750mm

At the column centreline, the slab was assumed to crack at 45^0 measured from the edge of the steel beam flange. Taking the width of the steel beam flange =102mm and the slab thickness =130mm, the uncracked width was:

$$B_{effective} = 102 + 2 \times 130 = 362mm$$

In the column zone, the effective width of the concrete slab had the curved shape shown in Figure 3.7. This double parabolic shape was adopted to avoid sharp change in stiffness which was expected to occur as a result of the sudden change in the slab width from 1750mm along the beam to 362mm at the column centre.

Since the loading took place in the lateral direction, the transverse reinforcing bars were neglected. The effect of these bars on the effective width of the concrete slab was assumed to be included in the proposed formula, given in Appendix II, to calculate this width.

(b) Model One (b)(the ¬ Shaped Sub-frame Resisting Closing Moments)

The applied force in this model is in the positive x-direction producing a closing moment. The shape of the effective width of the concrete slab in this model, as shown in Figure 3.8, is composed of two parabolas with a point of contraflexure at x=0.35L where L is the span of the beam.

The z co-ordinates of the nodes of the concrete slab elements were calculated according to the equation of the slab effective width. In other words the parabolic curve is composed of straight chords. Some of the concrete elements had angles between adjacent sides which were out of the preferred range of values specified in the software. A series of warning messages therefore appeared when the input data was checked in each load step.

The change in the slab effective width along the composite beam resulted in different cross-sectional areas of reinforcing bars. The anti-crack mesh is A193 fabric with cross-sectional area of 193mm^2/m. The area of reinforcing bars in each concrete element was calculated as follows:

$$A_{rebars} = 193 \times \frac{element\ width}{1000}$$

In order to facilitate the generation of reinforcing bars' elements, the concrete slab was divided into five strips. These strips are parallel to the steel beam with its width in the z-direction. The area of reinforcing bars was calculated for each strip and elements with this area were then generated.

Because the plane strain analysis was adopted, the set of reinforcing bars was created as a single element with the cross-sectional area of the group. This might have led to an overestimation of the effect of these reinforcing bars. Yielding could take place in the nearest bar to the column and as the crack propagates in the slab, further bars could start to be fully effective. Here the plane strain analysis introduces an artificially increased stiffness around the connection.

The boundary conditions, material properties, finite element mesh and other features of this model were similar to those in Model One (a).

3.2.2 Model Two (the ⊣ Shaped Sub-frame)

The geometry of this model (Figure 3.3) represents the connection between the edge column and a composite beam, where the column extends between the two midpoint heights of the columns of two stories.

The direction of the applied load causes the concrete slab to be either in tension or in compression, leading to the two different cases as before. These two models will be referred to as Model Two (a), in which concrete slab is in compressive

stress, and Model Two (b), in which concrete is in tension.

A set of boundary conditions was introduced at the point of load application and at the two points of contraflexure of the column. The lower point of the column was considered as a hinge. This means that no translation could take place while rotation was allowed at this point. Horizontal deflection and rotation were allowed at the upper point of contraflexure while vertical displacement was prevented. Again at the point of load application, horizontal displacements and rotations were allowed.

Model Two had material properties similar to Model One.

The finite element mesh of Model Two is shown in Figure 3.3 from which it is clear that the mesh is similar to that of Model One with the addition of the upper steel column. The finite element mesh of the upper column is composed of four zones: The first consists of three layers of elements with heights equal to the heights of the concrete elements i.e., 51, 54, and 25mm. The second part is a fine zone with a constant element height of 25mm, while the third region has an element height of 50mm. The finite element mesh of the upper part is a coarse one with element height of 150mm. These zones therefore reflect those in the lower column.

(a) Model Two (a) (The ⊣ Shaped Sub-frame Resisting Opening Moments)

The applied horizontal load in this model is a negative force producing an opening moment. The concrete slab effective width is constant along the steel beam and equal to 1750mm. In the column zone the slab has a parabolic shape as explained in Model One (a). The finite element mesh of Model Two (a) is shown in 3-D view in Figure 3.9.

(b) Model Two (b) (The ⊣ Shaped Sub-frame Resisting Closing Moments)

The concrete slab in this model is in the tensile stressed zone. The effective width of the concrete slab is assumed to be of a double parabolic shape as described in Model One (b). The finite element mesh for this model is shown in Figure 3.10.

The load-deflection curve for this model was expected to be similar in shape to that of Model One (b). The presence of the upper column was expected to add some extra lateral stiffness to the joint and consequently, Model Two (b) was expected to be only slightly laterally stiffer than Model One (b).

3.2.3 Model Three (The ⊤ Shaped Sub-frame)

The geometry for this model is that for the ⊤ shaped connection as shown in Figure 3.4. This connection was assumed to be composed of two adjacent ¬ shaped connections back to back. When one of the two ¬ shaped connections was subject to an opening moment, the other would resist a closing moment. In other words, the lateral stiffness of the ⊤ connection was expected to be the summation of the lateral stiffness of the two ¬ joint cases. In the frame investigated, the spans were 7 and 8 meters for the left and right bays respectively. The stiffness of the ¬ connections with a beam span of 8 meters is expected be laterally less stiff than that with a span of 7 meters. The spans to points of contraflexure of the composite beams in this model were 3500mm and 4000mm respectively.

Material properties of this model were the same as in model one.

The finite element mesh is shown in Figure 3.4 from which it is seen that fine mesh zones were created in the composite beam on both sides of the column. The column finite element mesh was the same as described in model one. The finite element mesh for the frame in 3-D view is shown in Figure 3.11 from which it is clear that the beam contained a fine mesh near the column from both sides. The column also had a fine mesh within the joint zone and immediately below it.

3.2.4 Model Four (the ┼ Shaped Sub-frame)

The geometry of this model represents the cross-shaped frame shown in Figure 3.5. The mesh of the sub-frame joint zone is shown in Figure 3.12. The composite beam extends along the x-axis from the mid-span of the left bay to the mid-span of the right bay. The finite element mesh of the beam is similar to that of Model Three. The slab on one side of the column will be in the tensile stressed zone while that in the other side will be in the compressive stressed zone. The concrete slab effective width was assumed to take the same shape as explained in Appendix II.

The steel column extended between the two mid-height points of stories with a total height of 4000mm. The finite element mesh generation of the column elements took place using the same procedure as described for Model Two.

A set of boundary conditions was introduced to this model to represent those constraining the actual connection. At the point of application of load, only the vertical displacement was prevented. The similar point in the second bay had the same boundary condition. At the point of the mid-height of the lower column, horizontal and vertical displacements were prevented. At the point of mid-height of the upper column, the vertical displacement was set to zero while the horizontal displacement and the rotation were left to be calculated by the programme.

Notes on the Basic Models

Comparisons between the load-lateral displacement curves of the basic four models are presented in chapter four. It was expected that the ┬ connection would have almost twice the lateral stiffness of the ┐ connection. Moreover, and because of the presence of the upper column, the ┼ shaped connection was also expected to be stiffer than the ┬ shaped connection.

As mentioned before, there are different possibilities for the actual size of the bolt-hole clearance, and for the construction tolerance as well. These physical sizes have been modelled using gap elements. Changing the gap size led to a significant change in the lateral stiffness of the connections studied.

The effect of changing the important variables on the behaviour of the ¬ shaped connection resisting opening and closing moments was studied.

3.3 Models of Stiffened Joints

The effect of changing the important variables of the ¬ shaped sub-frame together with stiffening modifications were studied. Although some of these options proved to be efficient in increasing the stiffness of the connection, they were excluded on grounds of practicality.

3.3.1 The ¬ Shaped Sub-frame with a Corner Tie

As one possible stiffening modification, a corner tie was rigidly connected at each end to both the steel beam and the steel column in model One (a). The point of fixity of the tie with the steel column was selected to be hidden above the false ceiling. The other point was selected on the bottom flange of the steel beam so that the tie was at 45^0 to the horizontal. The cross-sectional area of the tie was calculated to ensure that it remained elastic.

In the actual connection, a bar of diameter 16mm was suggested to be used as a tie on each side of the column web to provide symmetry. In the model, a single element with an area equivalent to that of the two bars is used because the plane strain analysis, with a single active plane was, adopted.

The element used to model the tie is the 2-D spar element. Although this element is a uniaxial tension-compression element, the effect of the corner tie was considered only in the connection resisting opening moment to avoid buckling

problems associated with compressed long members with small cross-sections.

The function of the tie is to transmit the horizontal force, from the beam to the column, without the large deflection required to close the tolerance gaps and create contact between the steel cleat and the bolt fixing the cleat to the beam flange.

The corner bracing option was considered impractical but provided an upper bound stiffness which could be realised within the connection. In other circumstances, it could be used to increase the lateral stiffness of frames to withstand wind or earthquake loads. This may be an acceptable option for old frames which were not designed to resist such high lateral loads. Other options for increasing the lateral stiffness of the frame were therefore looked for.

3.3.2 The Effect of Slab Reinforcement

This model was performed to study the effect of increasing the area of reinforcing bars on the lateral stiffness of the semi-rigid composite connections. A light A193 fabric had originally been used in all the four models. The option of increasing the stiffness of the connection by increasing the reinforcement of the concrete slab was assumed to be effective in the case of a closing moment, where the concrete slab is in the tensile stressed zone. Thus the cross-sectional area of reinforcing bars was increased only in the models which represent closing moment joints.

In this model, the cross-sectional area of reinforcing bars was increased to be 1% of the total cross-sectional area of the concrete slab. Based on the cracked shape of the slab, the increased area at the slab section with minimum width was $362\times130\times1/100=470.60mm^2$ while the original area was $193\times362/1000=69.866mm^2$. Apart from the increase in the area of reinforcing bars, the same features as Model One (b) were adopted. The stiffening effect of increasing the reinforcing bars' area was expected to start after the closure of bolt-hole gaps. The connection in this model did not contain a corner tie, in order to investigate the effect of increasing the reinforcing bars' area separately.

This option for stiffening may be carried out practically by the use of additional slab reinforcement of 4T16 instead of increasing the reinforcing bars as a percentage of the slab cross-sectional area. This alternative approach will be discussed later in this chapter.

3.3.3 The Effect of Seat Cleat Stiffening

In the connection investigated, there has been a stiffener plate welded to the seat cleat. In the previous analysis, this web plate has been neglected. The geometry, boundary conditions, material properties and the features of this model, other than inclusion of the seat cleat stiffener plate, are similar to those of Model One.

The seat cleat stiffener plate was modelled using the Two-Dimensional Isoparametric Solid Element (STIF42). A set of triangular-shaped elements has been created to accommodate the triangular shape of this part. The triangular shape is not recommended in STIF42 and warning messages appeared because of that. The alternative was to use the Three-Dimensional Isoparametric element, which has been used to model the steel columns and beams.

The stiffener plate was actually welded to the seat cleat which is in turn welded to the column. This was accounted for by using the same nodes in both the steel column and the seat cleat bracket. This means that the two parts were assumed to behave monolithically. Since the main objective of the numerical study is the investigation of the overall behaviour of the frame, modelling of two welded plates in this way was acceptable. Two closed vertical gap elements were placed to transmit the vertical reaction between the seat cleat and the steel beam flange. The first gap element was placed at the bolt position. The second vertical gap element was introduced between the end of the steel beam flange and the seat cleat.

At this stage, The assumption of a closed end gap was rejected because it was clear that the end of the beam and the column flange did not come in contact within the range of loading used. The bolt-hole gaps were assumed to be closed.

The effect of the seat cleat stiffener plate was investigated in both Model One (a) and Model One (b)

3.3.4 The Effect of Universal Beam Choice

The steel beam was changed to a heavier 305×102×28kg/m UB instead of the 250×102×25kg/m UB. This section is suitable, from the design point of view, for a span of 7 meters carrying a wide range of likely imposed loads. The column in this model was also changed, from the 254×254×89kg/m UC to a 254×254×73kg/m UC. Seat and web cleats were 150×90×10 and 80×60×8 respectively. The seat cleat stiffener was included in this model.

3.3.5 The Effect of Seat Cleat Angle

The option of increasing the lateral stiffness using corner bracing was excluded on grounds of practicality. The introduction of major changes to the common connection considered is not recommended.

However, increasing the lateral stiffness of the ¬ shape, and consequently any other connection configuration, can be accomplished by using a heavier seat cleat angle. This seat cleat section was changed from 150×90×10 to the heaviest angle section, 250×250×12mm. As explained earlier, only the upper leg of the angle, which is connected to the steel beam, has been modelled. The net cross-sectional area of the angle in all previous models was $100\times10-2\times18\times10=640mm^2$, while in this case the area is $100\times12-2\times18\times12=768mm^2$. The seat cleat stiffener plate has also been represented in this analysis, with a thickness of 10mm. The increased lever arm which resulted from the increase in the cleat section was expected to lead to a stiffer joint.

The steel beam and column were taken to be of steel grade 50 with tensile yield stress $355N/mm^2$.

The gap between the end of the beam and the column flange was assumed to be initially open with its full size of 6mm. This assumption was thought to be more realistic in the range of loading from 0.0 to 50kN.

3.3.6 The Combined Stiffening Effect of Reinforcement and Seat Cleat

The idea is the stiffening of the connection using a heavier seat cleat with a reasonable section of 200×100×10. This was combined with stiffening introduced by adding 4T16 as additional reinforcing bars. The steel beam is 305×102×28kg/m UB and the steel column is 254×254×73 UC. Both the steel beam and the steel column are of grade 50 steel. The seat cleat stiffener plate is included in this case. The end gaps were set initially open with 6mm gap width, the seat cleat bolt-hole gap was closed and the web cleat bolt-hole gaps were set initially open.

3.4 Summary

The major objective of the finite element study is to develop a realistic model for the analysis of semi-rigid composite joints using the finite element package ANSYS. The main requirement is to predict accurately the lateral stiffness of the joint. Prediction of the different aspects of the structural behaviour such as deformations and internal stresses for the joint main components are further items of interest. Different details and geometry are investigated to assist with the selection of the most appropriate details for use in frames in which the composite connection moment capacity is used to resist lateral (wind) loading.

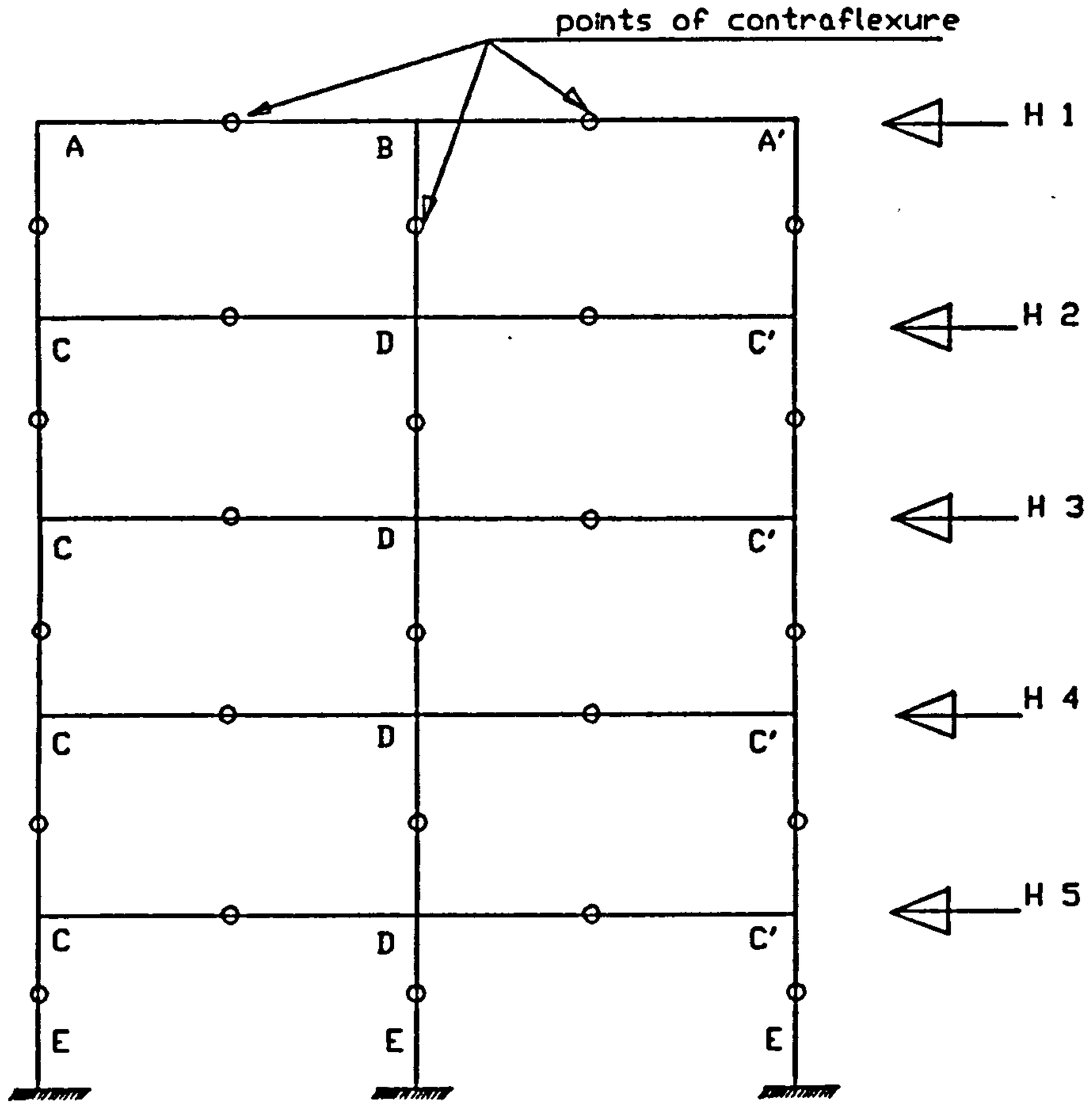

The stiffness of the building in providing resistance to lateral loading can be obtained by summing the contributions from each sub-frame, A to E, bounded by the points of contraflecture.

FIGURE 3.1

CROSS-SECTION OF THE BUILDING (UNDEFORMED)

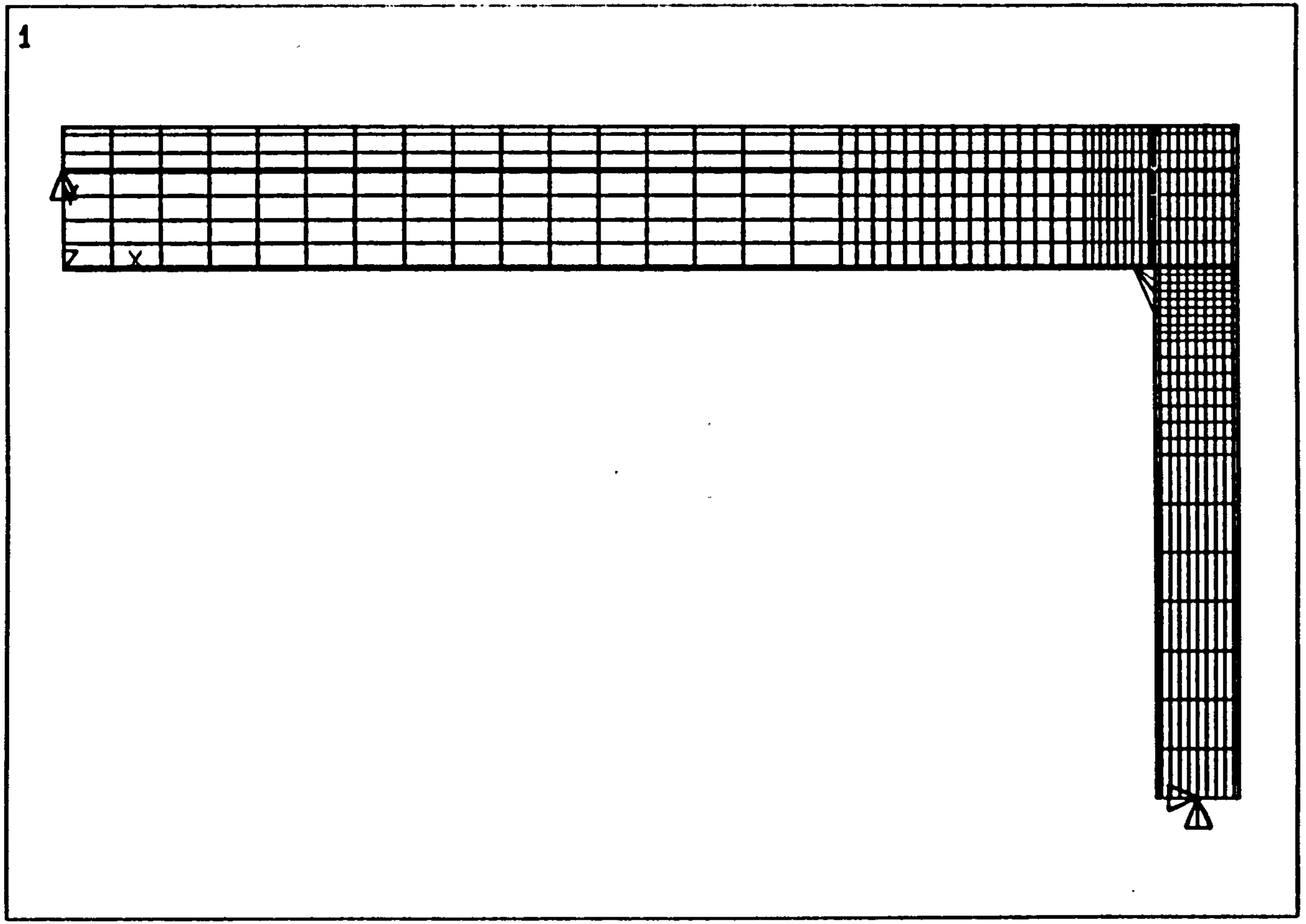

FIG. 3.2 MODEL ONE

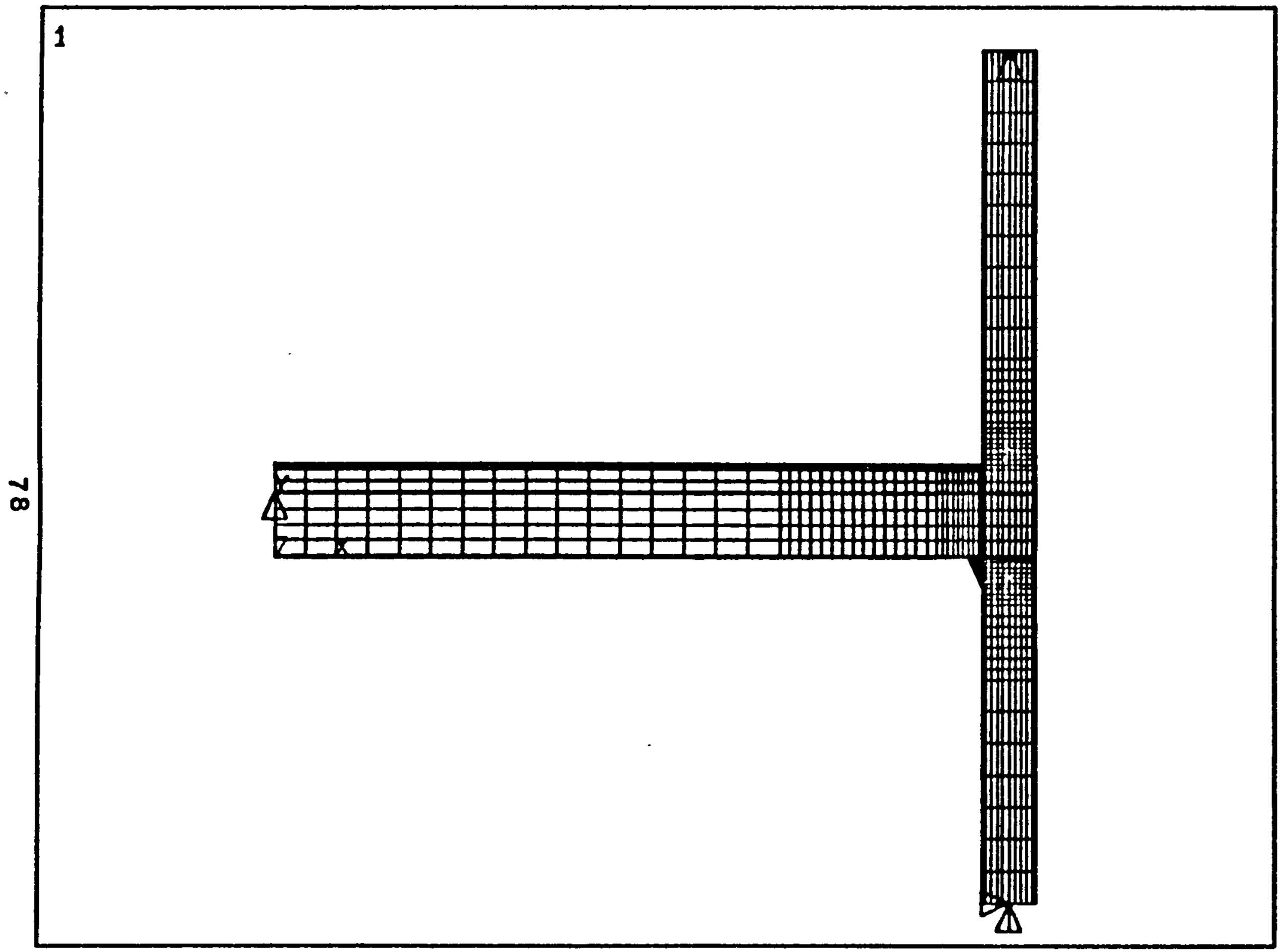

FIG 3.3 BOUNDARY CONDITIONS

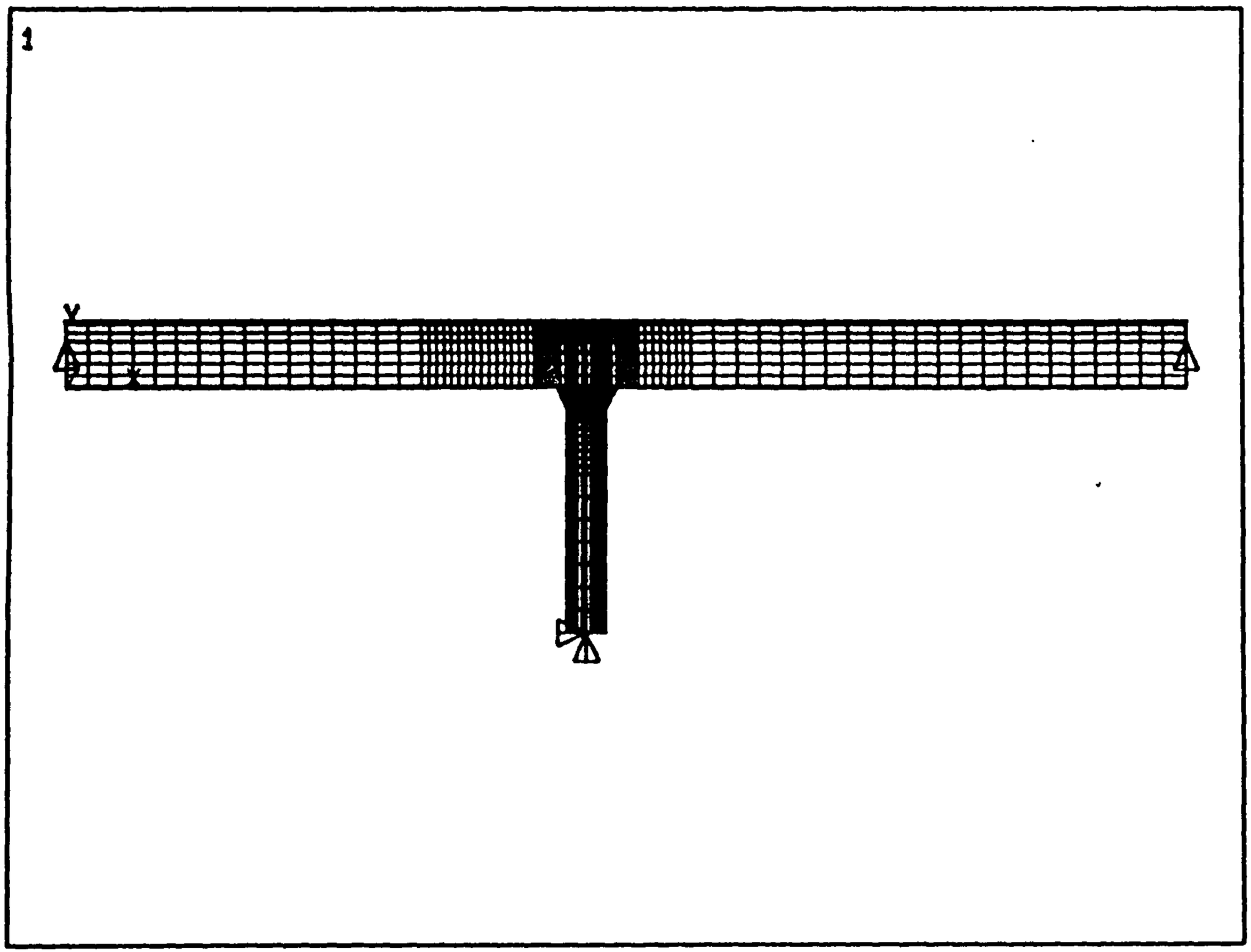

FIG. 3.4 F. E. MESH FOR MODEL THREE

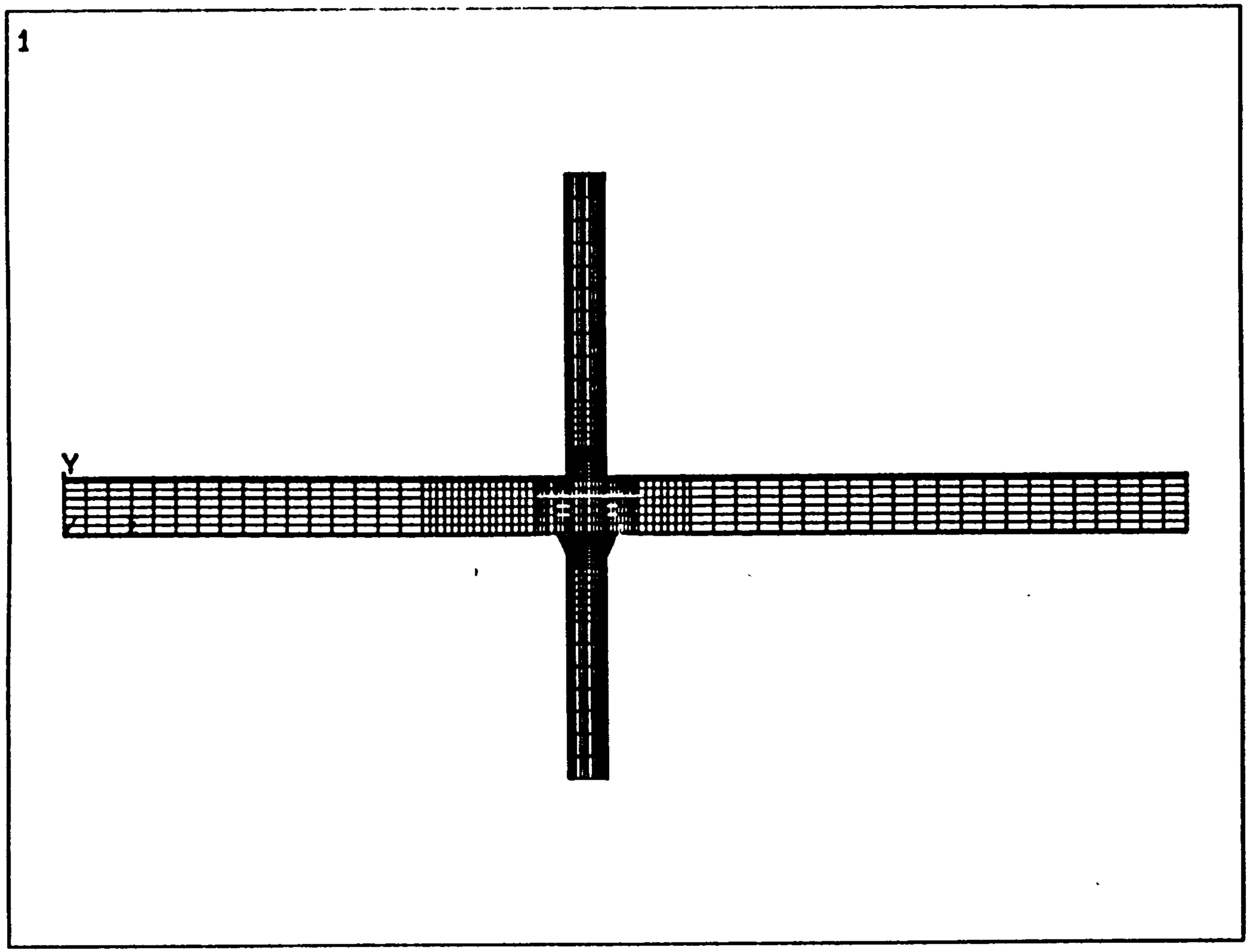

FIG. 3.5 FINITE ELEMENT MESH FOR MODEL FOUR (CROSS-JOINT)

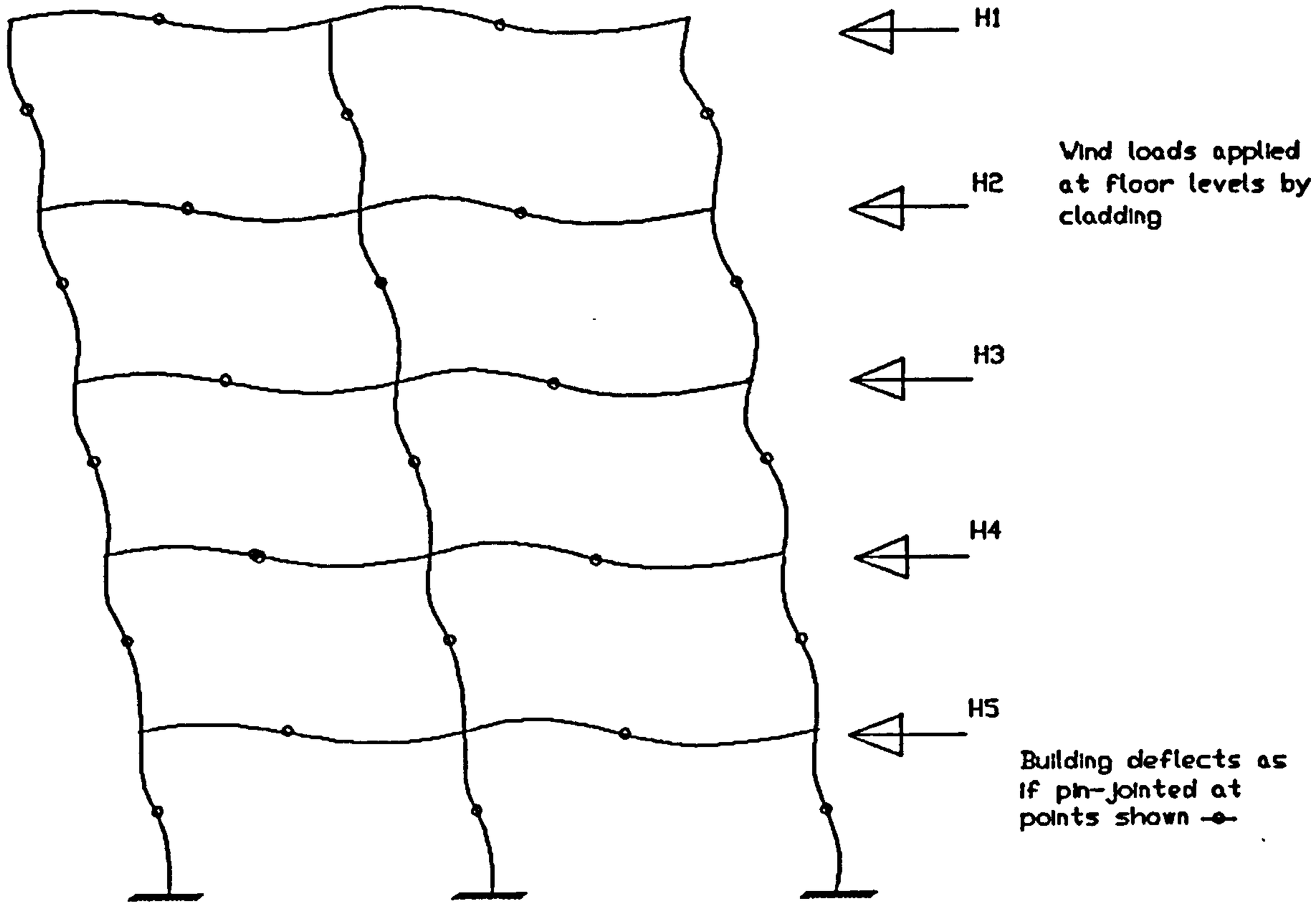

FIGURE 3.6

EXAGGERATED DEFLECTED SHAPE OF THE BUILDING DUE TO WIND LOADING

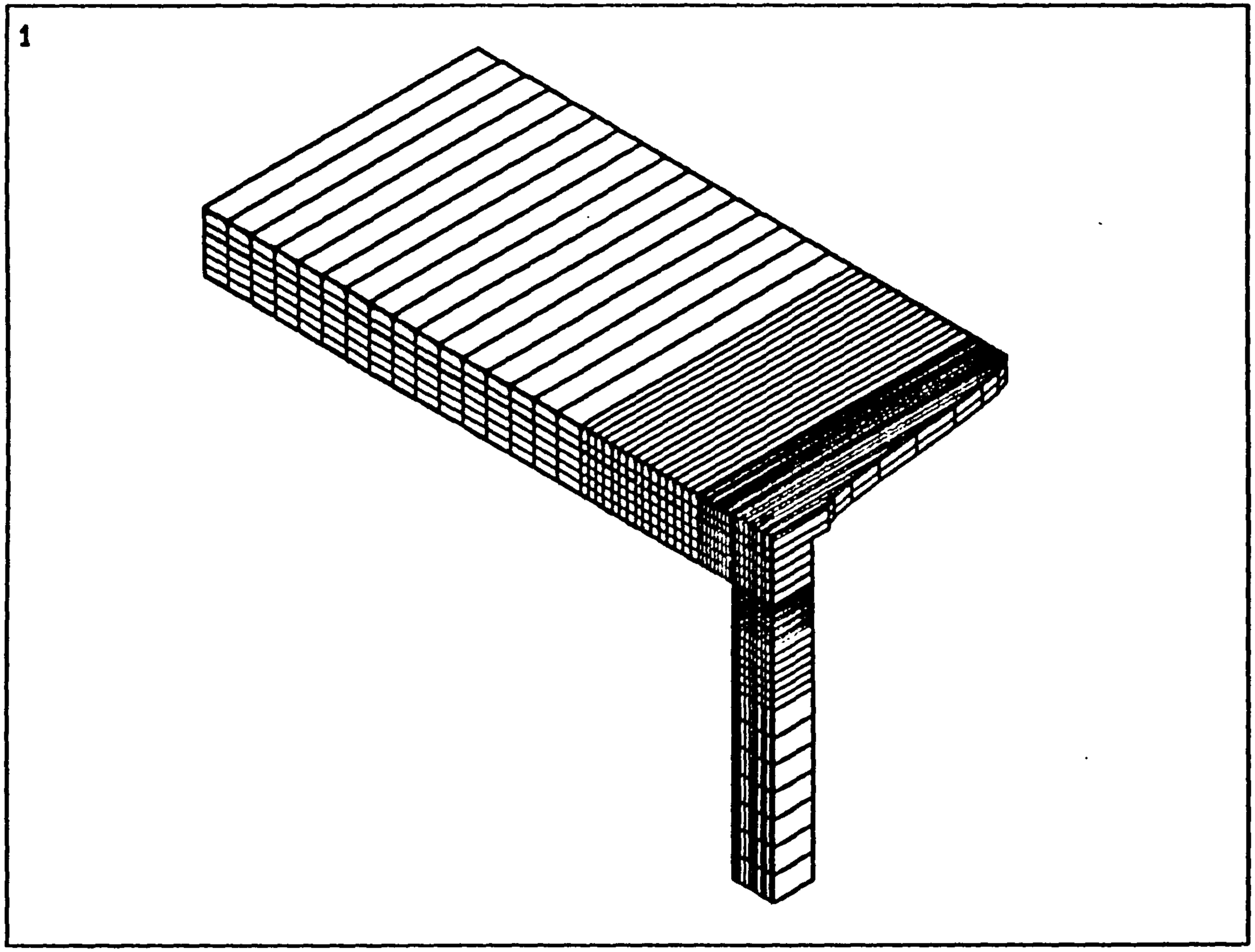

FIGURE 3.7

MODEL ONE A

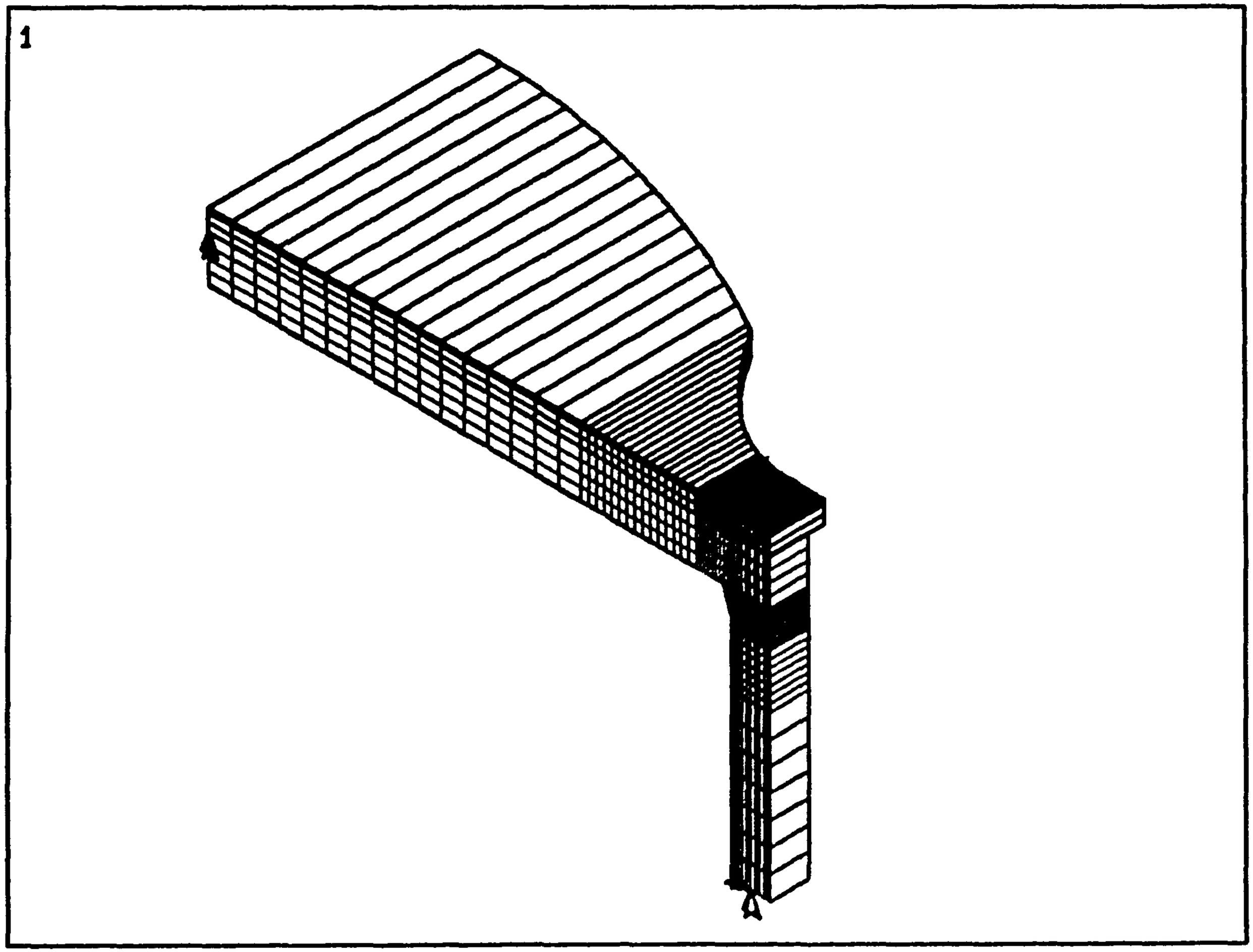

FIG. 3.8 MODEL ONE B (CLOSING MOMENT)

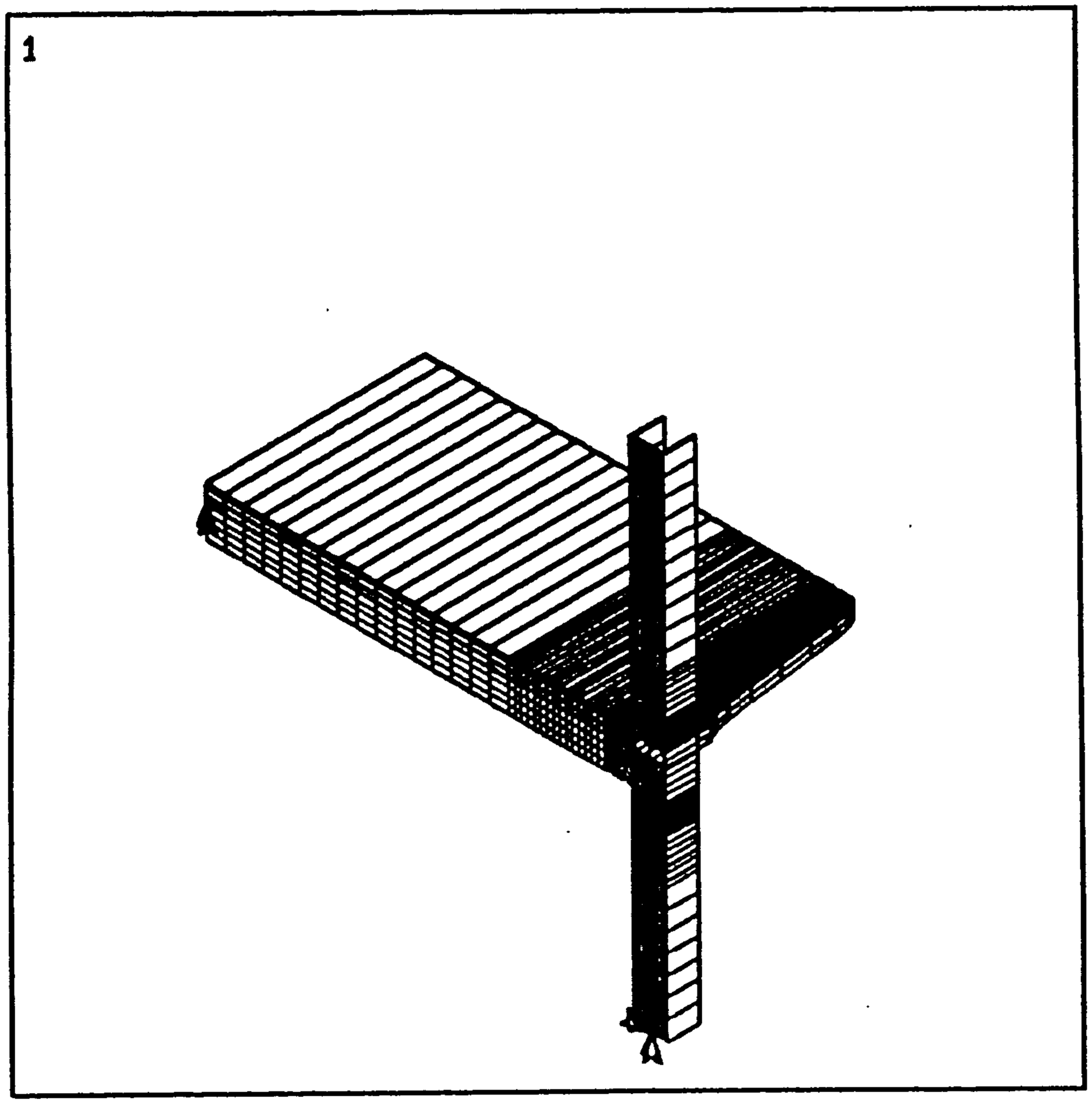

FIGURE 3.9
FINITE ELEMENT MESH OF Model Two a

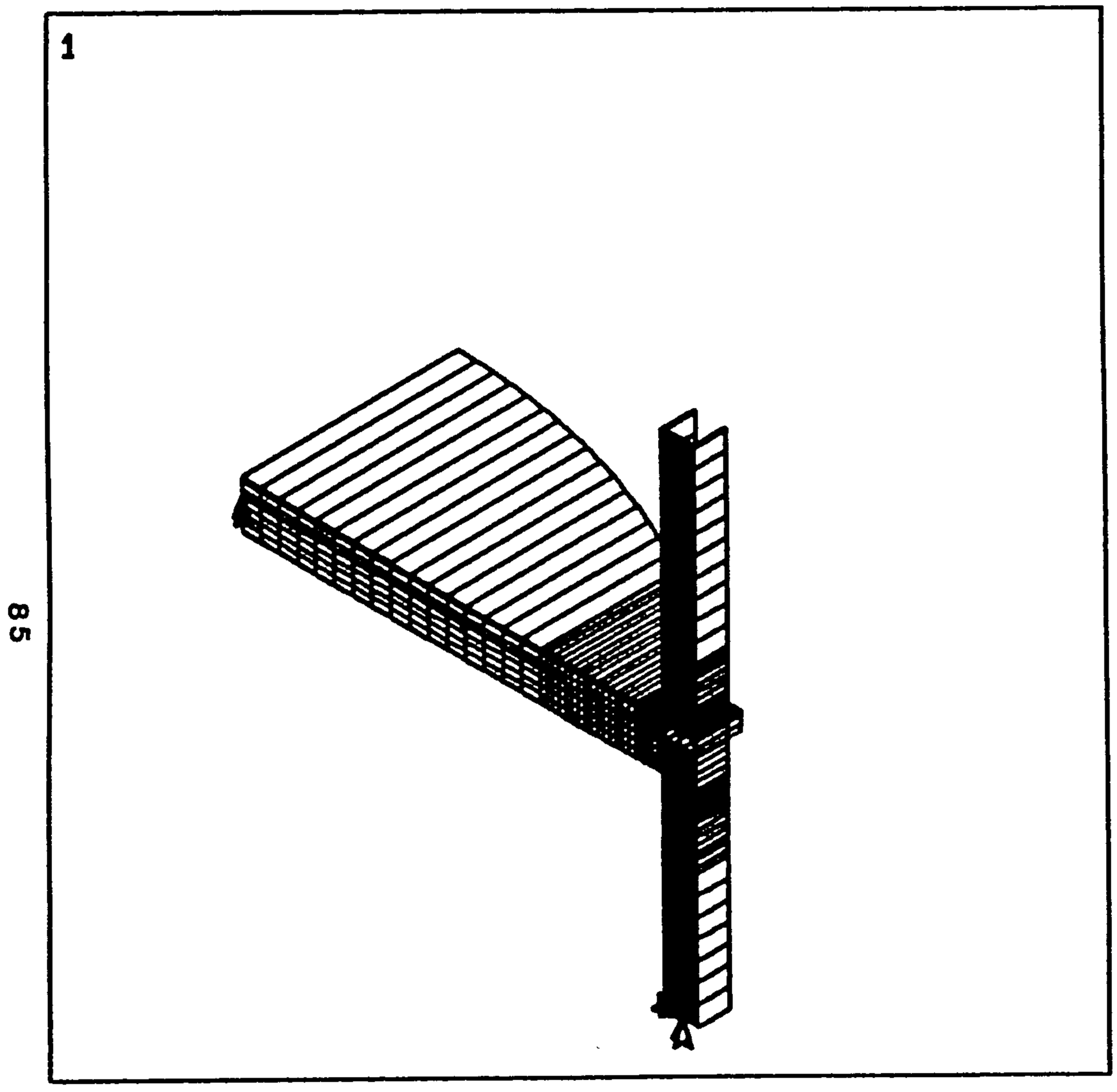

FIGURE 3.10

FINITE ELEMENT MESH OF Model TWO B

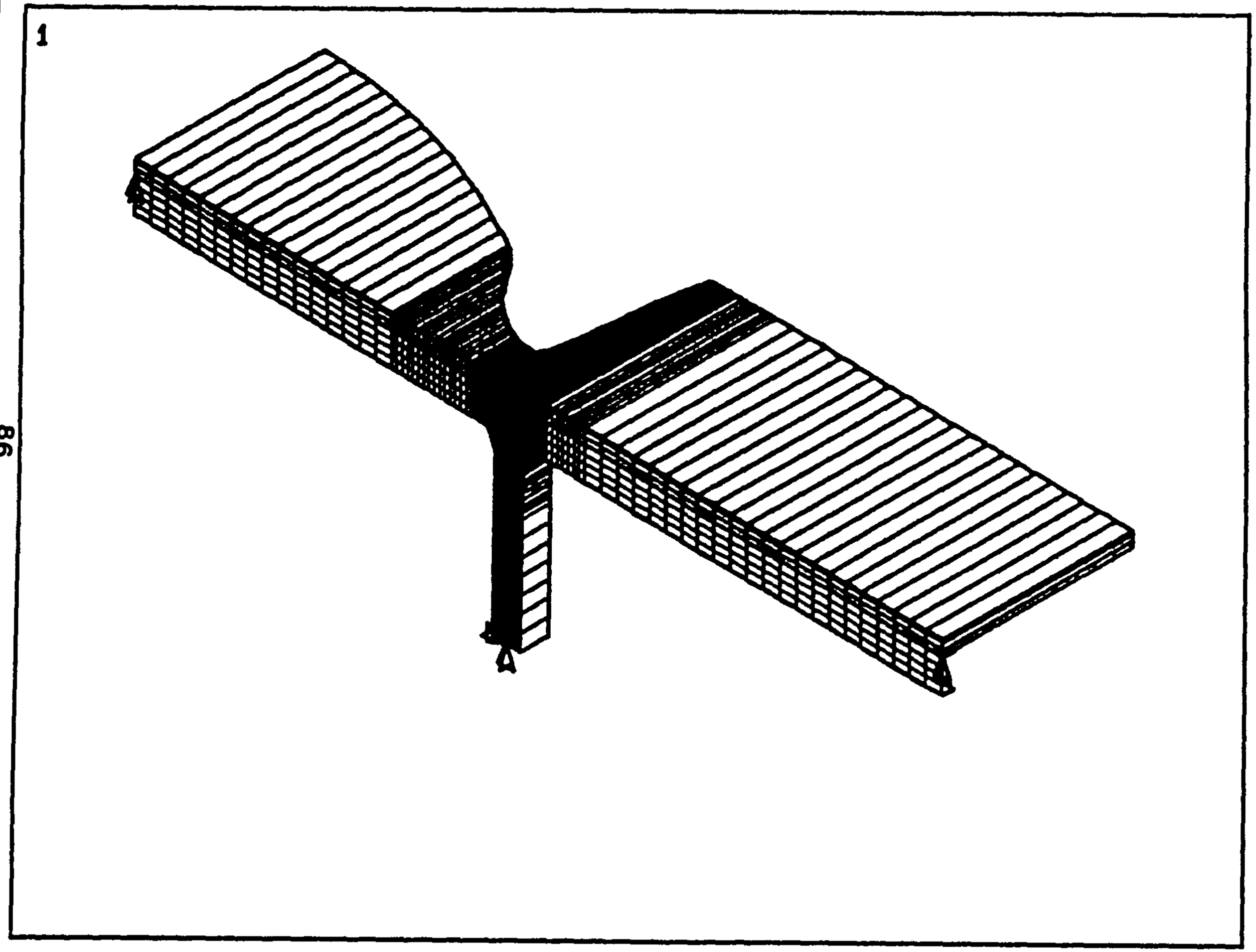

FIGURE 3-11

T-SUBFRAME

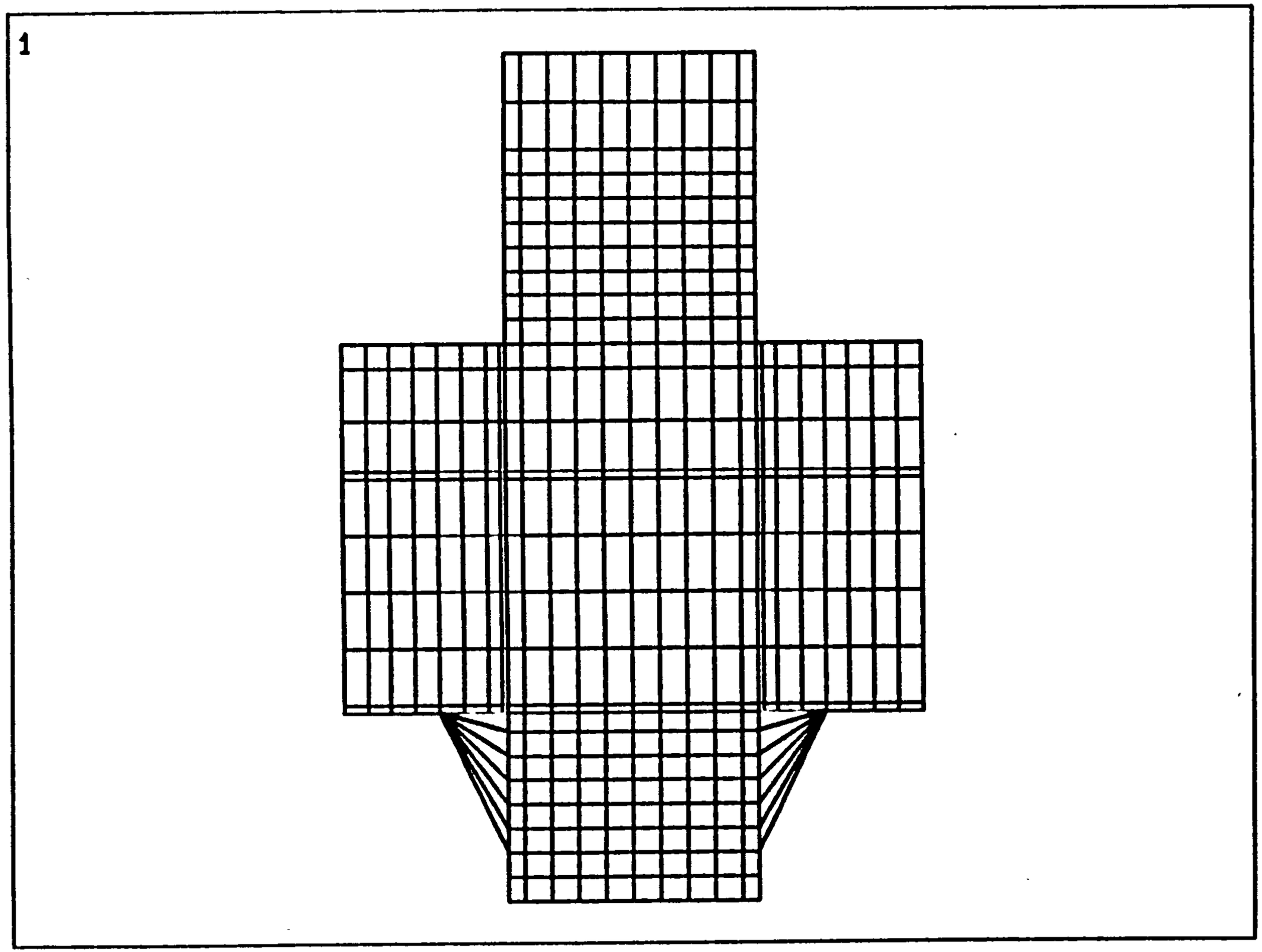

FIG. 3.12 FINITE ELEMENT MESH FOR MODEL FOUR (CROSS-JOINT)

CHAPTER FOUR

REPRESENTATION OF SHEAR CONNECTION IN THE NUMERICAL STUDY

4.1 Introduction

In all the models studied, the shear connection between the steel beam and the concrete slab was modelled by a system of spar and interface elements. This action is described by two interactions: traction orthogonal to the interface and shear in the interfacial plane, both of which are due to the presence of welded shear studs. The presence of the profiled steel decking minimizes, or indeed virtually eliminates, the contribution of adherence and friction to shear connection and so these effects were ignored.

Because of the importance of shear connection between the steel beam and the concrete slab to this research it was decided to examine the accuracy of the proposed system separately. A model was prepared to represent a push-off test. In this model, the shear connection in the composite beam was modelled using the proposed system of spar and interface elements.

A two-dimensional analysis was adopted. It avoids problems associated with the three-dimensional models regarding time and computer memory. This technique, which is presented in Chapter two, was adopted in the major part of the numerical study.

A comparison of the numerical results with the available experimental load-slip curve was made. The aim of which was to clarify the accuracy of representing shear connections in such way.

4.1.1 Push-off Test

The Push-off test for welded stud connectors embedded in solid slabs is documented in cp117. For slabs with profiled steel sheeting, reduction factors, k, have been specified [54]. The design shear resistance is given by:

$$P_d = \frac{k\,P_k}{\gamma_v}$$

where

γ_v is a partial safety factor.

P_k is the characteristic shear resistance of an isolated welded stud fixed directly to the steel beam.

k is the reduction factor for resistance of the shear stud to allow for the galvanised decking, slab boundary proximity and interaction with nearby shear studs.

Evans and Wright carried out 80 tests on T. R. W. Nelson [54] shear studs of the type which were used in this study as well. They modified the standard push-out test to accommodate the geometry of the profiled steel sheet.

4.1.2 Composite Beam Analysis

The longitudinal shear flow in composite steel and concrete beams is transferred across the steel flange-concrete interface by the mechanical action of the shear connectors. The dowel strength of the shear stud depends on the strength and stiffness of the stud material and also on the compressive strength and stiffness of the concrete in the zone directly in front of the stud [51,52].

Johnson developed a simple analysis method based on experimental results [19]. It is known as the linear partial interaction design and it assumes that the additional strength and stiffness of the beam resulting from shear connection between the steel beam and the concrete slab is a linear relation depending on the degree of interaction between the two. The ultimate strength of the composite beam with

partial interaction is expressed as follows:

$$M_{comp} = M_{plast} + \frac{N}{N_f}(M_{ult} - M_{plast})$$

where

M_{comp} = the moment capacity of the composite beam,
M_{plast} = the moment capacity of the steel beam,
M_{ult} = the moment capacity of the composite section with assumed full shear connection.
N = number of shear studs in the composite beam
N_f = the number of studs required for full shear connection.

4.2 Numerical Model Features

Using symmetry, one half of a push-off assembly was modelled. The idea behind this model is simplified in Figure 4.1. This model comprises a concrete slab, half of the steel beam, reinforcing bars, shear studs, interface and tie elements to represent the shear connection. The finite element mesh for this model is shown in Figures 4.2 and 4.3. The model was a two-dimensional one with the key options of the three-dimensional elements set to the plane strain analysis. The geometry was modified to accommodate the dimensions of the re-entrant profiled steel decking. One shear stud per trough was used. Perfect bond was assumed between concrete and reinforcing bars.

ANSYS elements (STIF45, STIF65, STIF1, STIF12, STIF42 and STIF3) were all employed to model the different components of the test assembly as described in chapter 2. The geometrical properties of the shear studs, gap elements, steel beam, and concrete slab were kept, generally, unchanged. However, small modifications were made to account for the change in the geometrical shape of the profiled steel decking.

The steel concrete interface was modelled using two dimensional interface (gap) elements introduced at the stud positions. The traction effect was modelled by a

steel beam to the nearest reinforcing fabric node. In tension, both gap element and beam were given the shear stud tensile properties. In compression, the gap element had a very high stiffness thus preventing unrealistic penetration of the stud into the beam. Shear connection was modelled using two spar elements which jointly had stress-strain properties similar to the load-slip curve of a single shear stud. The cross-sectional area of each spar element was 1mm. The interaction of the elements combine to model the shear stud and can be described with reference to Figure 4.1.

4.2.1 Finite Element Mesh

The finite element mesh is shown in Figure 4.2 through to Figure 4.4 from which it is clear that the open, trapezoidal-shaped profile of the steel deck was approximated by the triangular shape. Although the decking is seen as closed triangular prisms, the surrounding concrete elements have different nodes at the triangle's head which permit independent movement, as is the actual case. If closed prisms were used, an unrealistically stiff concrete slab would result.

4.2.2 Material Properties

(1) Concrete compressive strength was taken as 30.0N/mm^2. This strength value is a common value in lightweight concrete industry and was that achieved in the experimental study. Values of 1.909E4N/mm^2 and 0.2 were used for the initial Young's modulus and Poison's ratio respectively.

(2) Concrete tensile strength was taken as 1.85N/mm^2.

(3) Yield stress for reinforcing bars was taken as 460N/mm^2.

(4) Yield stress for the steel beam was taken as 355N/mm^2.

(5) Yield stress for the shear studs was taken as 450N/mm^2

(6) The stress-strain curve for the spar elements' material was deduced from an experimental load-slip curve. Two cases were considered, the first is the stress-strain curve of the spar element of length 150mm connecting interior studs. The second is the stress-strain curve of the end spar element the length of which was 75mm. Each shear stud was connected with two spar elements.

Figure 4.5 shows the proposed multi-linear stress-strain curve for the spar material which was used to represent the shear slip response of the shear studs. This curve is based on the load-slip curve of a push-off test which was carried out experimentally on a similar specimen.

Material nonlinearity for all joint components was considered in the analysis. However, full bond was assumed between reinforcing steel and concrete at all positions.

4.2.3 Boundary Conditions

A set of boundary conditions was introduced to represent the actual push-off test. For all the nodes on the plane y=0, displacements in the x and y directions as well as rotation around z-axis were set to zero. This was expected to represent the reaction and the friction of the thick plate of the fixed head of the test machine. On the plane of symmetry, displacements in x direction and the rotation around z-axis were also set to zero. At the top of the steel beam where loads are applied, nodes were constrained to a uniform displacement in the y-direction and were not allowed to rotate or to move in the x-direction. Boundary conditions and co-ordinate system are shown in Figure 4.2.

4.2.4 Loading

In the actual test, load is applied gradually until failure. In the finite element model, equal displacement increments were applied and the associated vertical

reactions were determined. Vertical deflections at the unloaded end of the beam were also recorded.

4.3 Numerical Results

The applied displacements were plotted against the vertical reaction per stud. The last value was calculated by dividing the total vertical reaction by the number of studs in the model (three in this model)

The load-slip curve is the major finding of a push-off test. The vertical displacement at the free end was plotted against the shear load of a single shear stud. The shear load per stud was calculated by dividing the total vertical reaction by the number of shear studs. The slip is affected not only by the elongation of the tie elements but also by the deformation of both the steel beam and the concrete slab. This was clear from the difference between the applied and the resulting deflections for a given load on the numerical model.

4.4 Comparison of Numerical and Experimental Results

The load-slip curve obtained from this model is compared with the experimental load-slip curve, which was used as an input stress-strain curve for the spar elements. The two curves are shown in Figure 4.6 from which the close agreement between numerical output and applied numerical input from the experimental results, is clear. Both the curves should end theoretically at 5mm elongation. The model appears to be more ductile (at higher elongations only). This may be attributed to two reasons. The first is that the finite convergence tolerance on the final slope of the non-linear stress-strain response for the shear connector tie elements. The second is that the maintained high tensile strength of the shear connector holding the concrete block against the steel beam. No account is taken in the model of the reduction in connector tensile strength when the connector is yielding due to high imposed shear stresses. This is irrelevant to the problem undertaken because such very high shear forces are not expected to result from

wind loads.

4.5 Summary

The aim of this part of the study was to examine the suitability of the method used to model slip at the shear connection. Study of the localised internal actions of the different components of the push-off test was not planned.

Shear connection between the concrete slab and the steel beam was studied numerically. The shear connection effect was modelled by a system of spar and interface elements in which the applied stress-strain curve for the spar elements was taken from the experimental load-slip curve of a single shear stud. The geometry and material properties of the model were to represent a push-off test. Good agreement was obtained between the applied response for the elements to model an individual shear connector and the output response of the entire push-off sample.

This model may therefore be used to model with considerable accuracy the load-slip characteristic of welded shear studs embedded in slabs with profiled steel decking. By changing the geometry of the model, different sheet profiles with different stud arrangements can be accommodated, as well as studs in solid concrete slabs.

The technique used in this model may also be employed to represent any level of shear connection in composite beams. This can be achived by changing the stress-strain curve of the tie element to accomodate the load-slip characteristic of shear studs.

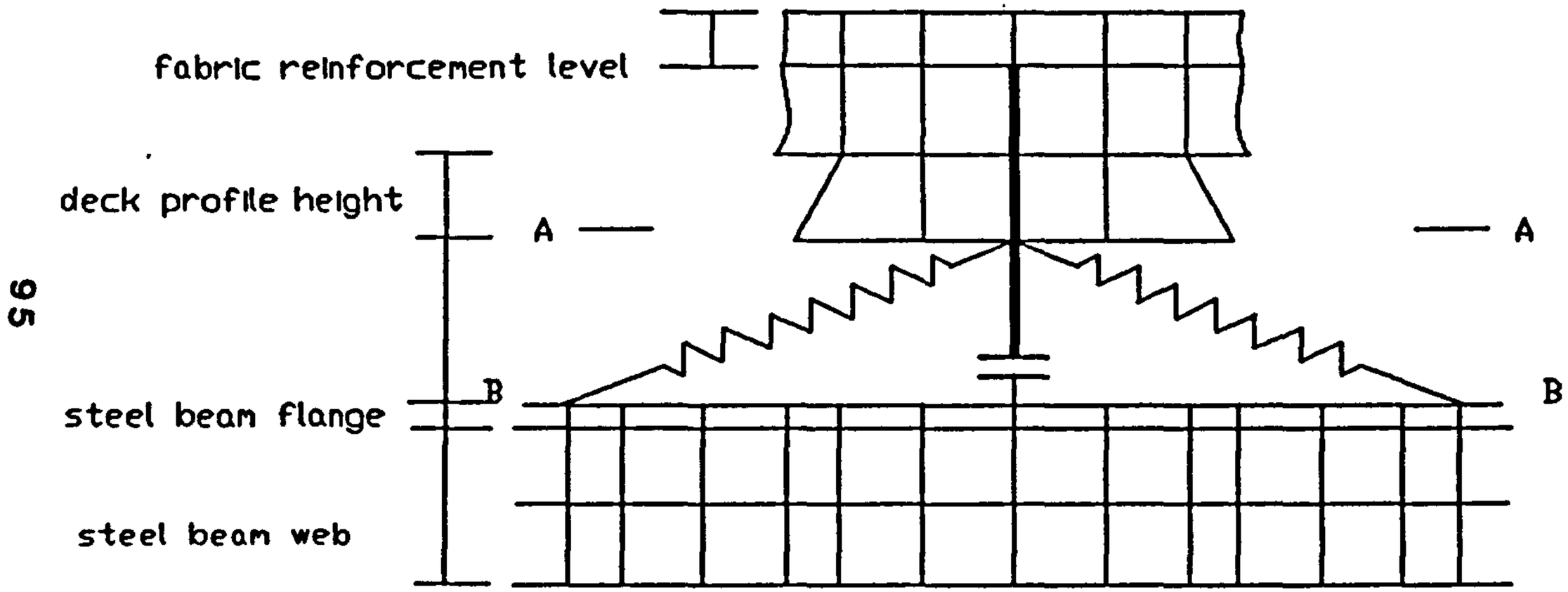

Section A-A and B-B coincide geometrically but are shown separated for clarity.

gap element

Spar element

FIGURE 4.1 SHEAR CONNECTION MODELLING

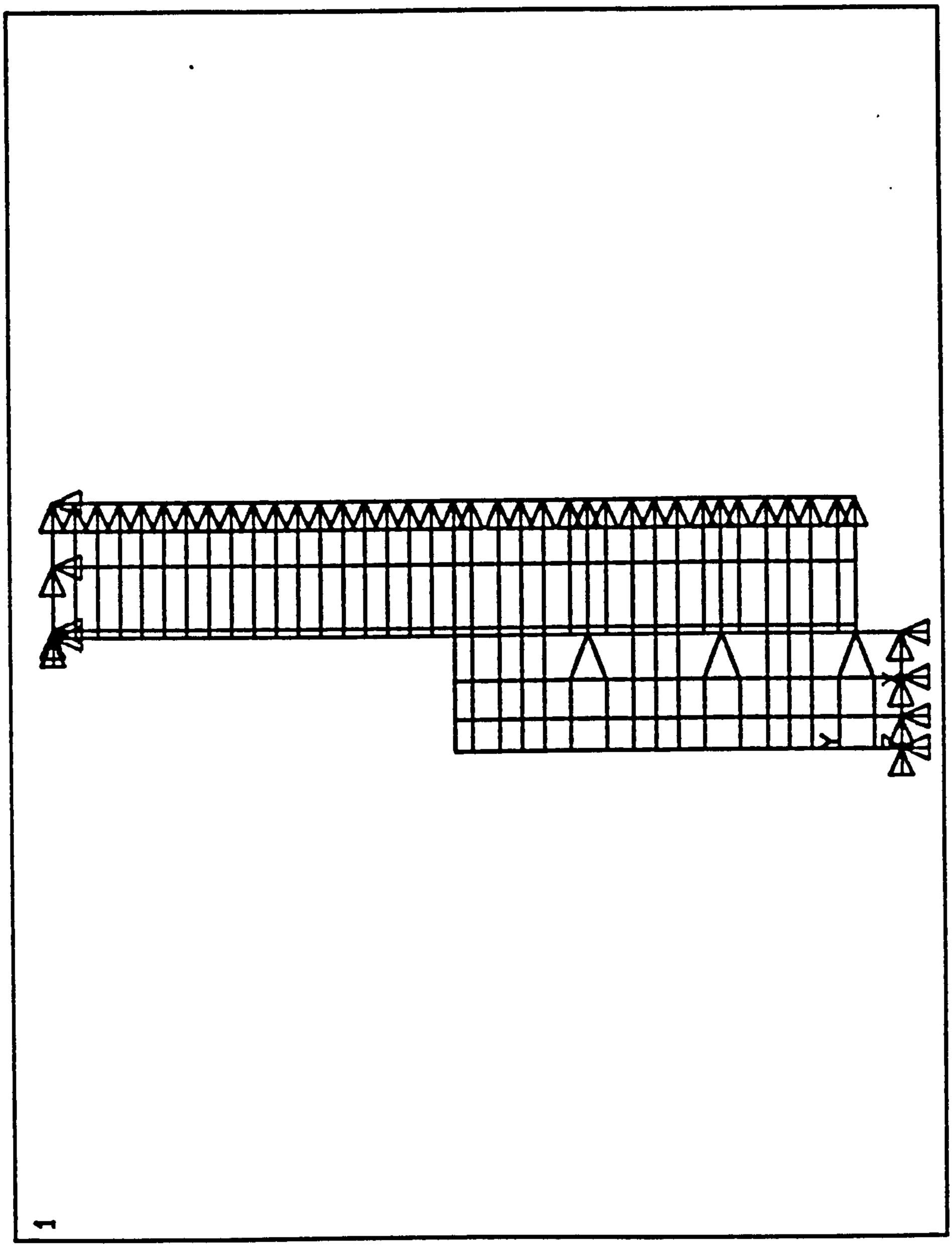

FIGURE 4.2 FINITE ELEMENT MESH 2-D

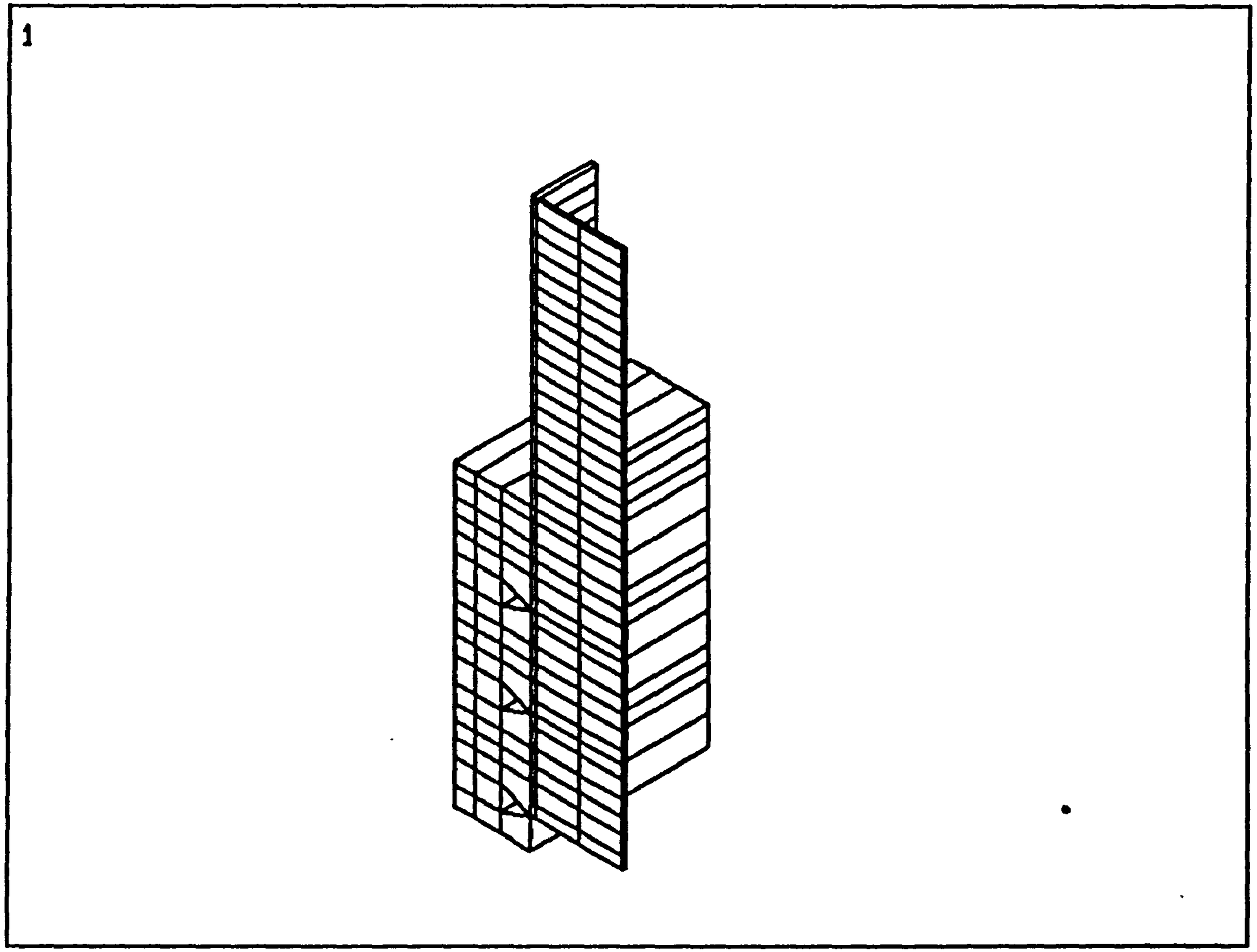

FIGURE 4.3 3-D VIEW OF THE MODEL

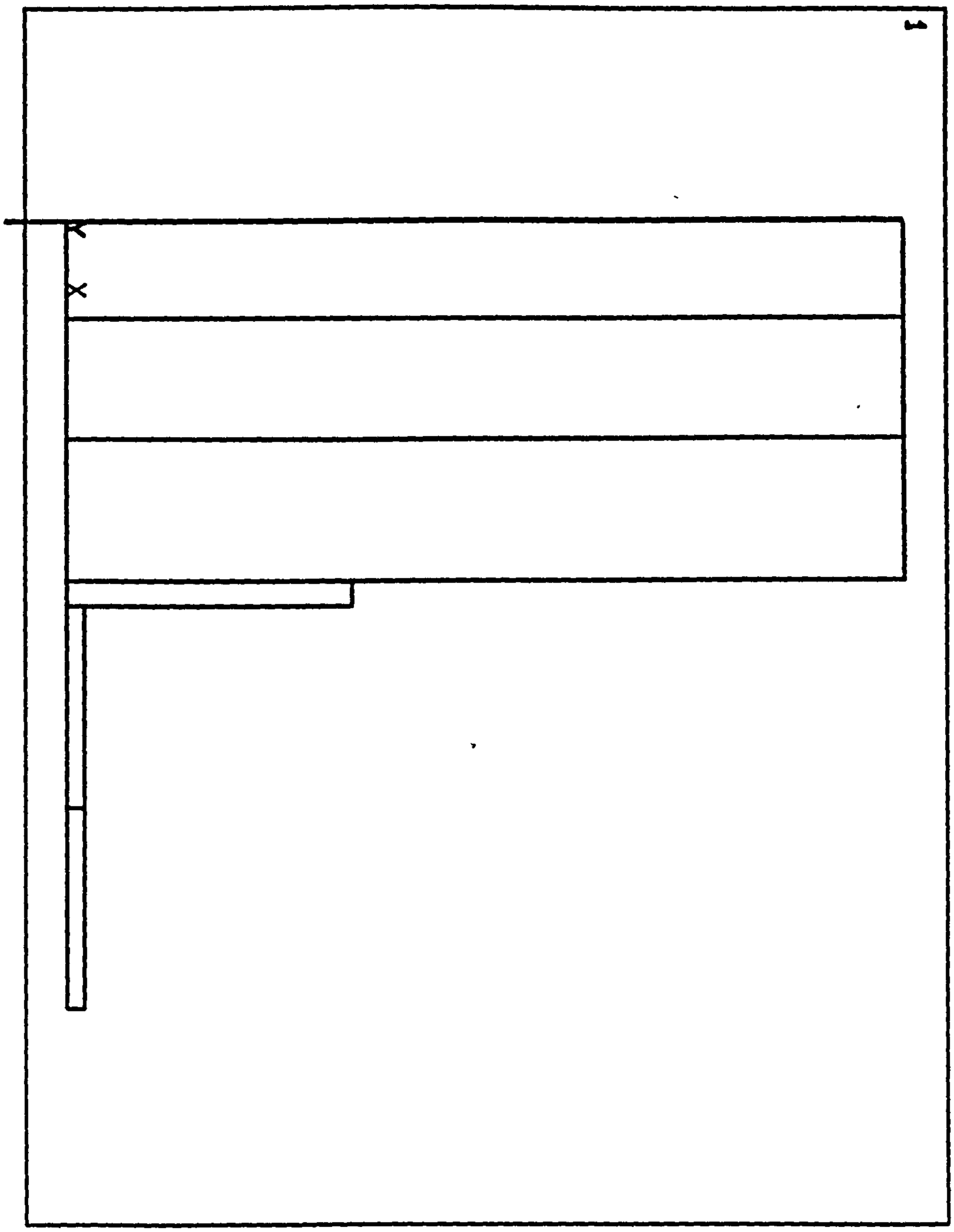

FIGURE 4.4 CROSS SECTION OF THE F.E. MODEL

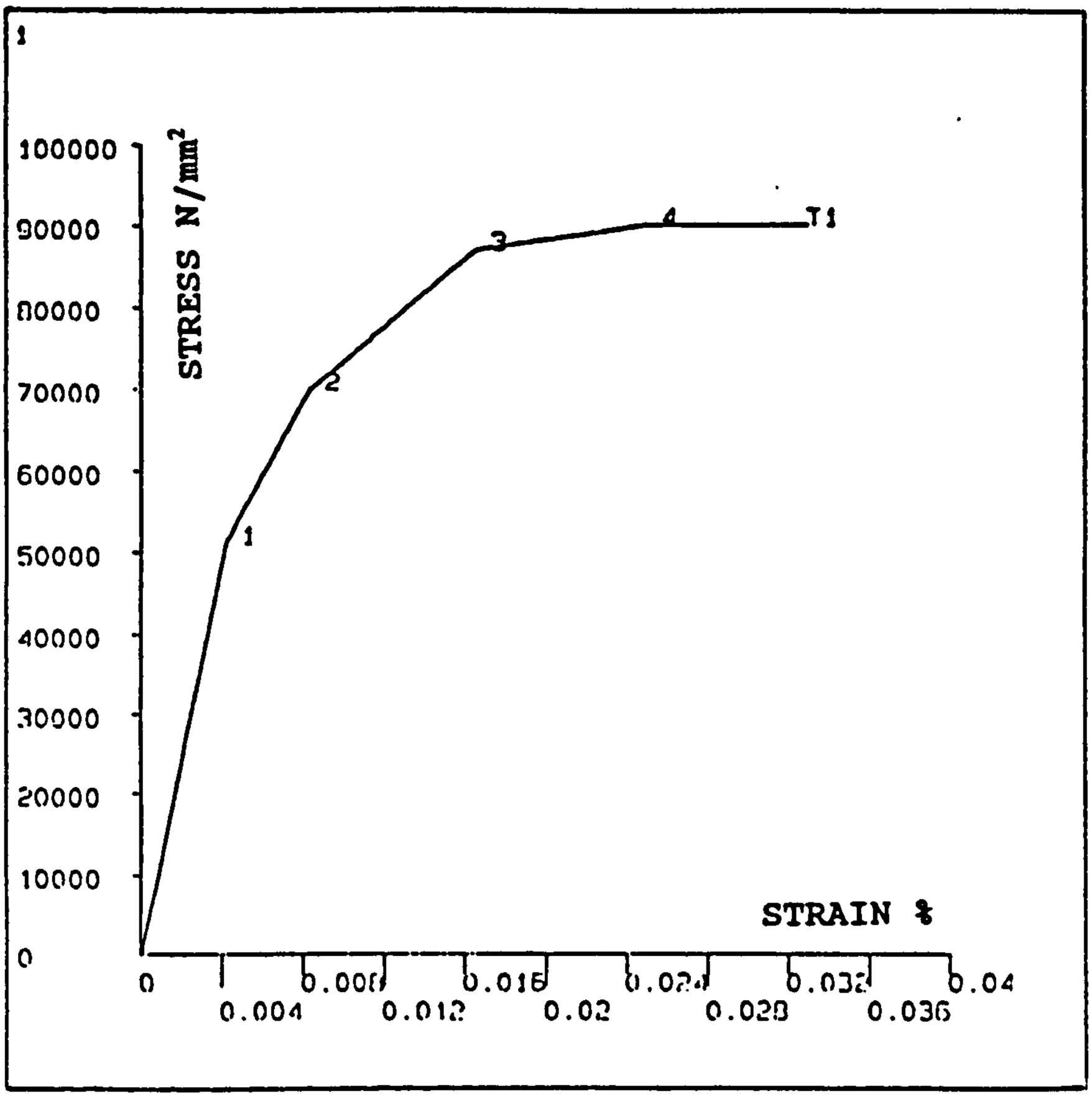

FIGURE 4.5: STRESS-STRAIN CURVE FOR INTERMEDIATE TIE

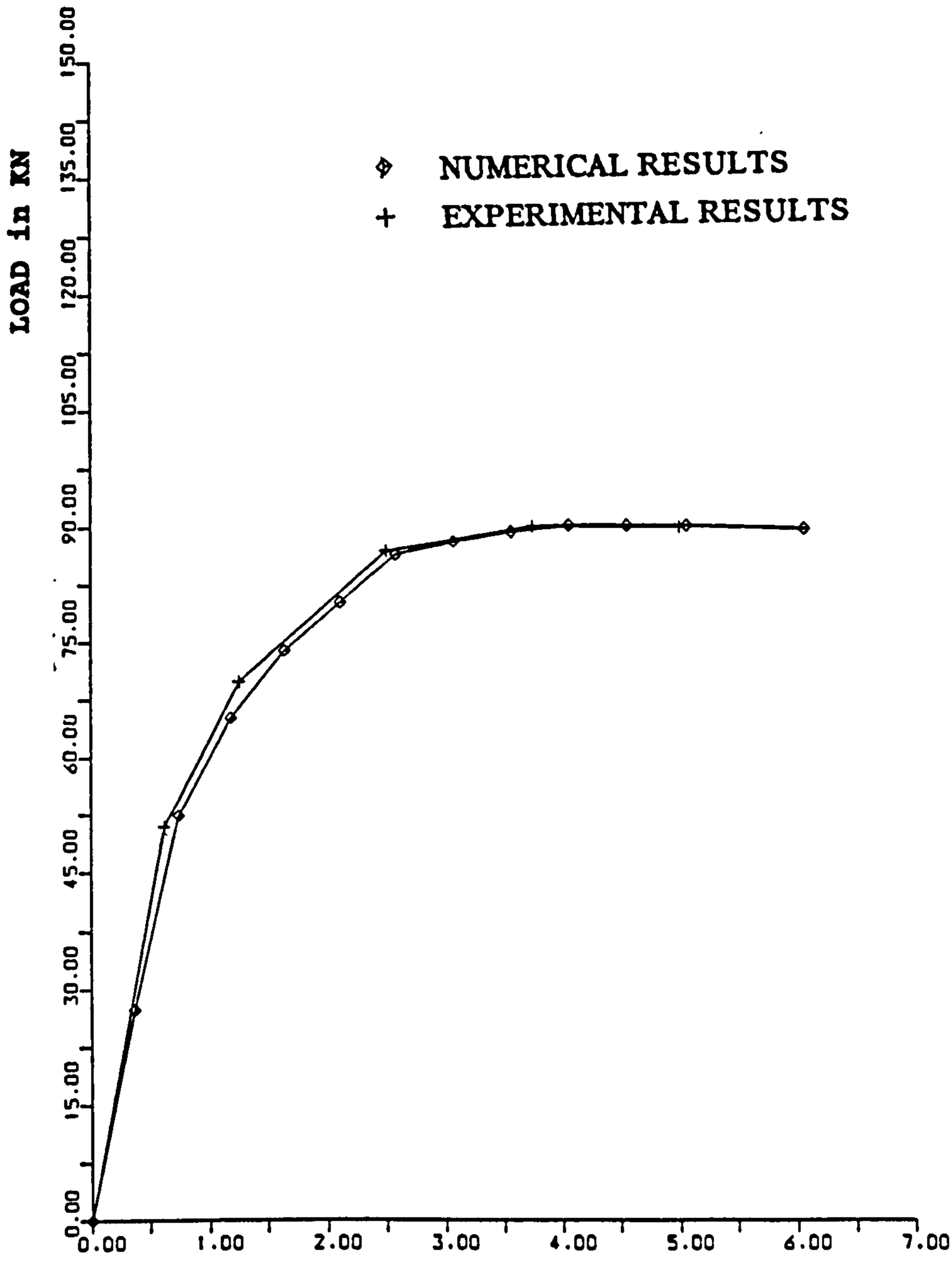

FIGURE 4.6: LOAD-DEFLECTION CURVE, PUSH-OFF TEST

CHAPTER FIVE

NUMERICAL RESULTS FROM 2-D MODELS

5.1 Introduction

In chapter two, finite element modelling of semi-rigid composite connections and the main features of ANSYS software programme have been discussed. Chapter three contains the models prepared to study the behaviour of the connection when subject to wind loads. In this chapter, the numerical results are presented. It was decided to compare the sub-frame stiffnesses by comparing the horizontal displacements of these sub-frames at the same loads. Moment rotation curves are not included in this chapter because of the large sway of unstiffened models and because these models were based on nominal material properties.

5.1.1 Horizontal Displacement

The values of lateral displacement were recorded at each node. For comparison, the deflection at the point of load application is taken as a measure of the lateral stiffness of the connection. The values of the lateral sway, as calculated by ANSYS, were plotted against the applied horizontal loads. The importance of the load-lateral sway curves arises from the following remarks:

(1) The load-lateral displacement relation represents the lateral stiffness of the frame subject to lateral loads.

(2) The point of load application is situated on the top flange of the steel beam. In the experimental investigation, the load was intended to be applied at the same point to facilitate the comparison between finite element and experimental results.

(3) The target lateral displacement is H/300 where H is the interstorey height. In case of the frame undertaken, this height is 4000mm. In the finite element model, one half of the column was considered. This means that the target lateral sway is equal to 2000/300=6.66mm. In other words, the lateral displacement should not exceed 6.66mm when the lateral load applied is 108kN for all the joints at one storey level.

Besides the lateral displacement at the point of load application, stress distribution in different parts was checked at different load steps as follow:

For each element type, a separate file containing the appropriate commands for writing the required data was prepared. This was carried out for the reinforcing bars, the concrete elements, the steel sections. Care was taken to check the occurrence of any plastic deformations in the steel sections. The status of the gap elements was also checked at each load step.

5.1.2 Element Stress

(a) Concrete Slab

In the case of a closing moment, concrete cracks take place if the input tensile stress is exceeded. The tensile strength of concrete was assumed to be 3N/mm^2 which is equal to one tenth of the compressive strength of 30N/mm^2. After the cracking of concrete, the tensile force will be resisted by reinforcing bars only. Crushing of concrete was expected to take place in connections resisting opening moment. In this case, compressive stresses will be distributed over the effective width. Concrete stresses were studied carefully to make sure that crushing would not take place in the range of loading applied.

(b) Reinforcing Bars

Tensile stress in reinforcing bars was checked at each load step. Yielding of reinforcing bars was detected by comparing the input yield stress of 460N/mm^2

with the calculated stress after each load step.

(c) Gap Elements

The two-dimensional interface may have one of three conditions: closed and not sliding, closed and sliding or open. Closed gap element can transmit force in the normal direction. This appears as an increase in the stiffness of the joint.

(d) Steel Sections

The input stress-strain curve for steel sections is a bilinear one with the first slope equal to Young's modulus and the second part has a slope equal to 5% of the previous value. If plastic strain appeared in a certain element, the stress at this element must have exceeded its yield stress. This method was used to detect the yield of steel elements. When the value of the plastic strain was zero, this meant that the element had not yielded yet.

5.1.3 Behaviour of Different Configurations

To represent all shapes of beam-to-column connections, four basic configurations were considered. The behaviour of each beam-to-column connection when subject to lateral load was studied. The deflected shape, the stress distribution in x and y directions are presented. The colour graphics in ANSYS are used in the plots. This was found to make it easier to interpret the plotted contour lines for stress and displacement distributions.

5.2 Preliminary Assessment of the Model

Since in the early stages of this research there was no experimental data available to judge directly the reliability of the numerical model, it was decided to compare the lateral displacements of the frame with the deflections of a rigid frame. In this section, the accuracy of the numerical results are discussed.

The numerical modelling has been serving as a tool to provide useful information which helped with the correct selection of the most appropriate options for stiffening the joint. It was also used to predict the behaviour of the connection in the range of loading similar to that expected from severe wind conditions.

The selection of the most representative arrangement regarding the geometry, amount of reinforcement and material properties in the experimental study is based on the finite element predictions.

5.2.1 Analytical Verification

The frame was analyzed as a rigid one. It was possible to find the displacement and the angle of rotation of the joint directly from the analysis computations provided. Longitudinal strains of members were ignored which allowed deflections to be measured at right angles to the original position of the members. Detailed calculations for this verification are presented in Appendix III. The lateral displacement is composed of two components:

$$d_{total} = d_\theta + d_h$$

$$d_\theta = H \times \theta, \qquad \theta = M \times \frac{L}{3EI_{beam}} \qquad radians$$

$$d_h = \frac{pH^3}{3EI_{column}}$$

where

L = Beam Span,
H = Column height
I_{beam} = Second moment of area of the composite beam
I_{column} = Second moment of area of the steel column
M = Applied moment =P.H

The second moment of area of the composite beam was calculated considering the frame with the steel beam 305×102×28 UB and the steel column of 254×254×73 UC and a modular ratio of 10. This value for the modular ratio was considered appropriate because of the use of light weight concrete and the early maturity loading. The following material properties were also used:

$$E_{steel} = 2.05\times10^{5} N/mm^{2}$$

$$E_{concrete} = 2.05\times10^{4} N/mm^{2}$$

Comparing the deflection calculated using the previous formula with the numerical results for the same frame analysed as a semi-rigid one, it was found that the semi-rigid composite frame has a lateral stiffness which is very close to that of a rigid frame.

5.2.2 Horizontal Deflection

The target value for the lateral displacement is H/300 where H is the height of the column measured from beam neutral axis to column point of contraflexure. The neutral axis of the composite beam was expected to be close to the upper flange. In all models studied, this height was taken equal to 2000mm from the top flange of the steel beam to the column point of contraflexure. The maximum value for the lateral displacement was 6.66mm while the allowable drift specified by UBC and ANSI is 0.5 % which in this case is 10mm. The moment-rotation curve was only drawn for the connections which satisfy horizontal deflection conditions.

The frame with a beam size of 305×102×28kg/m UB and a concrete slab width of 1750mm was considered as a rigid frame. The lateral sway at load 30kN was 6.23mm using the theoretical calculations. In the model with semi-rigid composite connection, the lateral deflection was 6.848mm. This means that a good agreement

with the theoretically obtained results was achieved.

It was intended to prepare a three-dimensional model which had the same geometry and material properties as one of the two dimensional models to compare their results. This model is presented in Chapter Nine.

5.3 Model One (The ¬ Shaped Sub-frame)

This shape was considered as the reference beam-to-column configuration. It has the advantage of relatively small number of elements and its stiffness can be considered as indicative of that of the other configurations. The ¬ shape joint includes seven variations on model one. All the Figures shown in this section are for beam section 305×102×28 UB and seat cleat 150×90×10.

(a) Model One (a)

When applying an opening moment, the deflected shape of the frame is as shown in Figure 5.1. In which the upper fibres of the concrete slab are compressed and the lower flange of the steel beam is in a tensile stressed zone. It is also seen that because of the rotation of the column the size of the tolerance became narrower on top. Because the concrete material is brittle, the concrete slab is slightly pushed outside the column outer boundaries.

Horizontal displacement (U_x) contour lines are shown in Figure 5.2 from which it is confirmed that the lateral displacement of the column is uniform in each horizontal section and increases towards its top. The continuity between the seat cleat stiffener plate and the steel column is also clear. Both the steel beam and the concrete slab have the same contours from the beam end to a point 600mm to the left of the column which means that shear connection is sufficient to transmit horizontal loads with a low level of slip. At the joint zone, and apart from the seat cleat, the shift between the column and the beam contours is clear which is expected because of the presence of the construction tolerance. This is an

indication that this gap is adequately modelled.

In Figure 5.3, the contour lines for the stress in x-direction (S_x) are plotted. The position of the seat cleat bolt is characterised by remarkable concentration of stresses. These stresses are distorted in a circular pattern where they are dissipated into the column. It is this stress concentration which indicates the potential advantage of corner stiffening or use of an enlarged seat cleat to increase the lever arm and hence reduce stress. The stress concentration at the point of fixation of the web cleat bolts within the beam is less severe. In fact, the presence of an open gap element between the web cleat and the beam did not allow any load transmission at this point. The concern here is to study the trend of stress contours not their absolute values which are dependent on the value of the applied load together with the different variables of the frame and of the connection itself.

At the axis of the column, stresses are concentrated by the group of shear connectors contained within the effective width and represented by a single shear stud. In fact, this effect is more complicated as the stress is transmitted to the column through the connection with the cross-beam.

Vertical deflection (U_y) contour lines are shown in Figure 5.4 from which it is seen that the outer fibres of the column are displaced upwards and the inner ones downwards. At the column axis, the value is confirmed to be zero. For the composite beam, all vertical displacements are negative. No separation between concrete and steel in the composite beam is predicted, as is clear from the continuation of the contours outside the joint zone. The concrete part within the column boundaries seems to move separate from the column. Vertical stress (S_y) contours are shown in Figure 5.5. This stress is concentrated at the point of the cross-beam shear connection which is situated at the column axis.

(b) Model One (b)

When the ¬ shaped sub-frame resists closing moment, its deflected shape is as shown in Figure 5.6. Compressive stresses are transmitted to the column through the seat cleat while the tensile stresses are mainly transmitted by the reinforcement.

Horizontal deflection contour lines are shown in Figure 5.7 from which it is seen that these contours are horizontal lines for the steel column. Contours are continuous between the seat cleat and the steel column.

Horizontal stress (S_x) contours are shown in Figure 5.8 from which it is clear that there are compressive stress concentrations at the seat cleat ends. Tensile stresses are transmitted through the floor slab composite decking and reinforcement. The tensile force in the reinforcing bars was calculated by the programme and its values will be discussed later. At a load 30kN, and apart from the local concentration at the column centreline, the maximum steel stress is 150N/mm^2. This means that no yielding of steel occurred.

Vertical deflection (U_y) contours are shown in Figure 5.9. For the composite beam, contours are almost vertical except where the beam rests on the seat cleat. The physical meaning of this is that the steel beam and the concrete slab are moving together in the vertical direction. For the column, contours are parallel and slightly inclined. The right angle between the steel column and the beam is becoming an acute angle. The outer fibres of the column are displaced downwards while the inner ones are displaced upwards.

5.3.1 Effect of Bolt-hole Clearance and Construction Tolerance

Gap elements which represented bolt-hole clearances were initially assumed open. This assumption represented the worst case from the stiffness point of view. Bolt gaps were set initially with the worst possible gap size of 2mm. In fact, this

assumption is not realistic because if the bolt is loose it will rest in the bottom of the hole with only 1mm clearance at each side. The assumption of initially open gap, of any size, also neglects the friction forces between the nut and the plate and assumes that the bolt will move loosely inside its hole until it comes in contact with the plate. The contact, which is represented by the closure of a gap element, leads to an increase in the stiffness of the connection. This appears as a change to a steeper inclination of the load-lateral deflection curve.

The second set of gap elements was introduced to represent the construction tolerance between the end of the beam and the column flange. These gap elements were set initially open with a gap size of 6mm.

The load-lateral displacement curve for this model is shown in Figure 5.11. It is clear that when both bolt-hole and construction tolerance gap elements are open, the connection is very weak and the lateral stiffness is very poor. This is clear from the large sway of the frame in the range of loading from 0.0 to 5kN which persists up to the target load. Use of bearing bolts in this type of connection made it more realistic to ignore the friction force. Consequently, for the cases which have bolt hole gaps, the stiffness is derived only from the composite slab, resulting in an extremely low stiffness and shallow initial slope.

The last two connections had end gaps of 6mm and the bolt-hole gaps were 1 and 2mm respectively. Their load-lateral deflection curves (Figure 5.11) are characterised by a very shallow initial part which means a very low lateral stiffness associated with the initially open gaps. After the closure of the bolt-hole gaps, the connection showed an increased lateral stiffness. Thereafter, the curves are parallel with a lateral stiffness similar to the previous one.

The assumption of initially opened bolt-hole clearance was rejected because of the excessive deflections shown in Figure 5.11. A closed gap could be achieved by the use of a suitable number of friction grip bolts. The friction force between the nut and the plate, which is dependent on the tightening force and the coefficient of

friction, is high enough to resist significant shear load before slippage. Another option is to weld the seat cleat to the steel beam. For any of these alternatives, no differential motion will take place between the bolt and the plate. This effect can be modelled by the introduction of closed gap elements. Unlike the bolt-hole gap, the interface elements which represented the physical gap between the beam and the column were set initially open with a gap size of 6mm. The contact between the end of the beam and the column flange was unlikely to take place.

With all bolt-holes closed, the lateral stiffness of the ¬ shaped connection increased considerably. A comparison between the two cases is shown in Figure 5.12 from which it is clear that the initial part of the curve which was nearly horizontal in the connection with open bolt and end gaps became inclined.

The maximum lateral stiffness is achieved by setting bolt-hole gaps initially closed and end gaps initially closed as well. In reality, this can be obtained with a change in the steel connection to an end plate or an extended end plate connection, or by welding the seat cleat to the steel beam. The seat cleat stiffener plate was not included in this connection and the steel beam was a 250×102×25 UB. The curve of closed gaps joint is linear until a load of 40kN where a small kink takes place. This change in the slope of the load-deflection curve means a loss of stiffness of the connection. The stress in reinforcing bars was 515N/mm^2 which means that the loss of lateral stiffness at this stage was due to yielding of the reinforcing bars.

The previous assumption of initially closed end gaps was considered unrealistic for the cleated joint. The bolt-hole gaps were assumed to be initially closed as before and the end gaps were set initially open with a gap size of 3mm. This assumption of the gap size considered one half of the construction tolerance to disappear after the sagging of the beam due to gravity loads. In the actual structure, the construction tolerance is maximum at the top of the beam and minimum at the bottom. An average value of 3mm was assumed and the load-lateral displacement relation for the connection is shown in Figure 5.12. Three values for the lateral stiffness can be distinguished. The first takes place from 0 to 20kN, the second

part is stiffer and takes place between 20 and 40kN while the third is parallel to the same part in the previous model with less stiffness than the second.

Because of the large and unacceptable sway, the moment rotation curve for this model is not included. The moment rotation characteristics of the frame are discussed in Chapter Eight where the actual materials properties are employed.

5.3.2 Effect of Reinforcing Bars

The effect of increasing reinforcing bars is studied next. This was considered a simple option for stiffening from the construction point of view. The reinforcing bars' area was increased to be 1% of the cross-sectional area of the concrete slab. The increased area was $1750 \times 130 \times 1/100 = 2275 mm^2$. This increase was expected to be most effective in the case of a closing moment, where the concrete slab is in the tensile stressed zone.

This option did not improve the initial, very poor lateral stiffness of the connection with open bolt-hole gaps. The effect started after the closure of bolt-hole gaps where the connection with increased reinforcing bars proved to be laterally stiffer than the same one with only the A193 fabric as shown in Figure 5.13.

To increase the area of reinforcing bars as a percentage of the slab cross-section, an additional reinforcement of 4T16 with cross-sectional area of $804.24 mm^2$ was used. In fact, the benefit of this option for stiffening is shown with both the shallow beam $250 \times 102 \times 25$ UB and with the heavier beam of section $305 \times 102 \times 28$ UB.

In the connection with a shallow beam, a loss of the lateral stiffness has occurred at a load of 20kN. This is explained by the yield of the reinforcing bars adjoining the column zone. A high stress of $545 N/mm^2$ was also observed in the upper bolt of the web cleat. The stiffener plate was not included in this connection. Local yielding of the ste2el beam also took place which is identifiable as a nodal stress

UNIVERSITY OF SOUTHAMPTON LIBRARY

which exceeded the yield stress of steel.

The load-lateral displacement curve of the connection with the beam 305×102×28 UB is linear. The lateral stiffness of the joint increased little with the additional reinforcement. This increase, which appears to be almost insignificant, is necessary to fulfil the target value for the lateral sway of H/300. The joint is very close to a rigid one and consequently the effect of the increase in reinforcing bars' area is relatively small.

5.3.3 Effect of Steel Beam Cross-section

Initially, the beam was 250×102×25 UB. Another, deeper beam of section 305×102×28 UB was also used. The frame with the deep beam proved to be laterally stiffer than that with the shallow one. The comparison is shown in Figure 5.14. This was expected theoretically and was proved to be correct numerically. The lateral sway of the frame can be resolved into two components : the first is the deflection of the column as a cantilever, the second is dependent on the angle of rotation (Θ) which is proportional to the second moment of area of the composite beam. This is explained in the analytical verification at the end of this chapter, but clearly a deeper beam increases the second moment of area.

5.3.4 Effect of Seat Cleat Stiffener Plate

A stiffener plate may be welded to the seat cleat. In model one, this part was not included at first and the seat cleat was modelled as a line element connecting the bolt position nodal point to a nodal point on the column flange. With the stiffener plate the lever arm of the moment has increased to be the distance between the reinforcing bars and the resultant of the forces transmitted by the seat cleat and the stiffener plate. The effect of the stiffener plate on the lateral stiffness of the joint is clear in Figure 5.15.

5.3.5 Effect of Seat Cleat Section

In the original connection used in the building on which this study is based, the section of the seat cleat was 150×90×10. This angle was modelled at first without its stiffener plate and then with the stiffener plate welded to it. The assembly of the angle and the seat cleat is rigidly fixed to the column to represent the weld. As an option for increasing the lateral stiffness of the connection, the seat cleat was replaced by a heavier one of section 250×250×1 After a discussion with steel fabricators and designers, who strongly resisted use of such heavy and unpopular sections, an intermediate seat cleat was included in the model. This third angle is of section 200×100×12. The longer leg of the unequal angle is the one welded to the column. As shown in Figure 5.15, the lateral stiffness of the joint increased with the use of a deeper angle. In case of opening moment, the tensile force produced from the bending moment is transmitted to the column through the horizontal plate of the cleat angle. An increase of the area of this plate will increase the moment capacity of the connection. This is another advantage of the heavier seat cleat.

5.4 Model Two

This model is similar to Model One except that Model Two has an upper column with 2000mm height. The deflected shape of this model when subject to opening moment is shown in Figure 5.17 on which the horizontal displacement contours are shown as well. From this figure, it is clear that the value of the lateral sway at the upper point of contraflexure is twice the value at the connection zone. Horizontal displacement contours for the column are parallel as explained in Model One. The stress distributions in vertical and horizontal directions were studied. It was found that the points of stress concentration are at the seat cleat ends, the upper bolt of the web cleat and at point of intersection of the cross-beam with the column web. The trend of vertical deflection contour lines is similar to those on the corresponding results for model one.

5.5 Model Three

The deflected shape of the frame is shown in Figure 5.18 in which the left joint is closed and the right one is open. Consequently, the left concrete slab is in a tensilely stressed zone and the right one is in a compressively stressed region. In the z-direction, necking of the effective width of the left slab will take place towards the joint zone.

Lateral displacement contours are shown in Figure 5.19 from which it is seen that the column and the beam have different contour lines for the lateral displacement. This is because of the presence of the physical gap between the two parts and slip at the shear connectors. The concrete slab is also separated from the steel column. Actually, a crack is expected to take place between the concrete slab and the steel column and no recovery of this crack is expected.

Vertical deflection contours are shown in Figure 5.20. For the left beam, deflections are positive. The right beam has negative deflections. For the steel column, contours are parallel and vertical. The load-lateral deflection curve for this connection is shown in Figure 5.23, in which the lateral stiffness of the joint is linear to a load of 100kN whereafter a loss of the lateral stiffness took place. This is explained by yield of the reinforcing bars.

5.6 Model Four

This model is similar to model three except that model four has the upper column. This will increase the lateral stiffness of the joint. The deflected shape of the whole frame is shown in Figure 5.24. The horizontal and vertical displacement contours and stress distributions are similar to model three.

5.7 Effect of Stiffening Measures

5.7.1 Effect of Corner Bracing

The effect of the corner bracing on the stiffness of model one is considered only in case of an opening moment. Although the option of increasing the lateral stiffness of the connection using this bracing was subsequently rejected, the load-deflection curve of the connection with the corner tie is shown in Figure 5.25.

Theoretically, the corner tie is a material-saving alternative for increasing the lateral stiffness. Moreover, it overcomes the problem of slip of bolts because even when it is bolted to the column and the beam, the tensile force in the tie will not cause it to slip inside the hole. However, as the cost of the connection is influenced heavily by the man-hours required for fabrication, this option was considered an uneconomical one.

5.7.2 Effect of Additional Reinforcing Bars and a Heavier Seat Cleat

The version of model one considered here is that with the combined effects of the preferred beneficial options studied. Thus this alternative uses a steel beam size of 305×102×28kg/m UB and a steel column size of 254×254×89kg/m UC. Bolt gaps are closed and end gaps are open with 6mm gap size.

The following two modifications are introduced:

(1) The seat cleat was increased to be 200×100×12 instead of 150×90×10.

(2) An additional reinforcement of 4T16mm was added to the A 193 fabric.

In the case of a closing moment, the lateral deflection at the point of load application was 6.45mm (at a load of 30kN). This means that with these options together, the frame can withstand wind loads without the use of any bracing.

For an opening moment, the lateral displacement was 6.16mm which is also less than the target value of 6.66mm.

The load-lateral displacement curve for this connection is shown in Figure 5.26 from which it is concluded that at 30kN, the lateral sway is less than the target value of 6.66mm and the load-deflection curve is linear to the maximum load reached which is 50kN in this case.

The connection was analyzed in both the opening and the closing moments and it was found that steel did not reach its yield stress and the concrete did not reach its crushing stress.

The physical gap between the beam and the column was assumed to be initially open and it was observed that this gap was still open after reaching a load of 50kN. This means that the assumption of initially open gaps between the beam and the column was a realistic one and the beam in this connection would not butt against the column face in the range of wind loading.

The maximum tensile stress in the reinforcing bars at a load of 30kN was 230N/mm^2 which is less than the yield stress. The maximum compressive stress in the concrete was 19.01N/mm^2 which means that no concrete element was crushed.

5.8 Summary

Using the finite element technique, two-dimensional models were developed to predict the behaviour of semi-rigid composite connections subject to wind loads. Four different configurations were considered with the ¬ shaped sub-frame taken as the basic model.

After carrying out the preliminary analysis on the four sub-frames, further numerical analysis was performed on the ¬ shaped sub-frame to investigate different options to increase its stiffness. The key factors which significantly affect

the lateral stiffness of the connection can be summarised as follows: steel beam section, reinforcing bars, seat cleat section, presence and cross-section of the stiffener plate, slip of the seat cleat bolts.

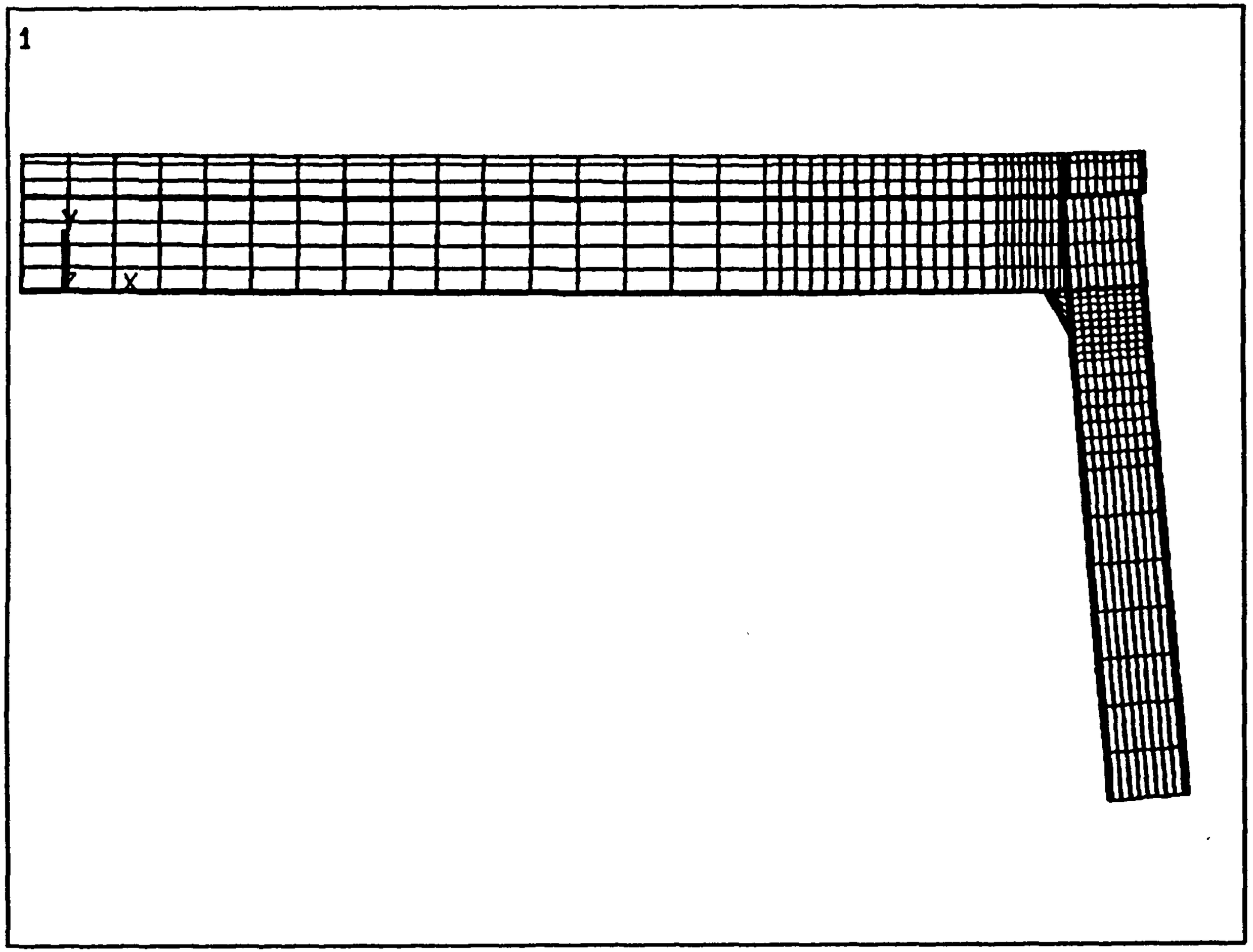

FIG. 5.1 DEFLECTED SHAPE, OPENING

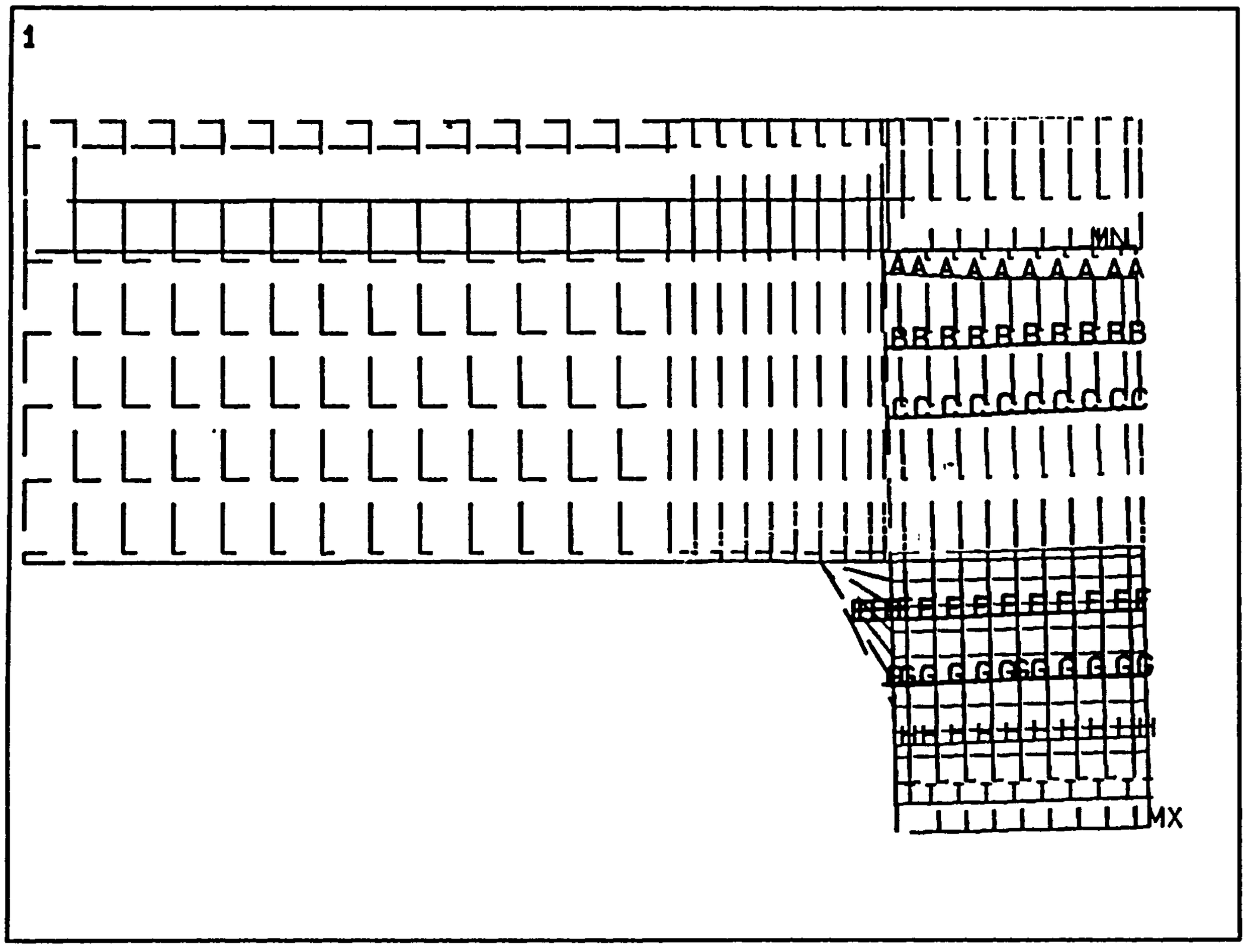

ANSYS 4.4A
SEP 22 1993
16:23:07
PLOT NO. 1
POST1 STRESS
STEP=7
ITER=20
UX
D GLOBAL
DMX =16.662
SMN =-16.638
SMX =-12.225

ZV =1
DIST=463.65
XF =3062
YF =84.45
A =-16.393
B =-15.903
C =-15.412

F =-13.941
G =-13.451
H =-12.961
I =-12.47

FIG. 5.2 UX CONTOURS, OPENING

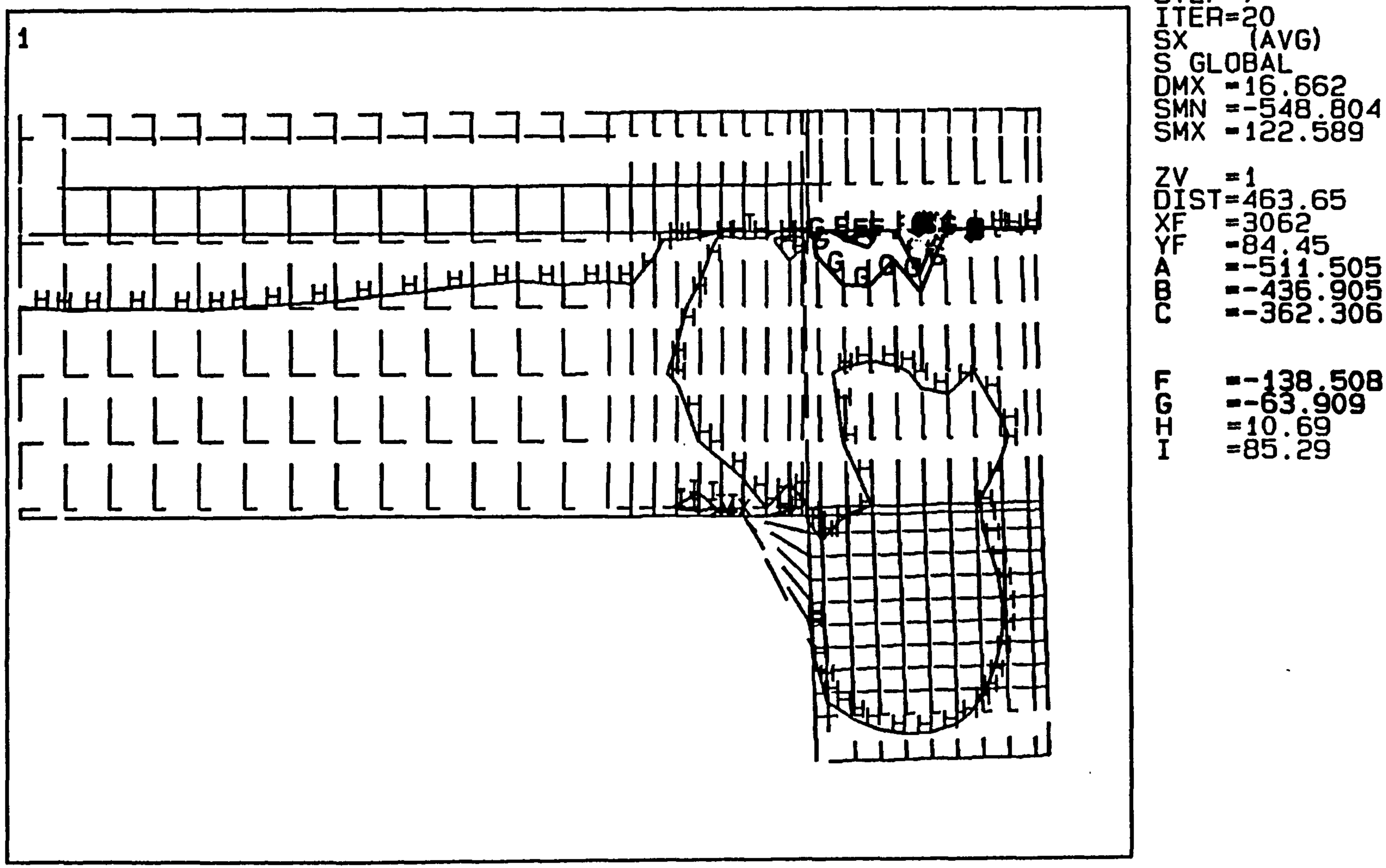

FIG. 5.3 SX CONTOURS

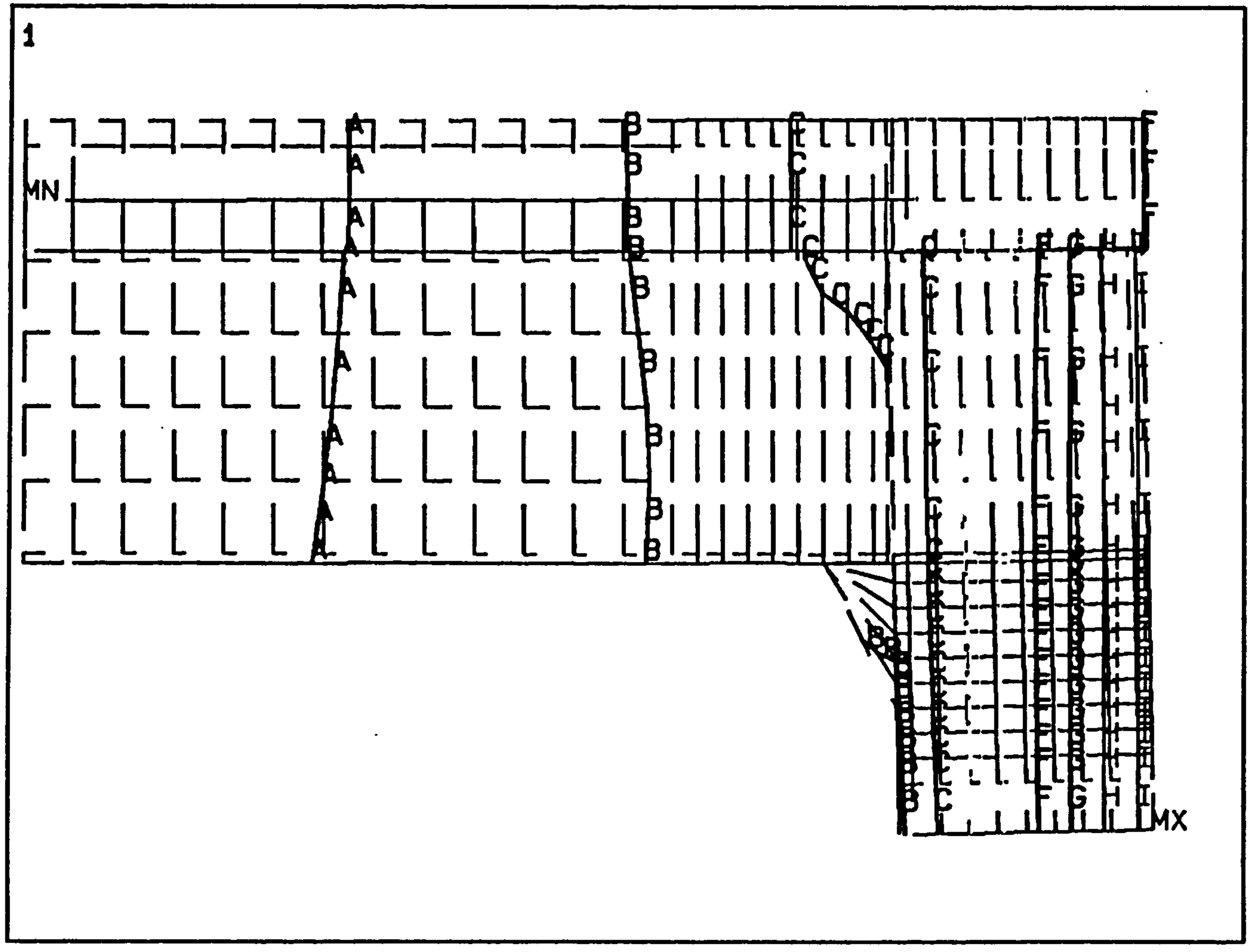

ANSYS 4.4A
SEP 22 1993
10:07:06
PLOT NO. 5
POST1 STRESS
STEP=7
ITER=20
UY
D GLOBAL
DMX =16.662
SMN =-1.37
SMX =1.063

ZV =1
DIST=463.65
XF =3062
YF =84.45
A =-1.235
B =-0.964555
C =-0.69426

F =0.116623
G =0.386917
H =0.657211
I =0.927506

FIG. 5.4 UY CONTOURS

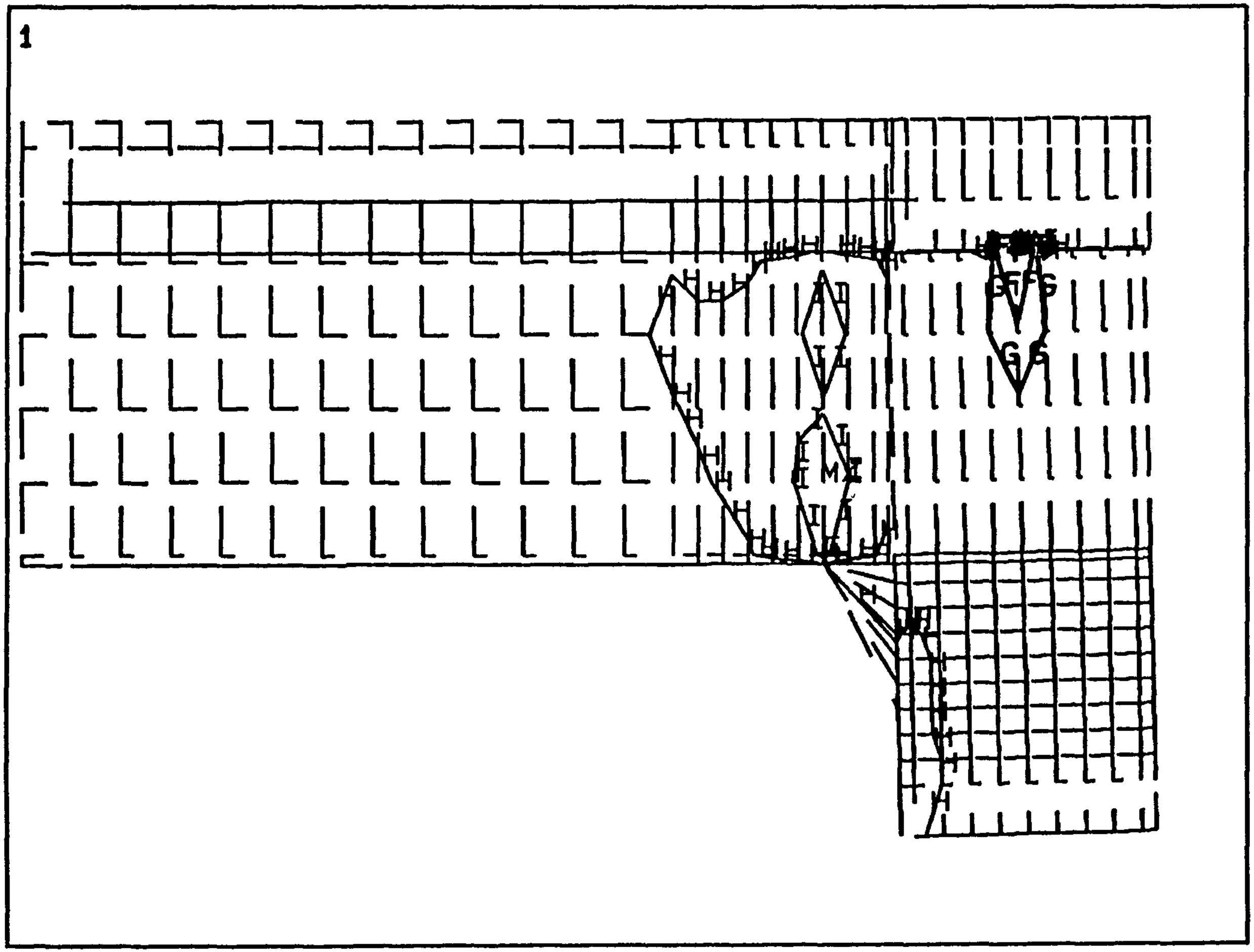

FIG. 5.5 SY CONTOURS, OPENING

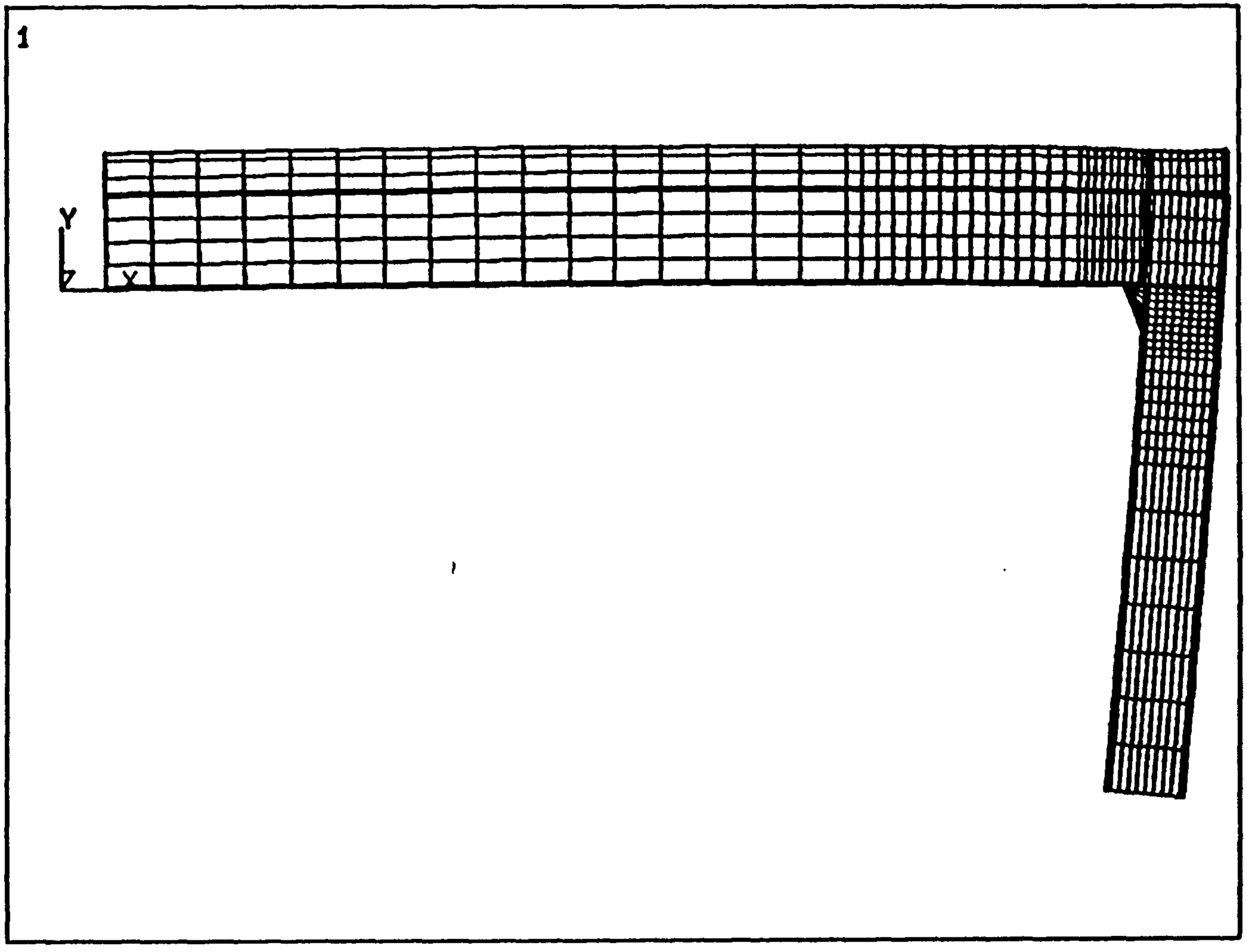

FIG 5.6 DEFLECTED SHAPE, CLOSING MOMENT

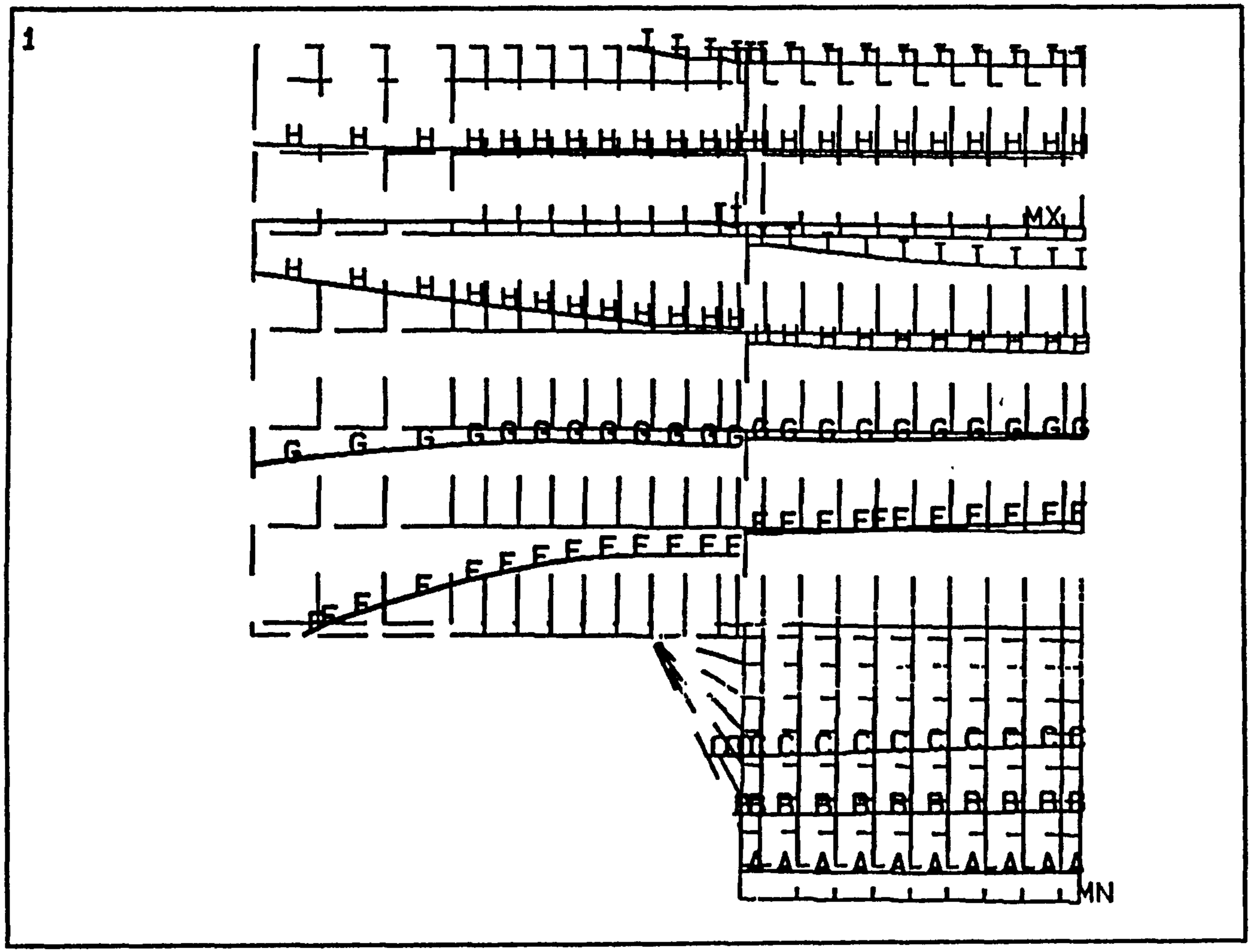

ANSYS 4.4A
JUL 6 1993
33:10:31
PLOT NO. 2
POST1 STRESS
STEP=1
ITER=20
UX
D GLOBAL
DMX =8.57
SMN =6.96
SMX =8.561

ZV =1
DIST=348.645
XF =3312
YF =121.95
A =7.049
B =7.227
C =7.405

F =7.939
G =8.116
H =8.294
I =8.472

FIG 5.7 HORIZONTAL DISPLACEMENT CONTOURS

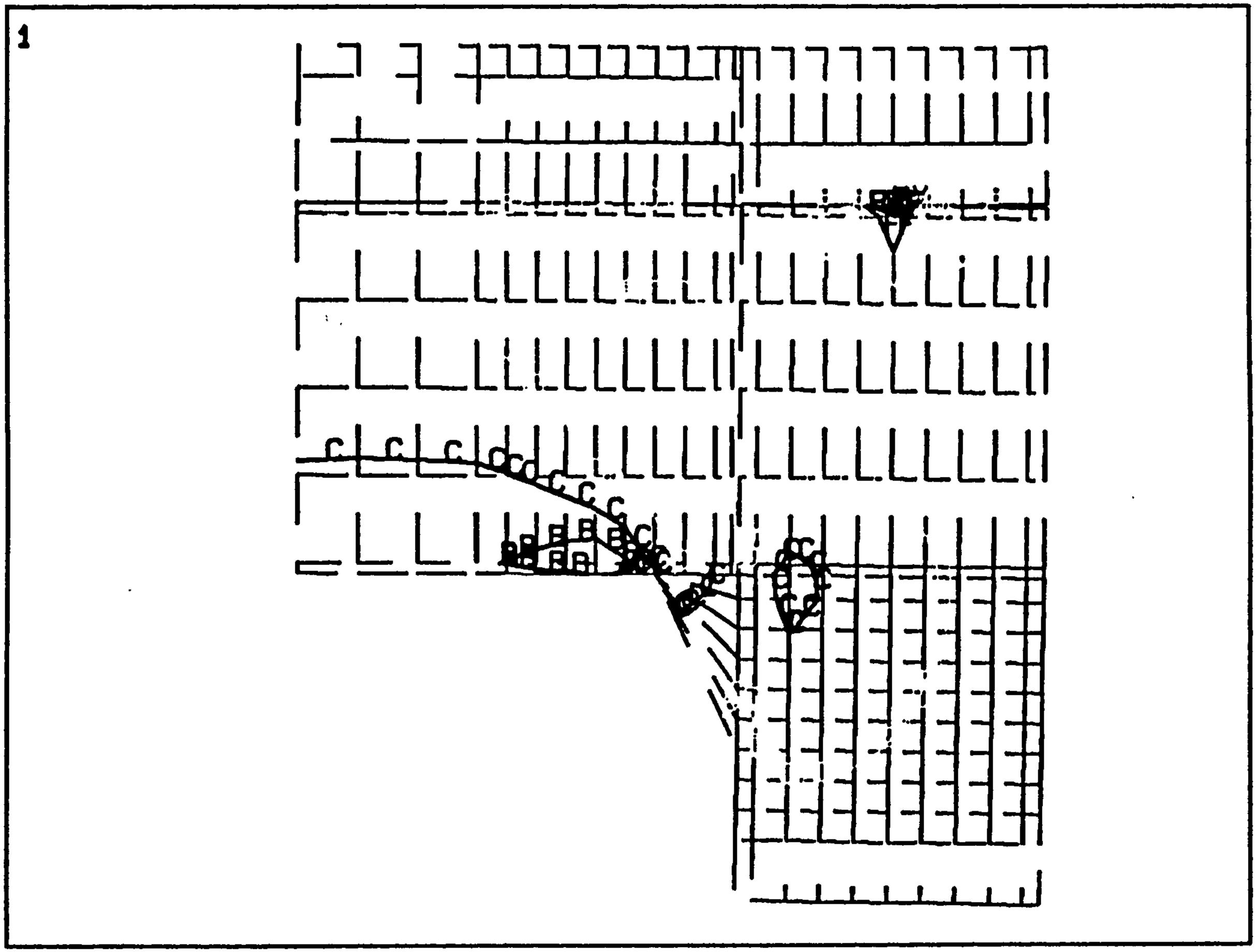

FIG. 5. 8 SX CONTOURS

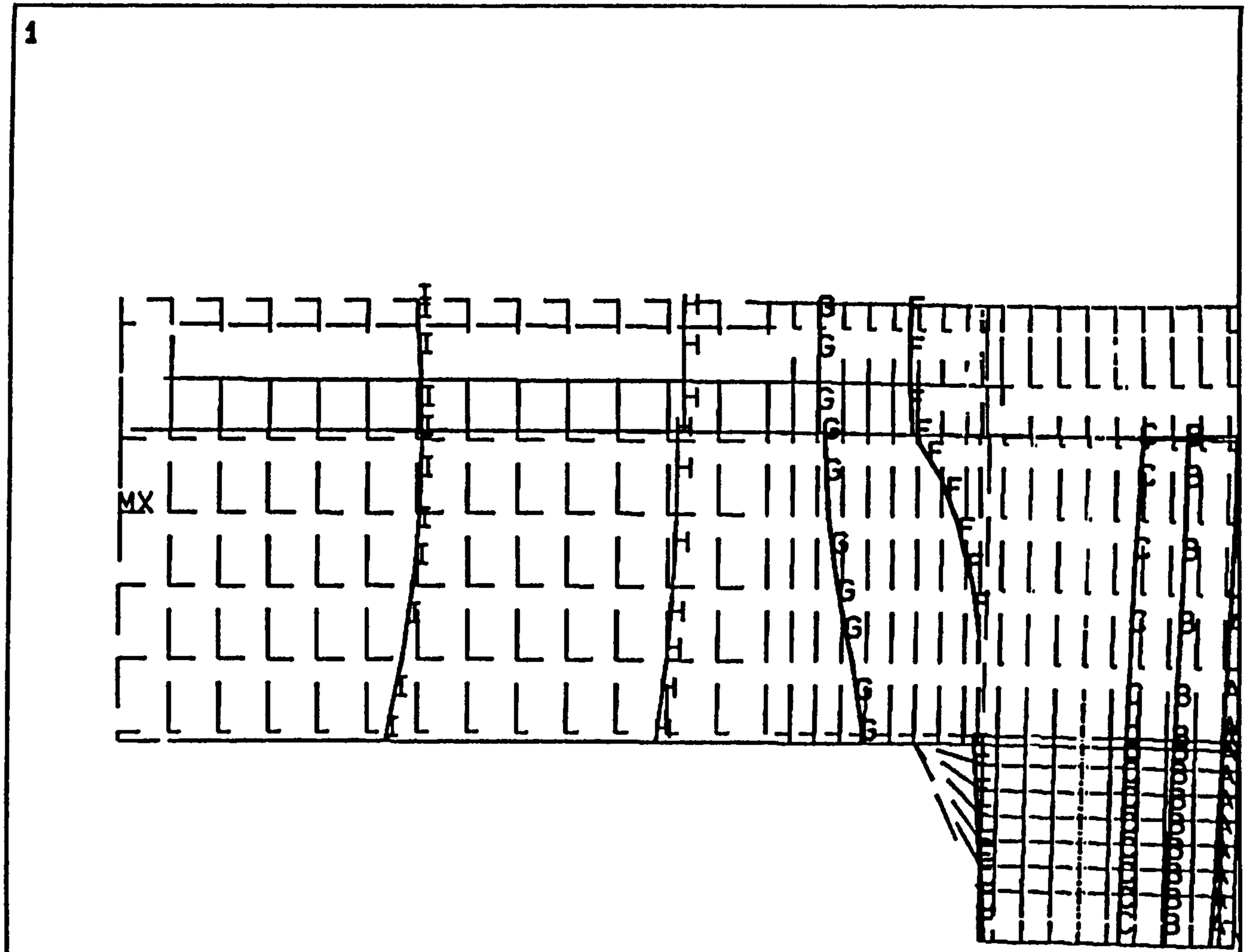

FIG. 5.9 UY CONTOURS

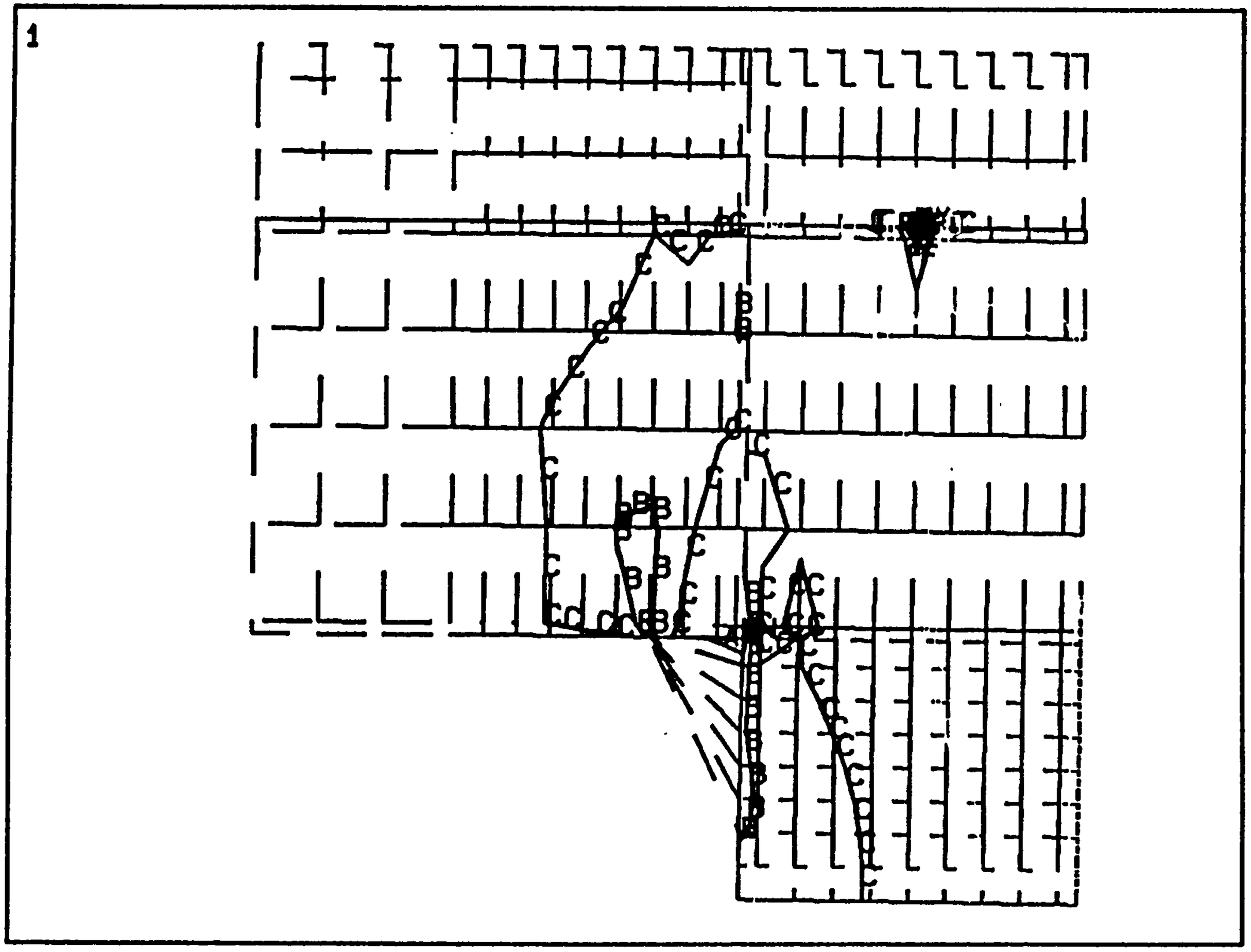

FIG. 5.10 STRESS CONTOURS IN Y-DIRECTION

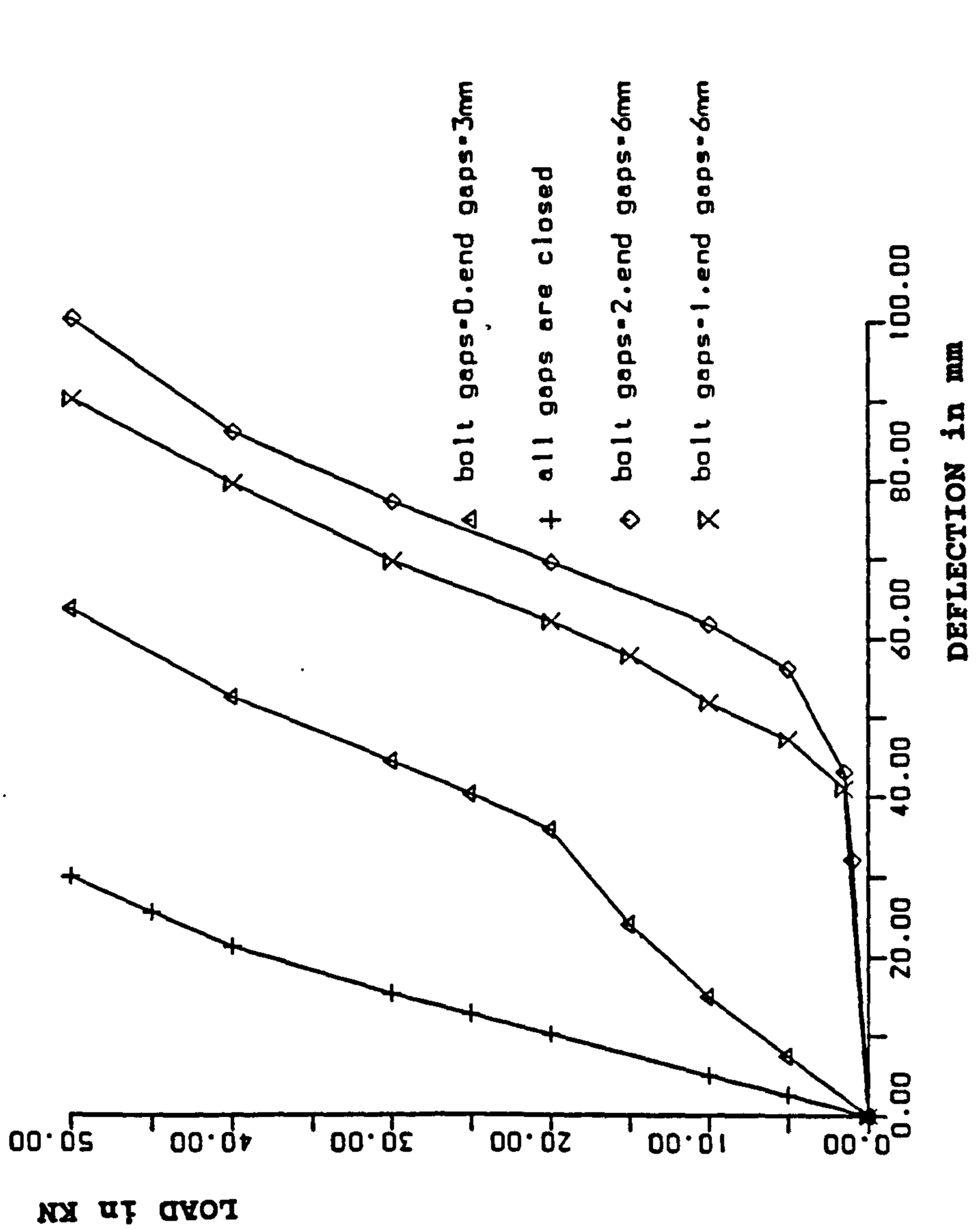

FIGURE 5.11: LOAD-DEFLECTION CURVE FOR SUB-FRAME, OPENING

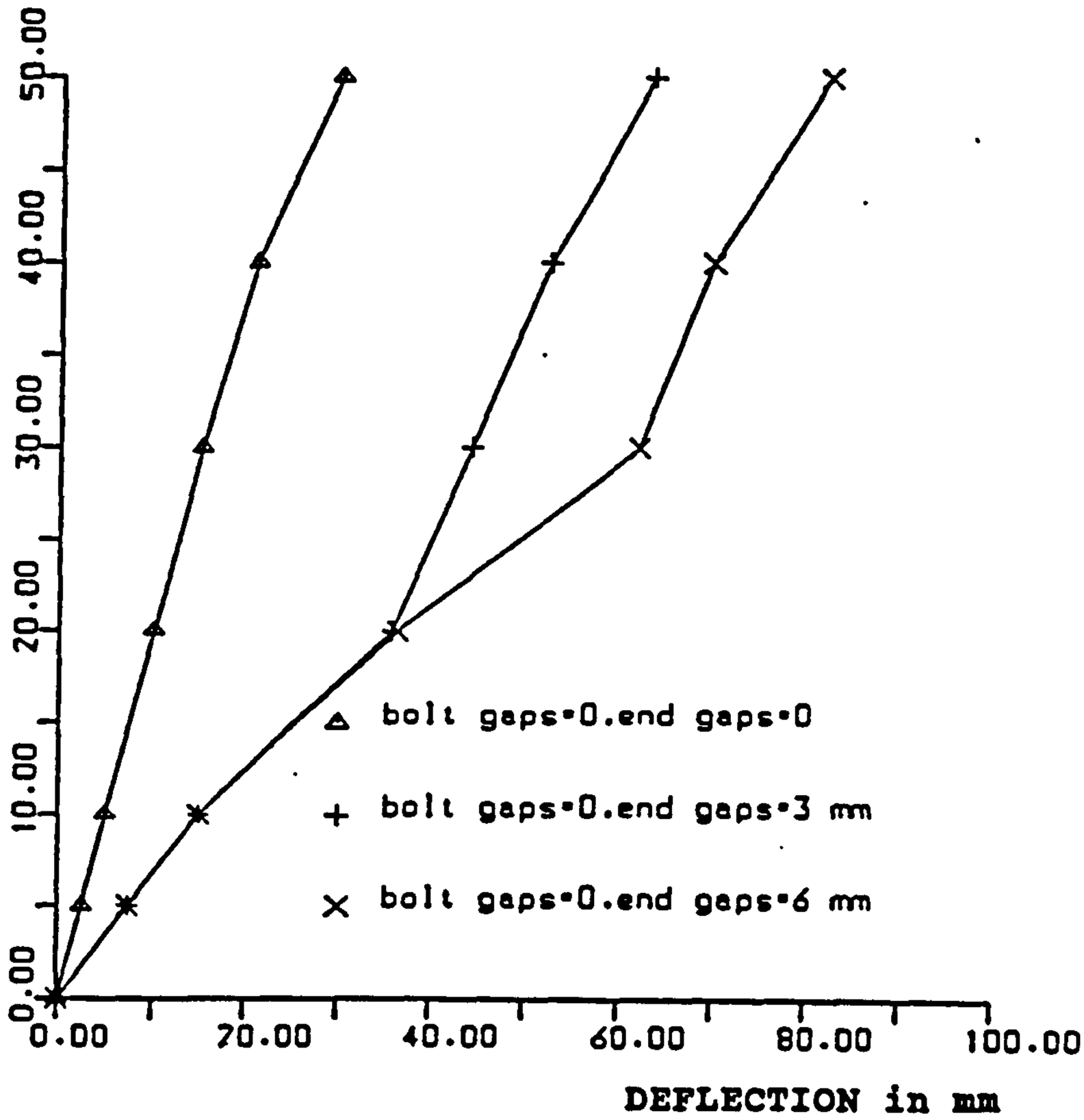

FIGURE 5.12: EFFECT OF END GAP SIZE

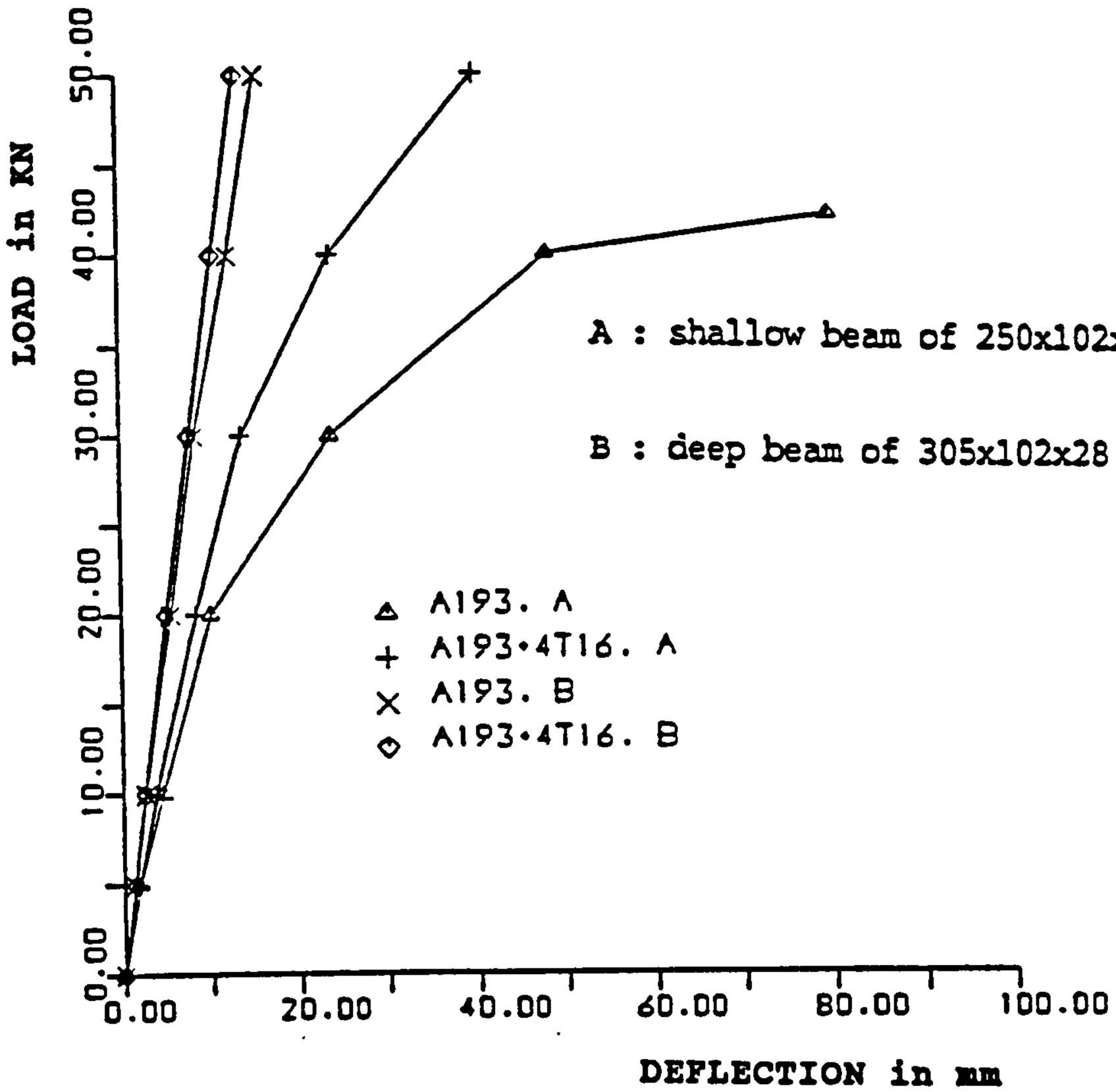

FIGURE 5.13: EFFECT OF REINFORCING BARS

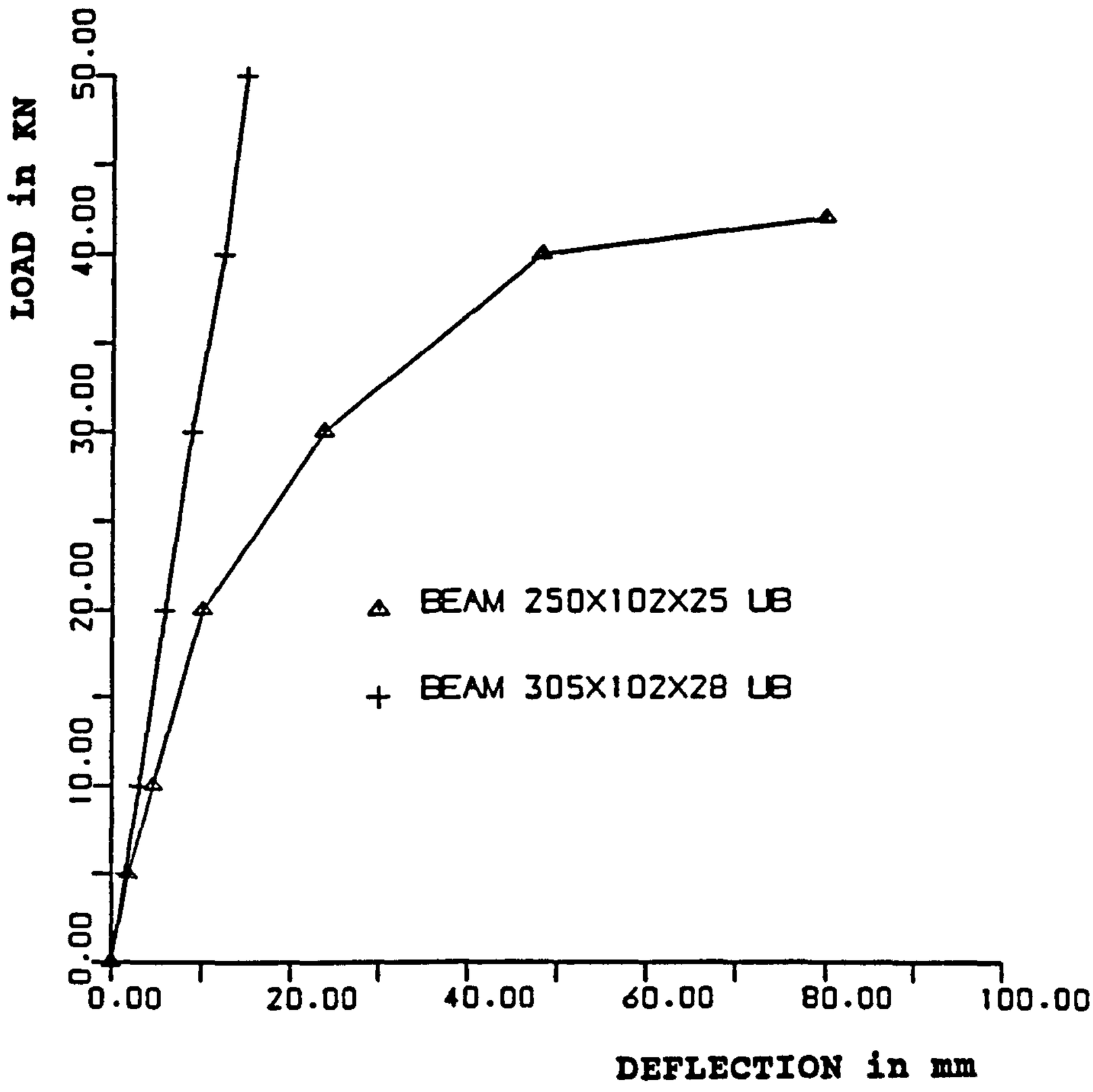

FIGURE 5.14: EFFECT OF STEEL BEAM SECTION

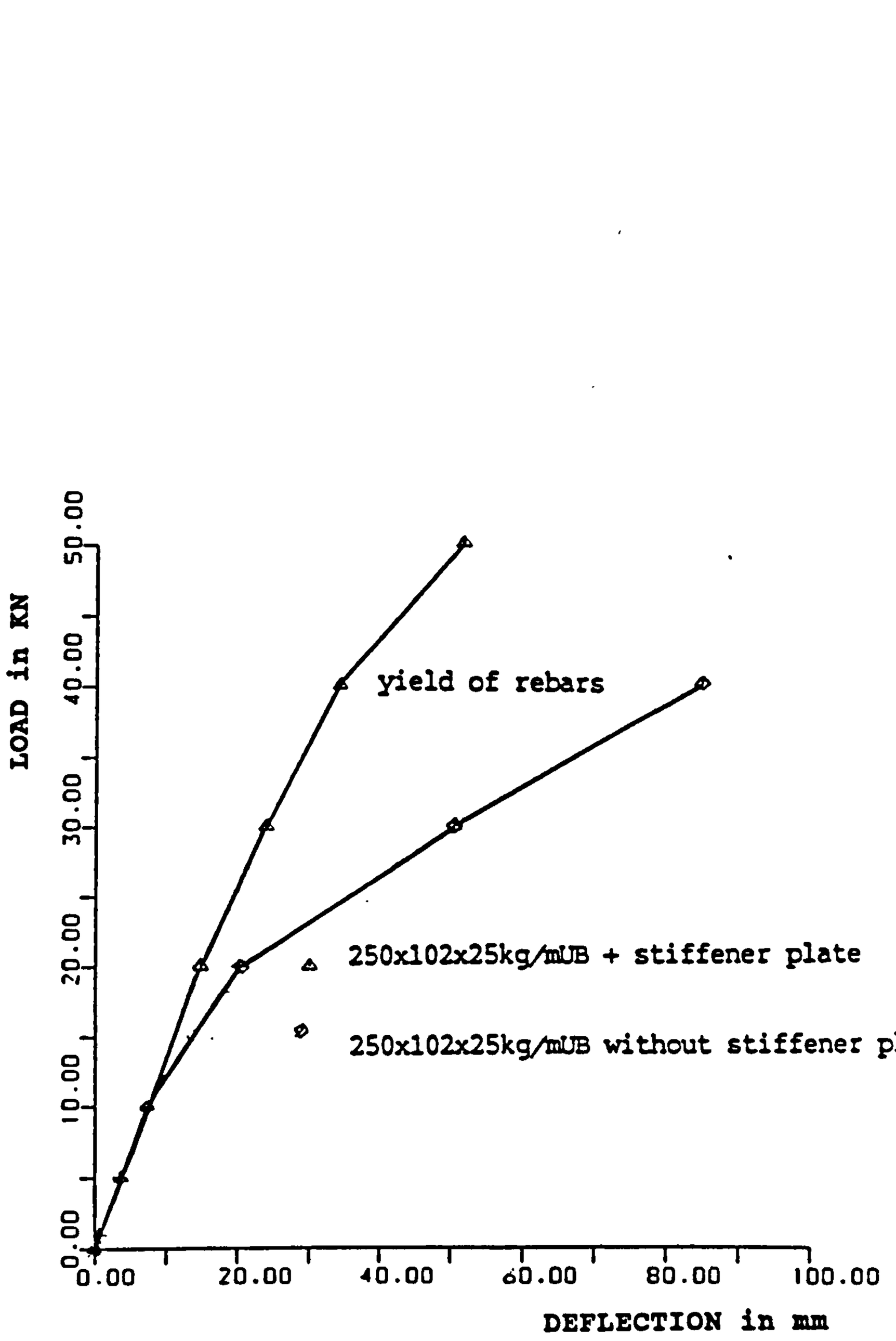

FIG. 5.15 :EFFECT OF SEAT CLEAT STIFFENER PLATE

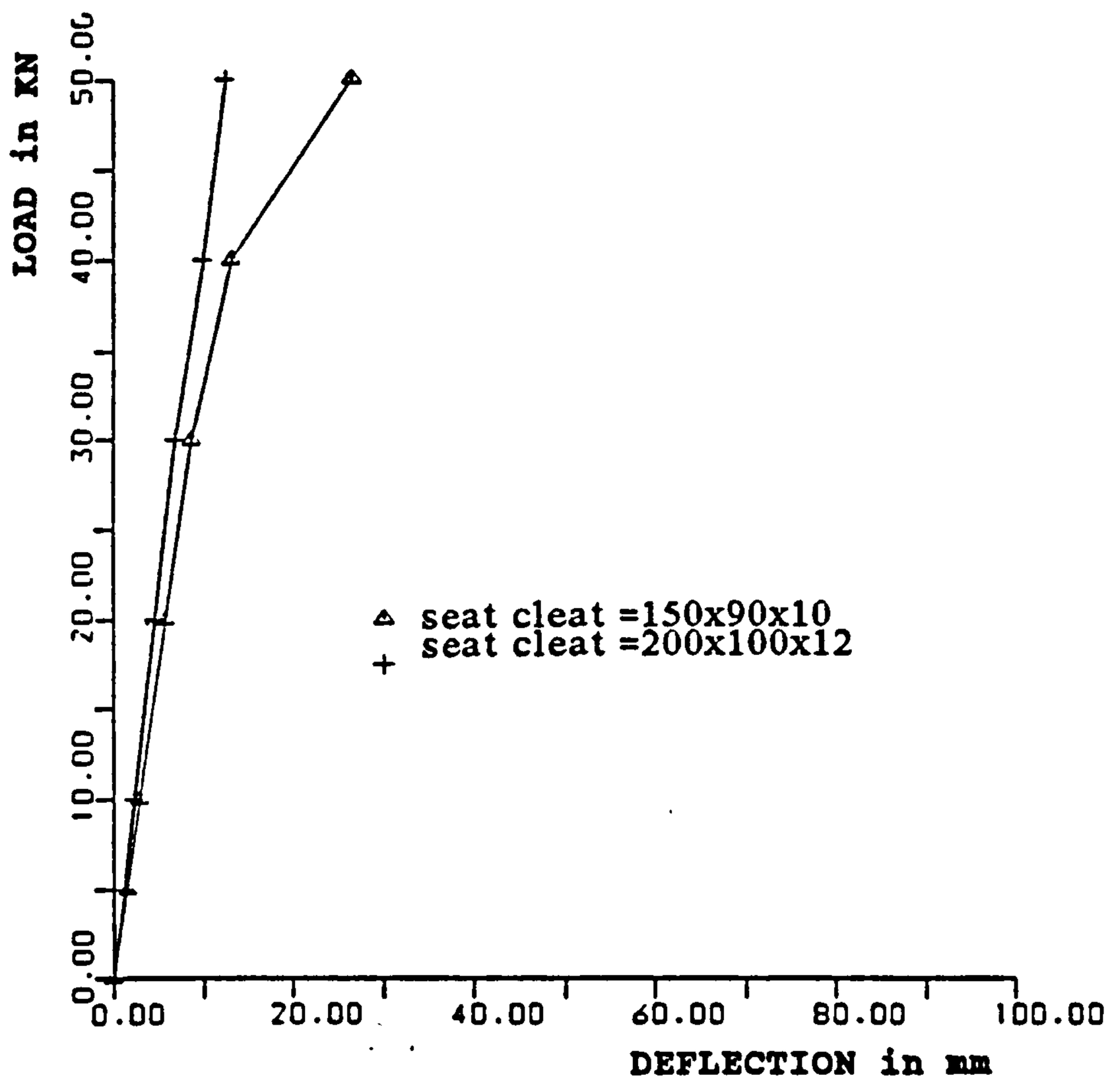

FIG. 5.16: EFFECT OF SEAT CLEAT SECTION

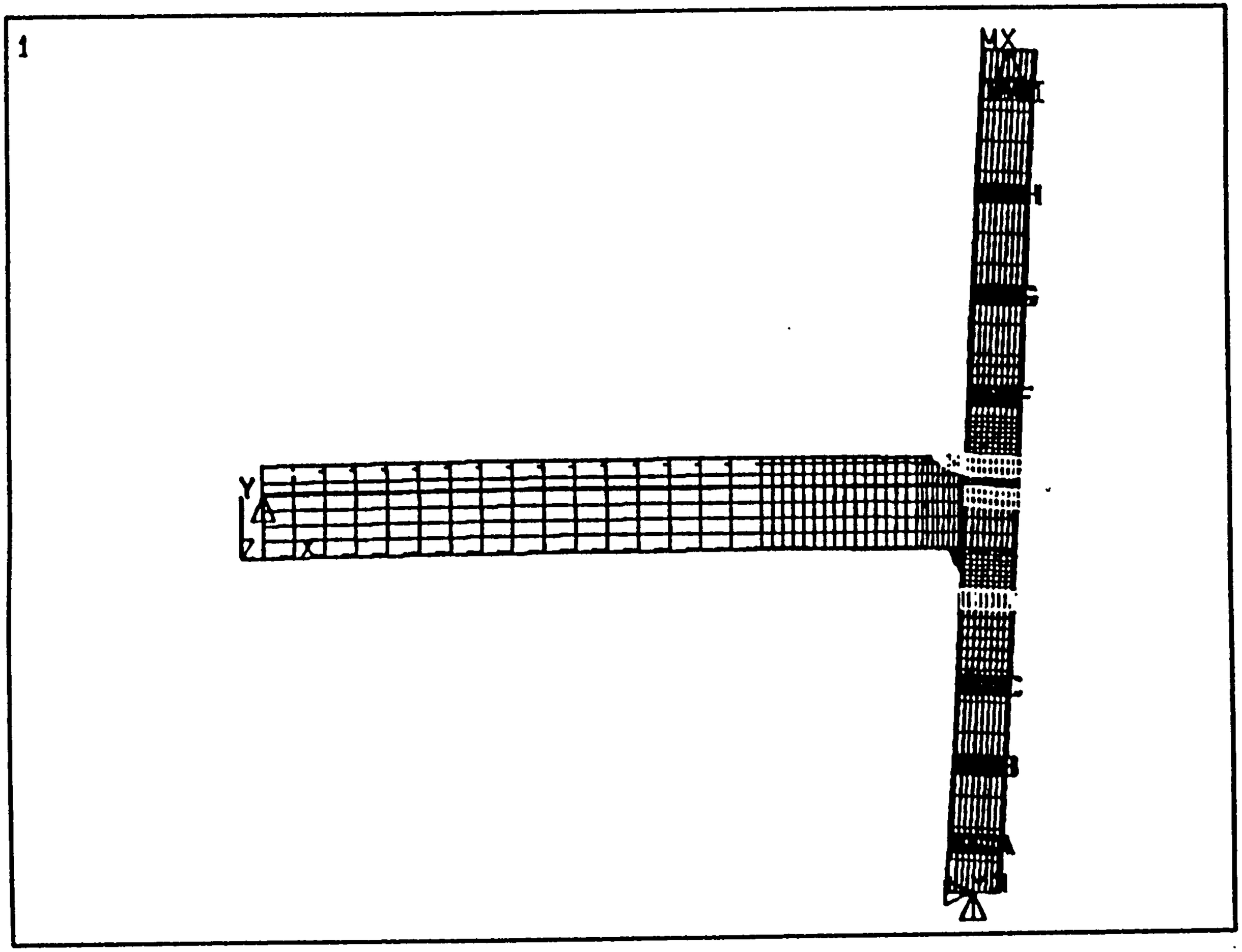

ANSYS 4.4A
JUL 7 1993
15:41:14
PLOT NO. 5
POST1 STRESS
STEP=1
ITER=20
UX
D GLOBAL
DMX =25.573
SMX =25.562
TDIS

ZV =1
DIST=2203
XF =1812
YF =382.65
A =1.42
B =4.26
C =7.101

F =15.621
G =18.462
H =21.302
I =24.142

FIGURE 5.17 UX CONTOURS , MODEL TWO

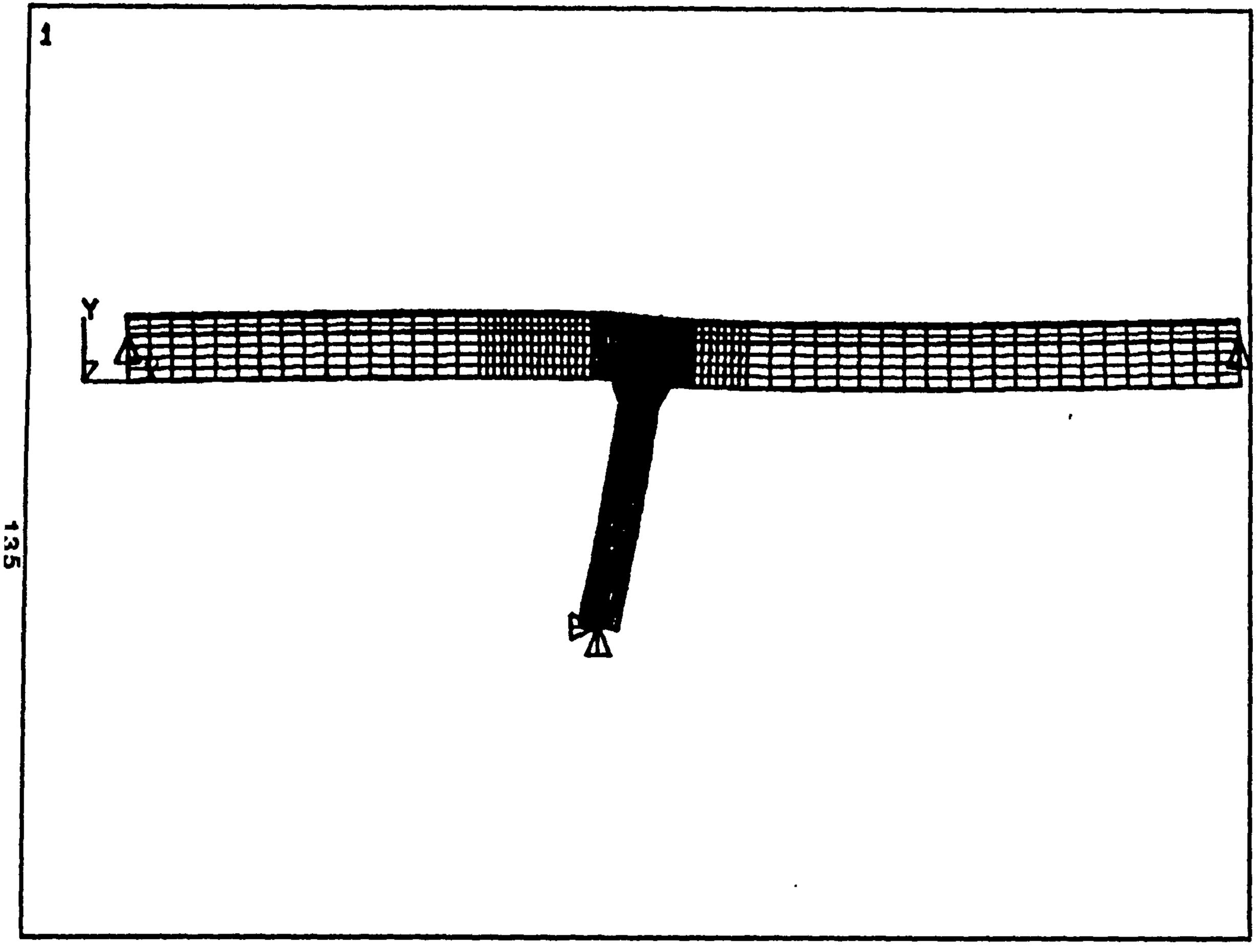

FIGURE 5.18 DEFLECTED SHAPE OF T-SUBFRAME

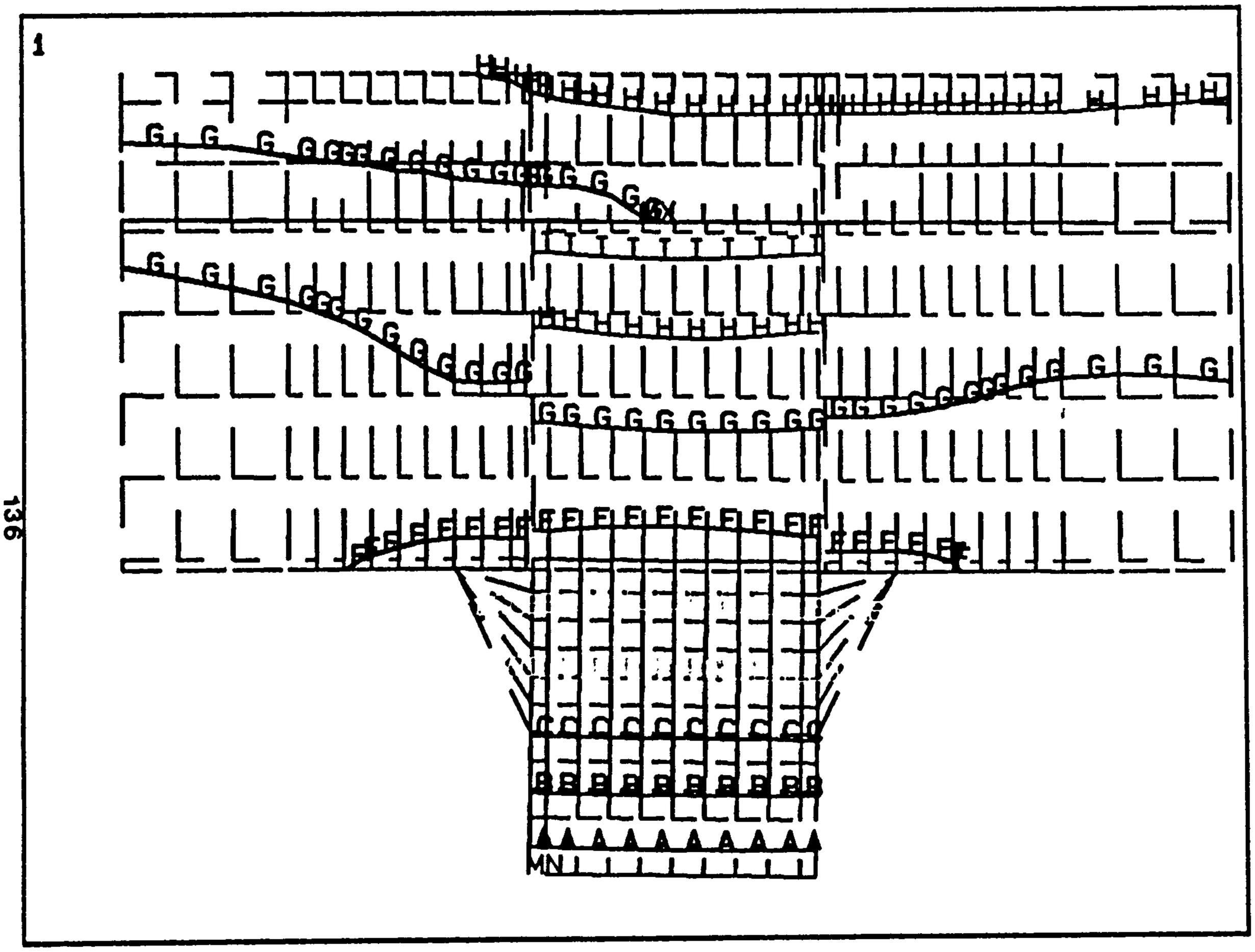

FIGURE 5.19 UX CONTOURS, T-SUBFRAME

60 kN

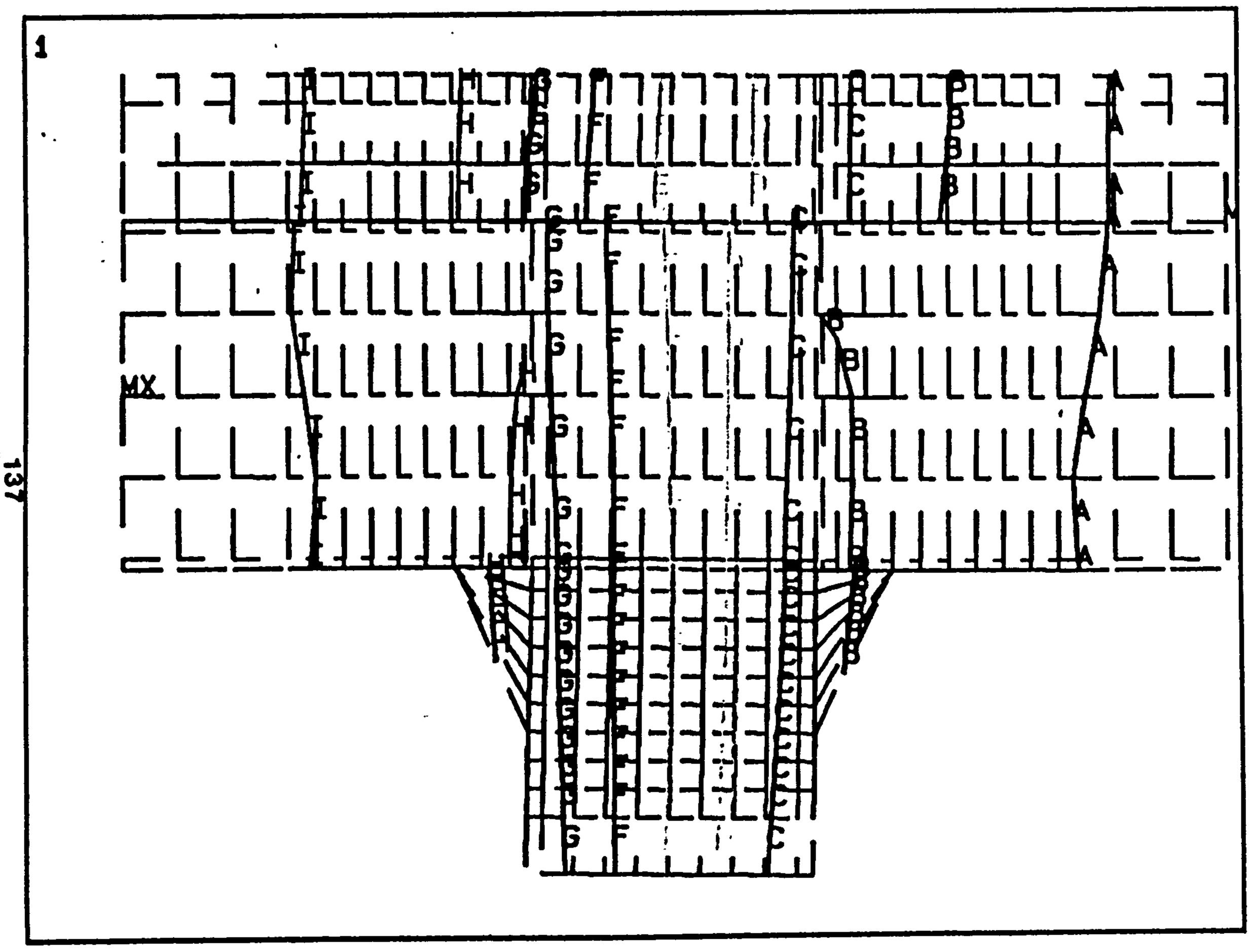

FIGURE 5.20 UY CONTOURS, ⊤ SUB-FRAME

60 kN

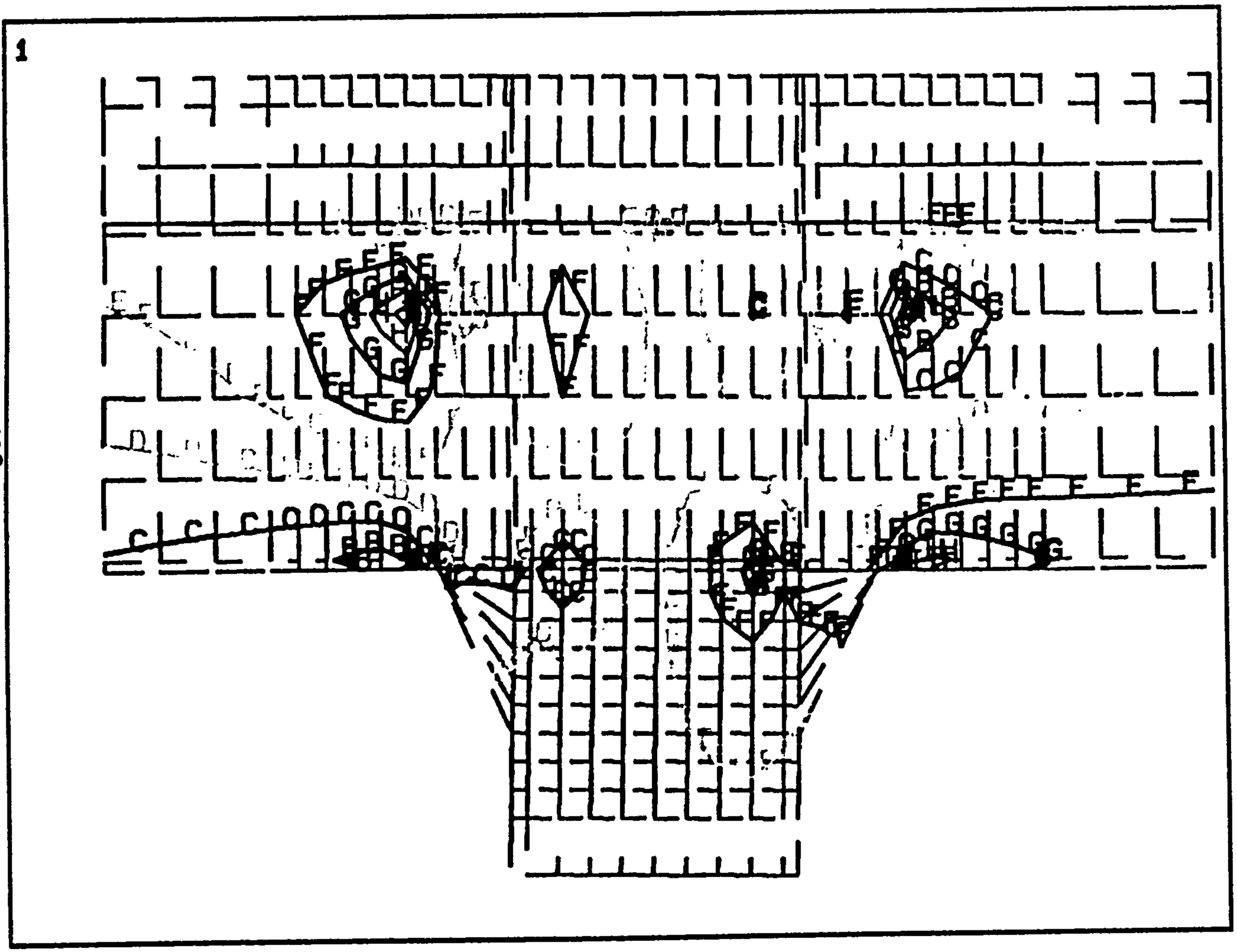

FIGURE 5.21 SX CONTOURS

60 kN

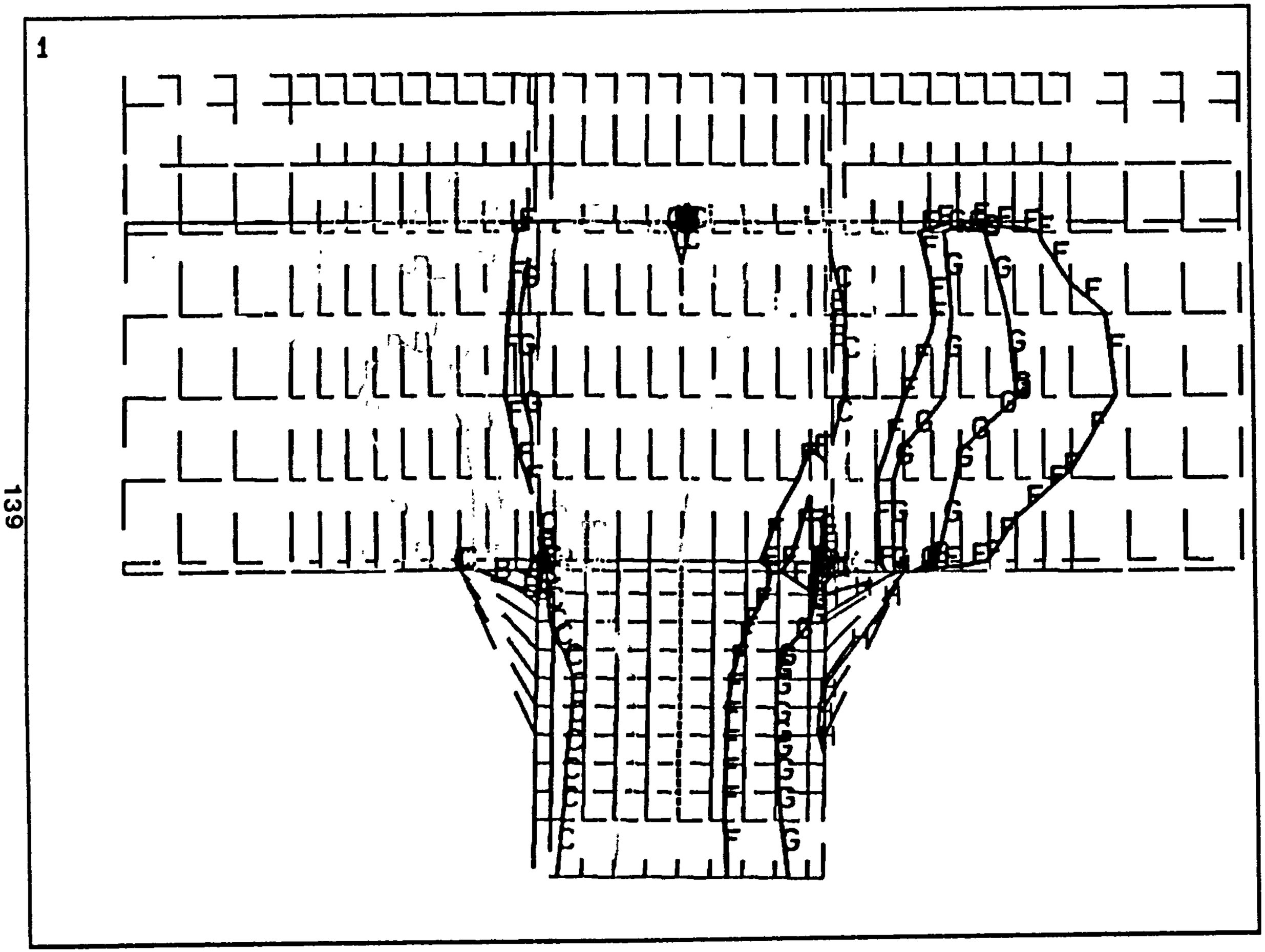

FIGURE 5.22 SY CONTOURS, T-SUBFRAME

60 kN

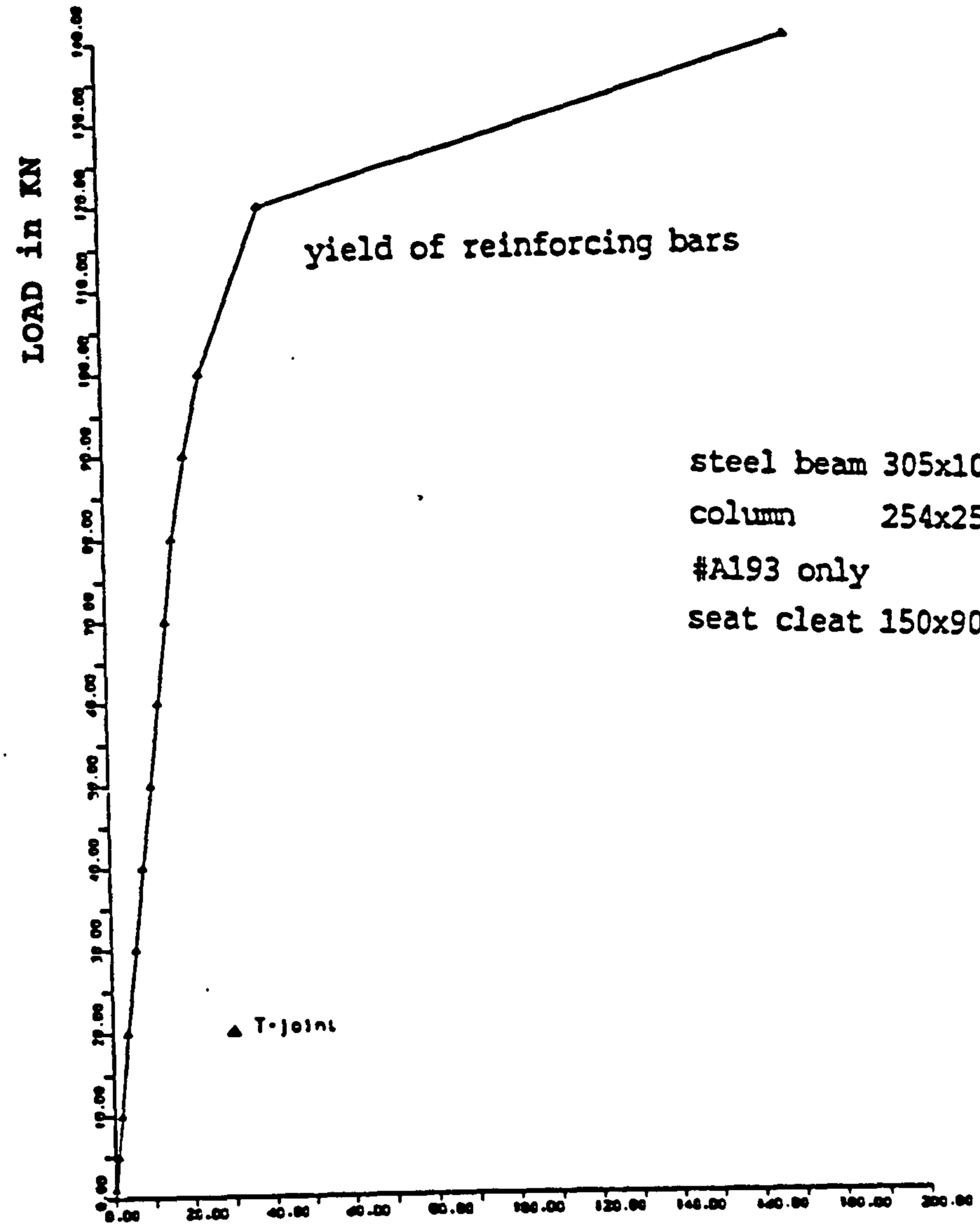

FIGURE 5.23: LOAD-DEFLECTION CURVE FOR ⊤ SUB-FRAME

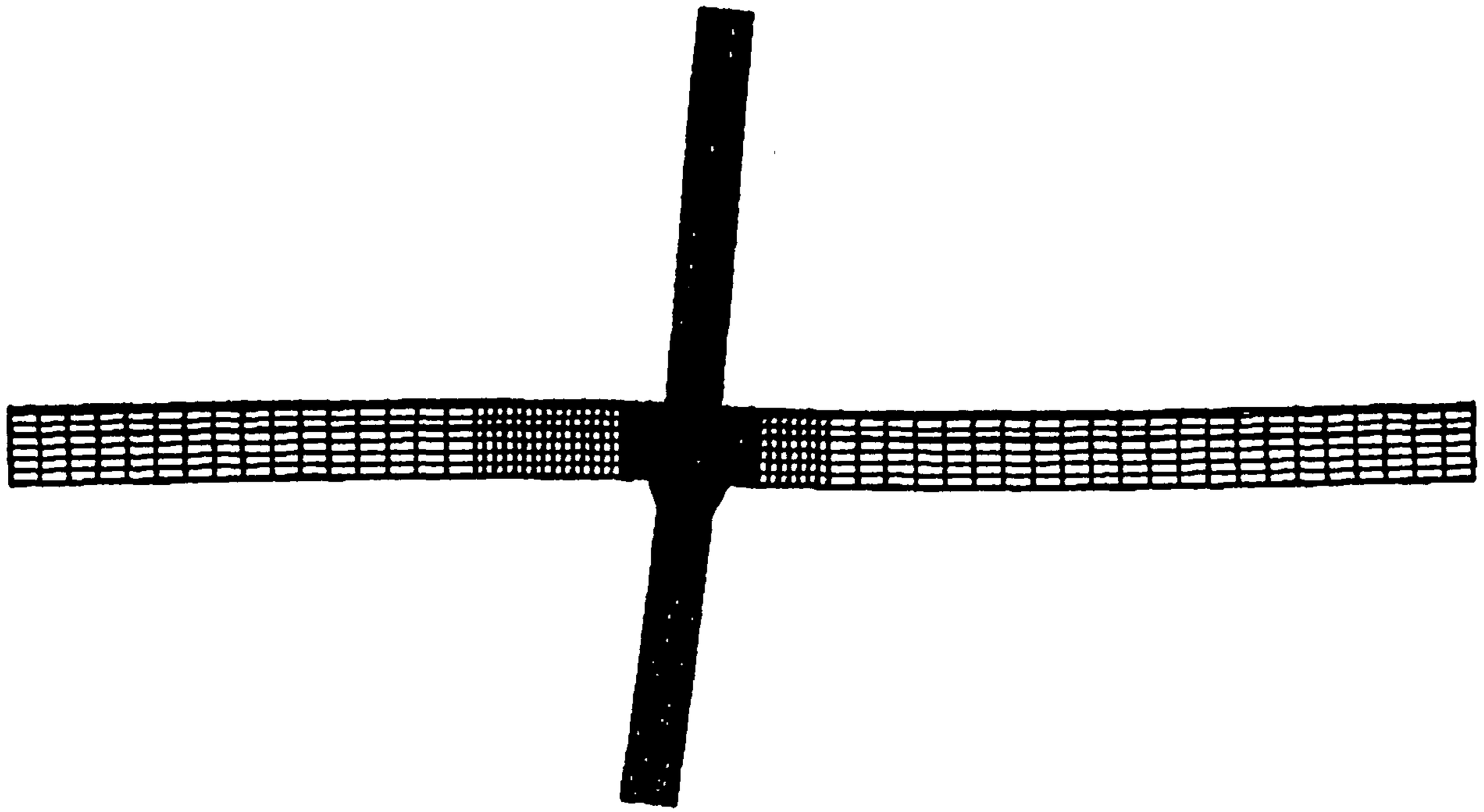

FIGURE 5.24 DEFLECTED SHAPE

cross-joint

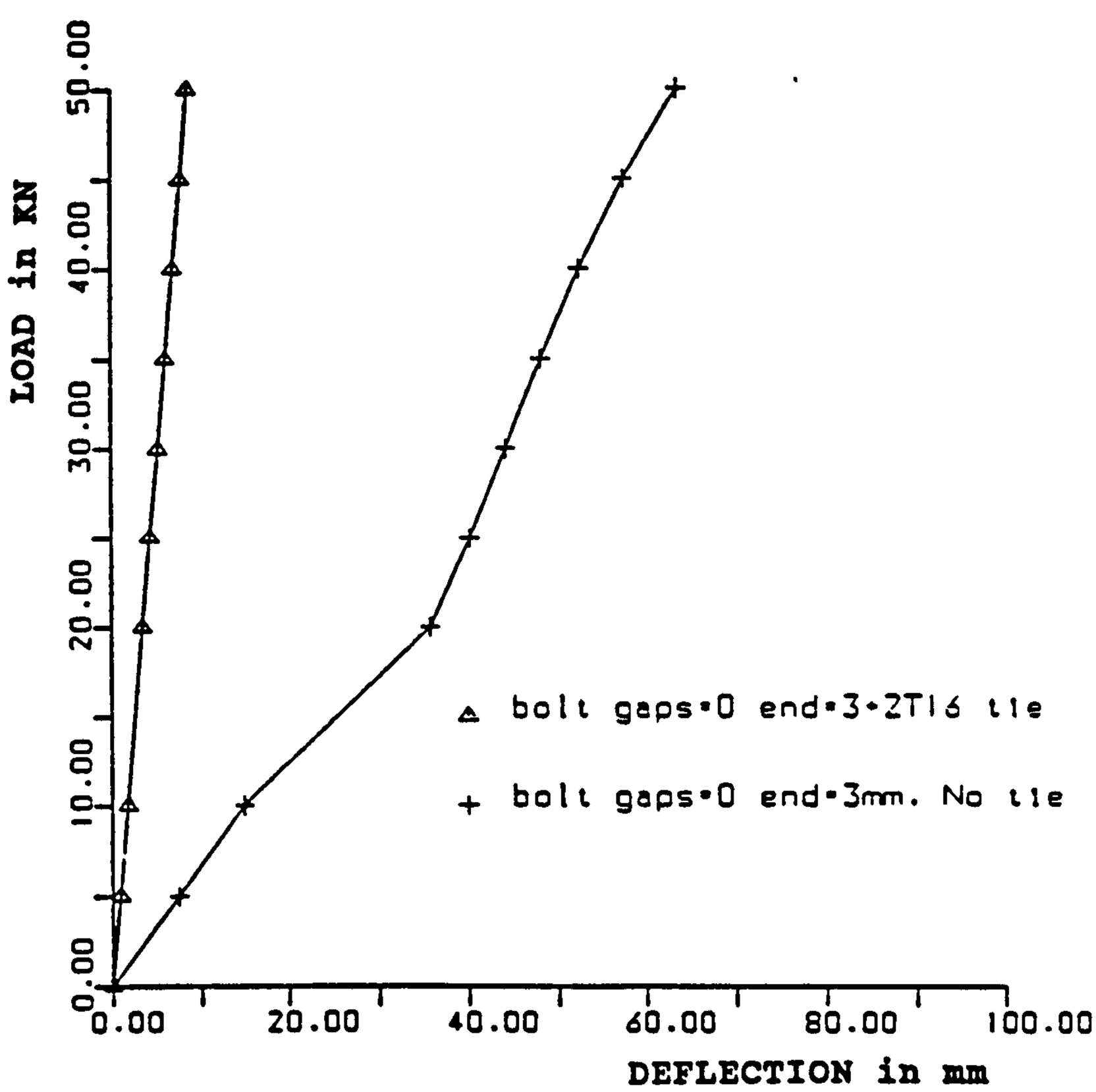

FIGURE 5.25: EFFECT OF CORNER BRACING

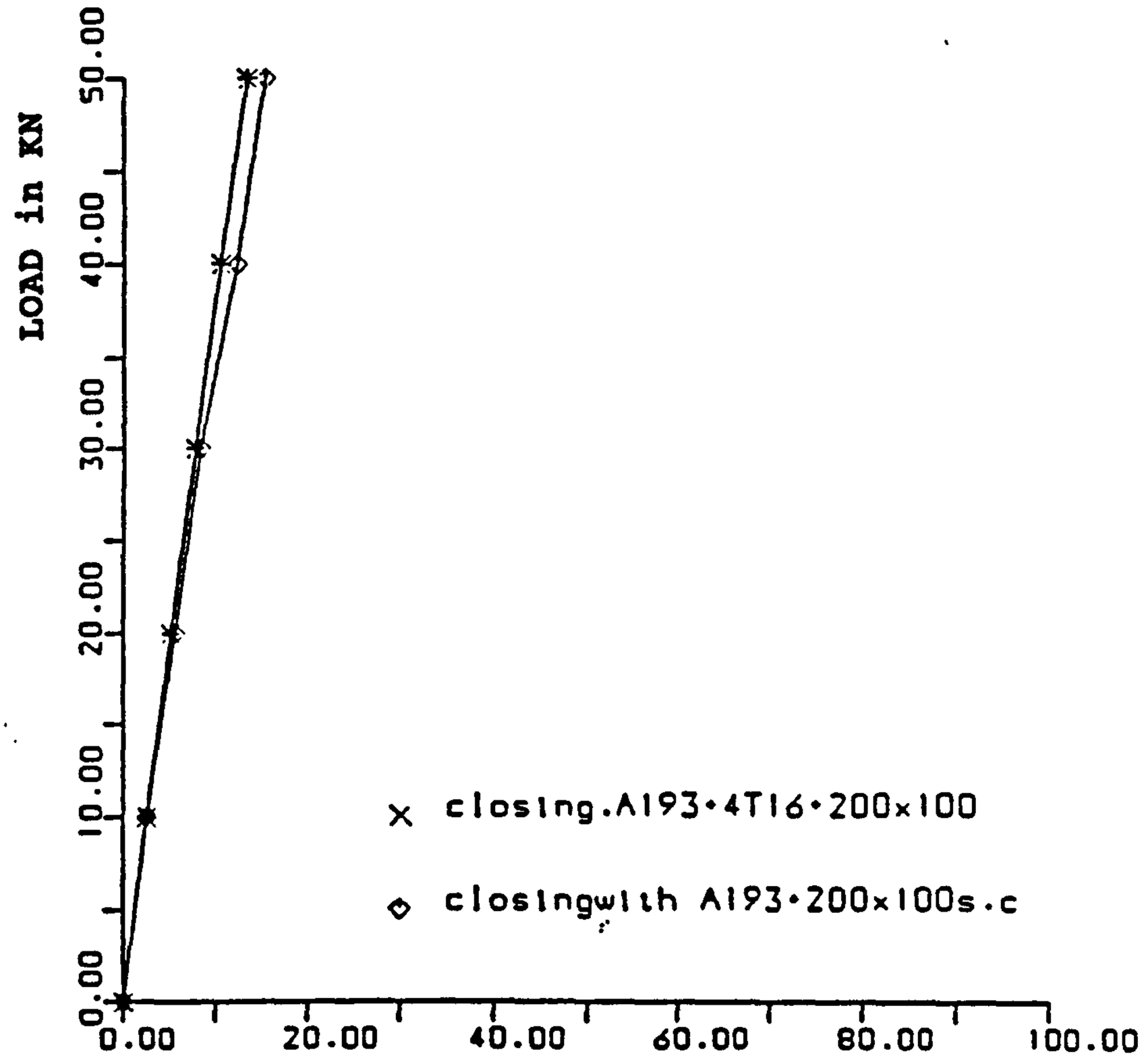

FIGURE 5.26: COMBINED EFFECT OF REINFORCING BARS AND SEAT CLEAT

CHAPTER SIX

EXPERIMENTAL PROGRAMME

6.1 Introduction

Determination of the performance of a structural connection under wind loads can be achieved by carrying out well prepared tests. Experimental investigation is always associated with high costs and time consumption. There is a lack of published test data that are directly representative of the construction arrangements currently much used in U.K. practice. Most of the previous tests were conducted on flat slabs (i.e with no metal decking) and employed much larger percentages of reinforcement (0.38% - 2.01%) than that provided by the mesh [2,9]. Because of the complicated interactions within semi-rigid composite connections, experimental studies are important to investigate overall behaviour and to confirm the accuracy of the finite element analysis predictions. The lateral sway of the frame, the crack pattern of the stressed concrete slab, and the vertical deflection of the composite beam can also be investigated.

Past experience [5,27] indicated that the degree of usefulness of a test is maximised if a complete report is provided, which should include (in addition to the moment-rotation or the load-deflection curves):

(i) All the data that would allow an identical test to be conducted in another laboratory;

(ii) The records of the deformation and displacement components measured, which would allow the influence of the various factors to be determined;

(iii) The effective stiffness values and level of moments, which characterise the

different phases of the overall joint behaviour.

6.1.1 Variables Affecting the Stiffness of the Connection

The complicated nature of composite connections arises from the fact that its different components contain different stiffness materials which are interacting together. The geometrical shape of the profiled steel sheet and the low load cracking of concrete are additional reasons for difficulty in the accurate prediction of the connection behaviour.

Variables which may have an effect on the connection's stiffness can be summarised as follows:

(1) Size and stiffness of the steel beam and column.
(2) Concrete properties i.e., compressive and tensile stiffness and strength.
(3) Presence and size of seat cleat.
(4) Presence and size of the seat cleat stiffener plate.
(5) Cross-sectional area, stiffness and yield strength of reinforcing bars.
(6) Depth of the concrete slab.
(7) Degree of shear connection between the steel beam and the concrete slab.
(8) Type of bolts used and their degree of tightening.
(9) Size and quality of fillet welds which are used to fix the connecting angles to the steel column.

All connection configurations identified as sub-frames A to E in Figure 6.1 were studied numerically. From the numerical predictions, each of the ⊤ and ┼ sub-frames were shown to be contributing to the stiffness of the building as multiples of the stiffness of the ¬ sub-frame.

The computation predicts the stiffness of each joint from the geometry and material properties. However, the accuracy of this prediction was unknown for the complex stress interactions which occur in the sample.

The experimental investigation was carried out to verify the safe behavioural prediction of this type of connection. Because of the high cost and time consumption required to make the sample, a single and representative connection of sub-frame type A was selected on which the experimental work was carried out. Some modifications were introduced during the tests to increase the lateral stiffness of the original connection.

The experimental work was carried out in the Heavy Structures Laboratory at the University of Southampton. In this section, layout of the test specimen, working drawings of the different parts of the connection, instrumentation and other details of the experimental work are presented.

6.1.2 Choice of the Sample Frame to be Tested

The frame tested is shown in Figure 6.2 from which it is clear that it was a ¬ shape, full-scale, half-storey, half beam span frame subassemblage, pin-jointed at the two support positions. The subassemblage beam span, which extended from the effective span mid-point to the column, was nominally 3500mm. The height of the subassemblage steel column was nominally 2000mm, from the assumption that the average total storey height is 4000mm. The overall slab thickness was 130mm and its width was 1750mm. This width was selected as one quarter of the total span of 7000mm. There were two reasons for the choice of the ¬ configuration in the experimental investigation. Firstly, because the free height and the span of the existing loading frame in the laboratory can easily accommodate it. Secondly, it was concluded earlier that multiples of the results for this shape could be considered as representative of the other configurations.

6.2 Materials and Geometry

A typical composite floor geometry was established for a steel framed building. To ensure representative geometries and easy assembly details, the experimental programme was discussed with **Gifford and Partners Consulting Engineers** and

with **Conder Southern Ltd**, steel fabricators. The position of the test frame in the typical building is shown in Figure 6.3.

6.2.1 Steel Components of the Composite Subassembly

The steel connection embodied within the composite beam-to-column connection comprised a seat cleat and a single web cleat. This connection is one of the most efficient, and it was recommended to be studied initially without major modifications. The two cleats were shop welded to the column and later bolted to the beam.

(a) Hot Rolled Sections

(1) The Steel Column

A 254×254×73kg/m universal column of grade 50 steel was used. All the cleats were shop welded. The column had the following nominal section properties and dimensions:-

Second moment of area I_x	= 11400cm^4
Elastic modulus Z_x	= 894.0cm^3
Cross sectional area A	= 92.9cm^2
Column depth D_b	= 254.0mm
Flange width B	= 254.0mm
Web thickness t	= 8.6mm
Flange thickness T	= 14.2mm
Plastic modulus Z_b	= 989cm^3

Horizontal shear loads are partially transferred directly between the column and the concrete slab, either by bearing or by the bond strength. While the bond strength was expected to have little effect, the I shape of the steel column allows the transmission of substantial forces by bearing. The steel column extended 100mm above the concrete slab to provide shear connection throughout the

concrete depth.

There was some deviation between the produced steel frame and the designed one. The actual column height was 2045mm. The steel column is shown in Figure 6.4 and the column base is shown in Figure 6.6.

(2) Steel Beams

A universal beam 305×102×28kg/m was used in the composite section. This beam had the following nominal section properties and dimensions:-

Second moment of area I_x	= 5421cm^4
Elastic modulus Z_x	= 351.0cm^3
Cross sectional area A	= 36.3cm^2
Beam depth D_b	= 308.9mm
Flange width B	= 101.9mm
Web thickness t	= 6.1mm
Flange thickness T	= 8.9mm
Plastic modulus Z_b	= 407.2cm^3

Fabrication details of the main steel beam are shown in Figure 6.6, the actual beam span was 3434mm.

Two steel stub beams were used to simulate the longitudinal beams. Span of each was 870mm and its section was 356×127×33kg/m universal beam as shown in Figure 6.7.

(3) Seat and Web Cleats

A 150×90×10mm seat cleat was shop welded to the steel column flange. Two M16, grade 8.8 bolts were initially used to fix the cleat to the main steel beam. Bolt holes were 18mm diameter with a clearance of 2mm.

The web cleat was also shop welded to the steel column and bolted to the steel beam by two M16, grade 8.8 bearing bolts. The section of this cleat was 80x60x8mm. The two stub beams had the same cleats as the main beam.

(b) Fabricated Steel Parts

(1) The Column Base

A heavy end plate was welded to the column to transmit loads into the simple hinge pin-joint. Details of the pin joint is shown in Figures 6.4 and 6.5. Welded stiffening webs ensured rigid connection between this plate and the 50mm diameter hinge sleeve. The hinge pin was 50mm diameter solid round bar. Similar stiffeners fixed the remaining length of hinge sleeve to their floor mounted base plate. The tubes were fixed to the base plate using two 152×89 channels. Each channel was 1200mm long.

Dimensions of the column base plate were 1200×1200×20mm with four 25mm bolt holes. These dimensions were selected for the following reasons:

(i) To ensure minor-axis stability for the column during loading.

(ii) To accommodate the existing floor bolt-hole positions.

(iii) To minimise the local deformation of the base plate. The long, welded, 152×89 channel sleeve stiffeners assisted in eliminating plate deformation.

(iv) To distribute load over a larger floor area.

(2) Beam End Support

There are two beam hinge fixing plates, one connected to each jack controlling either horizontal (Figure 6.8) or vertical (Figure 6.9) positions. The geometry of both these base plates was dictated by the following requirements:

(i) To ensure stiffness of the fixing plate to pin connection.

(ii) To match existing bolt hole positions on the jack.

(iii) To provide symmetrical restraint to the pin.

(iv) To permit free relative rotation of the jacks when the pin is displaced horizontally whilst maintaining its height.

At the loaded end of the beam, it was required to keep the point of load application in the same horizontal plane i.e., no vertical displacement was allowed at this point. This was achieved using a hydraulic jack as a vertical support to the beam end, as shown in Plate 6.3.

6.2.2 Bolts

Bolts are available in various grades depending on material properties, manufacturing tolerances, and nut and head size. In the U.K., the three most commonly used classes of steel bolts are black, precision, and high strength friction grip bolts [49]. The strength grade is given by figures separated by a point (in accordance with the ISO system). The first figure is one-tenth of the minimum ultimate stress in kgf/mm^2. The second is one-tenth of the percentage of the ratio of minimum yield stress to minimum ultimate strength. Black bolts are normally of grade 4.6; precision bolts are generally grade 8.8. High strength friction grip bolts are not recommended because they need close supervision to make sure that they are all tightened to the required torque. For bearing-type bolts subject to shear, the degree of tightening of a bolt is not of that importance.

Bolts may transfer loads by shear, tension or a combination of the two. They are usually installed in clearance holes, e.g., 2mm oversize up to M24 bolts. In many simple joints the bolts are considered to act in shear only, and the transfer of force through the connection is achieved by bearing of the plates on the bolt and so, bolt pre-loading is not necessary.

Initially, all the bolts were M16, grade 8.8 bearing bolts. All bolt holes were 18mm diameter. The stress at proof load for this type of bolts is given in table 13 of BS 3692 and is equal to 58.2kgf/mm^2. The tensile strength for it is 785N/mm^2=80kgf/mm^2.

All bolt holes were shop punched. This is allowed for statically loaded joints of limited plate thicknesses. The use of punched holes is restricted because of the concern over the embrittlement of the work-hardened material that immediately surrounds the hole.

As an option for increasing the lateral stiffness of the connection, high strength friction grip bolts were used instead of the bearing bolts which were initially used. The bolts were initially hand tightened with a spanner. An adjustable torque wrench was set to the required torque and each bolt was tightened to the required torque.

Crush washers were used with the HSFG bolts. The type used in this research was the dimpled ones. Proper preload was expected to crush the dimples and reduce their height but this did not occur uniformly. Tightening torque was also controlled by using an adjustable torque wrench. It was considered that torque control with a feeler gauge in the washers although desirable, is practically difficult and less accurate than the torque wrench.

Power driven tools are usually used for tightening HSFG bolts. They are not only heavier to handle but more generous clearances are usually essential for manipulation compared with an ordinary open-ended spanner. However, they offer considerable speed during the steelwork erection, and can be fitted with automatic torque limiting devices.

6.2.3 Decking

The profiled steel decking was a re-entrant trough profile, 51mm-deep deck with a pitch of 150mm and nominal gauge of 0.9mm throughout.

6.2.4 Reinforcing Bars

The concrete slab was reinforced by A 193 mesh. This mesh was cut to the slab dimensions. The mesh was kept in place by wiring it to the transverse ties which were used to keep the side shuttering restrained against concrete pressure.

A T16 high yield deformed steel bar was used as additional reinforcement to increase the lateral stiffness of the joint. This single bar was bent to be used as two bars projecting into the slab at 45° from the column. An 18mm diameter hole was drilled through the column web to allow the bar to go through. The length of each branch of the bar was taken as an anchorage length equal to 40 times the bar diameter.

6.2.5 Fasteners

(a) Nails and Screws

Hilti nails were used for light fixation of the profiled steel sheets to the steel beam prior to stud welding to keep the relatively thin and light sheets in place.

Hardened steel fastening pins were driven through the galvanized steel sheet and the flange of the steel beam. The nails used were the ENP fasteners which are suitable for fastening sheet metal to steel and concrete. A cartridge-actuated tool type DX650 was used in driving the nails. It uses safety cartridges which burn with time-lag control. This system is simple, economical, quick and independent from an external power source.

Self-tapping self-drilling screws, produced by "SFS Limited", were used to fix adjacent sheets together. The external threaded diameter was 5mm. An adjustable torque electric drill was used to drill these screws without shearing them.

(b) Shear Studs

The shear studs used were the Nelson headed stud connectors marked TRW Nelson. The material from which these made is low carbon steel to ensure satisfactory welding quality. The diameter of these studs was 19mm and the height was 95mm after welding. The following nominal mechanical properties were guaranteed by the supplier [54]:

The yield stress is 350N/mm^2, tensile strength is 450N/mm^2 and the elongation is 15%.

6.2.6 Concrete

The concrete mix was designed to give an average strength of 30N/mm^2 after 28 days. Concrete grades between 25 or 40 are usually specified, higher grades not being structurally necessary. Normal Portland cement was used. Lytag light weight aggregate with maximum size of 10mm and bulk density of 800kg/m^3 was used as coarse aggregate. The fine aggregate was normal sand. The mix proportions were: 1:2.5:1.59 (cement to sand to Lytag) with a free water cement ratio of 0.7 This mix was designed and tested by El-Shihy [52].

In current practice for composite frames, the concrete slab is cast using profiled steel sheeting. Shear connection is provided by welded shear studs. Techniques employed to produce the composite beam are explained later in this chapter.

6.3 Sample Assembly

6.3.1 The Steel Frame

The column base was fixed to the floor by 4 bolts in clearance holes and was braced horizontally against the adjacent column of the loading frame by two screw jacks. After the column base was fixed, the steel column was mounted to its base by introducing a 50mm diameter steel rod through the three tube sleeves of the column hinge. This rod was machined to move freely within the tube. The column was held vertically and the steel beam was connected to it by the four bolts of the web and seat cleats. The steel beam was then supported in the horizontal position by the vertical hydraulic jack.

A spirit level was used to check the level of the steel beam and a plumb bob was used to ensure verticality of the steel column.

The horizontal jack was fixed to the column of the loading frame and was hinged to the end of the steel beam. Finally the two stub beams were bolted to the column and their levels were checked.

The tightening torque for all the precision bolts was 14kgf.m. A spanner with 450mm lever arm was used to tighten the bolts and a torque wrench was then used to measure the torque. This torque was adopted as being consistent with the value expected of manual tightening with ordinary tools. Plain washers were used with the bearing bolts.

6.3.2 Decking Preparation and Sheet Fixation

Profiled steel sheeting is allowed to be used in building structures in composite design. Use of this sheeting in building provides many advantages as mentioned in 1.3.1. Profiled steel sheets used as permanent shuttering should be capable of supporting the wet concrete, reinforcement and construction loads.

Re-entrant profiled sheets were used. The gauge of the sheet was 0.9mm throughout. The sheet was cut to a length of 1750mm using a steel saw. Although trapezoidal timber blocks were used to absorb the loud noise which resulted during cutting, ear guards had to be worn during cutting. A square hole of 254×254mm was cut in the steel sheet to allow the column to go through the concrete slab. The ribs of the sheets extended in the direction perpendicular to the main steel beam and parallel to the two cross-beams.

Decking fixation was carried out by the use of shot fired nails which is the current practice. Hilti nails were used for this purpose. The idea behind the light fixation before welding of shear studs is to keep the relatively thin and light sheets in place. In situ, winds may take these sheets away if they were left loose.

The sheet was fixed to the steel beams by hardened steel fastening pins which were driven through the galvanized steel sheet and the flange of the steel beam. The nails used were the ENP fasteners which are suitable for fastening sheet metal to steel and concrete. A cartridge-actuated tool type DX650 was used in driving the nails. It uses safety cartridges which burn with time-lag control.

At both edges of the sheet, a fastener was driven to the longitudinal steel beam. Four fasteners fixed the sheets to the stub beams. The positions of fasteners were selected off centre from the web of the steel beams to ensure full penetration.

During concreting, the sheeting was assumed to stabilise the main beam which it spanned across. Therefore, to enable the sheeting to act as a shear diaphragm, fasteners were placed along the sheet seams in addition to along the steel beams. These fasteners also served to fix the sheeting prior to stud welding and to prevent relative movement during concreting. Shot-fired pins were used as fasteners to the steel beams while self-tapping self drilling screws were used to fix adjacent sheets together.

Self-drilling, self-tapping screws, produced by "SFS Limited", were used. The external threaded diameter was 5mm. These screws were used to connect each adjacent profiled steel sheet together. An adjustable torque electric drill was used to drill these screws without shearing them.

6.3.3 Shear Studs

Headed studs, which are the most widely used type of connectors, were used. The 19mm diameter stud is by far the most common, it is the one for which the majority of test data is available. The used studs were marked as made by Nelson. They were through-deck welded to the steel beam. This was carried out by a local sub-contractor. The diameter of shear stud was 19mm and its height after welding was 95mm. Spacing of shear studs was 150mm in the longitudinal beam and in the cross beams.

Welding of shear studs through galvanized profiled sheeting presents certain fabrication difficulties associated with construction site conditions. A power control unit provided the necessary current of 415 volts and long leads were used to supply electricity to the welding gun. The welding operation was relatively rapid, but it was clear that it is not suitable in a closed place because of the smoke. It is also not suitable for welding through sheet overlaps, to painted beams, or in wet conditions [54]. The sheet thickness was 0.9mm throughout which was less than the maximum thickness for through-deck welding of 1.25mm.

Visual inspection of shear studs showed that the weld to a stud connector formed a complete collar around the shank and was free from cracks and excessive splashes of weld material. It had a steel blue appearance. Two studs were tested by bending the shank of the stud through about 15^0, which is the site test given in draft Eurocode 4. The in-situ 15^0 bend method was also carried out on a single shear stud separately before welding to the main sample.

6.3.4 Concrete Forming and Placing

Concrete materials were divided into ten equal batches each of which was mixed separately. Although the concrete mix was sloppy, it was decided to use it as it was to keep the compressive strength at the level of 30N/mm^2 which is the common value in composite buildings.

A metallic access scaffold was constructed to provide safe path to the top of the steel beam. This access scaffold was strong and stable to provide a convenient and comfortable platform.

For safe and easy removal of the composite beam after the completion of the test, four lifting eyes were prepared of reinforcing bar. Positions of these eyes were selected to ensure balance of the composite beam when lifted. They were designed to carry the weight of the concrete slab and the beam.

The decking acted as an efficient working platform introduced for formwork and scaffolding, and need only be shuttered at its edges. Plywood shutters were placed around the re-entrant sheeting to give an overall slab thickness of 130mm. They were held in position by timber beams which were propped by Acrows. The corners were sealed by silicon Plasticine to reduce grout loss.

A set of 4 adjustable props with fork heads was used as temporary supports. Two 100×50mm softwood sections were used as longitudinal edge beams. 20mm plywood was used as edge shuttering. Opposite shutters were linked by 6mm threaded-ended ties arranged at 300mm centres. The ties went through the troughs of the steel sheets and M6 nuts were used to tighten them against the edge shuttering. A view of the test specimen at this stage of construction can be seen in Plate 6.1.

Slab reinforcement was an A193 mesh. The top cover was 25mm. The reinforcement was kept in place using lateral and longitudinal ties. The mesh was

cut to a width of 1710mm to allow 20mm cover at each side. The length of the mesh was 3460mm to allow 20mm cover at both ends.

The concrete was placed, carefully compacted using a poker vibrator, and levelled off using a timber beam.

The main and the control specimens were air cured for 24 hours and then were covered with a PVC sheet. The completed test specimen and loading frame are shown in Plate 6.2.

6.4 Testing of Materials

(a) Profiled Steel Sheeting

Tensile strength test was carried out on three test pieces of the steel sheet. Each was 25×250mm. A gauge length of 25mm was adopted for the measurement of elongation. The stress-strain relationship for the steel sheet is presented in Chapter Seven.

(b) Reinforcing Bars

Four test pieces were cut from the reinforcing mesh. Two of these were from the longitudinal bars and two from the transverse bars. It was thought that the welded point of the bar was a point of weakness because of the presence of a notch at this point. Every test piece contained two welded parts. The tensile strength test was carried out and the load-strain curve was automatically plotted for each of the specimens. A half bridge transducer with a gauge length of 25mm was used to measure the elongation. The idea behind the use of a transducer instead of measuring the actual movement of cross heads is to avoid the error resulting from slippage in the jaws.

(c) Concrete

Test samples were taken from different mixes. These samples included cubes to determine the compressive strength, small cylinders to determine the tensile strength, large cylinders to measure the modulus of elasticity, and beams to determine the flexural strength of concrete.

6.5 Loads and their Application

The frame was to be tested in three loading levels as follows:

(1) Construction stage loading in which wind loads were considered acting on the bare steel frame. The exposed area is the maximum probable area of the steel columns and beams.

(2) Construction stage loading with the profiled steel decking in place and attracting significantly greater wind load while contributing little to the stiffness.

(3) Composite floored building was considered in the third stage. In this state, the maximum wind load arises after the building is clad. Calculations of wind loads in the three stages are presented in Appendix I.

The test was carried out by gradual application of lateral loads which continued until a predetermined load was reached or lateral deflection was excessive. Load increments of 2kN, or 2.5mm horizontal deflection, were applied and limited by whichever occurred first. This increment was increased to be 5mm after the first test on the steel frame because of the large sway. After each load cycle, the frame was put back at its geometrical origin. Wedges were used to keep the vertical jack in position after each test session to ensure a subsequent start from the same point. During the test, some dial gauges went out of range and were reset when necessary to restore their effectiveness.

6.5.1 Loading Frame and Testing Machines

The loading frame was a steel one with 6700mm clear span and 3100mm clear height. Its end columns were 305×305×97kg/m UC and the top beam section was 610×305×179kg/m UB. Four 25mm bolts fixed the triangulated column base plate to the strong floor.

In this frame, the steel beam is rigidly connected to the columns. The connection between the steel beam and the steel column is an end plate one in which the end plate is 20mm thick. It is welded to the steel beam and bolted by 12 bolts each of diameter 20mm to each steel column. 20mm shear stiffeners are welded to the steel beam at 400mm centres. The lateral stability of the loading frame was checked numerically. It was decided to measure the lateral sway of this frame at each load step and the movement of its two columns at their lower points relative to the floor. Three dial gauges were used for this purpose and the adjacent loading frame, which was not in use at the time of test, was taken as a high level reference.

Two hydraulic jacks were used in applying the load. One of these jacks was fixed horizontally to the loading frame's column and the other was mounted vertically as shown in Plate 6.3. Both jacks had swivel hinged supports which allowed them to rotate at the fixed end. The moving end of both jacks were hinged at the connection to the test subassemblage as can be seen more clearly in Plate 6.4. Induced bending of the jack shafts was thus eliminated.

Both double-acting jacks had calibrated integral load cells and linear variable displacement transducers to provide both load and position control.

6.5.2 Stability of the Test Frame

To ensure the required in-plane response and to avoid any out of plane movements, the frame was restrained by a standard adjustable push/pull prop. The

lower plate of the prop was fixed to the floor and the top plate was fixed to the web plate of the steel beam using two G-clamps and two wood blocks as shown in the foreground of Plate 6.3.

6.6 Instrumentation of the Test Specimen Displacements

The target value for the lateral displacement was taken as H/300. Although the sway of the frame was the most important information, measurements of other displacements which may affect the stiffness of the joint were carried out. The instrumentation used in the test was prepared to measure the following parameters:

(1) Lateral deflection of the frame at the point of load application which was measured with respect to a suitable reference surface. This mounting frame which was composed of a welded steel frame with two horizontal plates was used also to support the dial gauges. This mounting frame is seen in Plate 6.3.

(2) Vertical displacement at the aforementioned point. This point was kept at the same level, and the purpose of the vertical dial gauge was to ensure that unobserved jack movement did not occur.

(3) Lateral sway of the outer surface of the steel column at two points. These two points corresponded to the bottom and the top of the steel beam.

(4) Changes in the size of the construction tolerance between the end of the steel beam and the steel column flange. The measurement of this gap was carried out before the application of any lateral load and after each load step using a linear resistance displacement transducer. This transducer was fixed within the column section and measured through a small clearance hole in the column flange.

(5) Slip between concrete slab and the top flange of the steel beam. This was carried out by a set of five resistance type transducers arranged along the span of the beam mounted as shown in Plate 6.5

(6) Play (slack) of the steel column support. This movement was measured vertically and horizontally to eliminate any effect of slack in the lower hinge. Two dial gauges were used in each direction, one each side of the column as shown in Plate 6.6.

(7) Lateral movement of one of the seat cleat bolt heads and the nut of the same bolt. Two transducers were installed using magnetic bases against the test beam web, one of the two was attached to the bolt head and the other was attached to the nut and is shown in Plates 6.7.

6.6.1 Transducers and Data Logger

All the transducers had 15mm stroke. According to their positions they can be divided into three groups:

(a) Group One

This group of transducers was concerned with measuring the relative horizontal movement between the column and the steel beam. Two transducers were used, one was installed at the lower flange of the steel beam and the second was attached to the end of the upper flange. The measurements of the lower one were taken as representative of the slip of the seat cleat bolts. The top measurements represented the crack width at the column-slab interface.

Two holes were drilled through the flange of the steel column to provide access to the steel beam flanges. The transducers were positioned horizontally having their arms compressed against the beam flanges. To mount these transducers on the steel column, both of them were fixed with a purpose-made aluminum plate bolted

to the column flange.

(b) Group Two

A set of five transducers was used to measure the slip between the concrete slab and the steel beam. Because of the geometrical symmetry, all these were mounted on one side of the steel beam. Five U-shaped steel mounting jaws were made to mount these transducers to the soffit of the concrete slab.

(c) Group Three

Two transducers were used to measure the relative displacement of the bolt head and the nut with respect to the steel beam flange. These measurements were taken to study the bolt movements under the applied loads. Magnetic bases were used to mount these transducers. A purpose-made aluminium bent bar was again used for the same purpose.

In addition to the above groups, a transducer was used to measure the vertical deflection of the beam at its mid-span.

A Solatron Orion data logger was used to record the readings measured by the transducers. The data logger provided an accurate conversion of the transducers' resistances in ohms to the required output in millimetres. A calibration rig was used to calibrate all the transducers before use. A built-in printer gave a hard copy printout for all transducers' measurements. The printed readings at each load increment allowed continuous assessment of the joint behaviour to be made as the test progressed.

6.6.2 Dial Gauges

All the dial gauges had 50mm strokes. They were used to determine the lateral deflection of the frame subassemblage and the movement of its lower support.

They were also used to measure the movement of the loading frame. According to the quantities to be measured and to their positions they can be divided into four groups:

(a) Group One

At the point of load application, two dial gauges were installed. The first was used to measure the horizontal deflection and the second measured the vertical deflection.

(b) Group Two

Two dial gauges were used to measure the horizontal deflection at the outer flange of the column. One of these was mounted at the level of the upper steel beam flange and the other at the level of the lower flange.

(c) Group Three

A pin joint was introduced at the column foot. There was some slack between the rod and the sleeve of the hinge. It was decided to measure the movement of the column foot vertically and horizontally at its two faces. The average of these readings was subtracted from the lateral sway of the frame. Four dial gauges were used to measure the displacements.

(d) Group Four

Three dial gauges were used to measure the lateral deflection of the loading frame at its two columns' bases and the third to measure the lateral sway.

6.7 Test Piece Modifications

During composite stage testing, the stiffness of the joint was critically dependant on the degree of fixity between the beam lower flange and the seat cleat. To compare the performance of the joint against the deflection criteria given in section 6.4.3, increasing degrees of fixity were tested as follows:

(1) Initial arrangement
(2) 2 HSFG Bolts
(3) 4 HSFG Bolts
(4) Welded Rigid

The frame with two 8.8 bearing bolts fixing the seat cleat to the steel beam was initially tested. The horizontal deflection exceeded the required value. It was concluded that modifications of the steel details were required.

6.7.1 Use of Two High Strength Friction Grip Bolts

As an option for increasing the lateral stiffness of the connection, the two 8.8 bearing bolts were replaced by two 10.9 HSFG bolts. The bolts were tightened with an adjustable torque wrench with the use of dimpled crush washers as torque control. Use of these bolts was found to be accompanied by some practical difficulties regarding torque control and bolts inspection. These bolts also showed readiness to slip earlier than expected when the applied load was reversed.

6.7.2 Use of Four HSFG Bolts

In order to use four HSFG bolts, it was required to extend the seat cleat to accommodate the two extra bolts. For easier welding at this stage, two 100×250×10mm plates were welded to the steel column flange, one at each side of the beam. At first, the two plates were prepared, cut, bevelled and marked. The bolt holes were then drilled to suit the existing ones. The bolts were tightened

before welding to avoid eccentricity of holes.

Welding was a full penetration single bevelled weld. Welding rods were selected according to BS639 [53] and were E51 44 BB. Care was taken to ensure that the plate would not be welded to the beam. The transducers which were close to the welding area were temporarily removed to avoid any damage by overheating. The bolts shear force (Q) due to wind was calculated as follows:

$$Q = \frac{P \times H}{d}$$

where P is the wind load, H is the frame height and d is the distance between the lower flange of the steel beam and the reinforcing bars in the slab. At external wind load of 30kN, the shear force Q is:

$$Q_{30} = 30 \times \frac{2045}{393.9} = 157.5kN$$

HSFG bolts transmitted the shear force between the steel beam flange and the seat cleat by friction, thus avoiding the movement of the bolt inside the hole.

6.7.3 Welding of the Seat Cleat to the Steel Beam

The relative movement was found to be the major reason for the large lateral sway. At first, it was thought that spot welding the steel beam to the upper leg of the seat cleat was possible. The Welding Institute, which was consulted, advised that spot arc welding of such thick plates was still in need of some development which meant it was not available at the time of the test.

Forming a puddle of fusion weld was the proposed solution for this problem. This means that a suitable hole should be drilled through the beam flange and then filled with welding material. This would have led to welding the beam and seat cleat together and a "shear stud equivalent" of the welding material would have transmitted shear forces between them.

Welding of the seat cleat edges was found to be the best way considering the laboratory facilities, the lack of access due to the presence of the slab, and the expected results. This may not be the best solution on site, but it was satisfactory to permit monitoring of the effect of the puddle welding.

The horizontal leg of the seat cleat was welded to the steel beam flange. The weld was designed to carry the total shear force of the connection.

For the seat cleat of section 150×90×10, the two parallel sides of the horizontal leg, 90mm each, were welded to the steel beam flange. The allowable stress for a fillet welds is 115N/mm^2 for grade 43 steel and 160N/mm^2 for grade 50 steel [57]. For leg thickness of 10mm, the throat thickness is 7mm and the permissible load is 1.12kN permm run of the weld.

Weld length required was thus 157.5/1.12=139.06mm.

According to the previous calculations, welding the two sides of the angle, with a total length of 180mm, was sufficient for safe transmission of the total shear force.

6.8 Summary

(1) Because of the high cost and time consumption required to make the sample, a single and representative connection was selected on which the experimental work was carried out. Some modifications were introduced during the tests to increase the stiffness of the proposed connection.

(2) The steel component of the composite frame joint was a seat and single web cleat one. The cleats were welded to the column and bolted to the beam with 2mm clearance holes for 16mm bolts.

(3) Re-entrant profiled steel decking was used as permanent shuttering and to provide composite floor action. Composite action between the slab and the

steel beam was provided by conventional shear studs welded through the decking to the top flange of the steel beams.

(4) Nominal grade 30 light weight concrete was used. Total thickness of slab was 130mm.

(5) Slab reinforcement was A 193 fabric to control cracking and as a fire mesh. Additionally, 2T16 reinforcing bars were used in the joint zone.

(6) A nominal construction tolerance of 6mm was allowed between the steel beam and the steel column. The actual width of this gap was slightly different after the assembly of the frame.

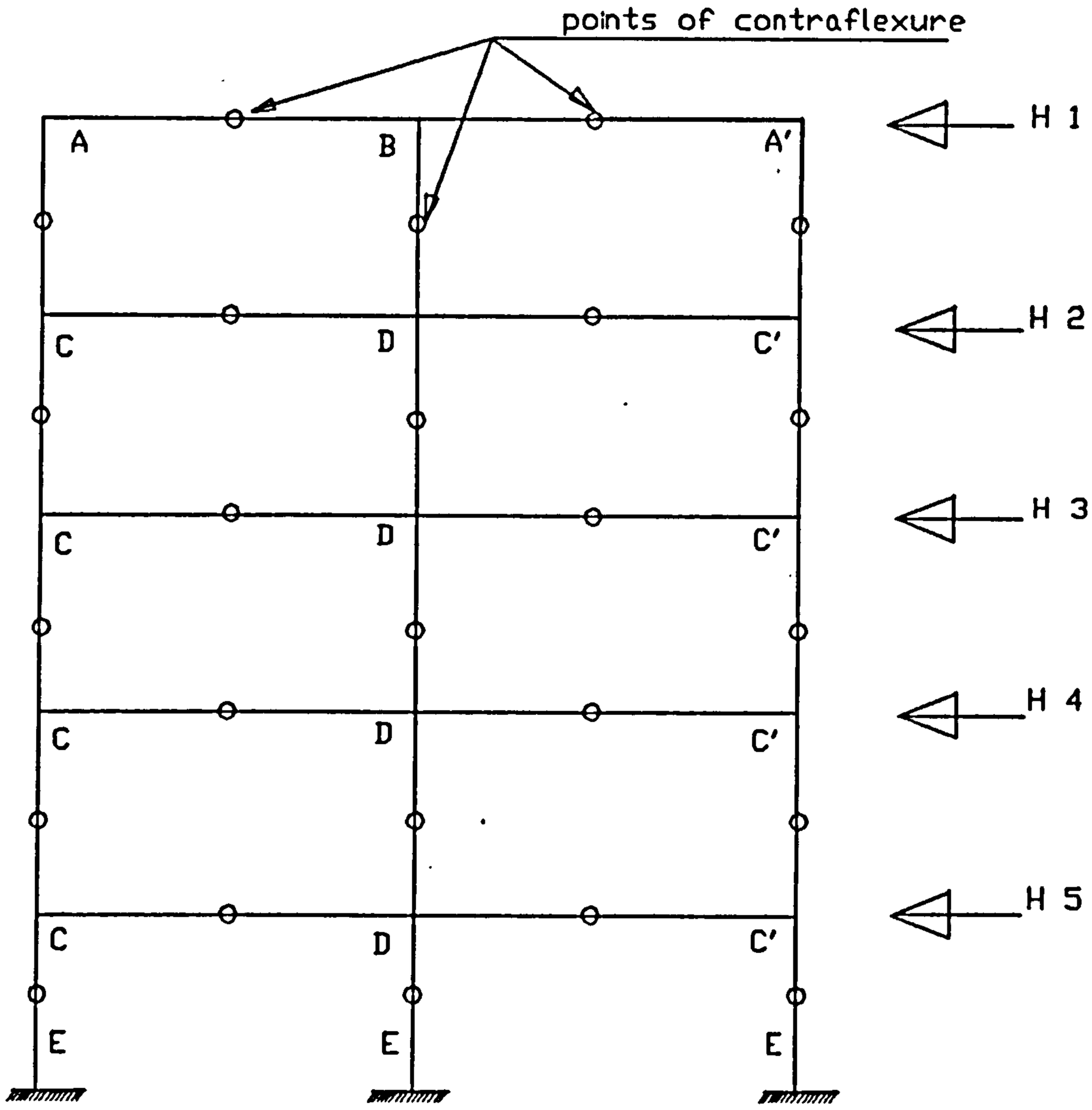

The stiffness of the building in providing resistance to lateral loading can be obtained by summing the contributions from each sub-frame, A to E, bounded by the points of contraflecture.

FIGURE 6.1

CROSS-SECTION OF THE BUILDING (UNDEFORMED)

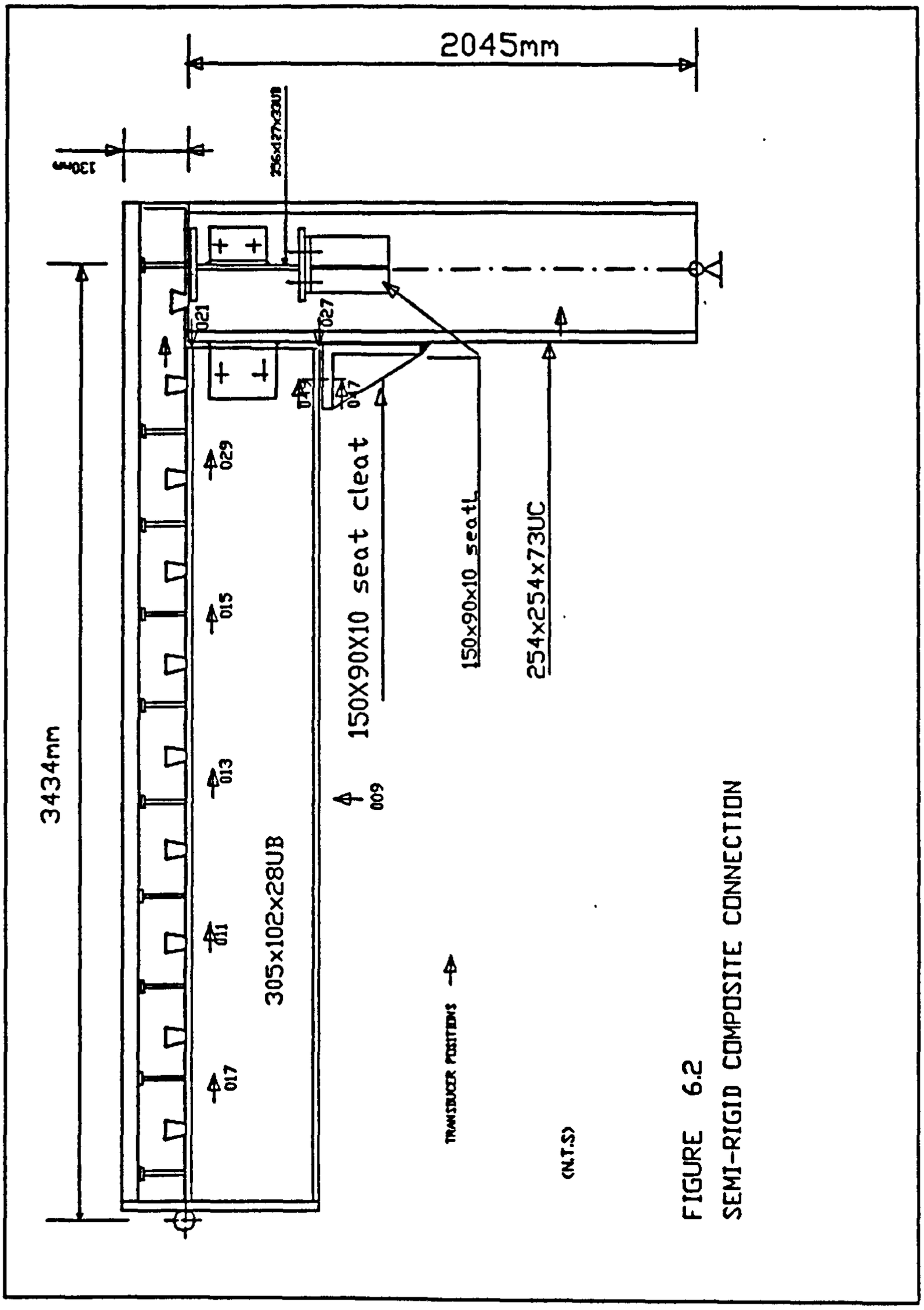

(N.T.S)

FIGURE 6.2
SEMI-RIGID COMPOSITE CONNECTION

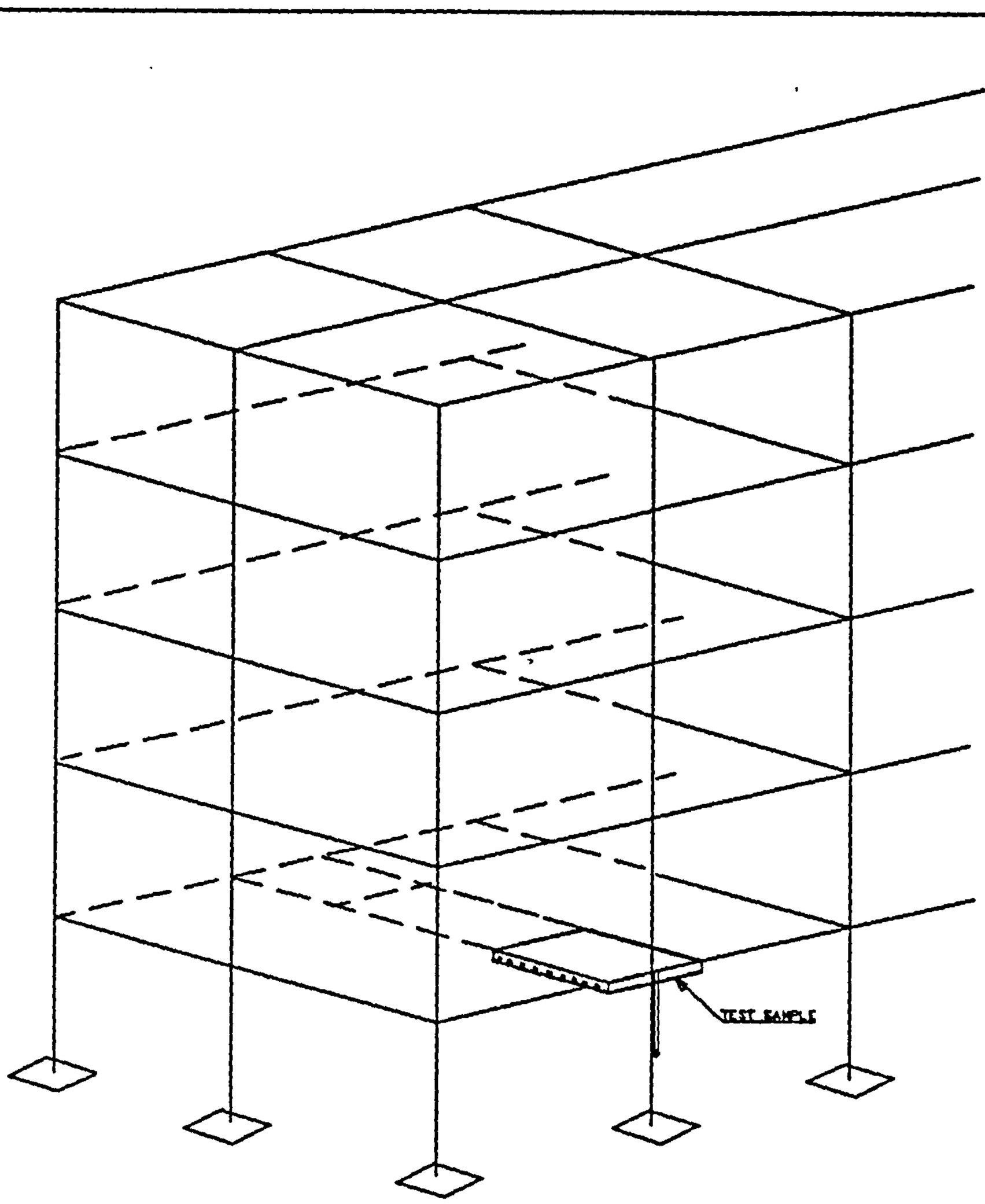

FIGURE 6.3

TEST PIECE POSITION IN A TYPICAL COMPOSITE BUILDING

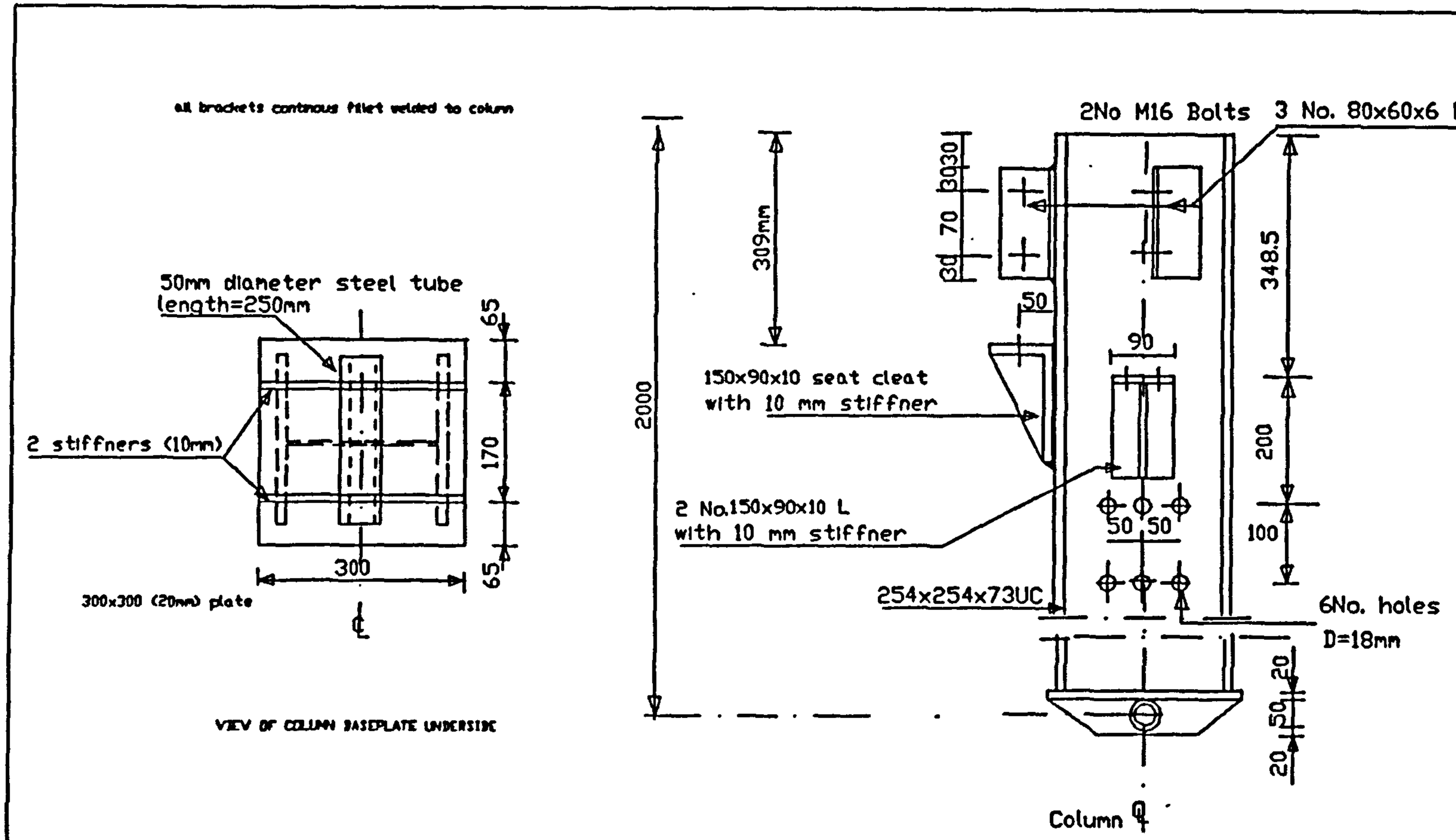

FIGURE 6.4

TEST JOINT COLUMN DETAILS

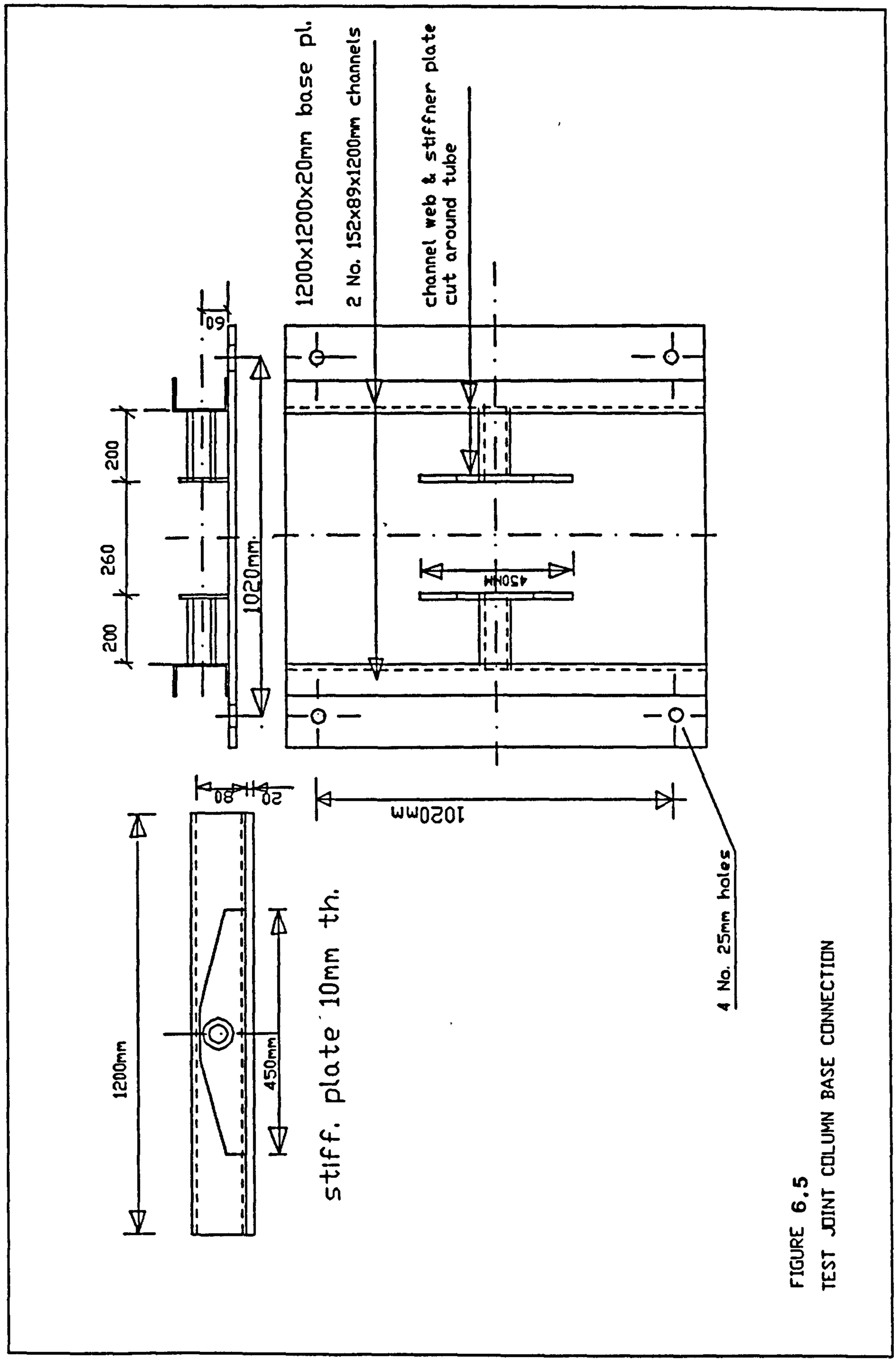

FIGURE 6.5
TEST JOINT COLUMN BASE CONNECTION

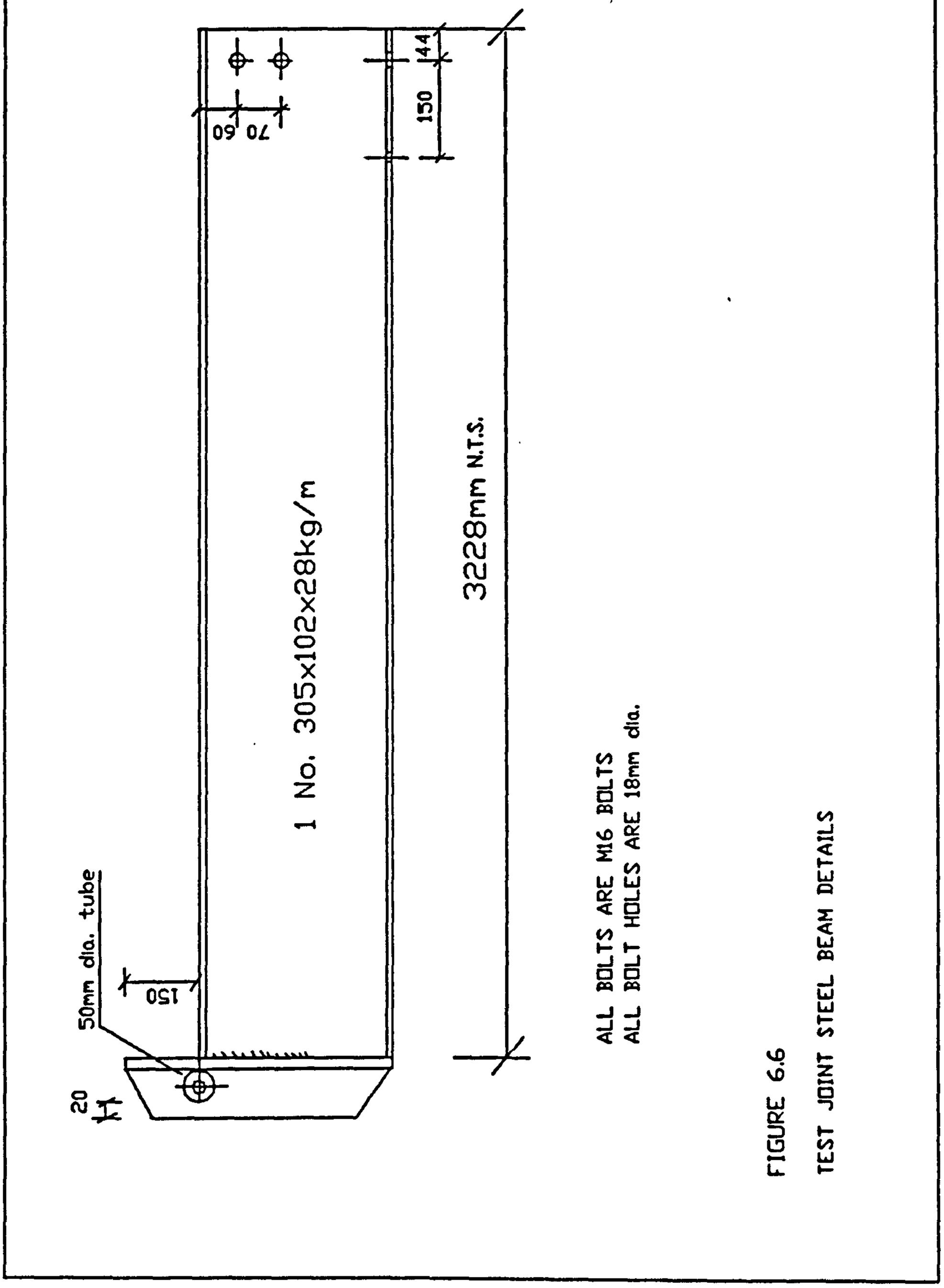

FIGURE 6.6

TEST JOINT STEEL BEAM DETAILS

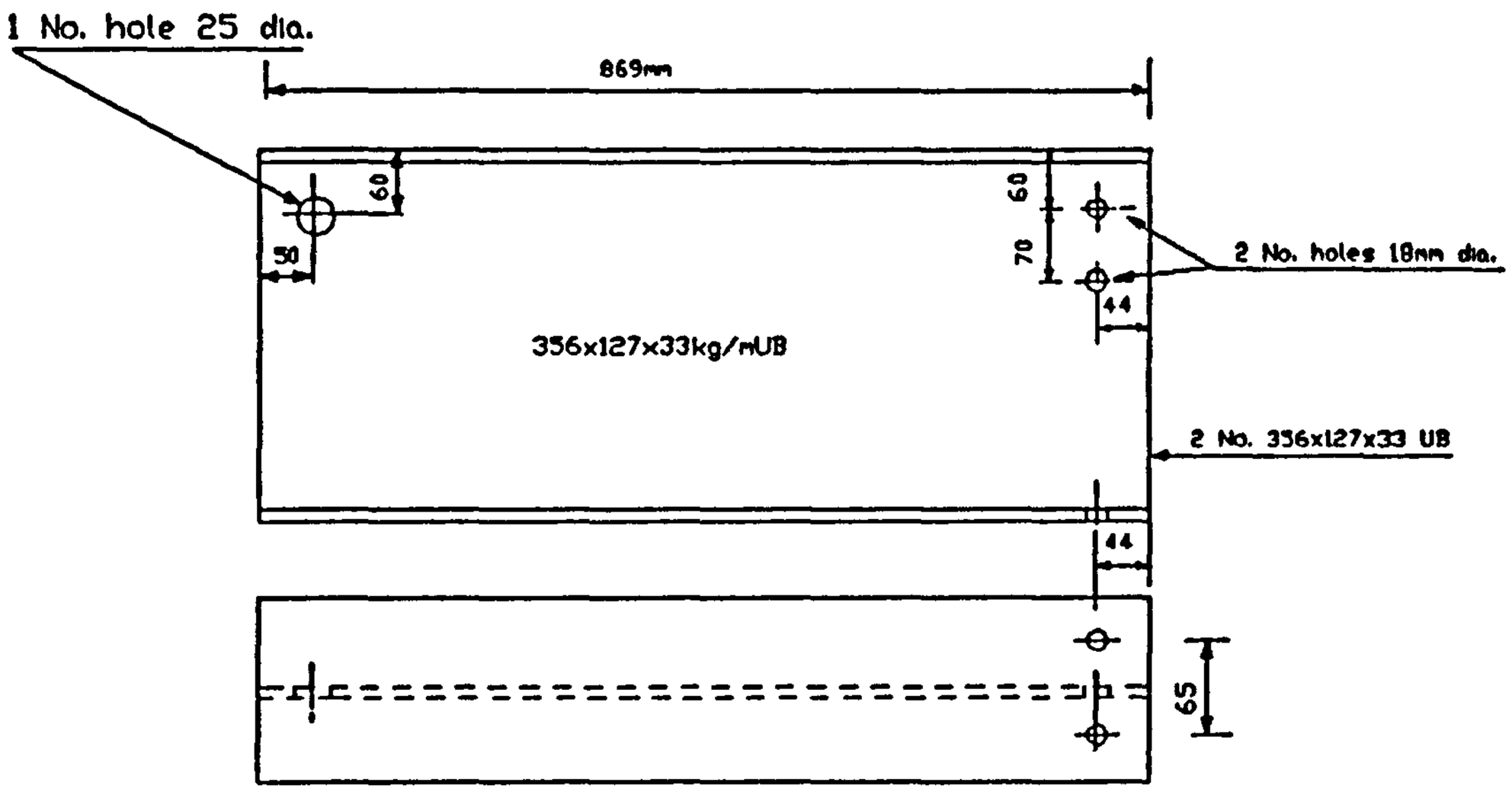

FIGURE 6.7

TEST JOINT STUB BEAMS

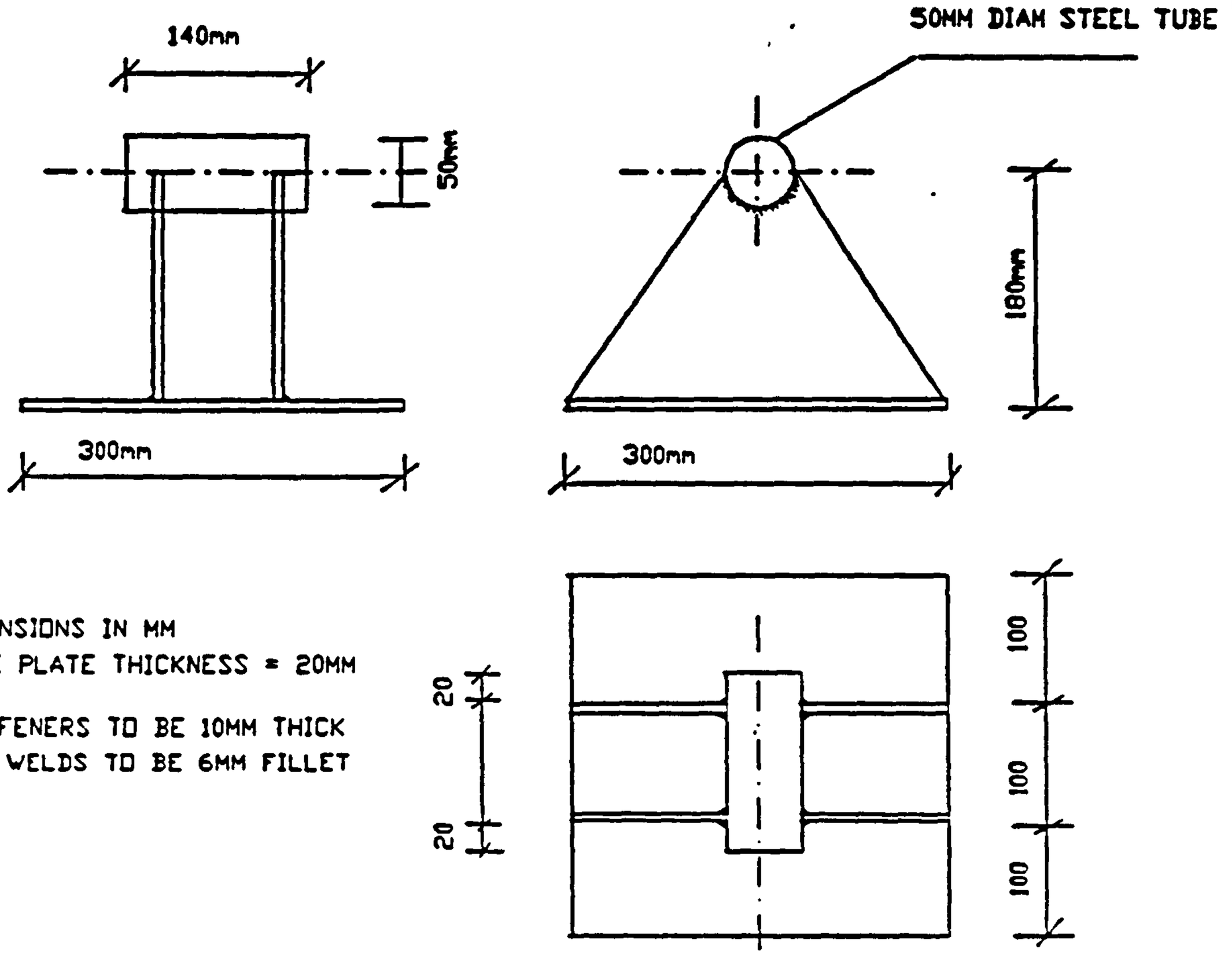

DIMENSIONS IN MM
BASE PLATE THICKNESS = 20MM

STIFFENERS TO BE 10MM THICK
ALL WELDS TO BE 6MM FILLET

FIG. 6.8: TEST JOINT LOADING JACK CONNECTION

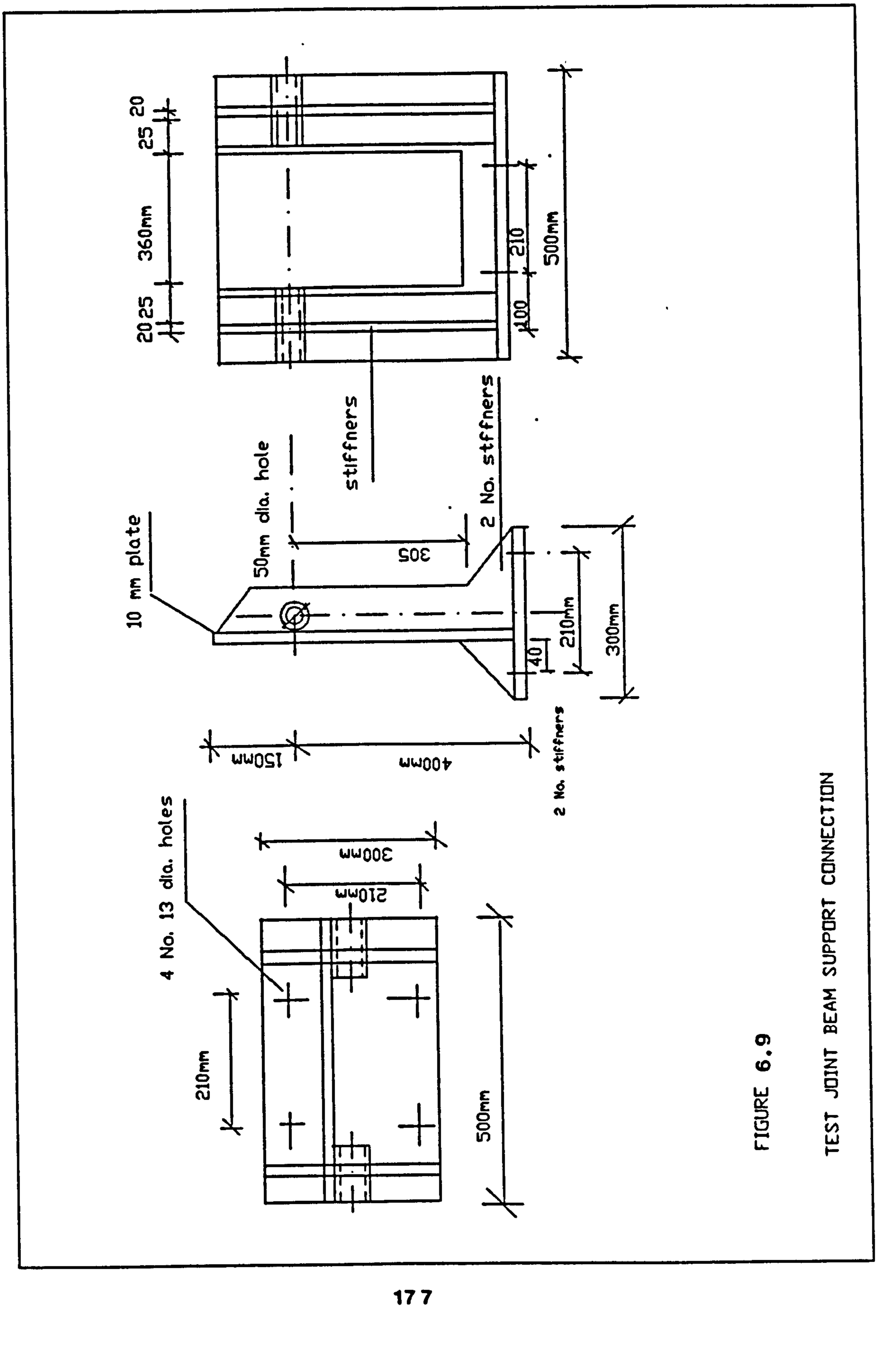

FIGURE 6.9 TEST JOINT BEAM SUPPORT CONNECTION

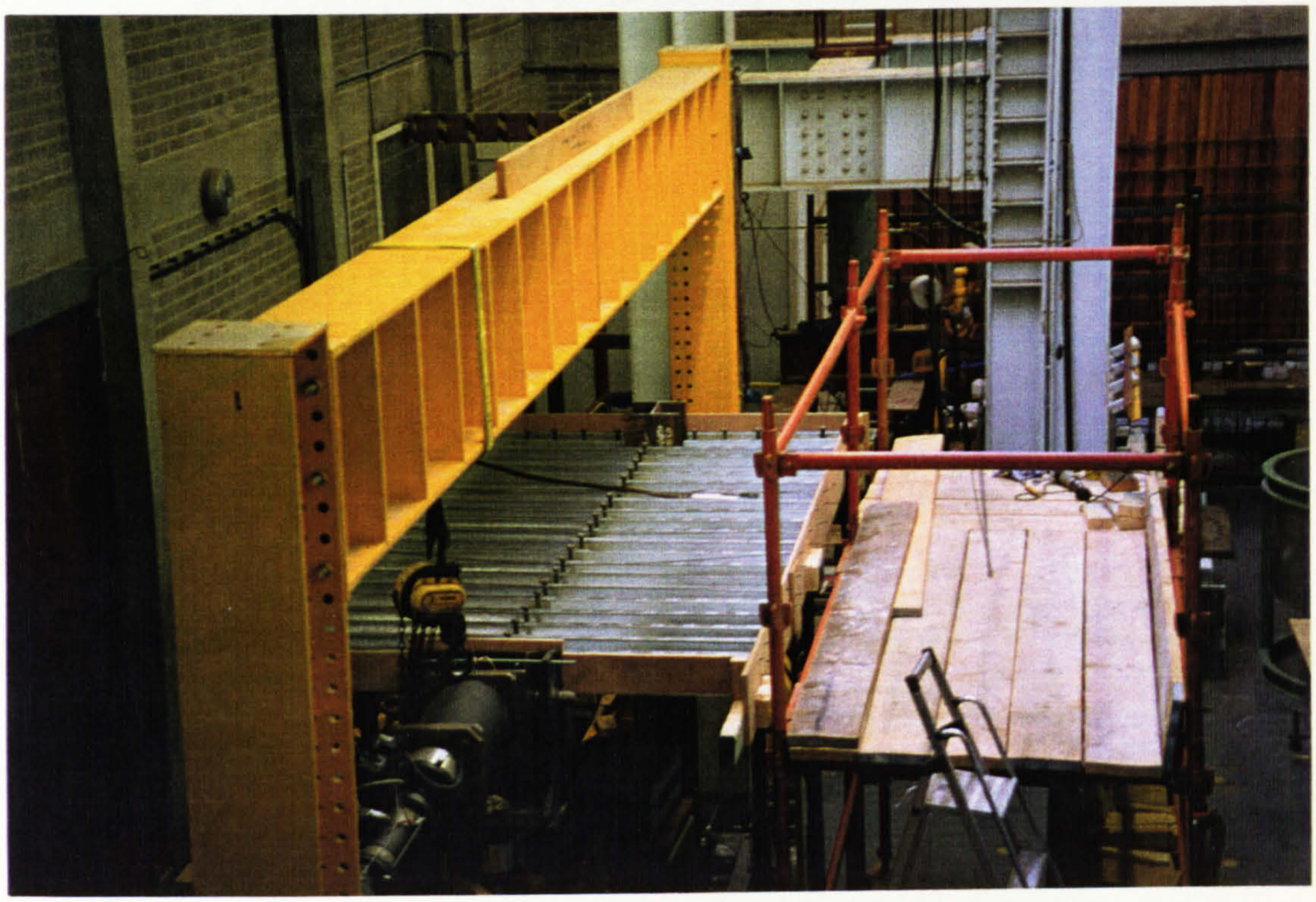

Plate 6.1: TEST PIECE UNDER CONSTRUCTION

Plate 6.2: COMPLETED TEST SPECIMEN

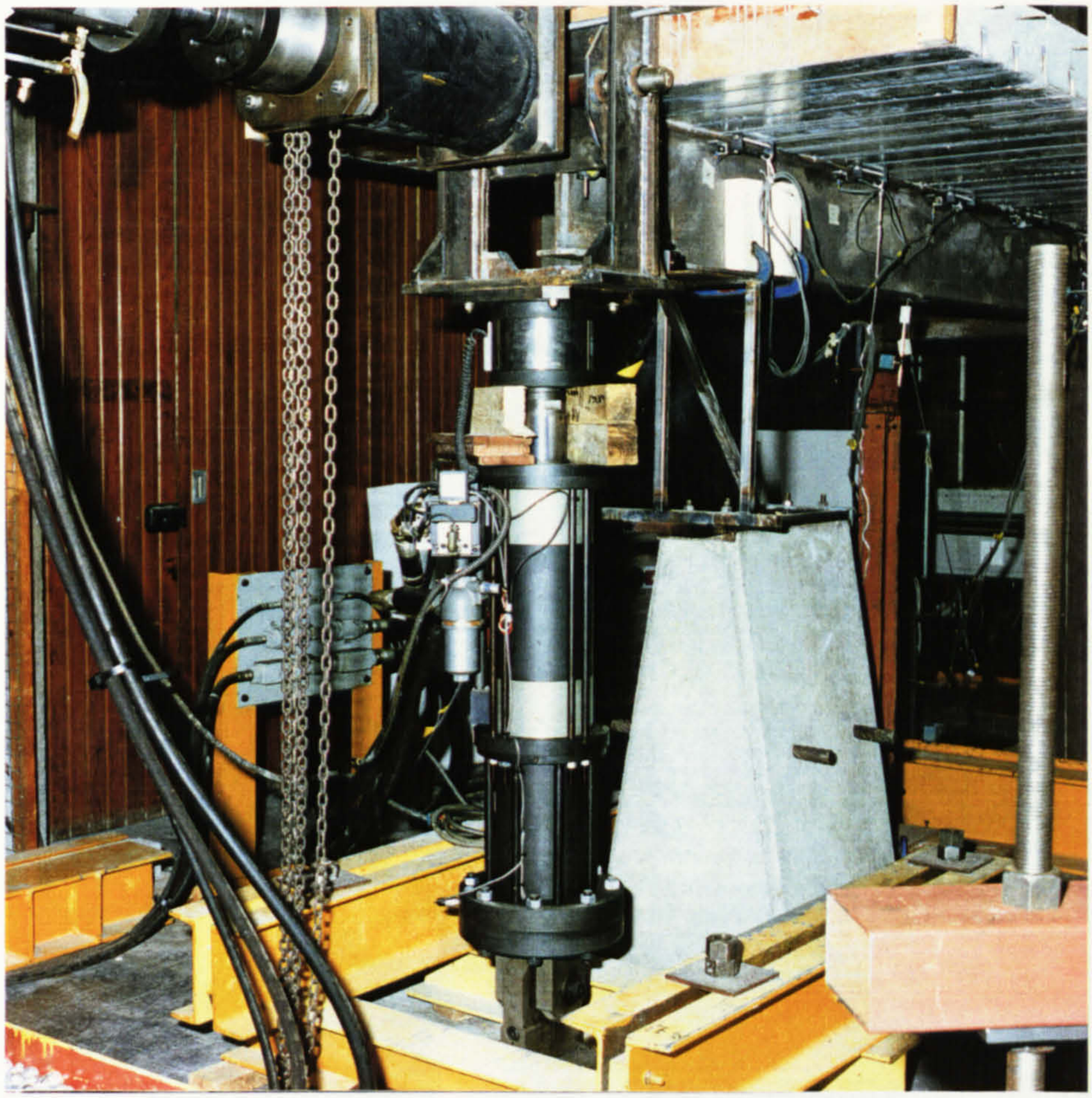

Plate 6.3: HYDRAULIC JACKS

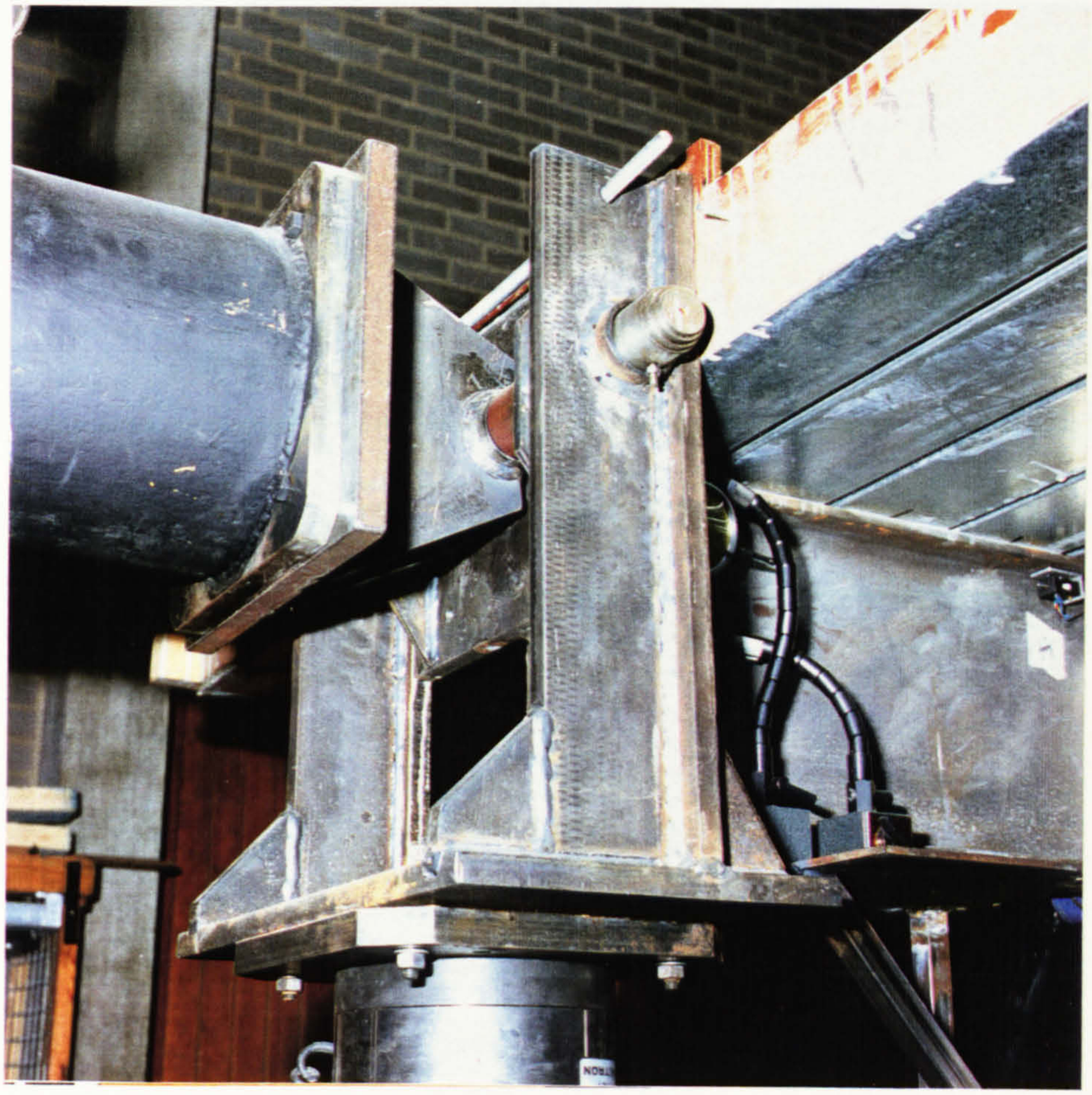

Plate 6.4: BEAM END HINGE

Plate 6.5: SLIP MEASUREMENT

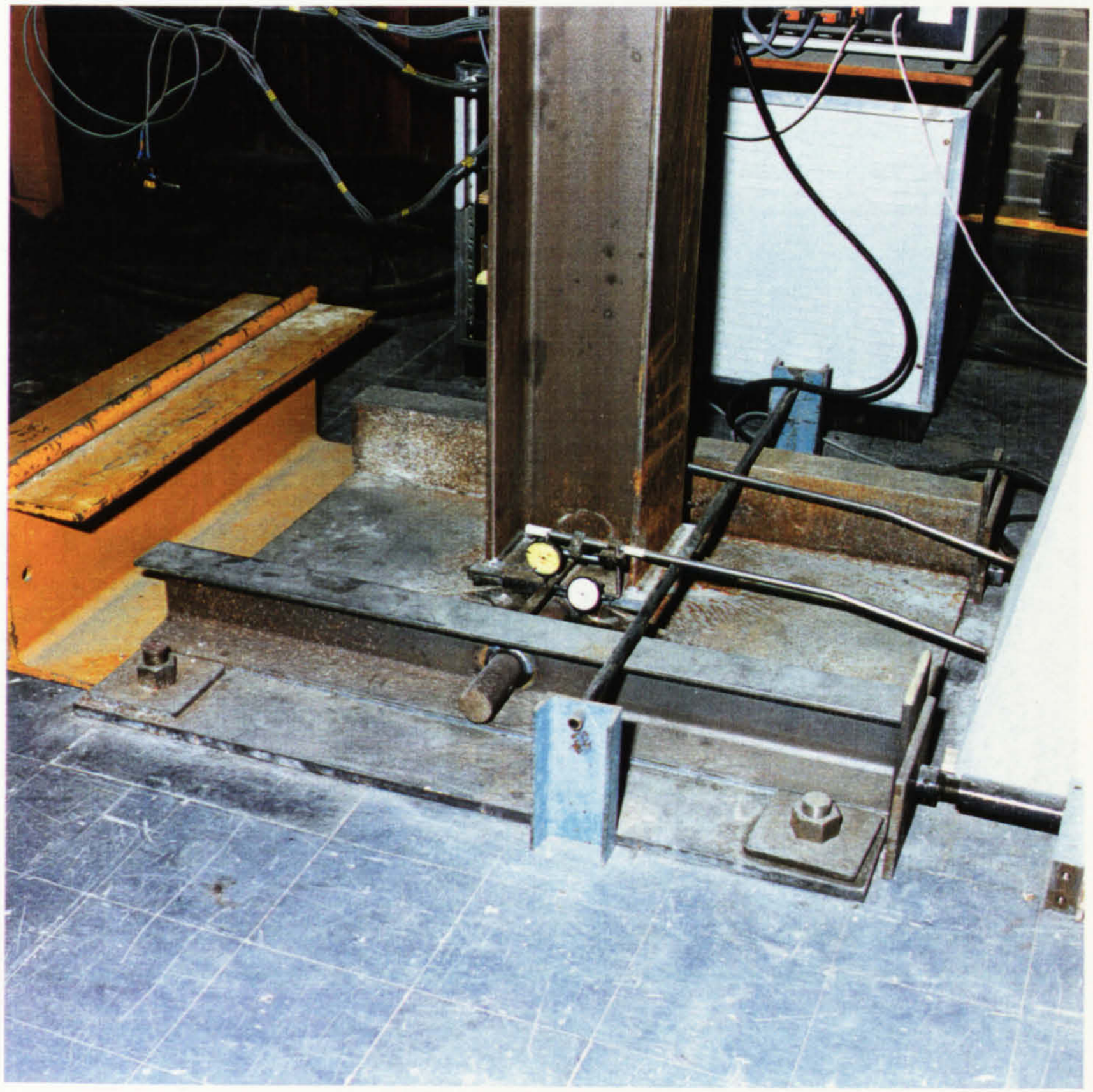

Plate 6.6: COLUMN BASE

Plate 6.7: CONNECTION WITH WELDED SEAT CLEAT

CHAPTER SEVEN

EXPERIMENTAL RESULTS

7.1 Introduction

The main objectives of the experimental work were to determine the accuracy of the numerical predictions and to investigate, without the expense of experimental tests, various options for increasing the lateral stiffness of the composite frame.

The lateral load per unit deflection of the frame was used as the measure of its lateral stiffness. These deflections are termed positive or negative, to represent the lateral sway for closing and opening moments respectively.

It is important to bear in mind that moderate lateral deflections are not dangerous but they are compounded by moments arising from the P-δ effect over a number of storeys. Deflection limitation minimises damage to the non-structural components. It is also required to avoid any objectionable vibration. Safety requirements are controlled by stress calculations. The maximum deflection of a simply supported beam according to BS 5950:1 due to imposed loads, is given as 1/360 of the span. This value is equivalent to 1/180 of the length of a cantilever. The BS also states that in a single storey building, the lateral deflection must not exceed 1/325 of its height [56], while the allowable drift specified by UBC and ANSI is 0.5 %.

The main test results for the frame are given in Figure 7.1 through to Figure 7.16. The applied horizontal loads were equal to maximum wind loads which would affect a typical five storey building at its first storey level anywhere in the U.K.

Before loading, all the dial gauges were inspected to ensure that they were correctly and securely positioned and an initial set of readings was recorded. The

transducers were also checked and scanned.

Care was taken to keep the beam loaded end at the same vertical position. After each load step, a complete set of readings was taken. This included transducer readings, dial gauge measurements and the values of the vertical and horizontal applied loads. Vertical and horizontal deflections of the two jacks together with the loads were recorded from the control panel of the testing machines.

The test was carried out by gradual application of lateral loads which continued until a predetermined load or lateral deflection was reached. Load increments of 2kN, or 2.5mm horizontal deflection, were applied and limited by whichever occurred first. Wedges were used to keep the vertical jack in position after each test session to ensure a subsequent start from the same point. During the test, some dial gauges went out of range and were reset when necessary to restore their effectiveness.

7.2 Steel Frame Load Response

Initially, the steel frame alone was loaded laterally to 9kN. This load represents the maximum wind load which may develop on a steel frame taking into account that the exposed area is the sum area of all steel beams and columns only. Loading was under displacement control. This means that the expected displacement could not be exceeded if the stiffness deteriorated suddenly.

7.2.1 Load-deflection Curves

The load-lateral deflection curve for the steel frame is shown in Figure 7.1 from which it is clear that large lateral deflections resulted from relatively small loads. The frame had a high initial lateral stiffness up to a load of 3kN which resulted from the joint friction force and is seen as a steep part of the curve near the origin. The initial response represents a stiffness which degraded as soon as bolt slippage occurred. Slip took place early since the slip capacity of the connection is

limited, as a result of poor tightening and lack of surface friction preparation. The curve is characterised mainly by an intermediate plateau which may be attributed to the slip of the cleat bolts.

The last part of the curve indicates higher stiffness which may be attributed to direct bearing of one or more of the seat cleat bolts.

The same trend was recognised in the second load cycle, with an even lower lateral stiffness during slippage of the bolts which may be explained as a result of the loss in the friction force due to lower surface roughness.

Luckily, even if storm force winds do occur, the probability of long exposure to wind for an incomplete frame is limited. Frame strength greatly exceeds that required at this stage, so any lateral sway can be easily restored before construction proceeds.

7.2.2 Non-linear Effects

(a) Bearing Stress

After the first load cycle, all bolts were removed and inspected. Bolt holes were also traced and visually inspected. It was thought that the use of set screws with their threaded shanks may have led to an increase in the lateral sway. The sharp threads of set screws, which are harder than the structural steel sections, may have cut into or recessed the surrounding plates. From the slight marks observed, it was concluded that this factor was not significant. Nonetheless, all set screws were subsequently replaced by bolts with plain shanks, even though these are becoming less common in practice. Overlapping of the steel plates was also observed. This showed that lack of fit in such steel frames may be expected to approach the 2mm hole tolerance, mainly due to positioning errors and distortion during cleat welding.

(b) Construction Tolerance Changes

Despite the large lateral deflection, no contact between the end of the steel beam and the steel column was observed. This meant that transmission of forces between the beam and the column by bearing was not imminent and should not be expected before the occurrence of unacceptable large sway. Slip of the seat cleat bolts occurred very early. The bolts were hand-tightened and consequently their shear slip resistance was small.

(c) Minimising the Bolt-hole Clearance

The movement of the bolts inside their holes, which is a result of the clearance, proved to have a major effect on the lateral displacement of the frame. The 2mm clearance in each bolt position may have led to a maximum of 4mm clearance in either direction within the lever arm of the bare steel connection: 2mm in the lower flange hole plus 2mm in the opposite sense for the web cleat hole. When bolts are centralised, the total clearance will be $\pm$2mm instead. In the steel frame, the movement of the bolts led to a sway of about 40mm. The ratio between the lever arm of the frame and the moment lever arm of the connection was 2045/204=10.02, which is much the same as the ratio between the frame deflection and bolt clearance of 40/4=10. It is concluded that any change in the bolt-hole clearance will have an effect on the lateral deflection equal to its value multiplied by about 10 in this case.

Reduction of the bolt-hole clearance was thought to be possible. The reduced clearance would lead to an earlier transfer of forces by bearing.

7.3 Decked Frame Load Response

The frame was re-tested after shot-fired fixing of the profiled steel sheets. The load-lateral deflection curve for this test is shown in Figure 7.2 from which it is clear that the first part of the curve again indicated a relatively stiff behaviour.

The curve became shallower at about 3.8kN. The frame showed another severe loss in its lateral stiffness close to 4.5kN. At 7kN, the frame started to regain lateral stiffness, which once more may be attributed to the bearing of the bolts. It seems that the load-lateral deflection curves for the decked and the bare steel frames are very similar.

Compared with the bare steel frame, the decked frame showed an insignificant increase in the lateral stiffness after the deck being fixed. This is clear from Figure 7.3. In fact, the additional area of steel rib exposure leads to a marked increase in the potential lateral load. In the previous case the lever arm was the distance between the top bolt of the web cleat to the soffit of the steel beam. Although the connection lever arm became longer, becoming the length between the deck and the soffit of the steel beam, the lateral stiffness of the frame was not significantly increased. This lack of increase in stiffness was because of the orientation of the steel deck, perpendicular to the main steel beam. The low resistance to transverse deformation of the first re-entrant profile above the joint was the reason for the lower restraint than expected at the beam's top flange level.

Again, the probability of long exposure to extreme wind for an incomplete frame is limited and any resulting lateral sway could be recovered if necessary.

7.4 Composite Frame Load Response

Testing of the composite frame was carried out in five stages. At first, the frame was tested with two grade 8.8 bearing bolts fixing each of the seat and web cleats. In the second stage, the two seat cleat bolts were tightened to their proof load. Thirdly, these two bolts were replaced by two HSFG bolts. The fourth case was to fix the beam's lower flange to the seat cleat by four HSFG bolts two of which were in double shear as explained in 6.7.2. Finally, the seat cleat was welded to the steel beam. This order was adopted to start with the simplest and cheapest practical option and proceed towards the maximum attainable lateral stiffness.

7.4.1 Composite Frame with Bearing Bolts

The frame tests commenced when the concrete compressive strength was 30N/mm^2. The maximum load in the first cycle of loading was 10kN in both directions, starting with the closing moment. Permanent reactions were necessary to return to the original geometrical position, which meant that unloading was associated with residual stresses. This may be attributed partially to the semi-plastic behaviour of the concrete slab but remains mainly due to bolt slip and subsequent reverse friction.

(a) Load-deflection Curves

The load-lateral deflection curve is shown in Figure 7.4 in which the response of the composite frame with 8.8 bearing bolts in two complete load cycles is shown. In the first one, and up to 10kN in both directions, the frame was stiff and the curve indicates linear behaviour. The maximum lateral deflection was 7mm. In the second load cycle, the load was increased to 15kN in both directions. In the positive direction, the two successive load cycles had similar load-deflection curves and the loading branches for both cycles were almost identical. The two unloading branches were parallel to each other and to the initial loading curve.

At a load of -12kN, the frame started to show sudden increase in the deflection which was not accompanied by an expected increase in the applied load. This indicated a loss in the lateral stiffness which again may be attributed to the slippage of the seat cleat bolts. The unexpected shape of the curve after that may be due to the unpredictable nature of the friction force.

The lateral deflection of the frame at 15kN was 12.5mm in the positive direction and was -20mm at -15kN. Since these values were already more than the target value of 6.66mm, the load was not increased beyond 15kN, thus avoiding permanent excessive damage of the concrete slab. Further modifications were planned to increase the lateral stiffness of the frame. Consequently, retaining the

slab integrity was essential.

Graphs of load against lateral sway were drawn for the three dial gauges positioned at the point of load application, the upper and the lower points of the joint. as expected, the three graphs have the same trend, as seen from Figure 7.5.

(b) Concrete Cracks

A crack started at the interface of the column flange and the concrete slab to a position marked **1** in Figure 7.6 which shows the development of cracks in the concrete slab through all the load cycles. The first crack started at a load of 9.96kN and it was very thin and hardly visible. A marker pen was used to locate the crack and the line was drawn beside it in order not to obscure it. At 14.5kN, the same crack spread right across to mark **2**. When the load was reversed, and at -14.5kN, another crack was recognised which penetrated most of the slab depth from its soffit.

The steel deck started to "ping" at a load of 7.22kN onwards to 9.96kN. This noise recommenced again at a load of -6.74kN and there were subsequent periods of noise and silent during the test. "Pinging" may be a result of local deformation and debonding of the decking.

The stiffness of the uncracked slab has a significant influence on the initial stiffness of the composite connection. Sudden reduction in the connection lateral stiffness at relatively low loads might be attributed to the loss of the stiffness contributed by the slab when cracks first appeared.

(c) Construction Tolerance Changes

The curve of the horizontal load-versus movement of the end of the steel beam relative to the column flange is shown in Figure 7.7 from which it is clear that slippage of the seat cleat bolts started at a relatively small load. It is also clear that

this curve has the same shape as the load-deflection one, which indicates the causal relation between the seat cleat slip and the lateral stiffness of the composite frame. As expected, movement of the lower flange of the beam was greater than that of the upper flange. This shows the effect of the presence of the concrete slab on the performance of the connection in acting as a fixed location pivot during rotation.

(d) Load-slip Curve

The load-slip curve shown in Figure 7.8 is based on the readings of the nearest transducer to the column, which was expected to have the maximum relative movement between the concrete slab and the steel beam. The curve is characterised by small values associated with the closing moment and relatively larger, although still very small values, in the opening moment direction. Maximum slip was about 0.1mm which corresponded with the loss in the lateral stiffness.

7.4.2 Comparison of Bare Steel and Composite Frames

Figures 7.1 and 7.4 respectively show the load-lateral sway curves for the bare steel frame and the composite one. From these figures, the increase in the lateral stiffness of the frame as a result of the presence of the composite slab is evident. This increase in the lateral stiffness of the frame is attributed to:

(1) A longer lever arm which is now the distance between the seat cleat and the slab reinforcing bars.

(2) The presence of the concrete slab, which limits the relative compression movement between the upper flange and the steel column.

(3) Instead of the web cleat bolts, the reinforcing bars resist tensile loads in the top of the joint.

Despite the increased stiffness, the lateral deflection was still larger than the target value of 6.66mm. This meant that still further modification needed to be introduced for stiffening up the frame.

7.4.3 Composite Frame with Fully Tightened Bearing Bolts

Use of fully tightened, grade 8.8 bearing bolts was considered next. This explored the performance of the connection with bolt slippage prevented as much as possible without resorting to the use of HSFG bolts.

The seat cleat bolts were tightened to their proof strength to reduce their potential slip. The two seat cleat bolts were tightened with an adjustable torque wrench to a torque of 28kgf.m which was calculated to correspond to the bolt proof strength. The load-lateral deflection curve of the frame in this case is shown in Figure 7.9 from which it is seen that the lateral stiffness of the connection increased when compared with the same connection with its bolts tightened to a torque of only 14kgf.m. The maximum stiffness is still not maintained throughout the target load range.

The intersection of the loading part of the curve with the unloading part is due to a vertical loading. There was an uncorrected accumulation of vertical deflections at the point of load application during part of this load cycle. The value reached was about 1.5mm before it was recovered by applying vertical load.

7.4.4 Composite Frame with Two HSFG Bolts

Slippage of the seat cleat bolts was the reason for the persistent loss in lateral stiffness. As HSFG bolts are designed to transfer loads by friction, they were expected to minimise this slip. The two seat cleat bearing bolts were therefore replaced by two HSFG bolts, grade 10.9. The web cleat bolts were not replaced for two reasons: Firstly, because they were close to the neutral axis of the connection, and consequently their effect was expected to be minimal. Secondly,

being in a very constricted position, their site inspection would be difficult.

(a) Load-deflection Curves

The load-lateral deflection curve for the frame with two HSFG bolts is shown in Figure 7.10. Comparing with the bearing bolt results, it is clear that the lateral stiffness increased with the use of HSFG bolts. The load was applied in the negative direction to -16 kN at which the sway was about 10mm. It was concluded that two HSFG bolts were still not sufficient to achieve the required stiffness. Because the edge cracks developed to the full slab depth, the load was not increased beyond 15 kN to avoid any further damage to the concrete slab.

(b) Construction Tolerance Changes

The deflection of the steel beam flanges relative to the column flange are plotted against the applied horizontal load in Figure 7.11. While the maximum deflection for the lower flange was 1.0mm, the upper flange moved just 0.125mm in the opposite direction. From these two readings, it was concluded that the effective centre of rotation of the connection lies 34.3mm below the top flange of the steel beam.

7.4.5 Composite Frame with Four HSFG Bolts

An additional plate was welded to the column flange on each side of the beam. This enabled the two bolts used in the previous test to act in double shear, and a further two HSFG bolts in single shear to be added.

It was recognised that the crushing washers were not completely deformed under the correctly applied torque. This means that the visual control method for the tightening of HSFG bolts is not very accurate, but is conservative.

Use of dimpled crush washers with the HSFG bolts in this case may have led to a loss of contact. When the bolt was tightened, the washers were not deformed to provide full contact. Consequently, only the three points or small rectangles were in contact with the steel plate. The major finding of the use of HSFG bolts is their readiness to slip earlier than expected when the prying moment was repeatedly reversed.

In this frame, two additional transducers were used to measure the movement of the seat cleat bolts nearest to the column. Measurements of the bolt head and nut were taken relative to the steel beam.

(a) Load-deflection Curve

The four bolts were tightened to 0.85 of their proof strength. The resulting load-deflection curve is shown in Figure 7.12, from which it is clear that despite the linear behaviour of the frame when loaded in the positive direction, its overall sway was still larger than the required value, and the load was just two thirds of the target load. In the negative direction, the lateral stiffness, indicated by the lateral deflection, was also lower than required even before slippage of bolts.

This cycle of loading was repeated later (next day) with the load increased to 30kN in the positive direction and to 24kN in the negative direction. The lateral sway at 28kN was about 12mm excluding the movement of the column foot support. This means that the target value of 6.66mm was still far exceeded. This may be attributed to the continued slippage of the seat cleat bolts which is clear from figure 7.13.

No bolt slippage was observed in the positive direction up to a load of 20kN. When the load was reversed, slippage started at a load of -17.5kN. The head of the bolt nearest to the column moved 0.38mm at a load of -20kN. It was also concluded that the lateral stiffness of the frame depends critically on the minimization of the relative movement between the steel column and the steel

beam. Although the slip load of the group of bolts used was calculated to be 150 kN, which is almost the same predicted value for the shear force of 1575kN, the loss of a significant percentage of the friction force after the first load reversal appears to be the reason for not achieving the full calculated load from these bolts without slippage.

(b) Concrete Cracks

This load case was characterised by the propagation of the previously recognised cracks to new positions marked 4, 5, and 7. Two new cracks were seen at 27.94 and 29.68kN. The positions of these two cracks was from marks 7 and 8 to the edge of the slab as shown in Figure 7.6.

No severe damage had happened to the concrete except for hairline cracking. The first crack appeared earlier and extended from the column flange tips to the edge of the concrete slab. Its width was changing according to the value of the applied load. Cracks which resulted from the opening moments started at the bottom of the concrete slab and extended to its top. Because of the presence of the steel decking, adequate detection of the start of these cracks and their precise propagation was difficult.

(c) Construction Tolerance Changes

To investigate the changes in the gap between the end of the steel beam and the steel column flange, the load-end gap changes' curve was recorded on Figure 7.13. The concentration was on the lower point of this gap. The presence of the concrete slab minimised the movement of the upper flange of the steel beam. The total movement of the lower flange was 2mm while that of the upper flange was only about 0.3mm in the opposite direction. From these two values, the centre of rotation of the connection is 5.45mm below the upper flange of the steel beam.

7.4.6 Composite Frame with Welded Seat Cleat

Welding of the horizontal lip of the seat cleat to the steel beam flange was the final option for increasing the stiffness of the frame. This was postponed until last because it is the most expensive on-site process, and consequently the one highly resisted by designers. The seat cleat was welded to the steel beam as explained in Chapter Six. Compared with bolting, site welded joints are time consuming and expensive. One can argue that the joint in our case is not a fully welded one, but contains a marginal part which is welded. Welding reduces options for alterations and remedial work. Purpose made safety enclosures in which to produce these overhead welds may be essential and would require suitable weather protection. Site welding may also involve considerable preliminary work, such as edge preparation. This together with fitting and inspection are further cost factors. Heavy-duty spot welding equipment may be a solution for many of the aforementioned problems.

(a) Load-deflection Curve

The load-lateral sway curve for this welded frame is shown in Figure 7.14 in which it is clear that the stiffness of the frame increased significantly. The maximum lateral deflection within a load interval between -30kN and 30kN was 17mm with the average of 8.5mm. At the specific target load of 27kN, the deflection was 7.65mm. The other advantage of this option is clear from the almost perfectly linear relationship between lateral load and the deflection, showing the elastic overall behaviour of this connection under wind loading.

(b) Construction Tolerance Changes

Welding the upper leg of the seat cleat to the steel beam prevented relative movement between the steel beam and the column. The elastic deformation of the welded parts and of the weldments are very small.

(c) Load-slip Curve

The load-slip curve is shown in Figure 7.15 from which its is clear that the relative movement between the steel beam and the concrete slab is very small. Slip was measured at 5 positions along the beam. Comparisons of slip values at these positions confirm the previous conclusion.

(d) Concrete Cracks

In this modification, slip at the flange-seat cleat interface was prevented by welding. Consequently, no new cracks were observed. From this it is concluded that in the previous load cycles bolt slip accelerated the formation of cracks in the slab and caused consequent loss of stiffness. At this stage, the full section of the concrete slab was cracked and the tensile forces were transmitted by the reinforcement.

(e) Horizontal-vertical Load Relationship

Vertical loads were applied to keep the balance of the frame. External Loads should be in equilibrium. In other words, the following relation should be valid to avoid overturning of the frame:

$$P_h \times H_c = P_v \times L_b$$

where

P_h = Applied horizontal load
H_c = column height
P_v = Applied vertical load
L_b = beam span

$$P_h \times 2045 = P_v \times 3434$$

The relation between the vertical and the horizontal applied loads, in figure 7.16, is fixed for all load sequences, regardless of any changes in the details of the

beam-to-column connection.

7.5 Material Testing

Besides the main test sample, the experimental programme included testing of samples of reinforcing bars, profiled steel sheet and concrete.

(a) Reinforcing Bars

The tensile strength test was carried out on samples cut from the longitudinal and transverse bars of the fabric. The longitudinal bars showed higher yield and ultimate strengths. This may be attributed to work hardening induced during the straightening process of the longitudinal bars. The stress-strain curve for the fabric is shown in Figure 7.17.

It was found that no fracture occurred at any weld point which means that it is not a point of weakness in the bar. The average yield strength was 618.4N/mm^2. Besides the fabric, the same test was carried out on a test sample from the additional reinforcing bar, and its yield strength was found to be 596.8N/mm^2.

(b) Profiled Steel Sheeting

Tensile strength test was carried out on three test pieces of the steel sheet. The average yield strength was 325.58N/mm^2 and the average ultimate strength was 386.04N/mm^2. The stress-strain relationship for the steel sheet is shown in Figure 7.18.

(c) Concrete

The compressive strength values of concrete were 18.6, 23.9, 30.6, 33.1 and 34.2 at the ages of 7, 14, 21, 42 and 90 days respectively. The stress-strain curve of concrete at the age of 21 days is shown in Figure 7.19.

Since the results obtained after 21 days were representative of the lower bound of concrete strength in composite construction, side shuttering was removed and testing of the composite frame started.

Young's modulus of concrete when the composite beam was firstly tested was $1.909 \times 10^4 N/mm^2$. The tensile strength was determined by the indirect tensile strength test and was found $1.85N/mm^2$. The flexural strength of concrete was also determined and was found to equal $3.24N/mm^2$.

7.6 Summary

The load-lateral deflection characteristic was the most important information required for the connection tests undertaken. Some other measurements were also required to justify the performance of the numerical models which were prepared to study the connection in greater detail.

Although only a single sample was prepared, it is felt that with the introduced modifications, it served as more than a single test frame. The results obtained showed some points directly related to the effect of bolt slip on the lateral stiffness of the frame. This factor was the common governing reason for the large sway of the frame. The strength and stiffness of the composite sub-frame were also found to be substantially increased by minimizing the slip of the seat cleat bolts.

The steel frame showed large sway under relatively low loads which indicated that final checking of the under-construction frames would be essential after high winds to restore any deflections. Frame strength greatly exceeds that required at this stage, so any lateral sway can be easily restored before construction proceeds. Compared with the bare steel frame, the decked frame showed an insignificant increase in the lateral stiffness after the deck fixation.

Test results showed that slip of the cleat bolts was the common governing reason for the large lateral sway of the frame. In the composite frame, the strength and

stiffness of the connection were found to be substantially increased by minimizing clearance of the seat cleat bolts.

Introducing some modifications to the connection to increase its lateral stiffness was carried out experimentally as follows:

(1) Increasing the tightening torque of the bearing bolts to its proof strength load.

(2) Use of HSFG bolts which was found to be accompanied by some practical difficulties regarding torque control and bolt inspection. These bolts also showed readiness to slip earlier than expected when the prying moment was reversed.

(3) Site welding of the seat cleat proved to be effective in increasing the lateral stiffness of the connection. It is required to solve some practical problems to facilitate this process on site.

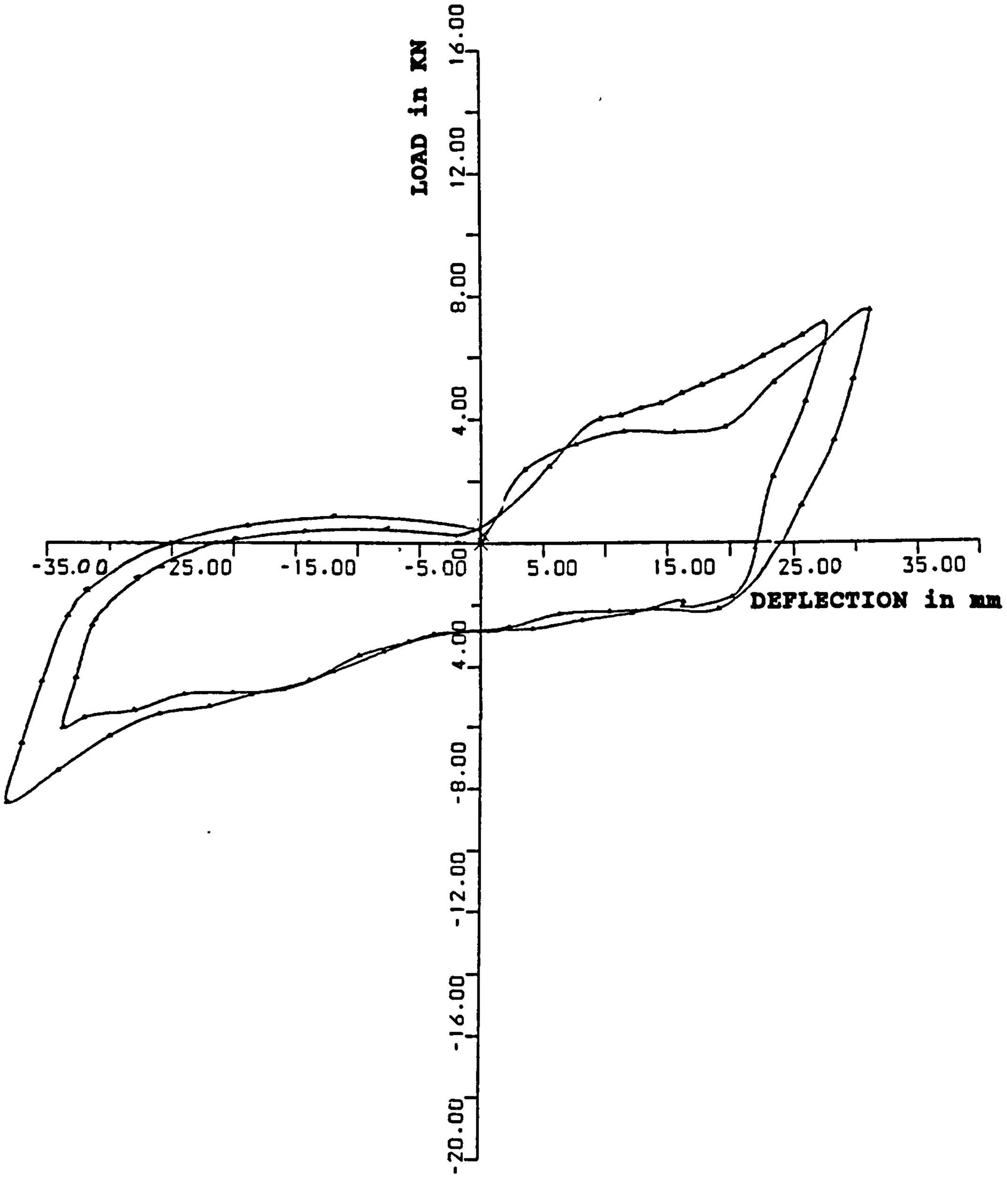

FIGURE 7.1 : LOAD-DEFLECTION CURVE FOR THE STEEL FRAME

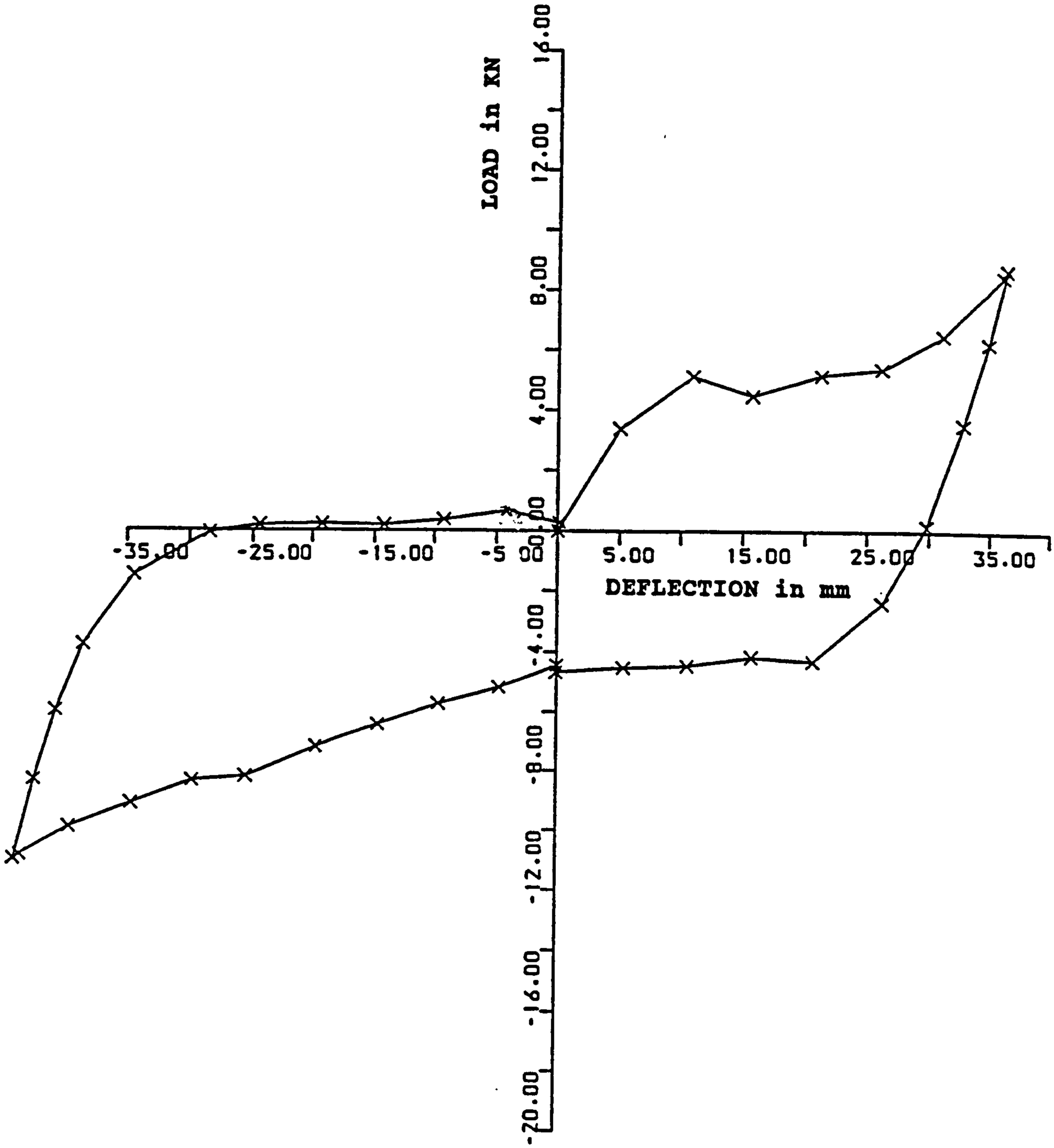

FIGURE 7.2 : LOAD-DEFLECTION CURVE FOR THE DECKED FRAME

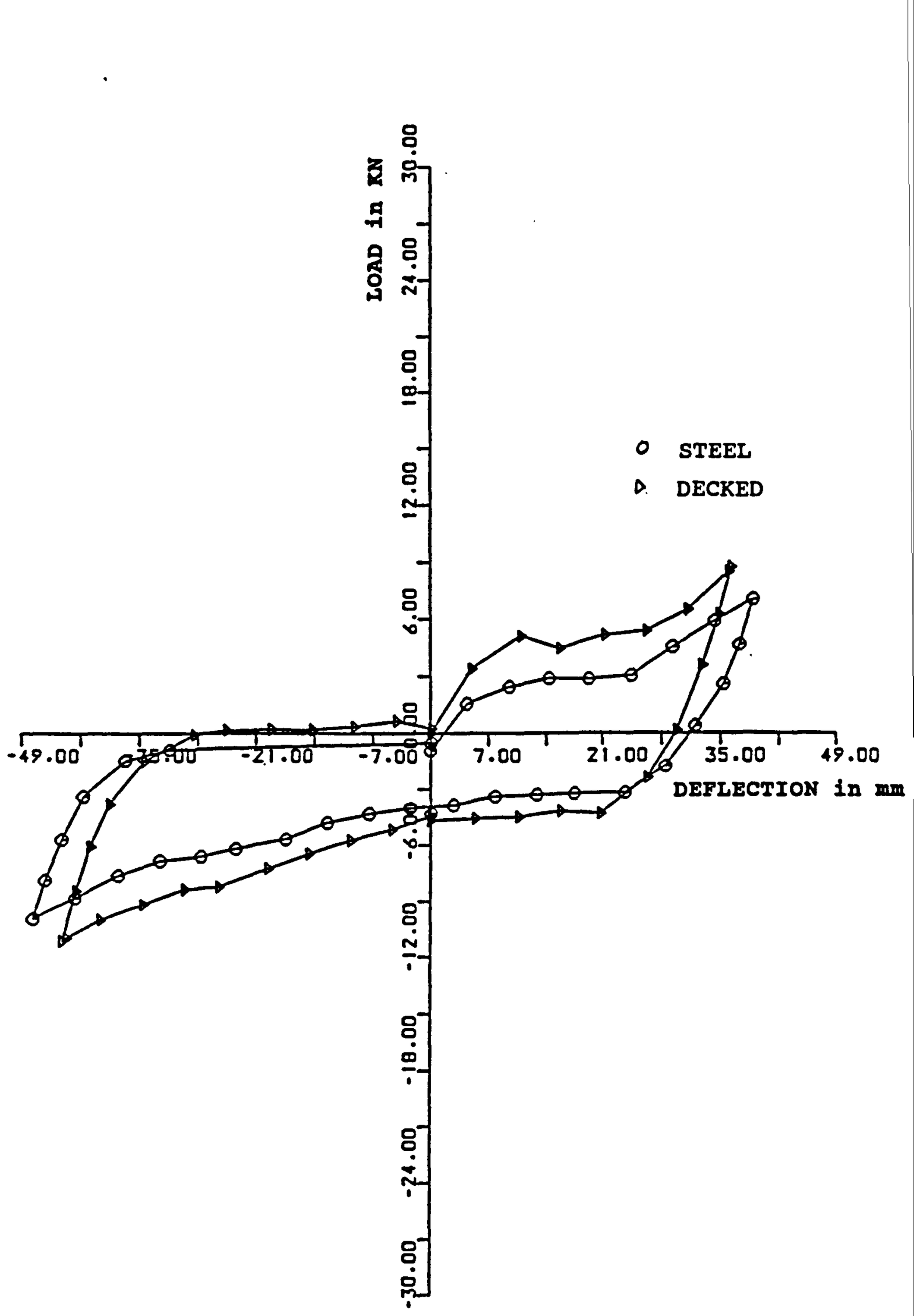

FIGURE 7.3 : COMPARISON OF STEEL AND DECKED FRAMES

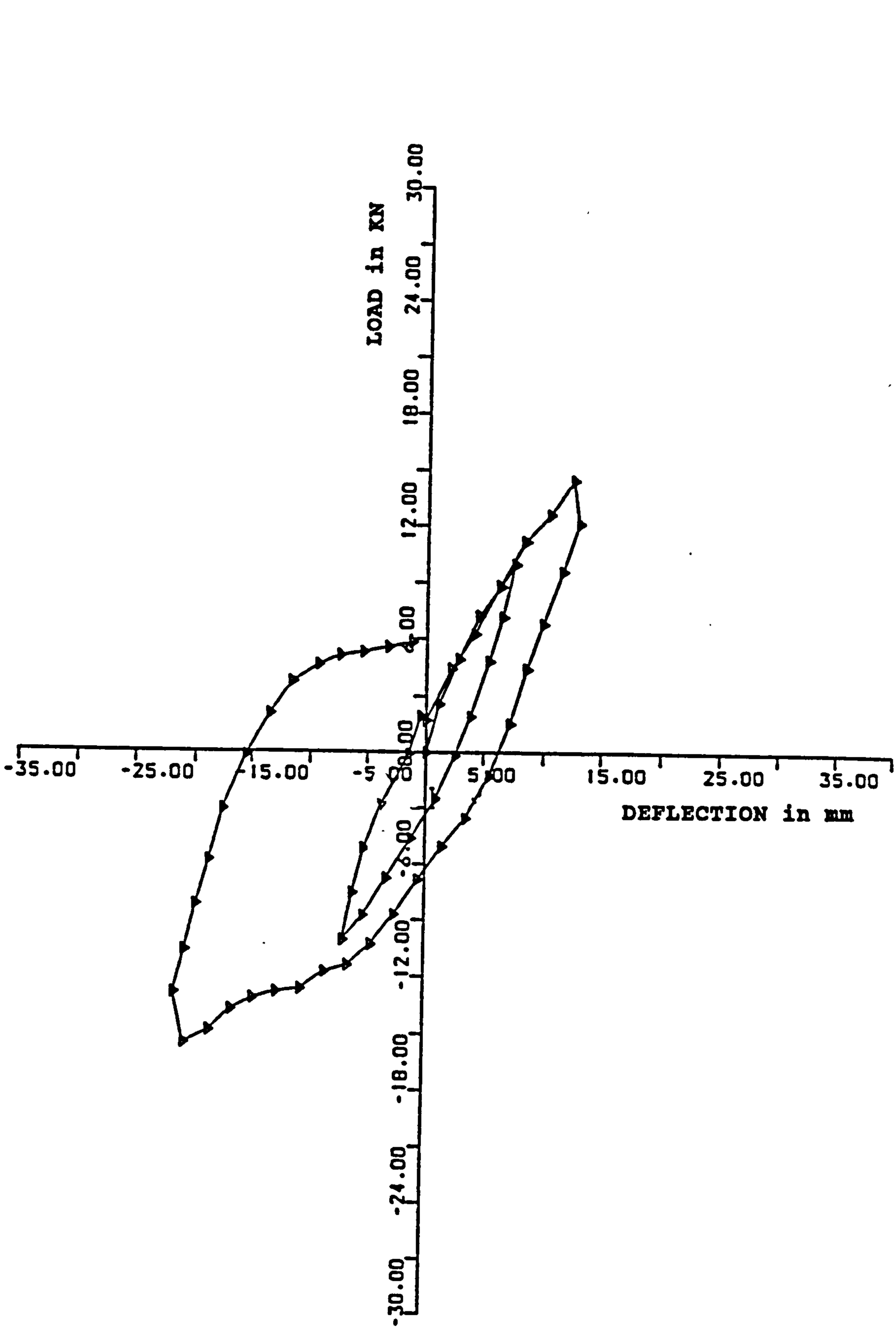

FIGURE 7.4 : LOAD-DEFLECTION CURVE FOR THE COMPOSITE FRAME WITH 8.8 BEARING BOLTS

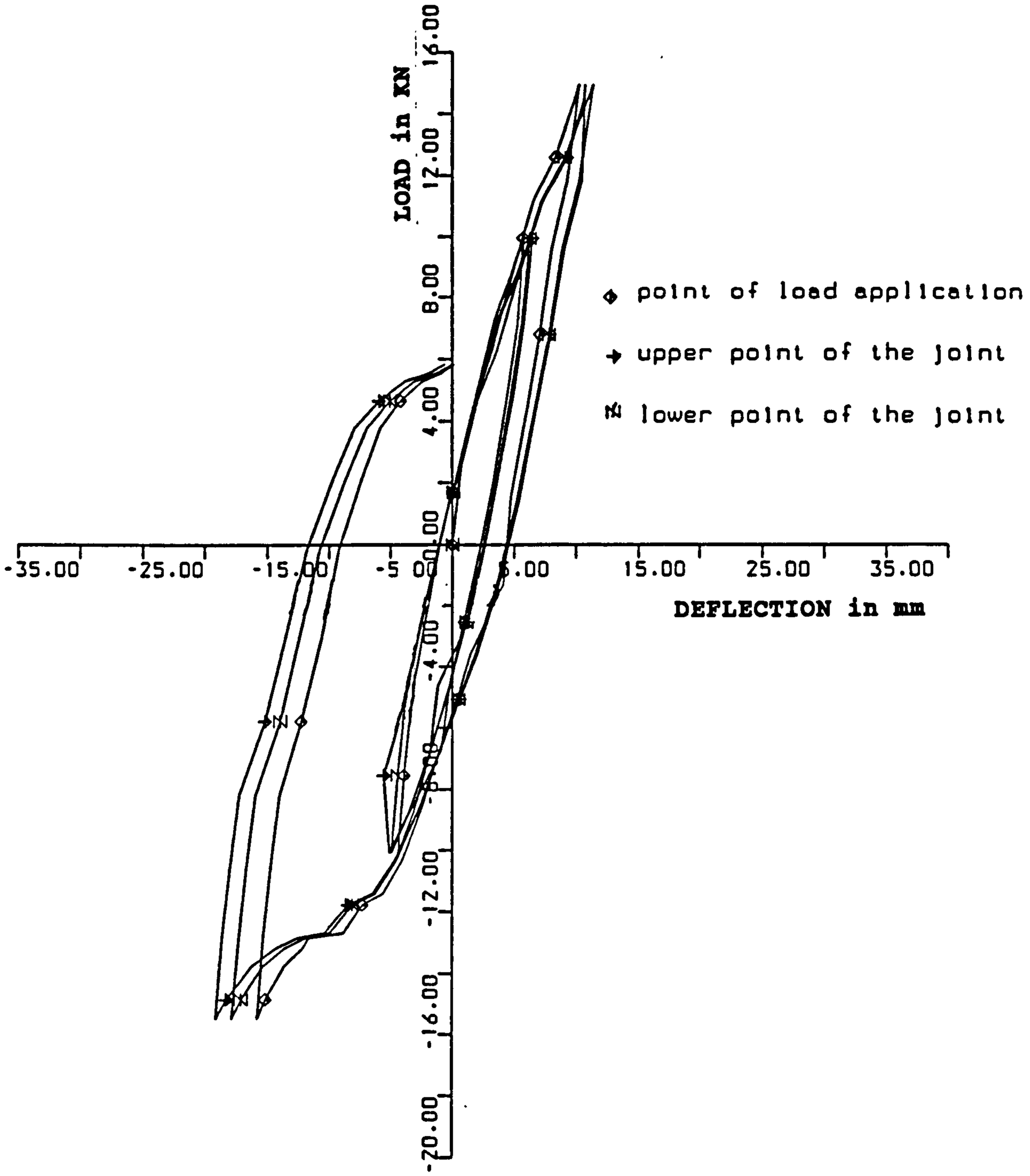

FIGURE 7.5 : LOAD-DEFLECTION CURVES FOR UPPER AND LOWER POINTS OF THE JOINT, COMPOSITE FRAME WITH 8.8 BEARING BOLTS

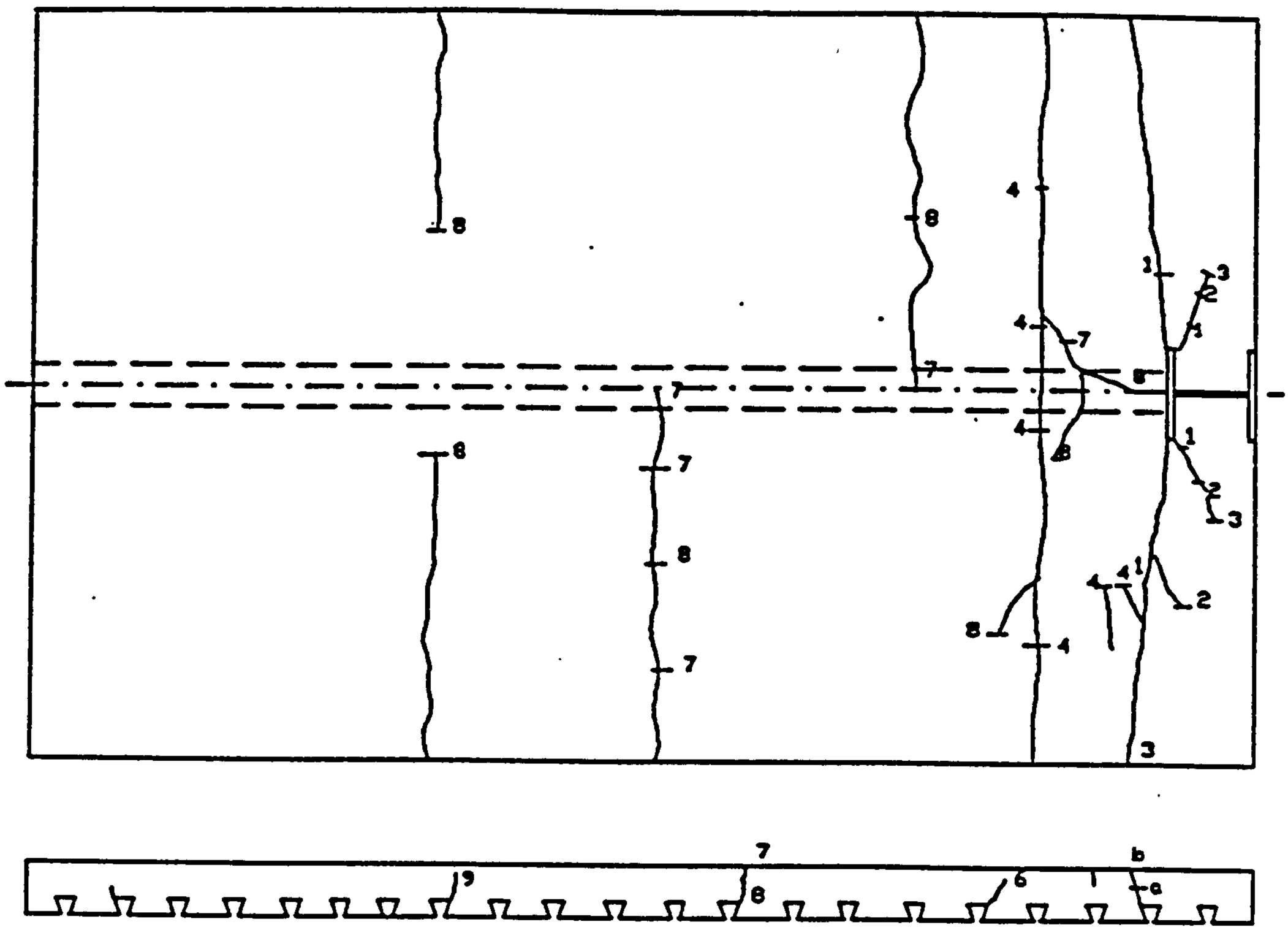

POINT		LOAD
1		10.55
2		14.5
3		-14.38
4		15.07
5		19.9
6		-17,08
7		27.94
8	TOP	29.68
8	BOTTOM	-23.92

FIGURE 7.6 : DEVELOPMENT OF CONCRETE CRACKS

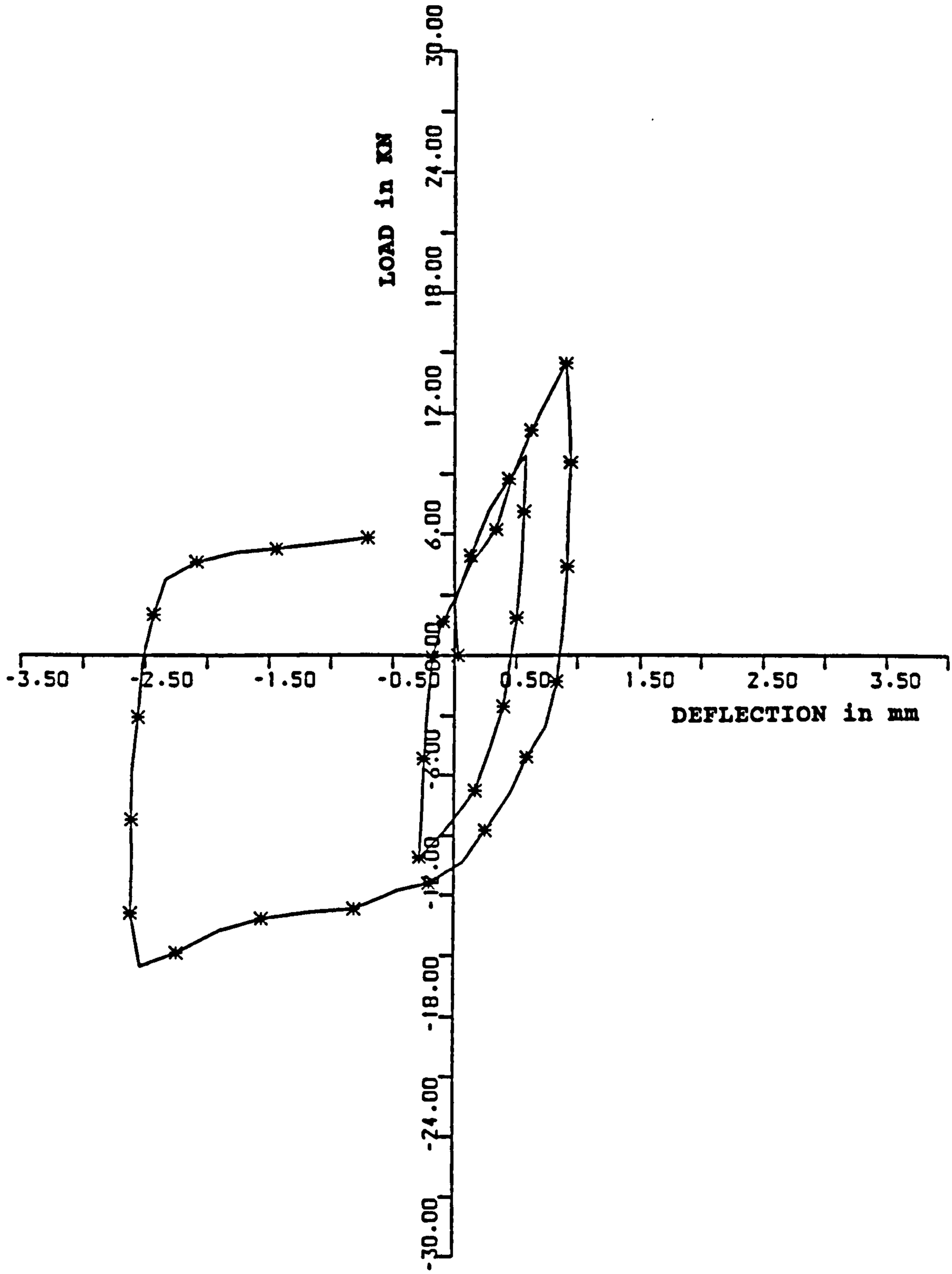

FIGURE 7.7: GRAPHS OF LOAD-LOWER FLANGE MOVEMENT FOR COMPOSITE FRAME WITH 8.8 BEARING BOLTS

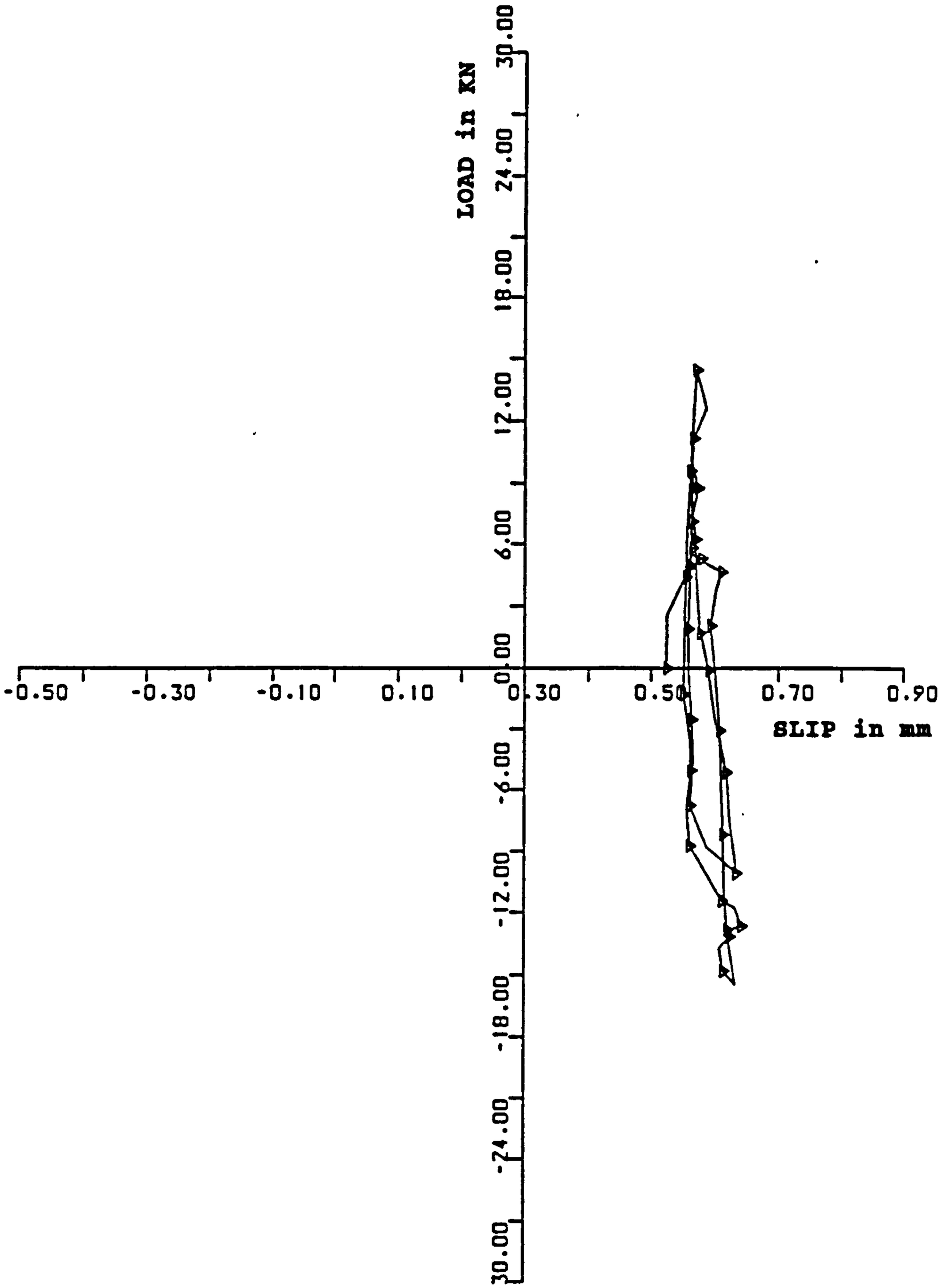

FIGURE 7.8 : LOAD-SLIP CURVE WITH 8.8 BEARING BOLTS

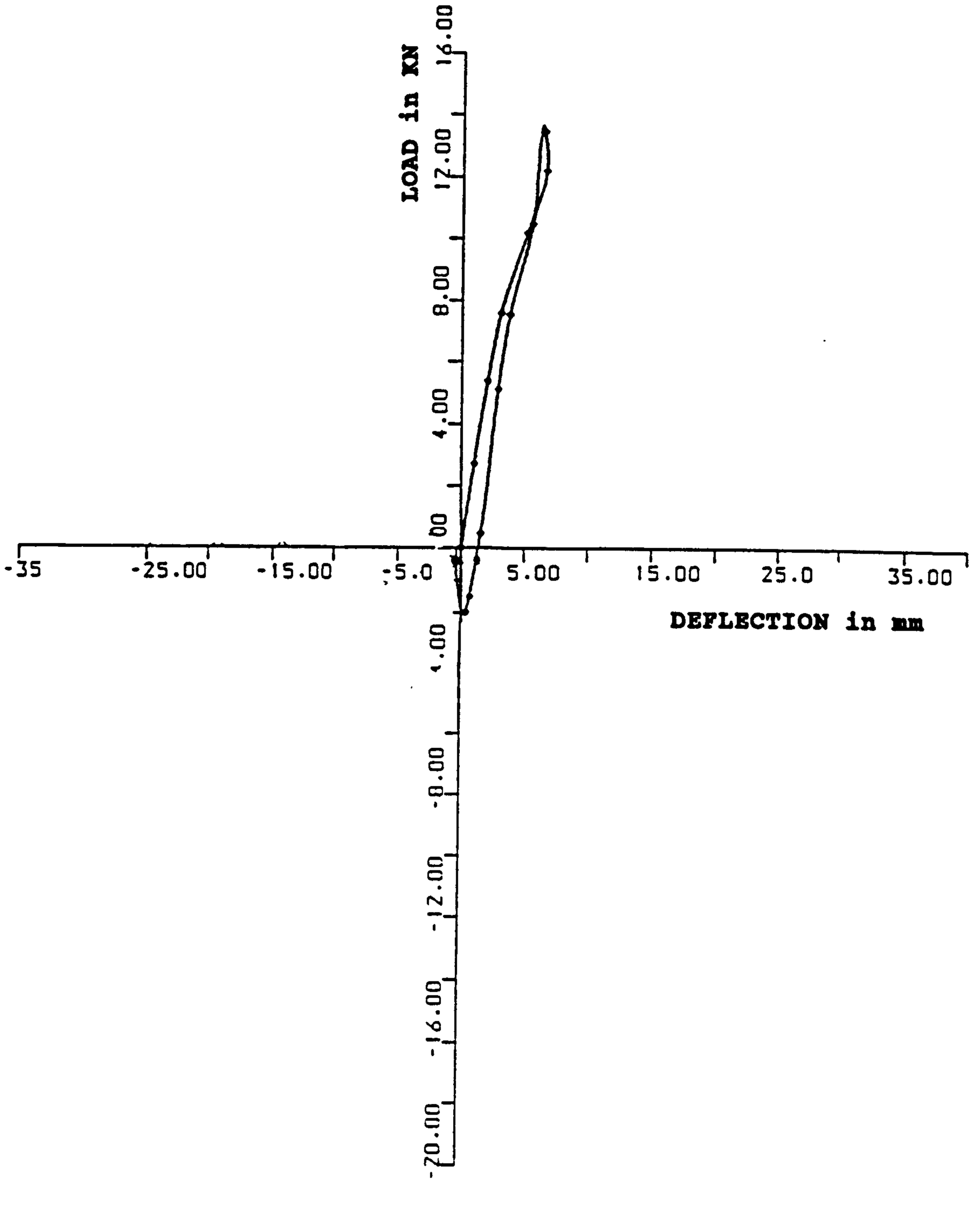

FIGURE 7.9 : LOAD-DEFLECTION CURVE FOR THE FRAME WITH FULLY TIGHTENED 8.8 BEARING BOLTS

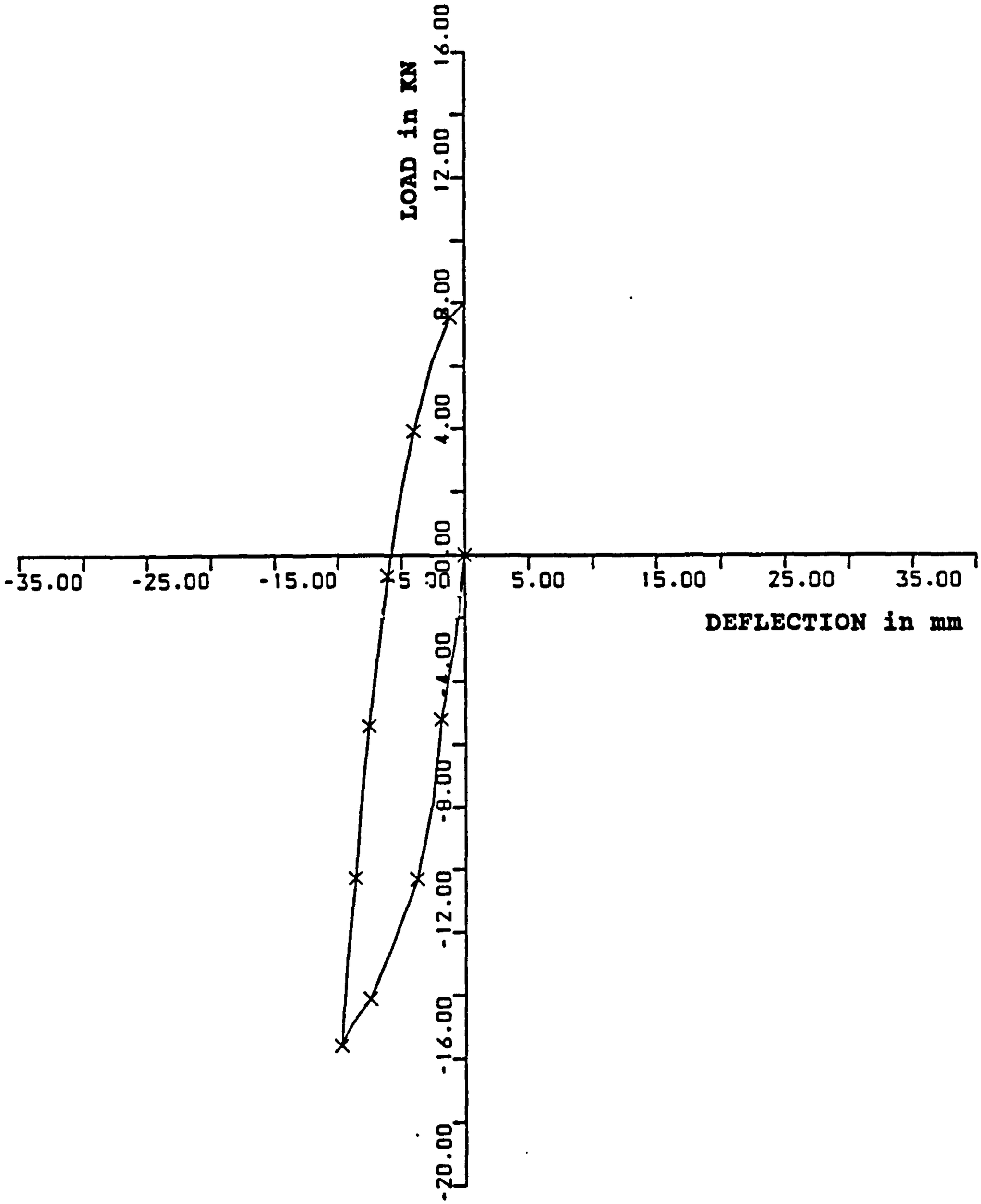

FIGURE 7.10: LOAD-DEFLECTION CURVE FOR COMPOSITE FRAME, SEAT CLEAT BOLTS ARE REPLACED BY HSFG BOLTS

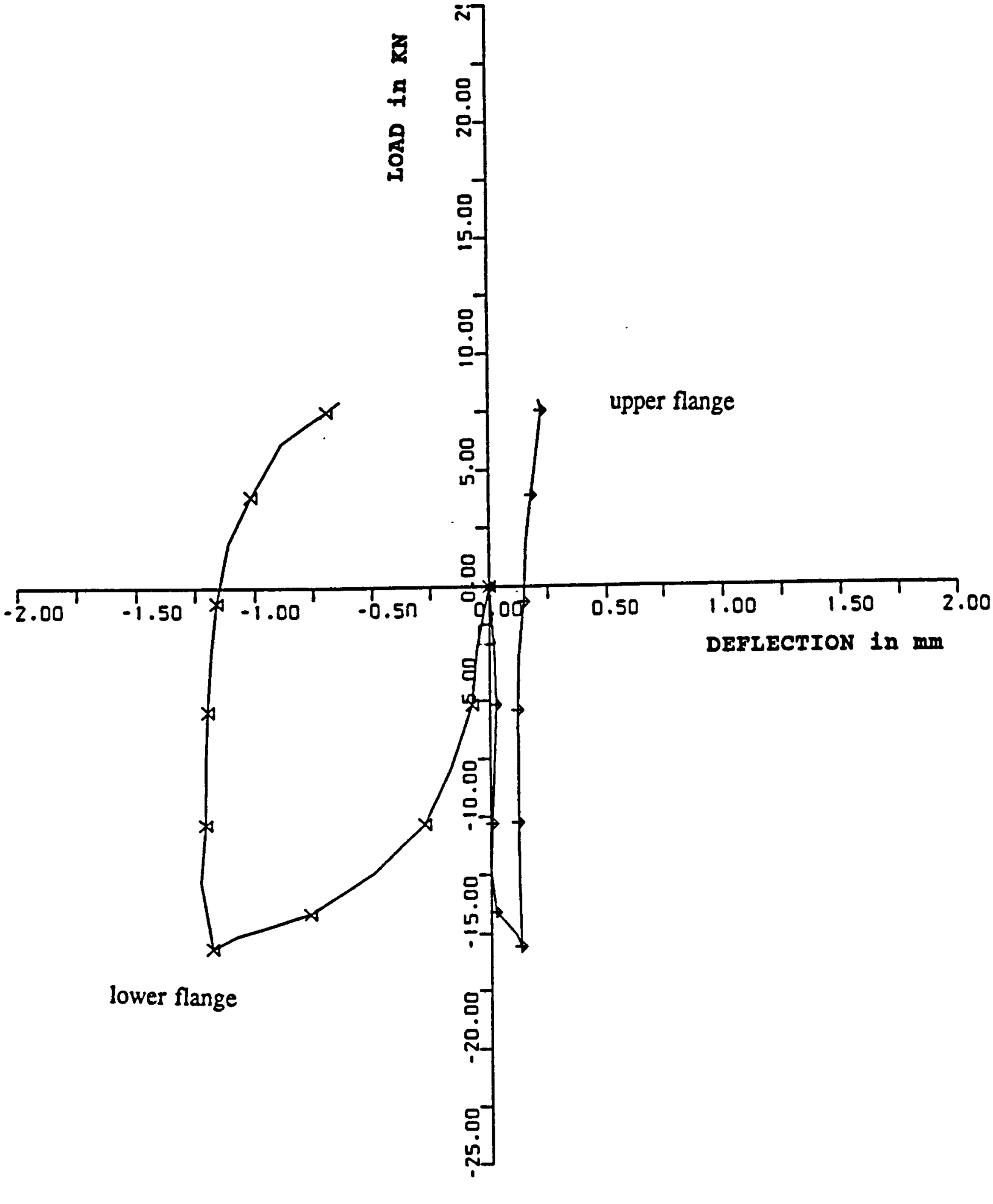

FIGURE 7.11: LOAD-DEFLECTION CURVES FOR THE UPPER AND LOWER FLANGES OF THE STEEL BEAM, SEAT CLEAT BOLTS ARE HSFG BOLTS

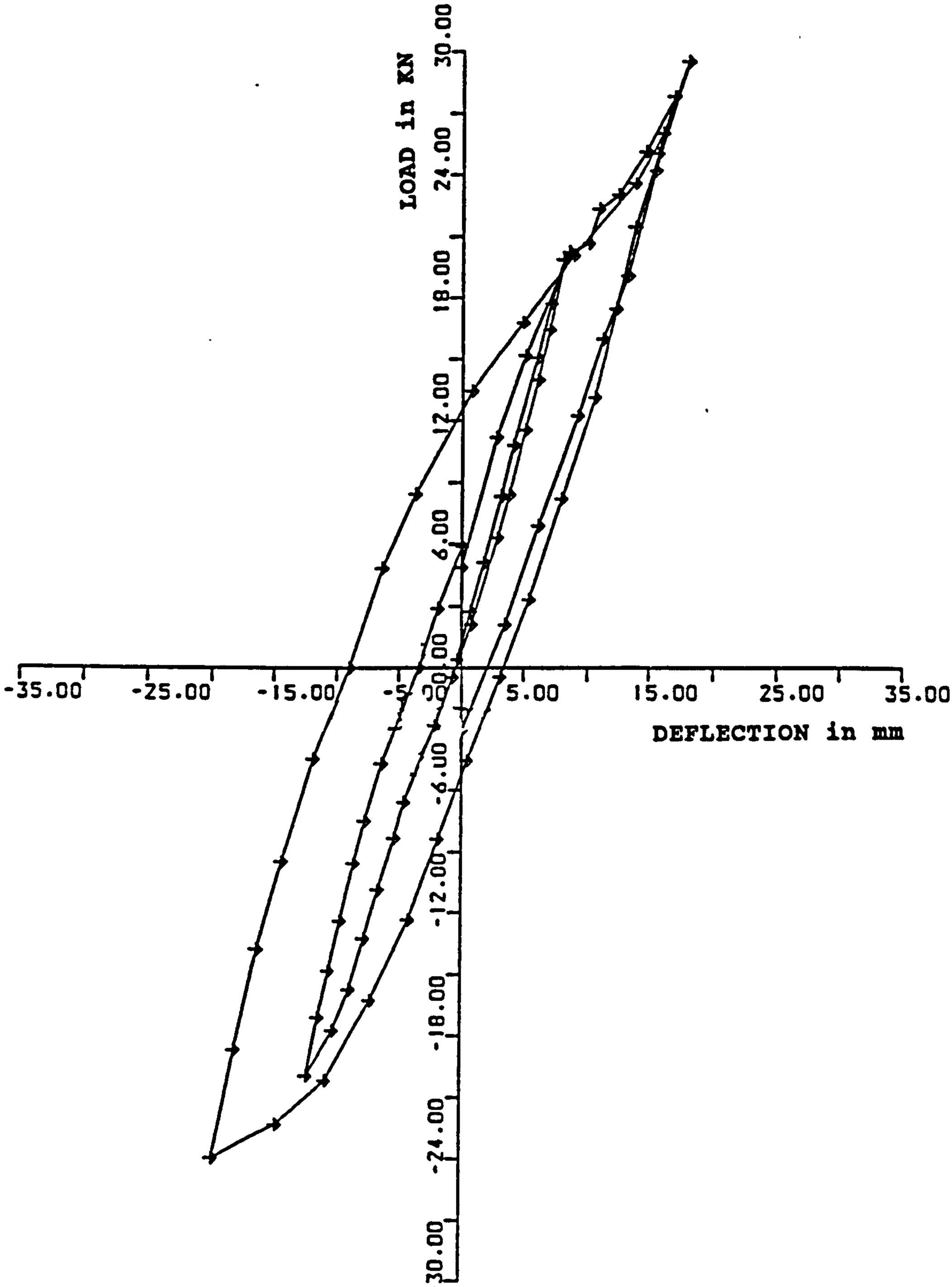

FIGURE 7.12 : LOAD-DEFLECTION CURVE FOR THE FRAME WITH 4 HSFG BOLTS

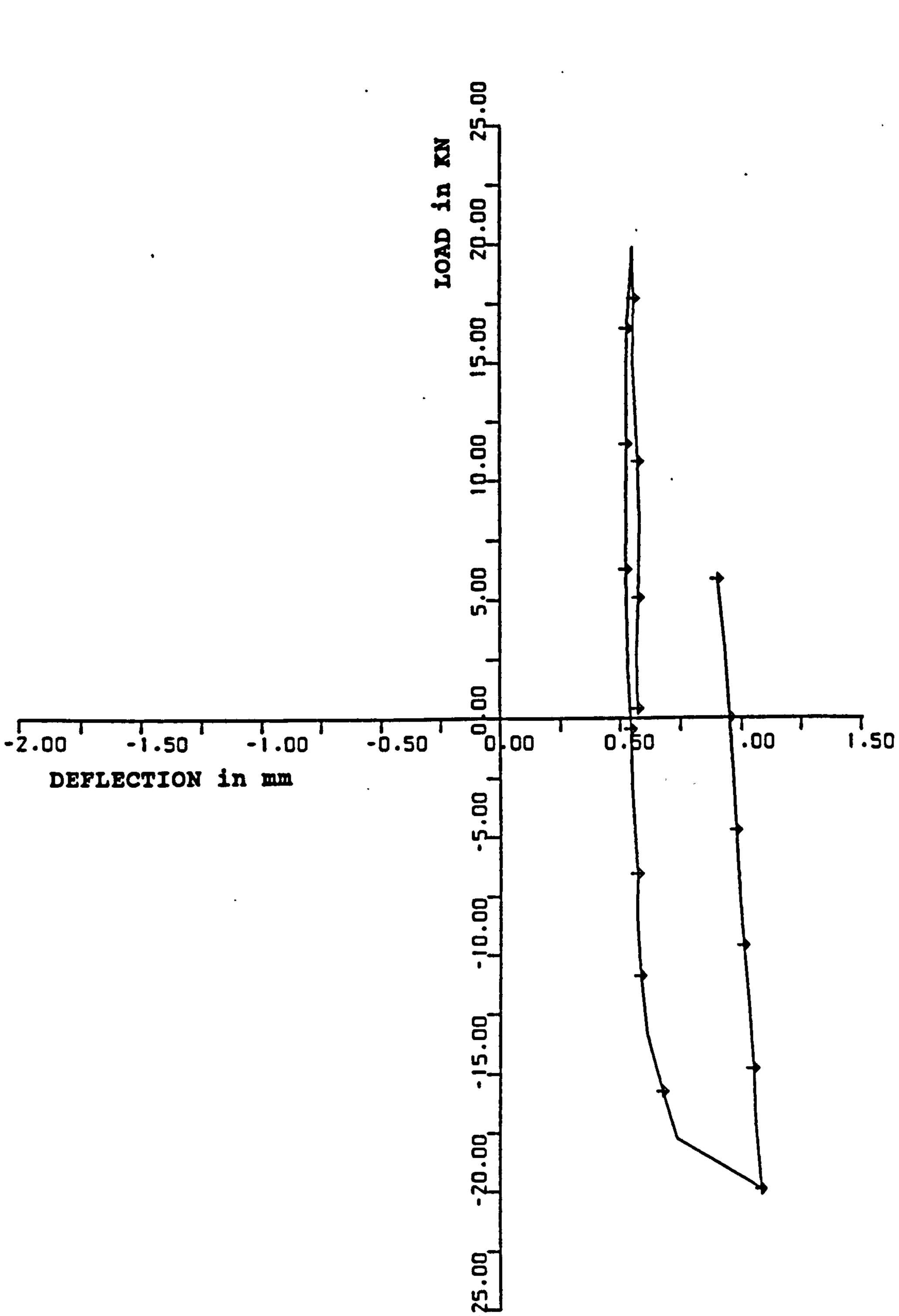

FIGURE 7.13: GRAPHS OF LOAD-END GAP CHANGES, COMPOSITE FRAME WITH FOUR HSFG BOLTS

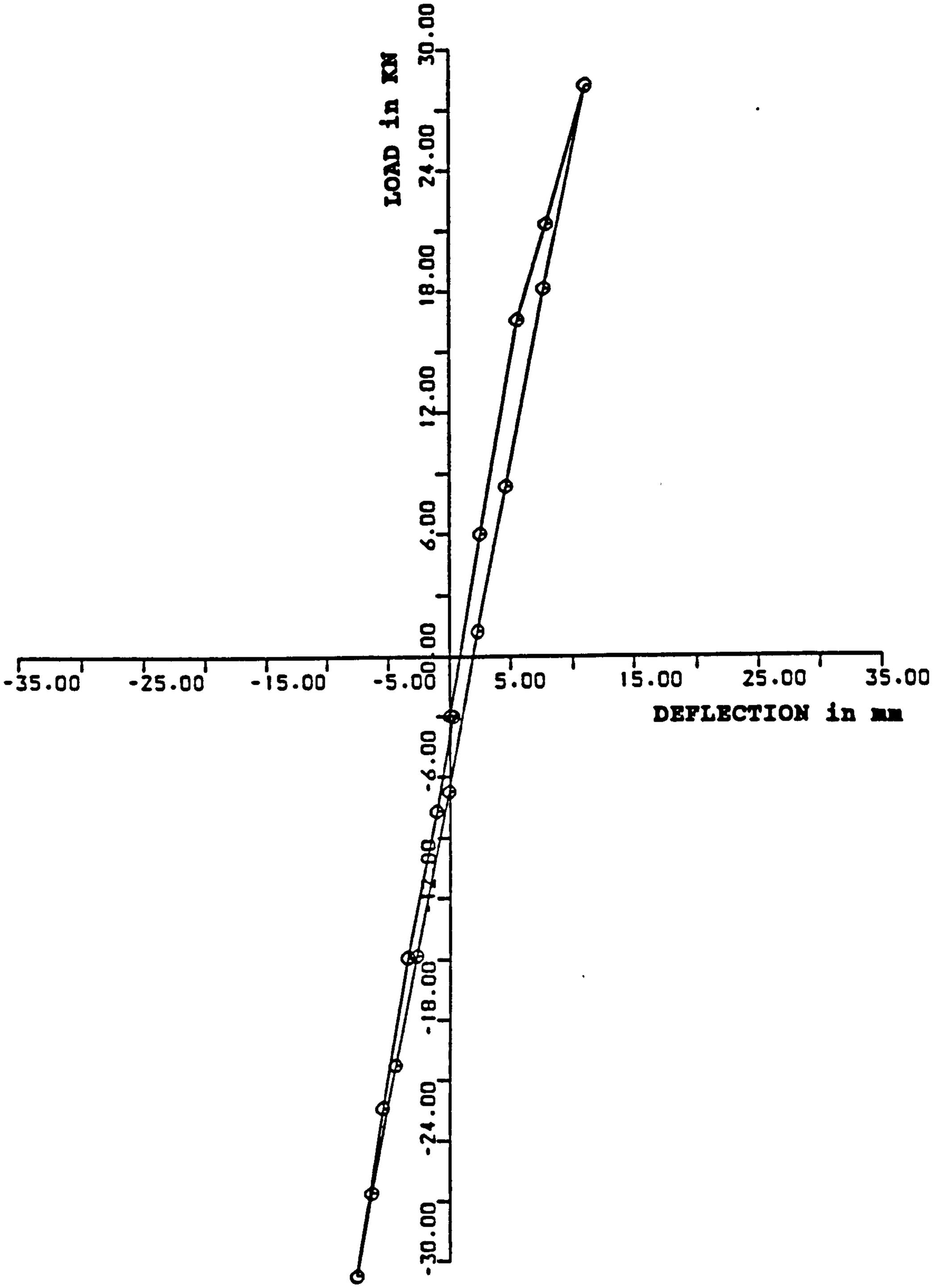

FIGURE 7.14 : LOAD-DEFLECTION CURVE FOR THE WELDED FRAME

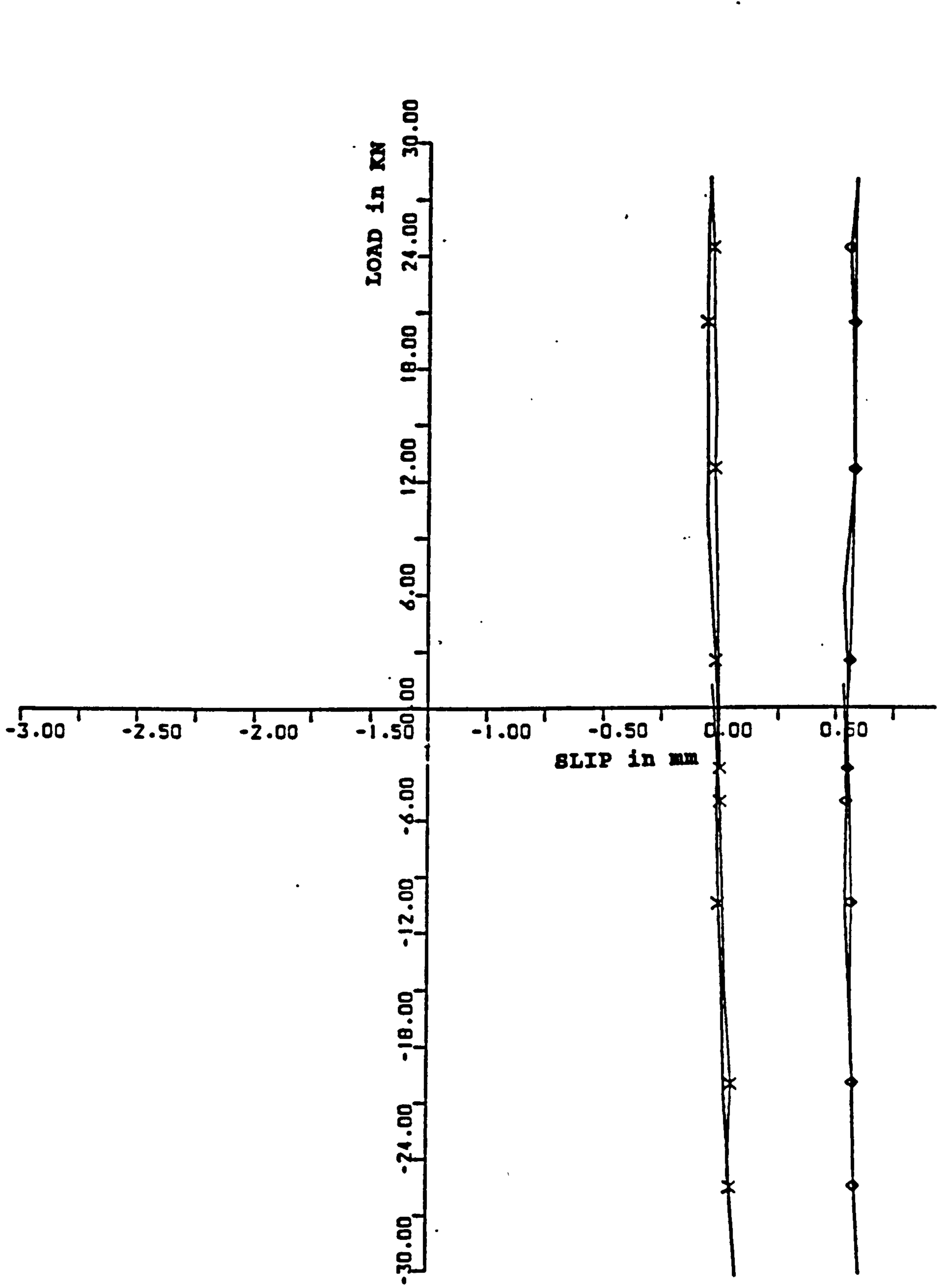

FIGURE 7.15 : LOAD-SLIP CURVE FOR THE WELDED FRAME

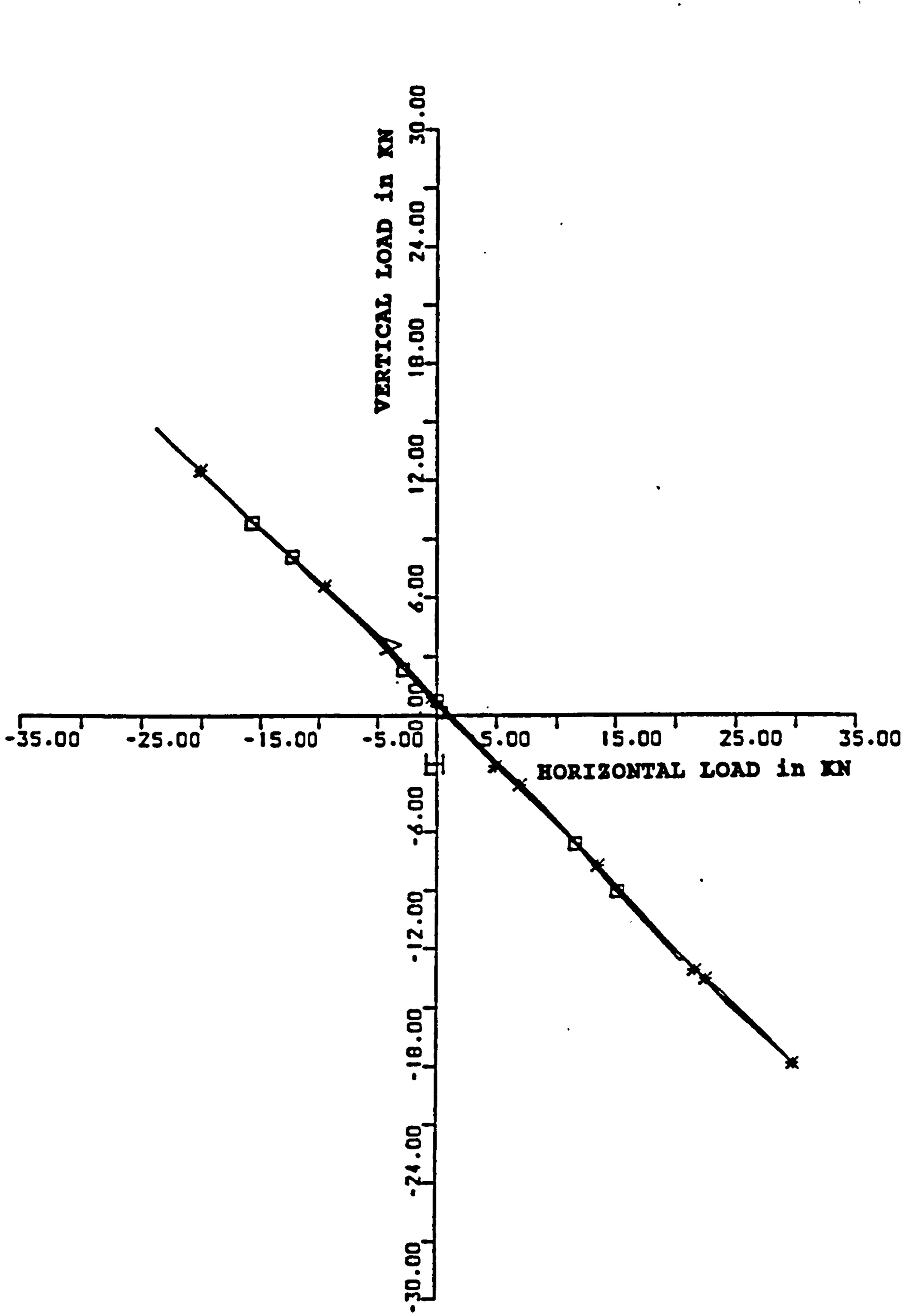

FIGURE 7.16 : HORIZONTAL-VERTICAL APPLIED LOAD RELATIONSHIP

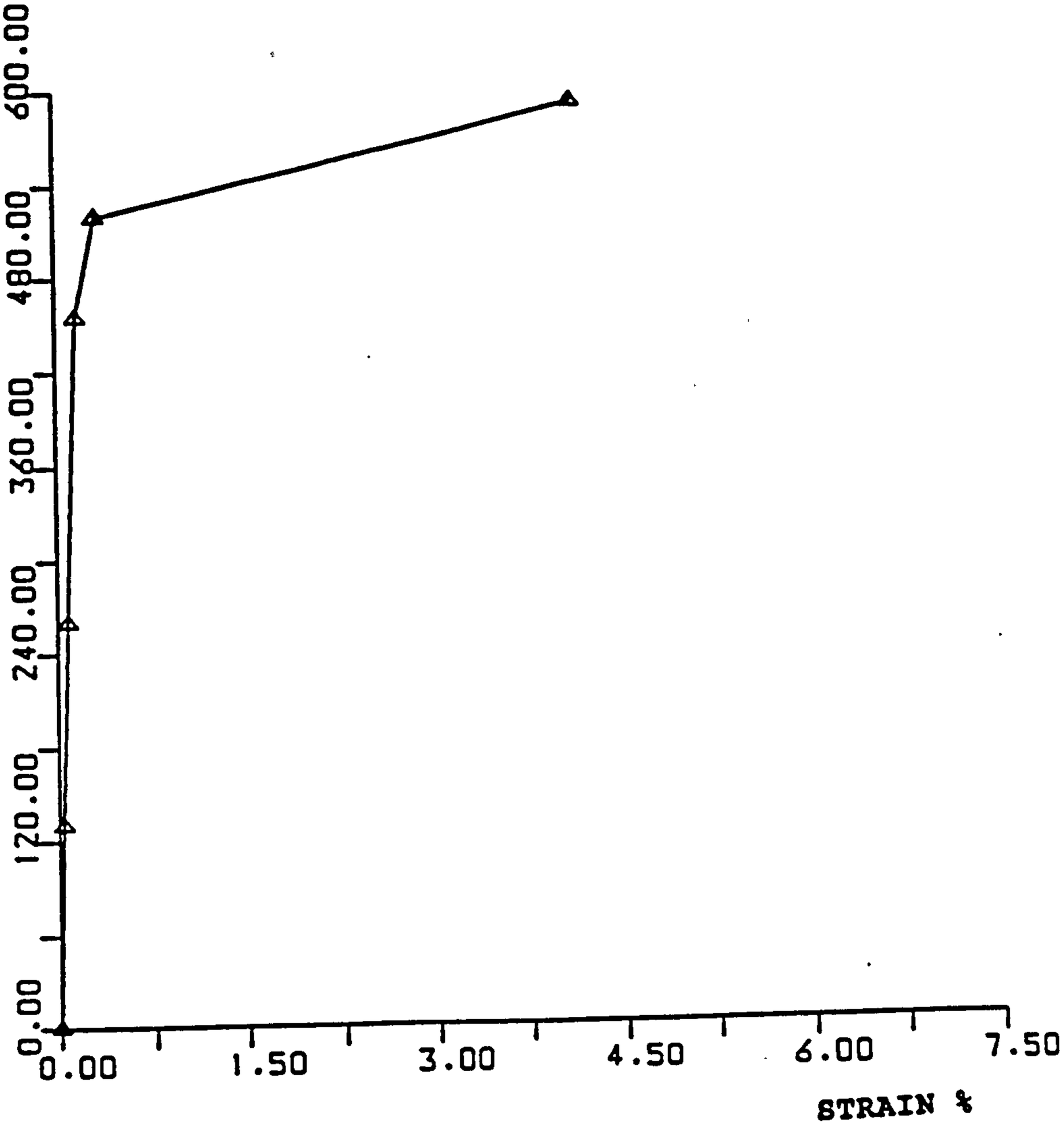

FIGURE 7.17 : STRESS-STRAIN CURVE FOR THE FABRIC

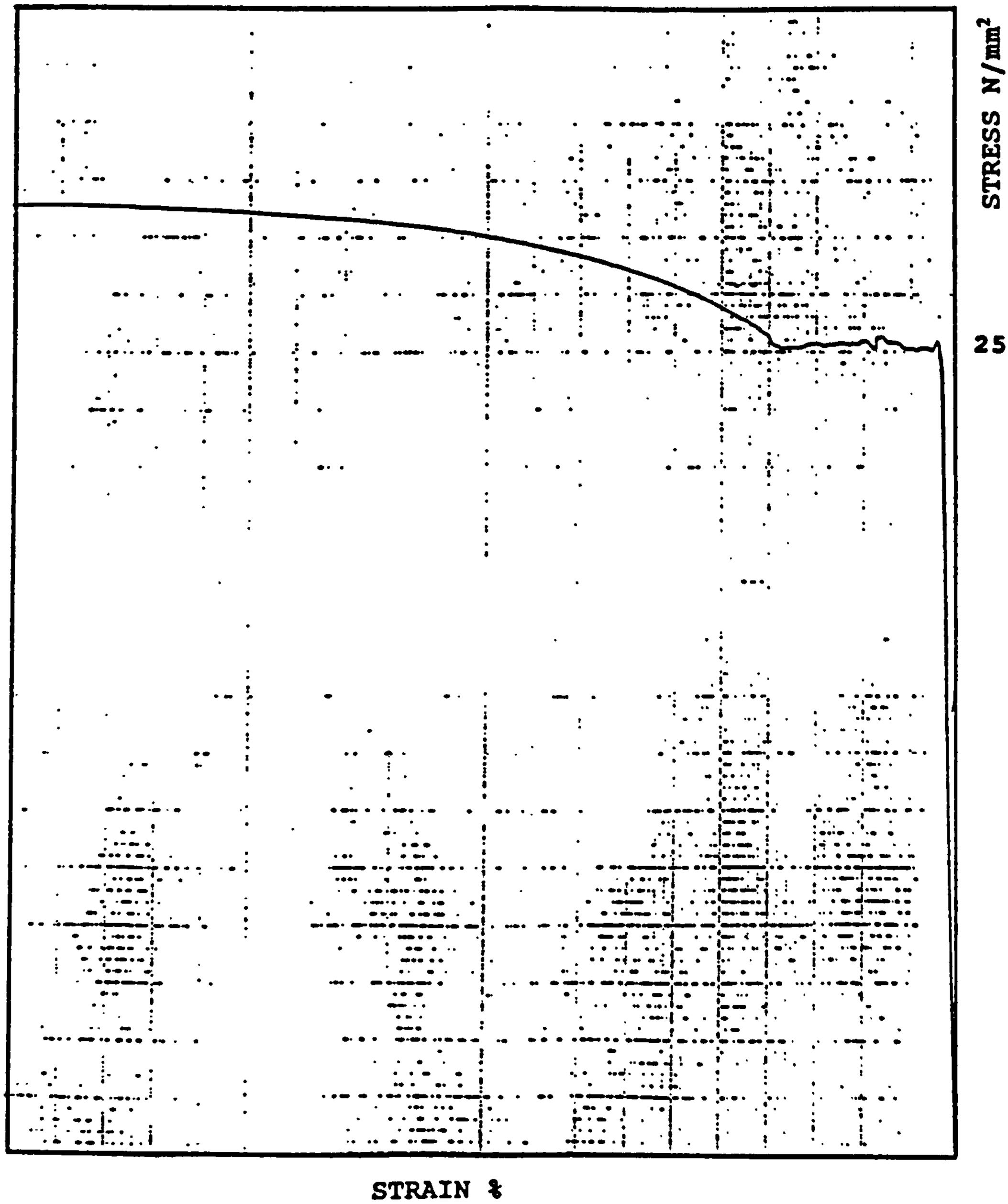

FIGURE 7.1 8: STRESS-STRAIN CURVE FOR THE STEEL SHEET

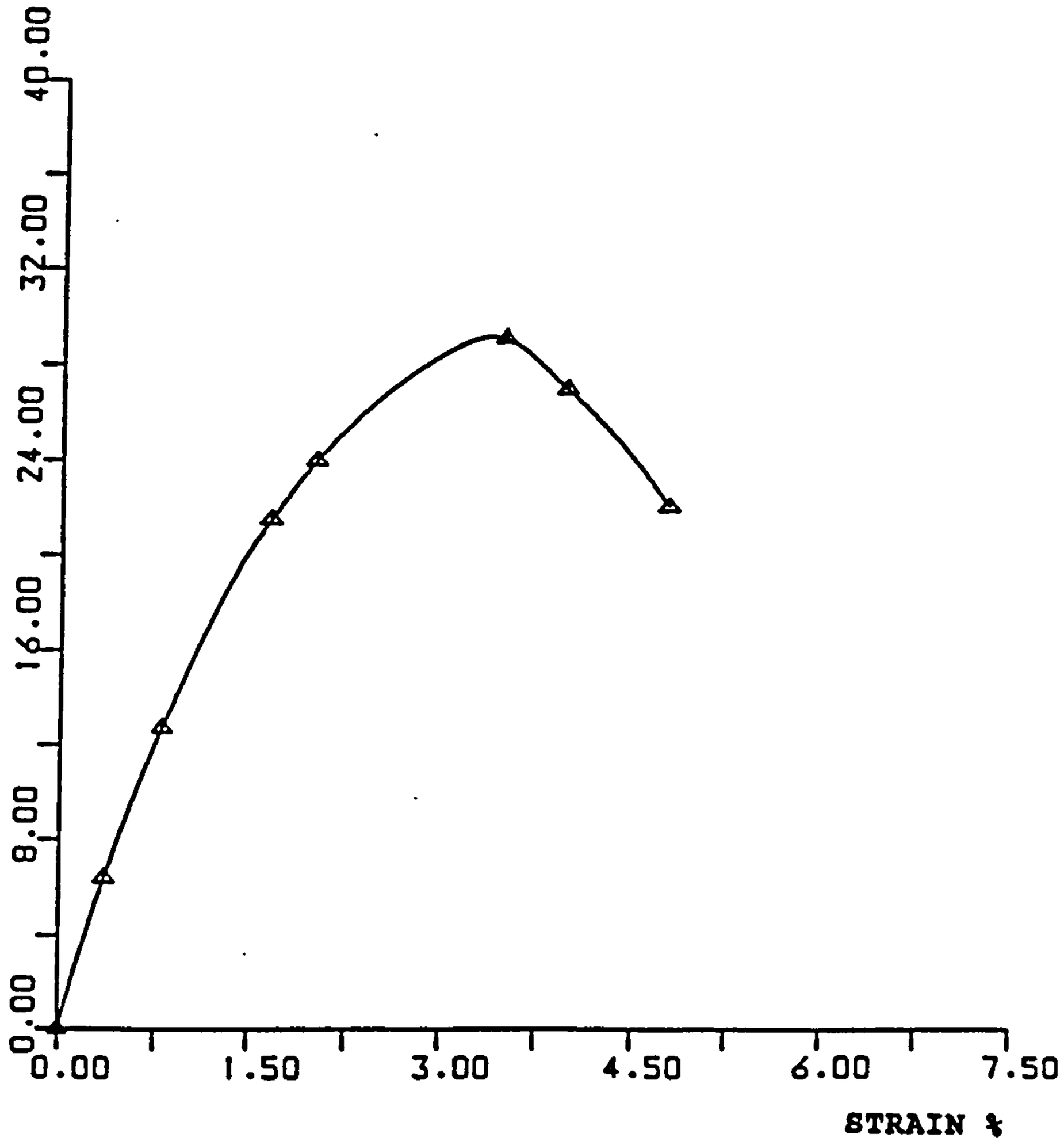

FIGURE 7.19 : STRESS-STRAIN CURVE FOR CONCRETE

CHAPTER EIGHT

MODIFIED 2-D NUMERICAL MODEL OF THE TEST SAMPLE

8.1 Introduction

In the preliminary 2-dimensional numerical analysis, assumed material properties and geometries were adopted. Since there were some differences between the measured and the assumed values, a 2-dimensional model which had the test piece geometry and material properties was prepared. In this chapter, this model is presented, its results are discussed and compared with those obtained earlier from model One with nominal geometry and material properties and with the experimental results as well.

The aim of preparing this model was to examine the accuracy of the preliminary numerical predictions and to investigate the sensitivity of the numerical results obtained from 2-D models to material and geometrical deviations. Attention is drawn to the fact that none of the key parameters affecting the stiffness of the joint was changed. These include the bolt-hole gaps, presence of seat cleat stiffener plate, steel beam and steel column sections.

The current numerical results are also compared with the experimentally obtained values to examine the accuracy of the 2-dimensional numerical study when based on actual geometry and material properties. Comparisons with the 3-dimensional numerical results are presented in Chapter Nine.

In the current model, the ¬ shaped sub-frame is represented as a 2-D model. The steel column and beams' sections are the same as in the test specimen. The only option for increasing the stiffness was the additional reinforcement of 2T16. The assumption of no slip between the seat cleat and the steel beam as in the case of

welded seat cleat was adopted in the current model.

8.2 Numerical Model Features

A finite element mesh similar to that adopted for model One was used in the present model. ANSYS elements (STIF45, STIF42, STIF65, STIF1, STIF3, STIF12) were all employed to model the different constituents of the composite frame. The material properties of the concrete elements and reinforcing bars were those obtained experimentally. Some geometrical changes were introduced to account for the change in the dimensions of the steel beam and the column.

8.2.1 Geometry Changes

(1) The steel column height was increased from 2000 to 2045mm.

(2) The steel beam span was reduced from 3500 to 3434mm.

(3) In the preliminary models, the effective width of the concrete slab was assumed to follow parabolic shapes. In case of closing moment, reduced width of 362mm at the column face was assumed. In the current model, and based on the experimental observations, the full width of the concrete slab was assumed to be effective in closing as well as in opening moments.

(4) The seat cleat gap elements were removed to represent welded plates while those of the web cleat were set initially open to represent the case of ignored friction forces, i.e., slip of web cleat bearing bolts was allowed from the early stages of loading.

(5) The gap width of the construction tolerance gap elements had the values of 5mm for the lower flange level and 3.5mm for the upper one.

8.2.2 Material Changes

(1) Concrete tensile strength was reduced from 3.0 to 1.89N/mm^2. This value was the experimentally measured tensile strength of concrete. Values of 1.82x10^{4}N/mm^2 and 0.2 were used for the initial Young's modulus and Poisson's ratio respectively. The previous value for Young's modulus was 2.05x10^4 while the same value for Poisson's ratio was used.

(2) Yield stress for reinforcing steel was taken as 618.4N/mm^2 instead of the previous nominal value of 460N/mm^2.

Material nonlinearity for all joint components was considered in the analysis.

8.3 Numerical Results

The basic numerical results of the current model are discussed in this section. Comparisons with the preliminary 2-D model are also presented. The case considered herein is that with initially open web cleat bolt-hole gaps and no seat cleat gaps. The load was increased from zero to 30kN, with load increments of 5kN, in both directions.

(a) The Concrete Slab

In the closing moment, and because of the lower concrete tensile strength, cracks started at an early stage of loading. Until cracking, the joint behaviour is mainly governed by the concrete tensile strength. After the cracks started at a moment of about 21kN.m, tensile forces are transmitted by the fabric and the additional reinforcement. The first crack which was perpendicular to the steel beam took place at the interface between the steel column and the concrete slab. With increasing load, the number of cracked elements increased and the width of the already cracked ones increased as well. Despite that, the maximum crack width recorded was 0.5×10^{-2}mm.

In the opening moment, the maximum compressive strength in concrete was 17.37N/mm^2 which indicated that crushing of concrete element was not imminent. This value was 19.1N/mm^2 in the preliminary model. The difference between the two values must be attributed to the assumed shape of the concrete slab with narrower width over the longitudinal beam.

(b) <u>The Reinforcing Bars</u>

The longitudinal bars of the fabric were modelled as a single reinforcing bar which had the same cross-sectional area as the fabric. This cross-sectional area was 337.75mm^2. Additional reinforcement of 2T16 was also introduced as a single straight bar in the same active plane.

In the early stages of loading, and before concrete cracking took place, low tensile stresses developed in these reinforcing bars, leading to linear behaviour of the load-tensile stress curve as seen in Figure 8.1. Cracking of concrete elements, which started at 10kN, caused a marked change in the slope of the load-tensile stress curve. This was a direct result of tensile concrete stresses being transferred to tensile stresses on the reinforcing bars. The maximum tensile stress in the reinforcing bars at a load of 30kN was 206.4N/mm^2 from which it is concluded that yielding of these reinforcing bars was not imminent. In the similar model with assumed properties the tensile stress was 200.1N/mm^2. The difference between the two values may be attributed to the increased moment due to longer lever arm in the current model. The expected effect of the geometrical changes on the stiffness of the joint is presented in appendix III.

(c) <u>Load-deflection and Moment-rotation Curves</u>

The load-lateral deflection curve for this model is shown in Figure 8.2 from which it is clear that the maximum deflection was 12.98mm at 30kN. The curve is characterised by an insignificant loss in the lateral stiffness associated with the concrete cracking due to opening moments. For the closing moment, the curve is

linear with the maximum lateral displacement of 11.89mm.

Compared with the similar model with nominal properties, the lateral stiffness of the current frame at the early stage of loading is higher. This is seen from the load-horizontal deflection curves of the two models shown in Figure 8.2. This may be attributed to the wider effective width assumed in the current model. The lower value for concrete tensile stress in the current model of 1.89N/mm^2 was previously 3.0N/mm^2, and this may have contributed an insignificant difference.

In the closing direction, the current model had lower stiffness, which is closer to the experimentally obtained value. This was expected since its geometry and material properties were identical with the test piece. The transition from being stiffer at early stage loading to comparable stiffness at the maximum working load is due to the more extensive cracking within the load range associated with the lower tensile concrete strength.

The moment rotation curve for this model is shown in Figure 8.3 from which the linear behaviour of the joint in the range from 0 to 30kN in both directions is clear. The maximum rotation was 2.04×10^{-3} at a moment of 61.35kN.m.

The rotations were calculated by selecting two points on the outer face of the steel column at levels 0.0 and 308.9, which correspond the two dial gauges in the test specimen, calculating the angle of rotation of rotation Φ as follows:

$$\Phi = \tan^{-1}\left[\frac{\delta_{upper} - \delta_{lower}}{308.9}\right]$$

Where δ_{upper} and δ_{lower} are the lateral deflection at the upper and the lower points respectively. The curve is deduced from the load-lateral deflection values and its trend is the same with a change in the slope at the points of concrete cracking.

(d) Steel Sections

No plastic strain was recorded in both opening and closing moments. The maximum recorded stress in steel was 153.4N/mm^2 which means that yielding of steel elements was still far away. Stresses were concentrated at the point of fixation of the seat cleat to the lower flange of the steel beam and at the nodes combining the stiffener plate and the column flange. The same trend, with the maximum stress of 150N/mm^2, was recorded in the preliminary model.

8.4 Comparisons with the Experimental Results

Comparisons with the experimental results were made taking into account that the compared frame reached a state at which the concrete slab has already cracked and residual stresses were expected to affect the comparisons.

(a) Load-deflection Curve

The load-horizontal deflection curve obtained from this model is compared with the experimentally obtained one in Figure 8.4. The comparison showed that there was a difference in the initial stiffness of the connection in the closing moment direction. The experimentally obtained stiffness is less than that obtained numerically. This may be attributed to the absence of the concrete slab contribution because of the cracks which had formed during previous load cycles.

In the opening moment, although the linear behaviour of the two curves is clear and they are close to each other, the difference between them may be attributed to the following reasons:

(1) The experimentally obtained curve has not had its start at the origin because of the residual stresses and plastic deformations. It was decided to draw it shifted from the origin for clarity.

(2) The numerical model had perfect material properties while the test piece had not had such perfect properties. The frame was repeatedly loaded and its performance is expected to be affected by residual stresses and plastic strains, especially in the concrete slab.

(b) The Concrete Slab

In the case of opening moment in the preliminary models, the effective width was assumed to follow the parabolic shape shown in Figures 8.5 and 8.6 for closing and opening moments respectively. In the current model, and based on the experimental observations, the full width was assumed to be effective. Cracks appeared close to the column at the top of the slab and extended rapidly to the full width with increased loads. The cracked shape of the concrete slab showed that cracks were perpendicular to the steel beam. This meant that the previous assumption of parabolic effective width was not accurate once cracking was fully developed.

(c) Load-slip Properties

The load-slip curve for the concrete slab in the test and in the 2-D numerical model are shown in Figure 8.7 from which it is seen that the two curves have the same linear behaviour. The offset along the deflection axis at zero load is arbitrary, and maintained only for clarity of the figure. This result was expected since a remarkable difference in the load-slip curve, which is a measure of the shear connection in the composite beam, would have led to a significant difference in the stiffness of the joint, and this did not occur.

8.5 Summary

A 2-D model which had modified geometry and experimentally measured material properties was prepared. Comparisons with the similar 2-D model which had assumed geometry and nominal material properties were made. The aim of this

was to examine the accuracy of the preliminary numerical predictions. It was found that both models had the same order of stiffness and stress in different constituents with minor differences due to change in geometry and input material properties. It was concluded that as far as the overall behaviour of the joint is concerned, marginal deviations in geometry and material properties have insignificant effect on the results. The only difference which might in some circumstances be significant is the load at which initial cracking occurs. The solutions from both models converge prior to concrete cracking and after cracking has occurred in both cases. This conclusion is valid if and only if the key variables affecting the joint were known and kept unchanged. The most important of these variables is the slip in the seat cleat bolts.

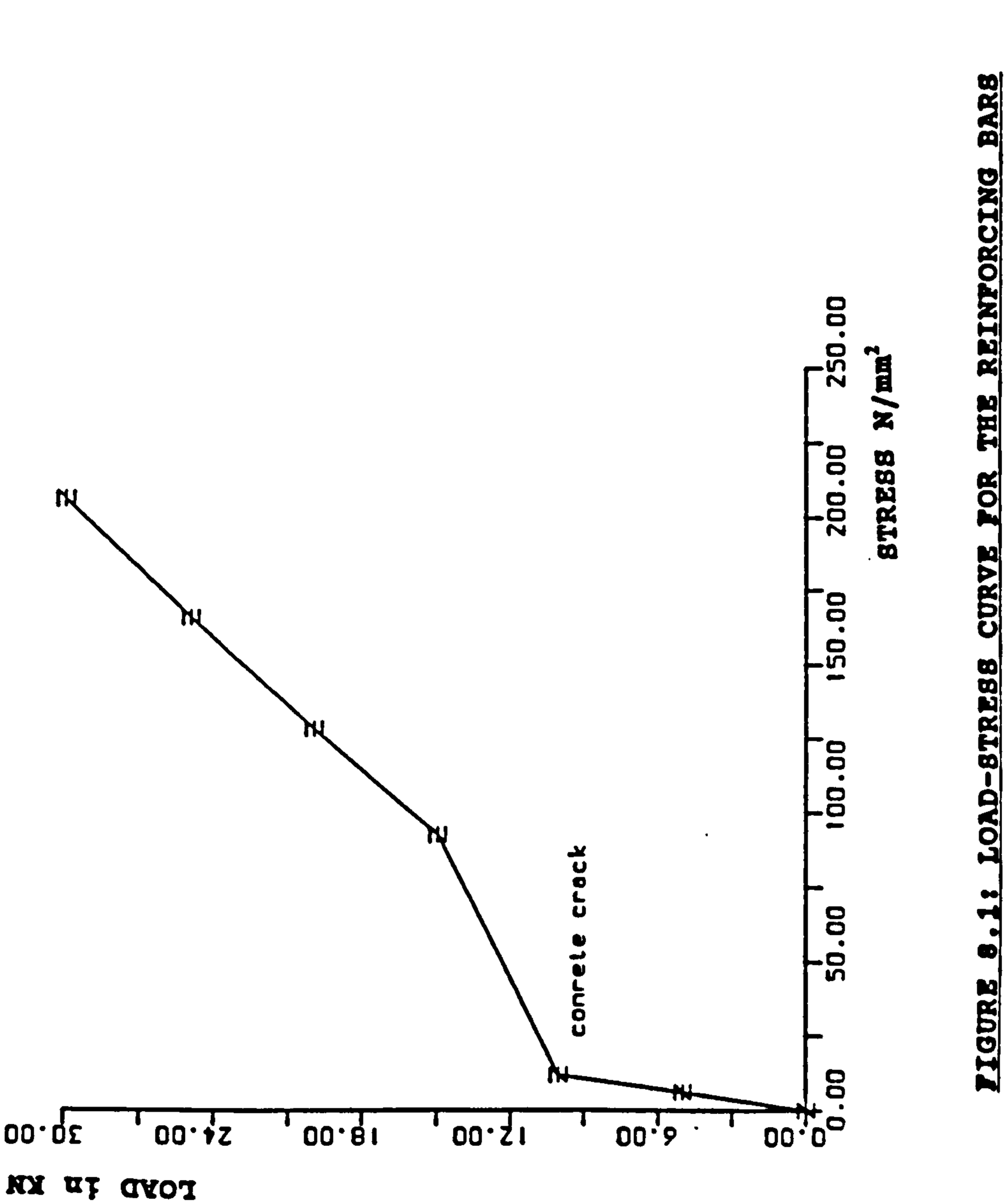

FIGURE 8.1: LOAD-STRESS CURVE FOR THE REINFORCING BARS

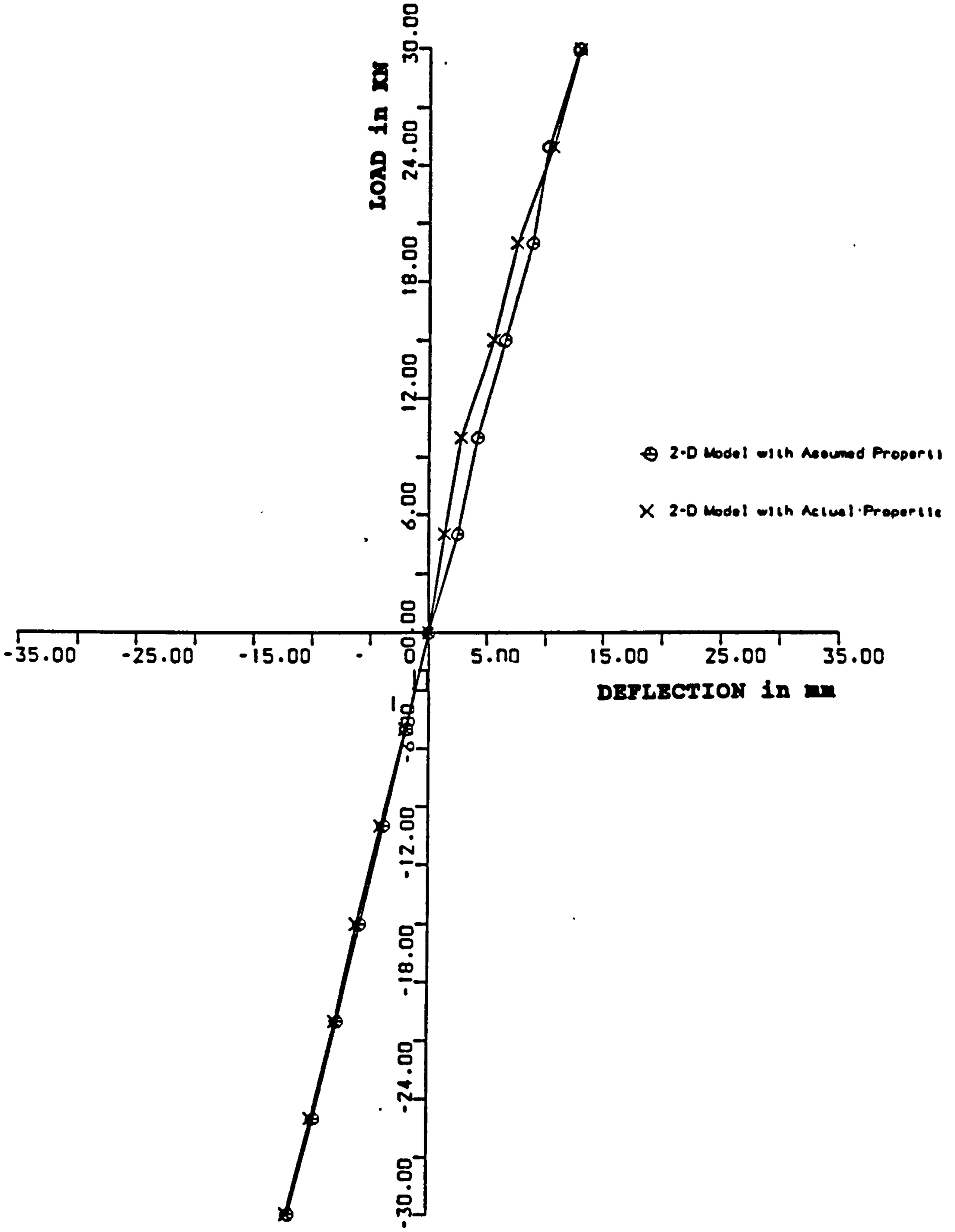

FIGURE 8.2: LOAD-DEFLECTION CURVE, COMPOSITE FRAME WITH WELDED SEAT CLEAT, 2-D NUMERICAL RESULTS

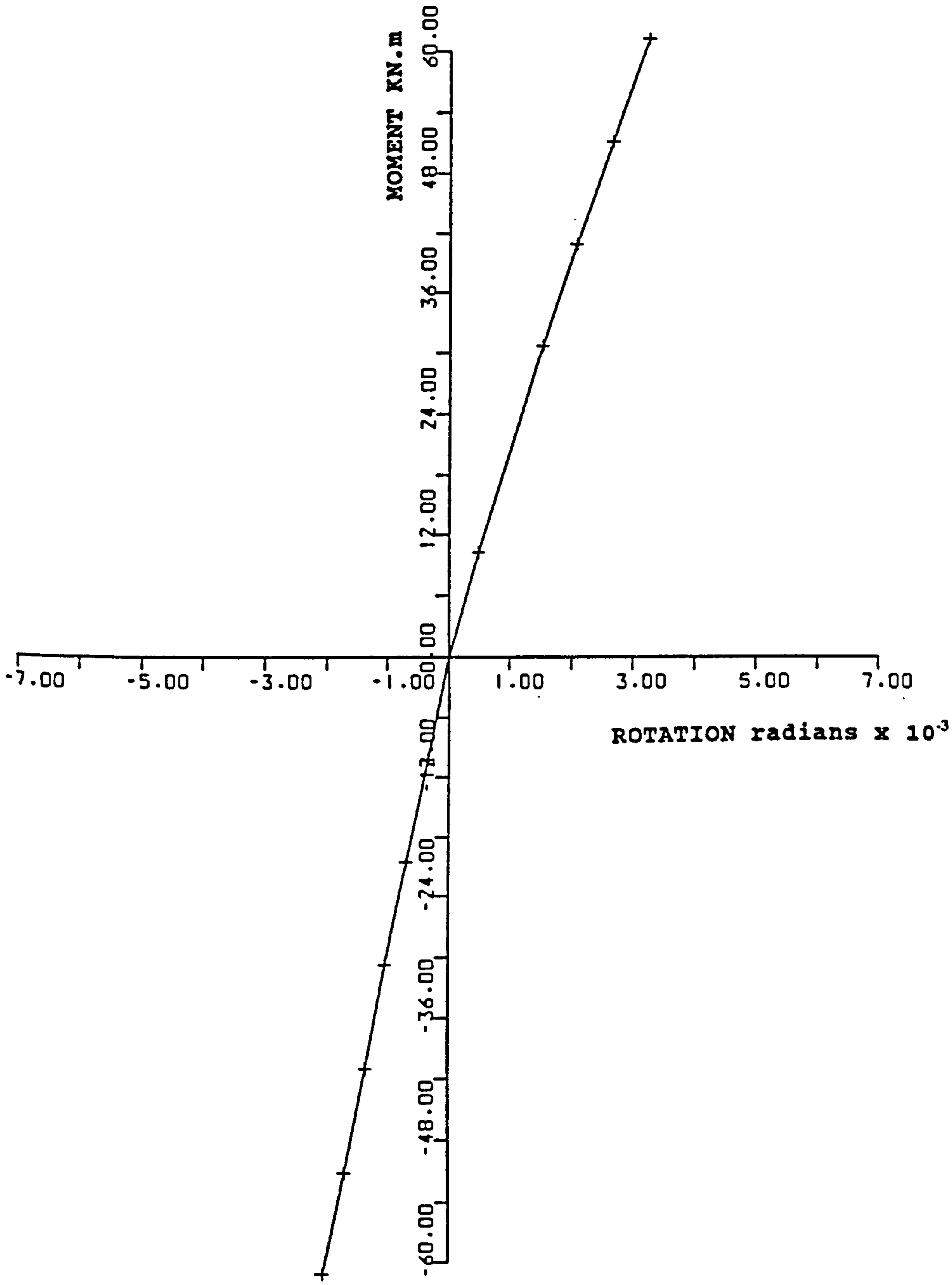

FIGURE 8.3: MOMENT-ROTATION CURVE, COMPOSITE FRAME WITH WELDED SEAT CLEAT, 2-D NUMERICAL RESULTS

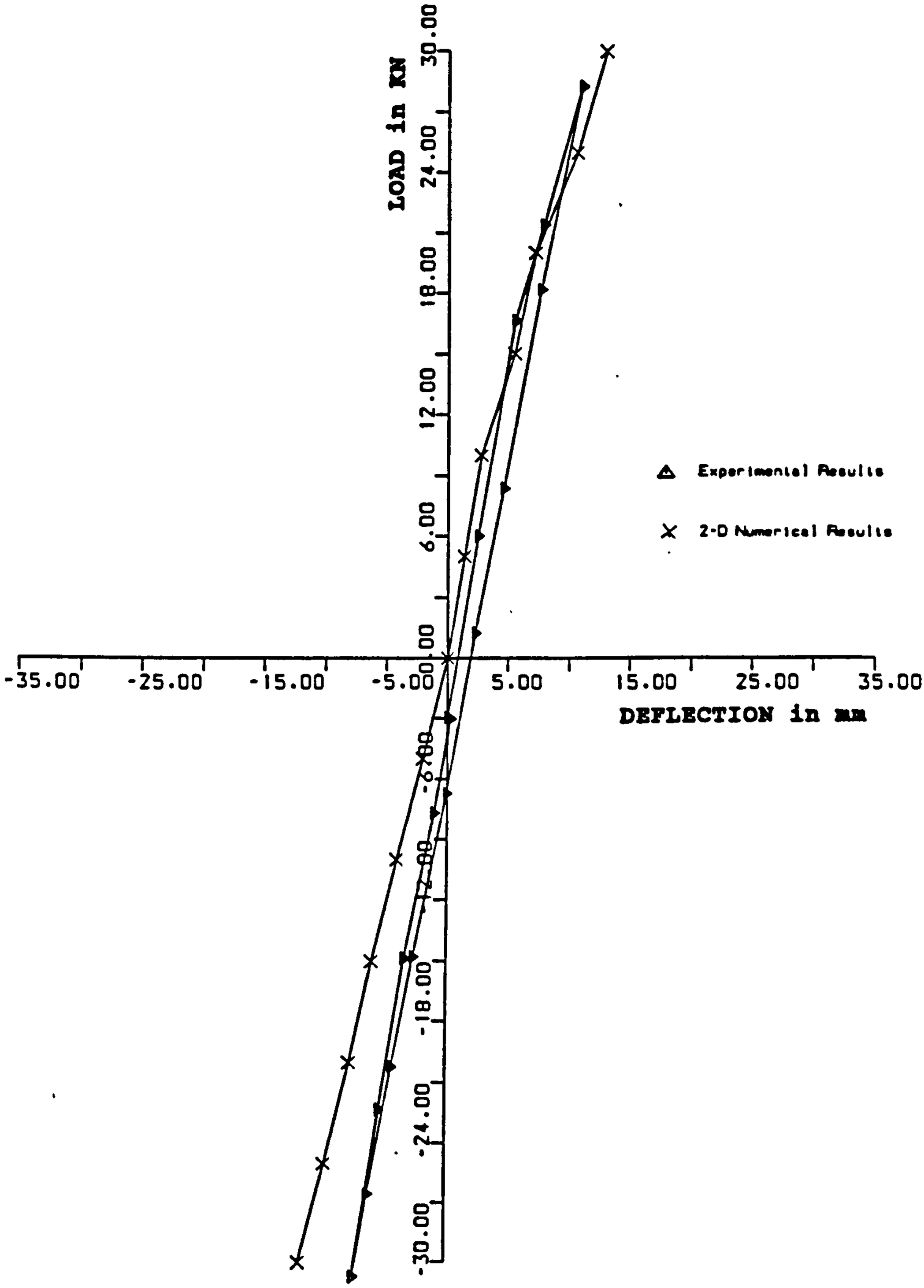

FIGURE 8.4: LOAD-DEFLECTION CURVE, COMPOSITE FRAME WITH WELDED SEAT CLEAT, EXPERIMENTAL & 2-D NUMERICAL RESULTS

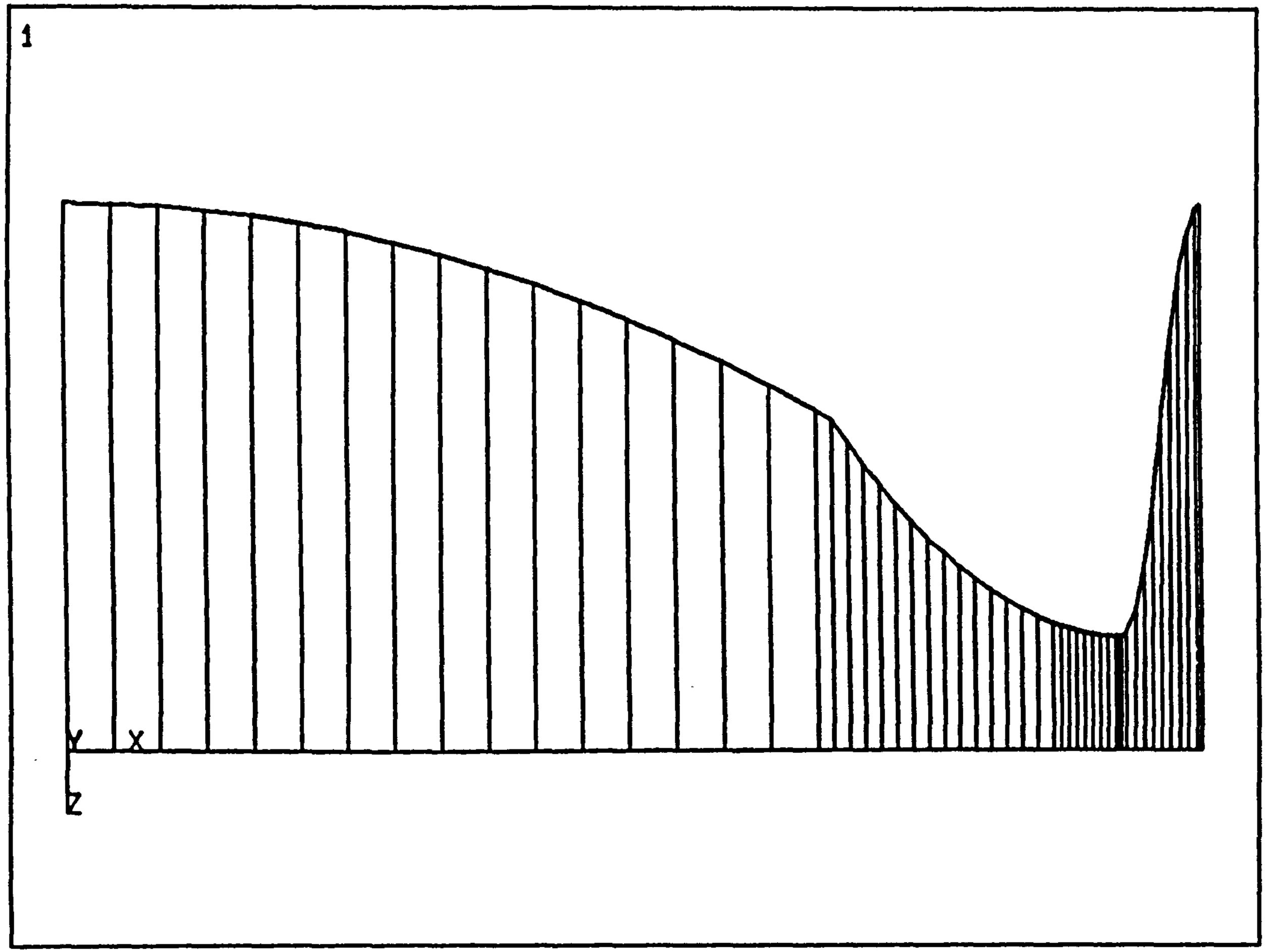

FIGURE 8.5: ASSUMED EFFECTIVE WIDTH IN CLOSING MOMENT

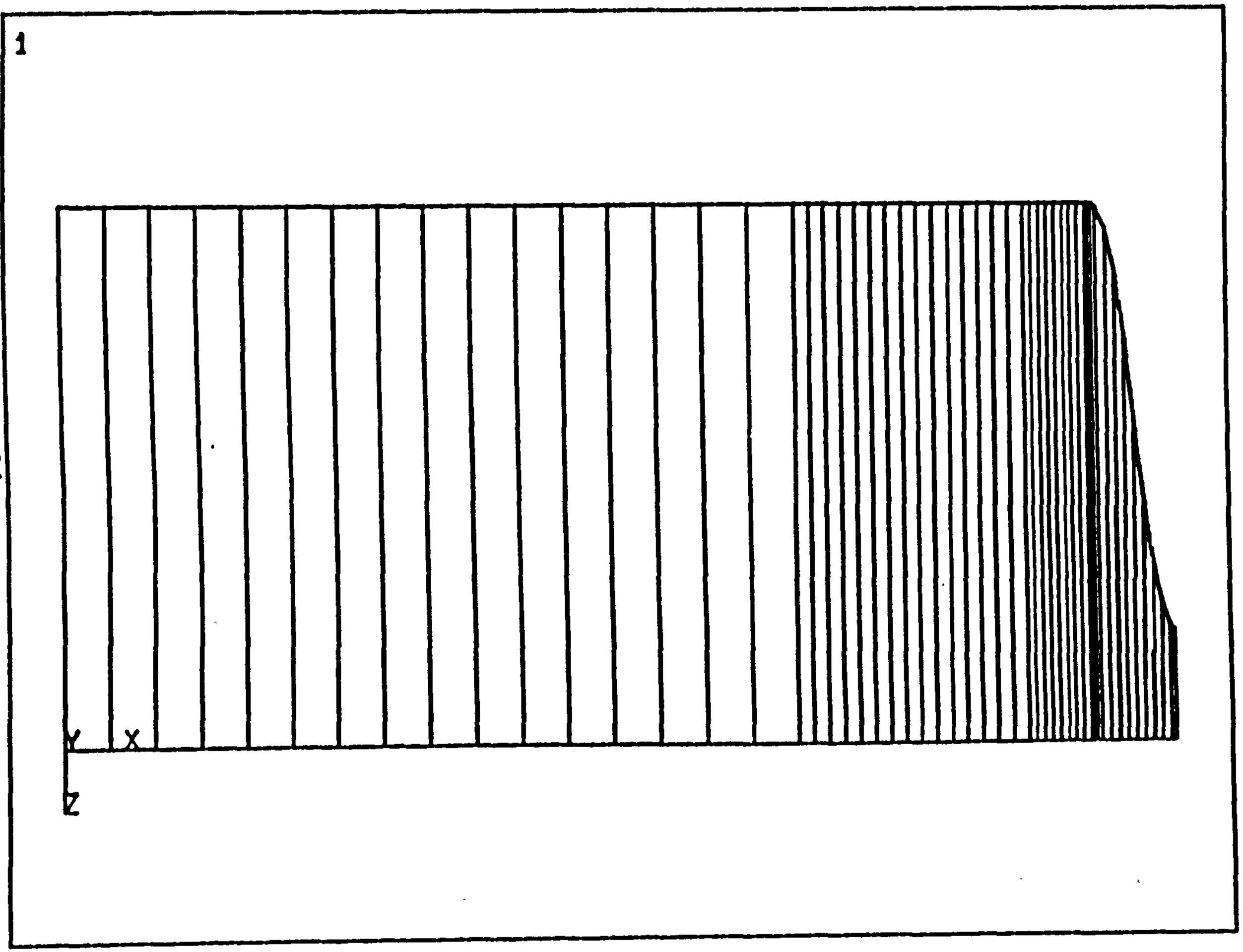

FIGURE 8.6: ASSUMED SHAPE OF THE EFFECTIVE WIDTH OF THE CONCRETE SLAB, OPENING

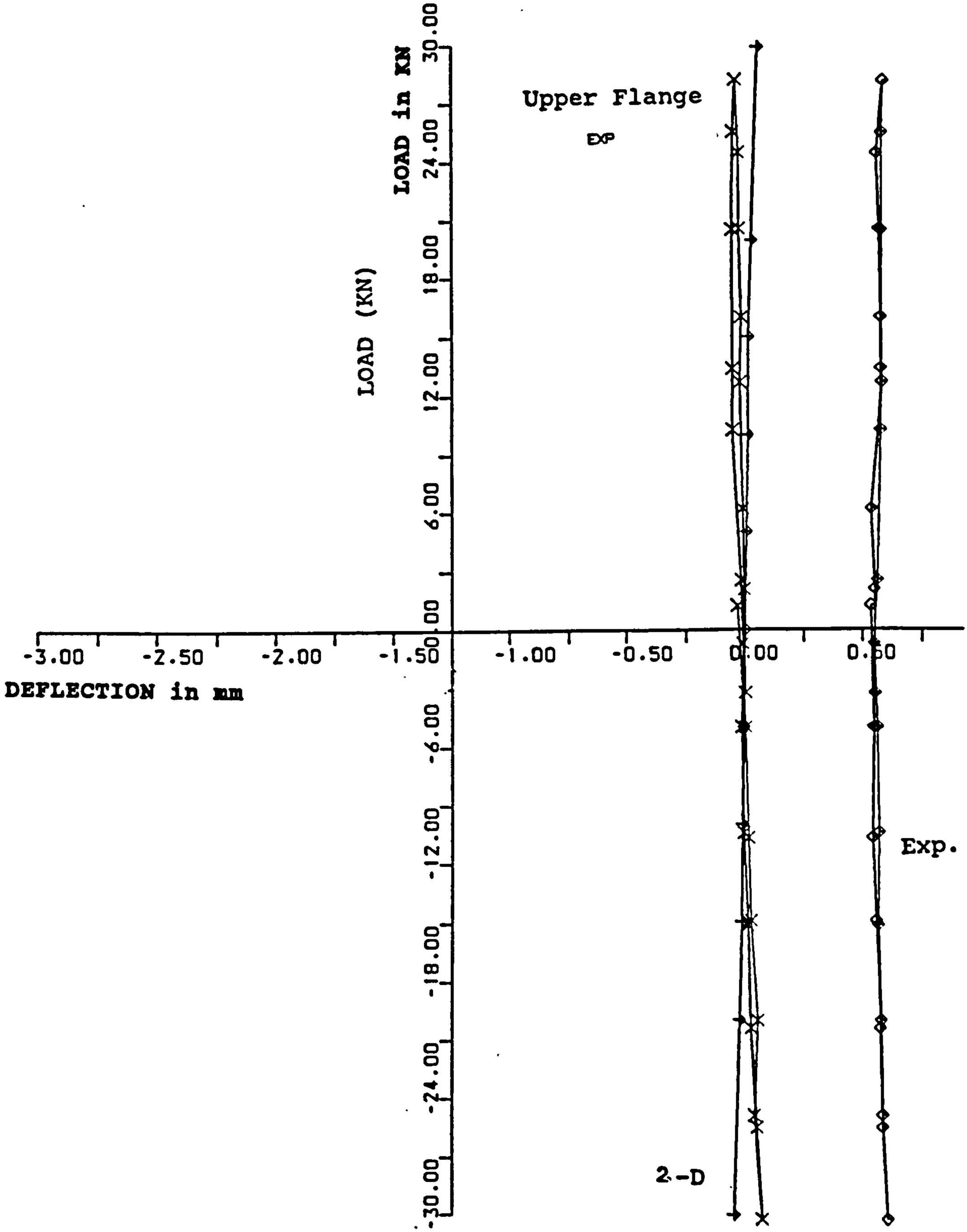

FIGURE 8.7: GRAPHS OF LOAD-END GAP CHANGES & LOAD-SLIP, COMPOSITE FRAME WITH WELDED SEAT CLEAT

CHAPTER NINE

THREE DIMENSIONAL MODEL OF THE TEST SAMPLE

9.1 Introduction

It was assumed that the finite element analyses of the joints would be sufficiently accurate using a 2-dimensional model. This assumes negligible shear lag effects within the composite floor and between the beam web and flanges. The accuracy of this assumption for components with such large aspect ratios in the third dimension is not obvious. Numerical errors may also be increased in the matrix solution procedures.

In order to check the accuracy of the two-dimensional numerical analysis, a three-dimensional model with the same geometry and material properties as the ¬ shaped model was prepared. In a three-dimensional analysis, problems of the computer capacity and running time are always expected if the aspect ratio is kept within its recommended range of 1-3.

The 2-D analysis, which was adopted in this study, proved not only to minimize the running time and the required memory size. Its results were found to be within the expected values for the lateral sway and stress distributions. However, its capability of representing the problem correctly is investigated in this chapter.

Leon and Lin carried out a three-dimensional analysis in which the composite connection model was dealt with in two steps. Firstly, the angle cleats were separately studied and the multilinear stress-strain constitutive laws were determined. Secondly, the connecting angles were substituted by truss elements, which had the predetermined laws, and were included in the overall three dimensional system of columns and beams [41,43].

In the different attempts to increase the lateral stiffness of the tested frame, it was proved that the slippage of seat cleat bolts was the reason for the low lateral stiffness (large horizontal sway). When the seat cleat was welded to the steel beam, the lateral stiffness increased dramatically. The frame with the welded seat cleat is considered for comparative purposes in this chapter.

9.2 Numerical Model Features

Only one half of the frame is considered in the analysis, thus taking advantage of the symmetry of the specimen. The steel beam was 305×102×28kg/m UB, the column was 254×254×73kg/m UC. The steel connection between the two was a web and seat cleated one. The model represented the ¬ shaped connection.

In order to keep the aspect ratio within a reasonable value, it was required to divide the concrete slab and the steel sections into a large number of elements. This would have led to a large number of elements, which consequently would have led to problems regarding storage capacity and solution time. Another technique was therefore adopted, in which fewer elements with condensed material properties were used to represent a larger number of elements which were remote from the plane of symmetry.

In this joint configuration, no slip in the seat cleat angle was possible due to the tolerances of bolt holes. In the 2-D models, this was achieved by introducing an initially closed gap element between the seat cleat and the steel beam. Keeping this element closed allows the transmission of forces between its nodes. In this three-dimensional model, the seat cleat was constructed using the same nodes as the beam and the column, thereby considering the welded plates to behave monolithically.

9.2.1 Element Types Used

The element types used to construct the three dimensional model did not vary significantly from those used in the two dimensional models. The concrete element (STIF65) was used to model the concrete slab elements. Unlike the 2-D analysis, it was used with its key options adjusted to get the 3-D performance. Three dimensional isoparametric elements were also used to model the steel sections of the column and the beam. The shear studs were modelled using two dimensional beam element. Reinforcing bars were modelled using the three dimensional spar element. Web and seat cleats were represented by two dimensional beam elements while the stiffener plate was modelled with the two dimensional plate element. Features of these elements are presented in the ANSYS manuals [37].

9.2.2 The Finite Element Mesh

The finite element mesh for this model is shown in Figure 9.1 through to Figure 9.5. Following the aforementioned technique, each of the steel beam flanges was divided into two elements in the z-direction. One of these elements had the ordinary steel properties, while the other had an identical aspect ratio and its material properties were multiplied by the number of elements it replaced. In other words, to keep the number of elements to a minimum, many steel elements were substituted by condensed material elements. The web plate was modelled with a row of elements as shown in Figure 9.2. The same technique was used to model the steel column and the concrete slab as seen from Figures 9.3 and 9.4. Geometrical symmetry about the z-axis was used and only one half of the frame was modelled.

The element mesh matched that for the two-dimensional analyses in the x-y plane with different zones of element sizes, which led to different aspect ratios. In both the column and the beam, the finest mesh was in the most highly stressed joint zone.

9.2.3 Material Properties

Based on the results of the experimental investigation, described in Chapter 7, the material properties used as input data in the programme were those obtained experimentally. These properties are presented in 7.4.1 and are summarised as follows:

(1) Concrete compressive strength was taken as 30N/mm^2

(2) Concrete tensile strength was taken as 1.85N/mm^2

(3) Yield stress for reinforcing bars was taken as 618.4N/mm^2

(4) Yield stress for shear studs was taken as 450N/mm^2

(5) Yield stress for steel sections was taken as 355N/mm^2.

(6) Modulus of elasticity for all steel parts was taken as 2.05×10^5N/mm^2.

9.2.4 Shear Connection

The shear connection between the steel beam and the concrete slab was again modelled using the technique which was described in Chapter Seven. The shear studs and the connecting ties were created in the x-y plane, which was the plane of symmetry. Each individual shear stud in the experimental work was modelled separately.

9.2.5 Boundary Conditions and Loading

A set of boundary conditions was introduced to represent the actual three dimensional frame. Because of the symmetry around the x-y plane, only half of the frame was modelled. The assumption of the presence of points of contraflexure at mid-height of columns and mid-span of beams in such frames when subject to wind load was used. The beam's free end was restrained vertically and was allowed to move horizontally and to rotate. The column lower point, at its centreline was allowed to rotate but not to move in any direction.

As for the two-dimensional analysis, the load was applied as incremental forces at the upper node of the steel beam flange.

Load was applied in small increments of 2kN at first and then the load increment was increased to be 6kN. Maximum applied load was 30kN in each direction. The number of iterations needed to achieve convergence varied between load steps and with the direction of loading.

9.3 Numerical Results

The basic results of the three-dimensional numerical analysis are discussed in this section. Load values used through the discussion are twice those obtained from the analysis to allow for the symmetry in geometry. In other words, only half of the actual test loads were applied to the finite element model because only one half of the frame was modelled.

In contrast with the two-dimensional analysis, only one case was considered. This represented the final modification to the test piece in which the seat cleat was welded to the lower flange of the steel beam.

(a) The Concrete Slab

Concrete cracked in the closing moment when its tensile stress exceeded the preset value of 1.85N/mm^2. The first crack started at 10kN and was perpendicular to the beam centreline as shown in Figure 9.6. With increasing load, cracks extended towards the slab free edge. When cracking of the condensed concrete elements occurred at 20kN, a crack perpendicular to the steel beam with the full width of the slab was detected. At this stage, tensile stresses are transmitted by the reinforcing bars. Cracks were mainly concentrated in the region close to the inner column face. The maximum crack width was 3×10^{-3m}m.

When opening moments were applied the concrete elements were mainly compressively stressed. The maximum recorded concrete stress was 18.6N/mm^2 which was less than the preset value for f_{cu} of 30N/mm^2, and consequently, concrete crushing did not occur. This was checked by reviewing the suitable concrete stresses associated with the concrete element used (STIF65).

(b) Load-deflection Curve

The load-lateral deflection curve for the frame is shown in Figure 9.7 from which it is concluded that at a load of 10kN, and due to concrete cracking, a loss of the lateral stiffness occurred. This loss is not very significant, and from the straight line relationship which followed it can be concluded that no yield of reinforcing bars took place. In the negative direction, the curve is linear which indicates that no loss of the lateral stiffness occurred. No crushing of concrete elements, which were compressed in the opening moment loading, took place.

Horizontal deflection contours in the joint position showed that the maximum sway took place at the upper surface of the concrete slab. The trend of the contours is to decrease down the column, with zero displacement at the column lower support. Horizontal deflection contours in the column are parallel and horizontal as expected. The same trend was obtained earlier in the 2-D analysis. The column and the welded stiffener plate behaved monolithically as they are modelled with the same nodes.

(c) The Reinforcing Bars

The reinforcing bars transmitted the tensile forces to the shear stud at the column centreline at which a group of four studs were employed to represent the cross beam. Figure 9.8 shows the load-maximum tensile stress curve. The longitudinal bars within the model were represented by three bars. The bar positioned at the

plane of symmetry had the maximum tensile stress values while that at the edge had the lowest values. A change in the slope of the load-tensile stress curve is recognised at a load value of 10kN indicating start of concrete cracks which was associated with an increase in the reinforcing bars' stress. A second and marked increase was also recognised at 20kN indicating cracking of condensed concrete elements. A third change which did not affect the stress remarkably is seen at 25kN and may be attributed to the full penetration of concrete cracks. The maximum tensile stress was 253.83 which confirmed that yielding of reinforcing bars was not imminent.

(d) The Steel Sections

No plastic strain was recorded in the range of loading used in both directions. The localised yield due to stress concentrations in the area of contact between the bolts and the surrounding plates could not be recorded in this model.

9.4 Comparison with 2-D Model

A comparison was made between the current 3-D model and the 2-D one which had the same features. The comparison comprises the load-deflection relationship, the concrete slab behaviour, the maximum stress in the reinforcing bars and the load-slip characteristics.

(a) Load-deflection Curves

Load-horizontal deflection curves obtained from both models are shown in Figure 9.9. From this figure, it can be seen that in the closing moment both curves had almost the same initial stiffness. Because of the concrete cracking, the two curves diverge from each other. Finally, and starting from 24kN until the maximum load of 30kN, the two curves had the same stiffness. This last behaviour may be

attributed to the full cracking of the concrete slab in both models and resisting the tensile forces by the reinforcement which had the same cross-sectional area in both models.

In the opening moment part, although both the current 3-D and the 2-D models had the same order for stiffness with a linear behaviour for both curves, the 3-D model had slightly higher stiffness, which is closer to the experimental values for stiffness. This was expected since 3-D models are generally more accurate than 2-D models, as shown in Figure 9.11.

(b) The Concrete Slab

In the 2-D model, a certain effective width was assumed. It was concluded from the experimental work that this assumption was not correct. This may be attributed to the absence of the transverse reinforcement in the 2-D model. In the current model, the full width of the concrete slab was modelled and the concrete was allowed to crack according to the development of concrete stress. This means that the effective width is controlled by the presence and the propagation of cracks which take place when the preset value of concrete tensile stress is exceeded. This technique proved to be more accurate in representing the actual behaviour of concrete. The major disadvantage of this approach is that because of the employment of condensed concrete elements, cracks start at higher stresses than the actual case.

(c) The Reinforcing Bars

Load-maximum tensile stress curves for the reinforcing bars in both models are shown in Figure 9.10. From this figure, it is clear that the reinforcing bars' stress in the 2-D model had lower values than the central bars in the 3-D model and higher value than the outer ones. In the actual case, the contribution of reinforcing

bars in resisting tensile stresses is proportional to their distance from the centreline of the composite beam. This shows that the current model represented the reinforcing bars more accurately than the 2-D models in which all longitudinal bars are represented as a single bar in the plane of symmetry.

9.5 Comparison with the Experimental Results

Comparisons with the test results were made. The case considered was the frame when the seat cleat was welded to the steel beam. This modification was introduced, as explained in Chapter seven, after several load cycles. during which the concrete slab was cracked. This was not the case in the finite element model.

(a) Load-deflection Curve

In the closing moment, and because this comparison is made with the frame after several load steps during which cracks took place, the 3-D model showed higher stiffness. This is seen from Figure 9.11. The occurrence of cracks in the model caused the two curves to intersect. The stiffness at the maximum load of 30kN is of the same order with a difference in value of 0.35mm.

In the opening moment part, the two curves had the same linear behaviour and are seen as two parallel lines because of the offset of the experimental results due to residual stresses.

(b) The Concrete Slab

In the current model, the first crack started at 10kN as seen from figure 9.6 and was perpendicular to the beam centreline. With increasing load, cracks extended towards the slab free edge. This was, generally, similar to the development of concrete cracks in the concrete slab of the test sample. The fact that cracks started

and propagated in previous load cycles with the slip in the seat cleat bolts led to the difficulty of a direct comparison. In other words, and before loading, the slab in the 3-D model was a perfect one while that in the test was an already cracked one. Apart from this, the pattern of cracks, and the direction of their propagation, was perpendicular to the composite beam as in the test. They were mainly concentrated in the region close to the inner column face which was observed in the early stages of loading during the test. Cracking of the condensed concrete elements, which occurred at 20kN, was expected to start earlier and spread more steadily towards the edge.

9.6 Model Assessment

The major finding of this model is the ability of the three-dimensional model to represent such complex composite problems correctly. The technique of substituting a number of elements by an element which had condensed material properties proved to be successful. It avoided the problems of running time and wave front limitations while representing the problem more closely. The model is more accurate in studying the behaviour of the concrete slab in such structures than the 2-D models.

9.7 Summary

A 3-D finite element model for the analysis of semi-rigid composite connections subject to wind loads is presented in this chapter. The model has been verified by comparison with the results of experimental tests carried out as a part of this study and very good agreement has been obtained. The material properties were also obtained, except for steel sections, experimentally. The steel UB and UC section properties could not be measured without cutting samples from the test sub-frame, which would have precluded its further use. The model can be used to study the behaviour of composite frames under gravity loads and for the study of composite bridges.

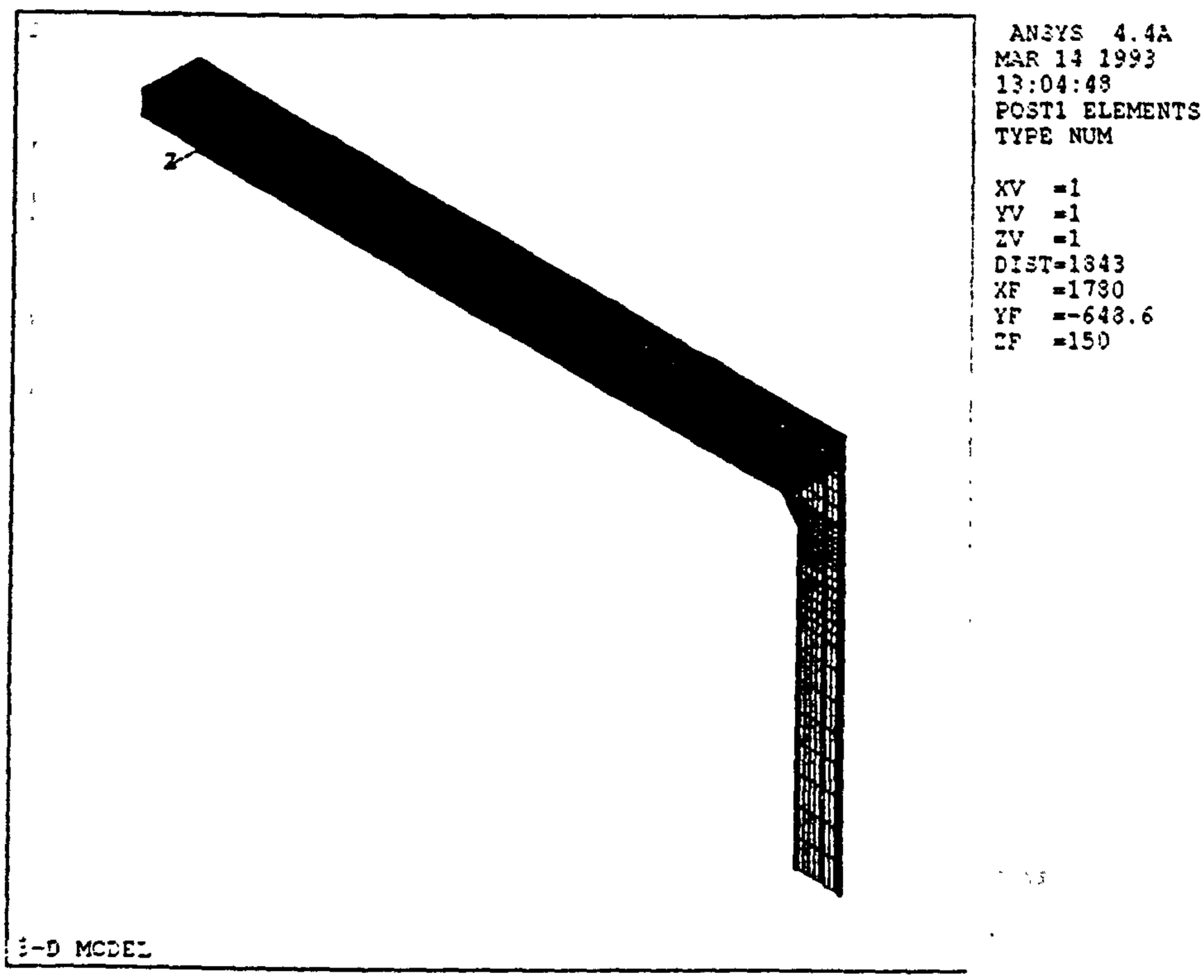

FIGURE 9.1 3-D MODEL OF THE L-SUBFRAME

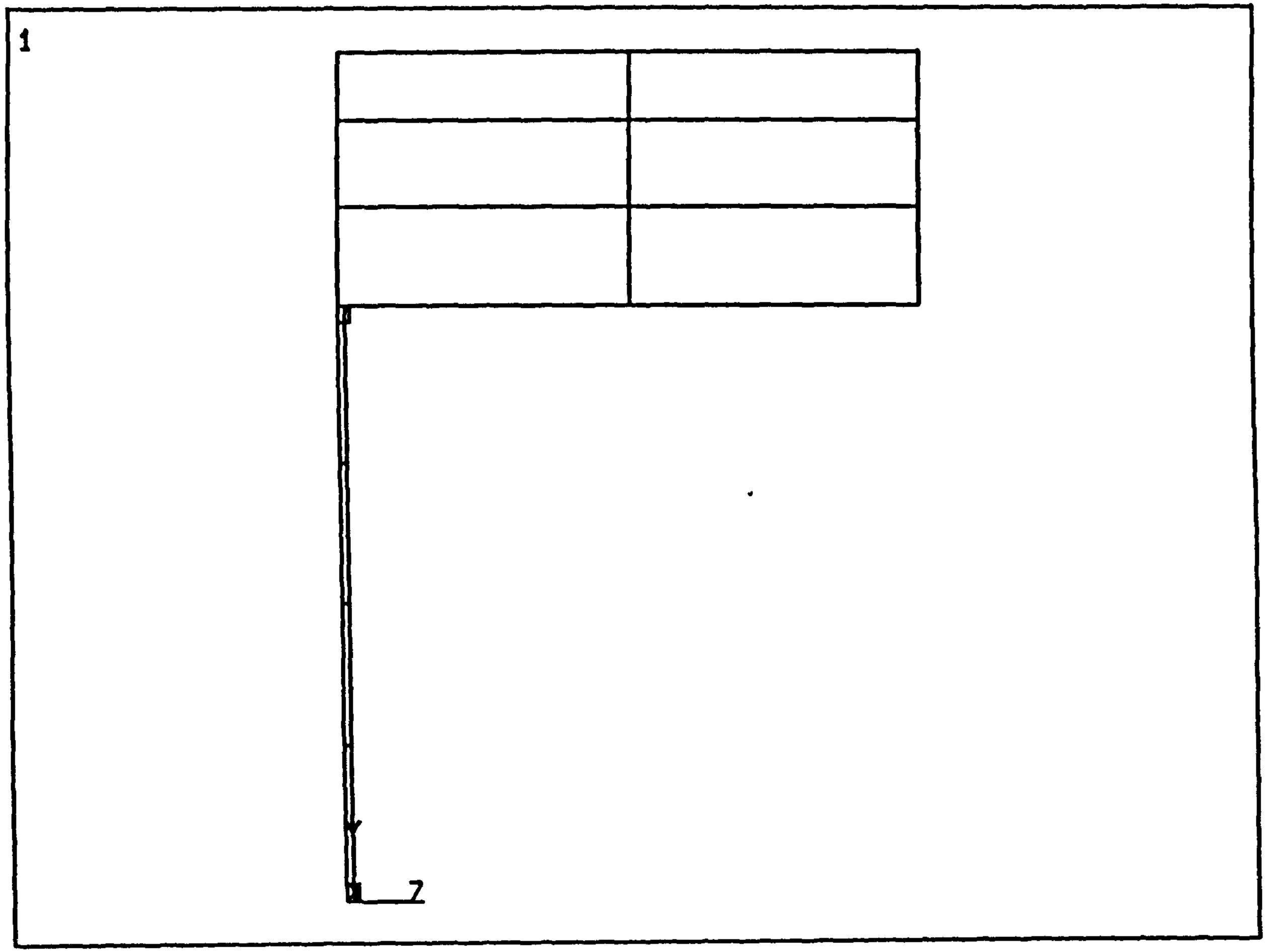

FIGURE 9.2 CROSS-SECTION OF THE COMPOSITE BEAM

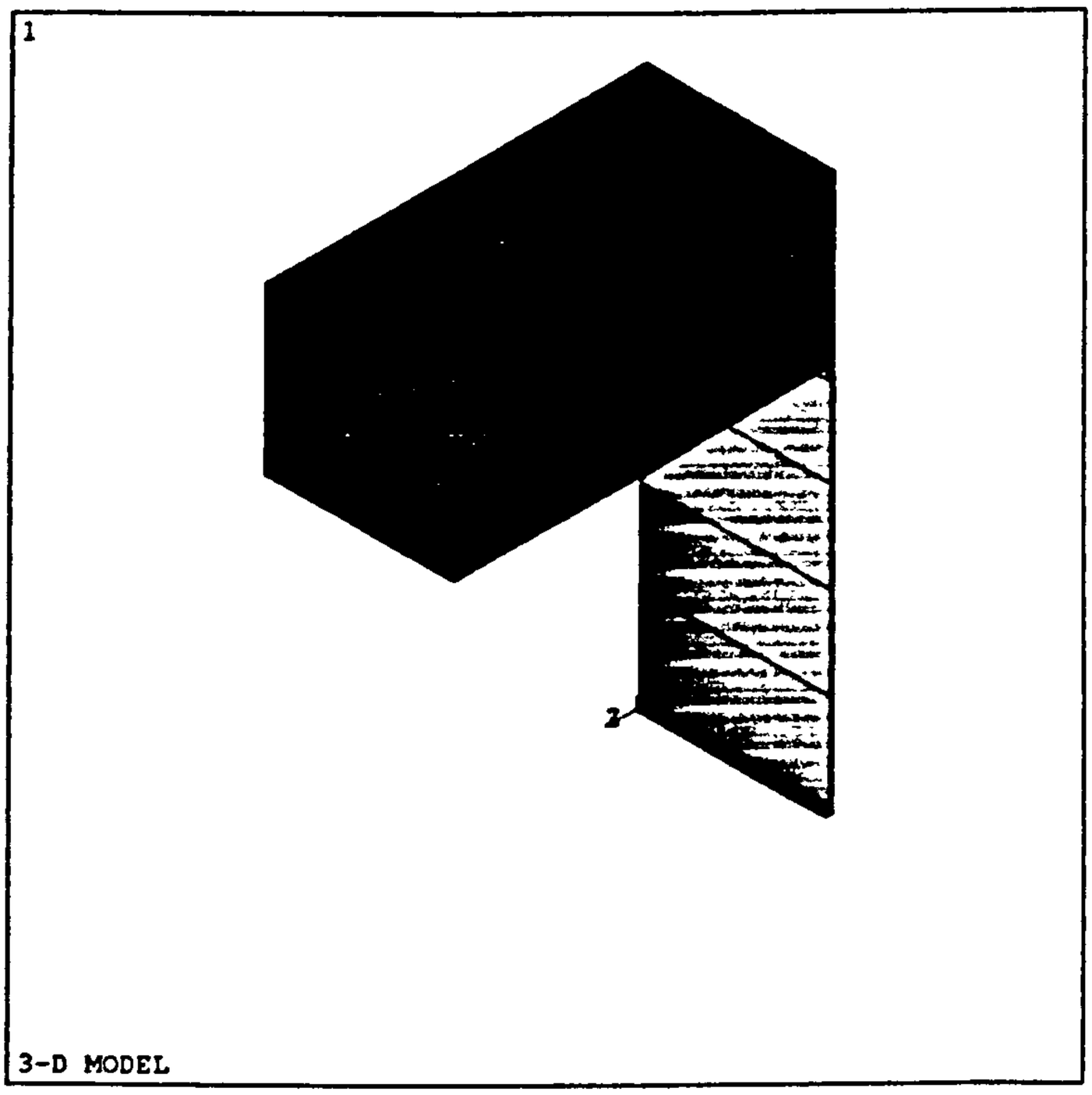

FIGURE 9.3 CONCRETE AND STEEL ELEMENTS IN THE 3-D MODEL

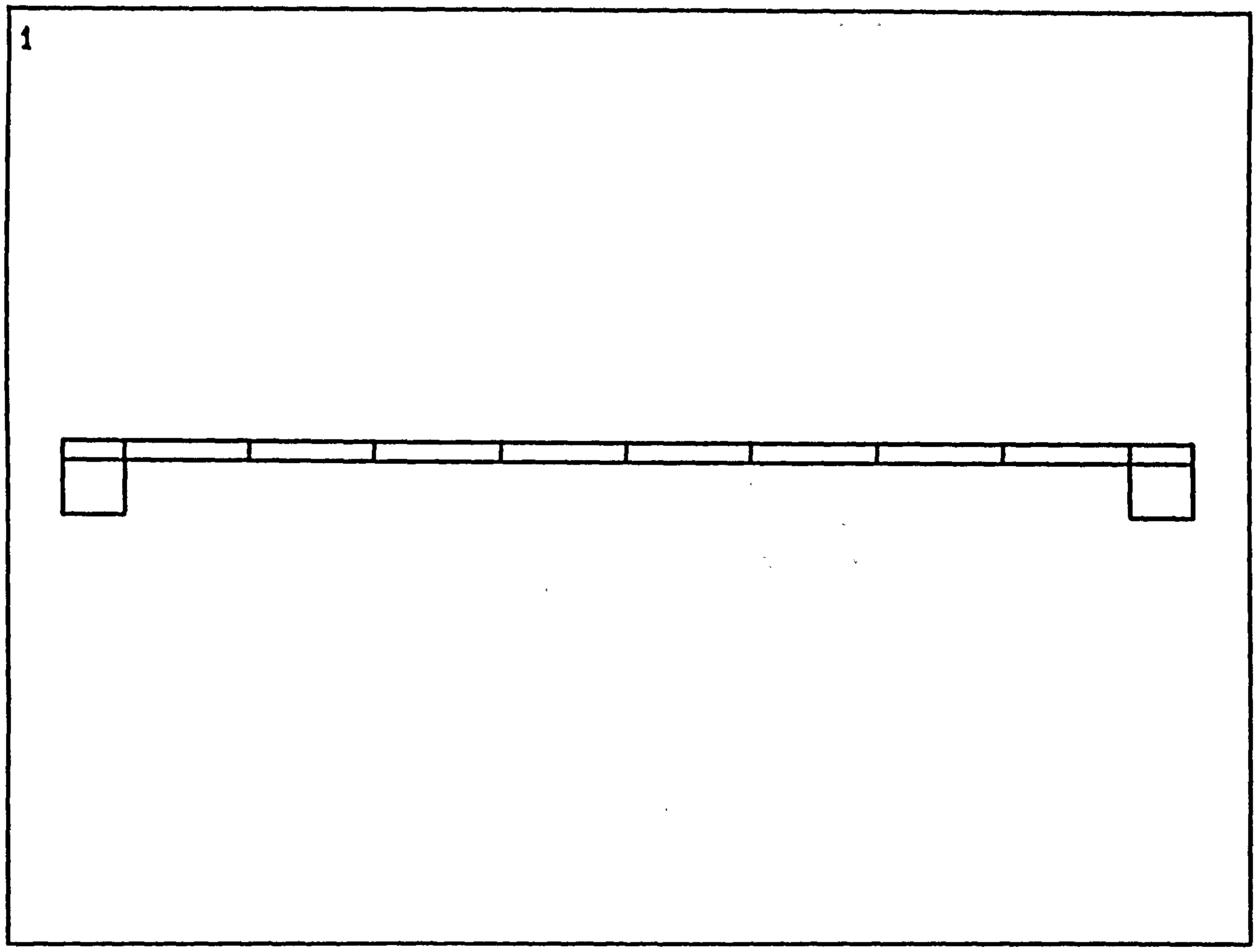

FIGURE 9.4 CROSS-SECTION OF THE COLUMN

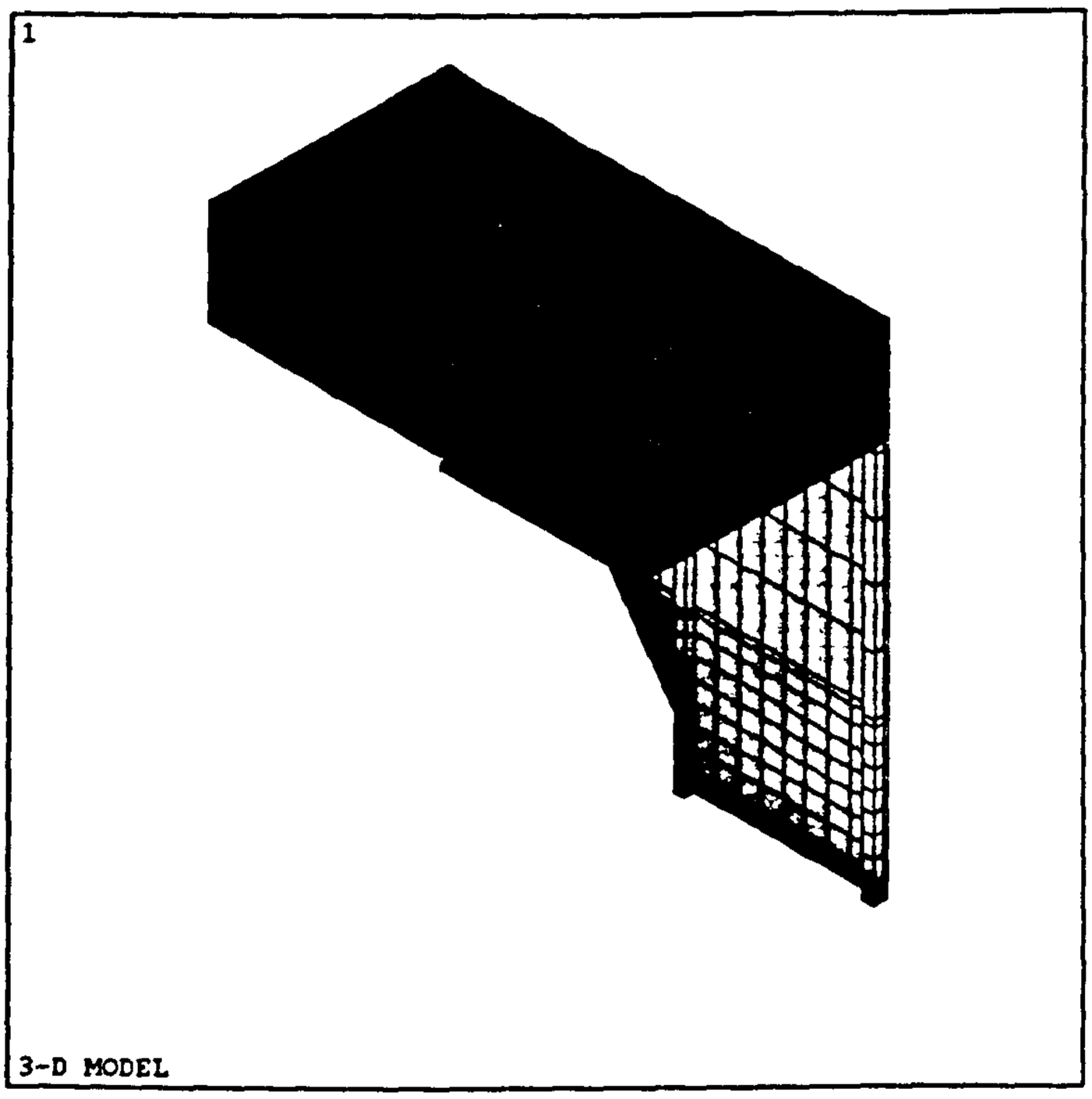

FIGURE 9.5 3-D VIEW OF THE JOINT

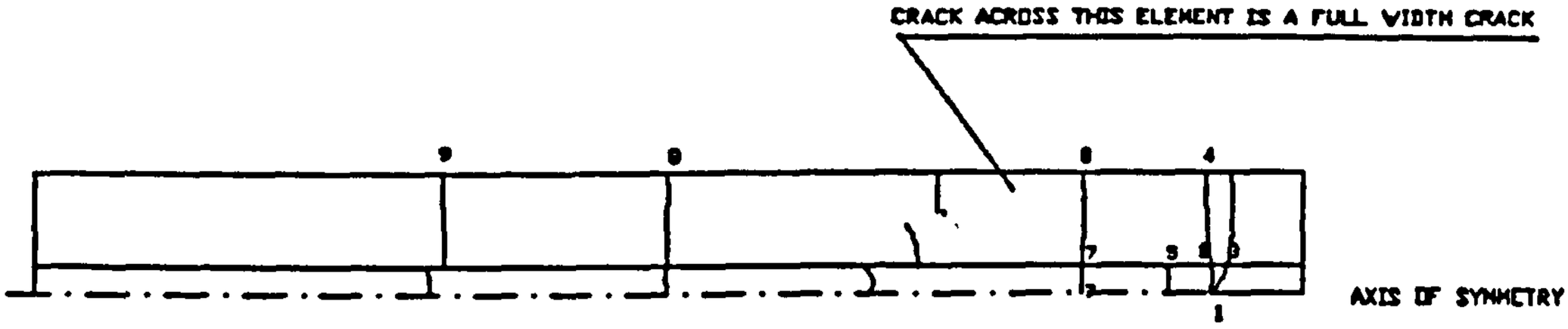

ELEMENT INTERIOR BOUNDARIES ARE OMITTED FOR CLARITY

CRACK PATTERN IN THE 3-D MODEL (PLAN VIEW)

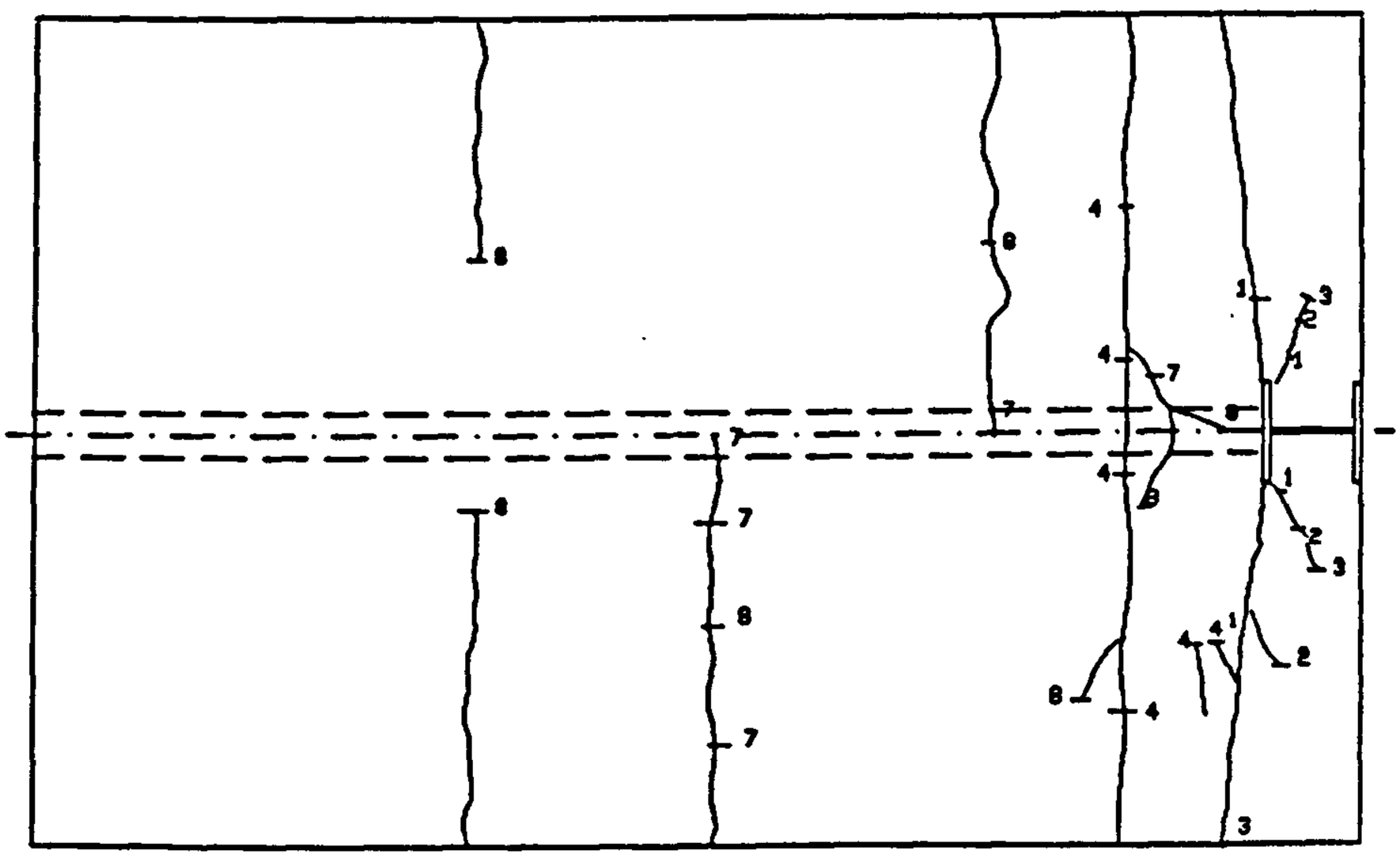

CRACK PATTERN IN THE TEST PIECE

FIGURE 9.6: CRACK PATTERN IN THE 3-D MODEL & IN THE EXPERIMENTAL WORK

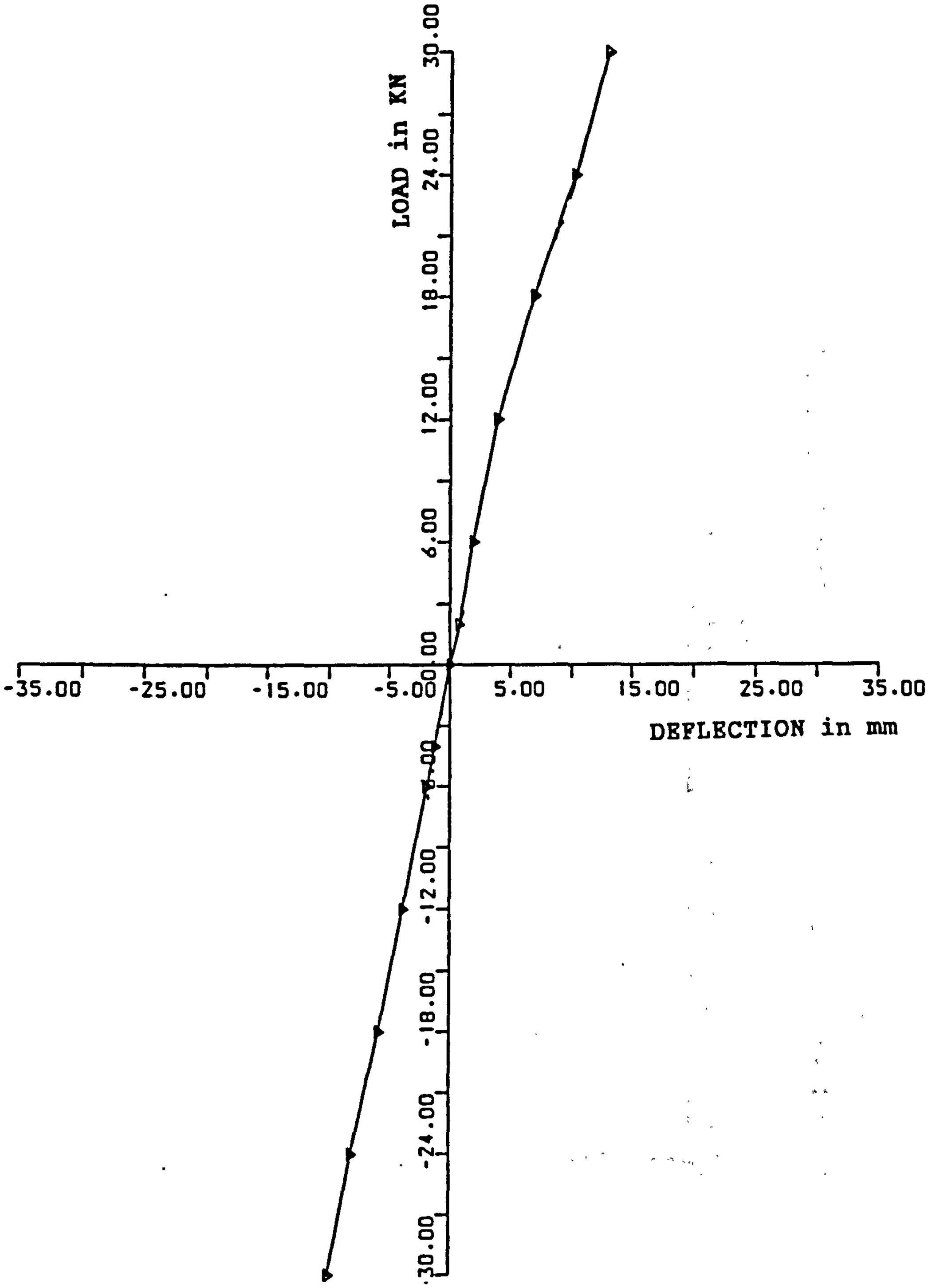

FIGURE 9.7: GRAPHS OF LOAD-LATERAL SWAY, COMPOSITE FRAME WITH WELDED SEAT CLEAT, 3-D NUMERICAL RESULTS

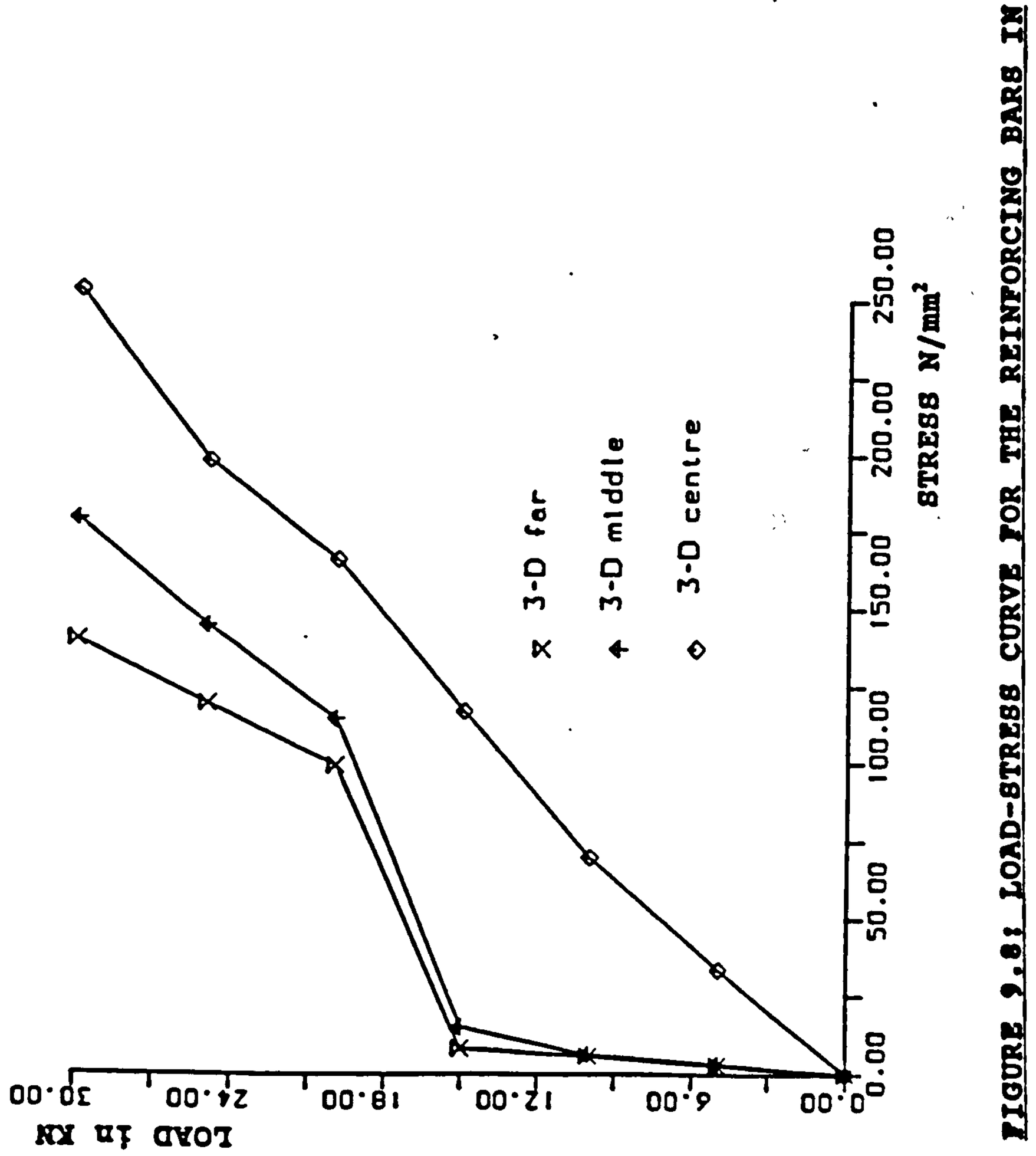

FIGURE 9.81 LOAD-STRESS CURVE FOR THE REINFORCING BARS IN THE 3-D MODEL

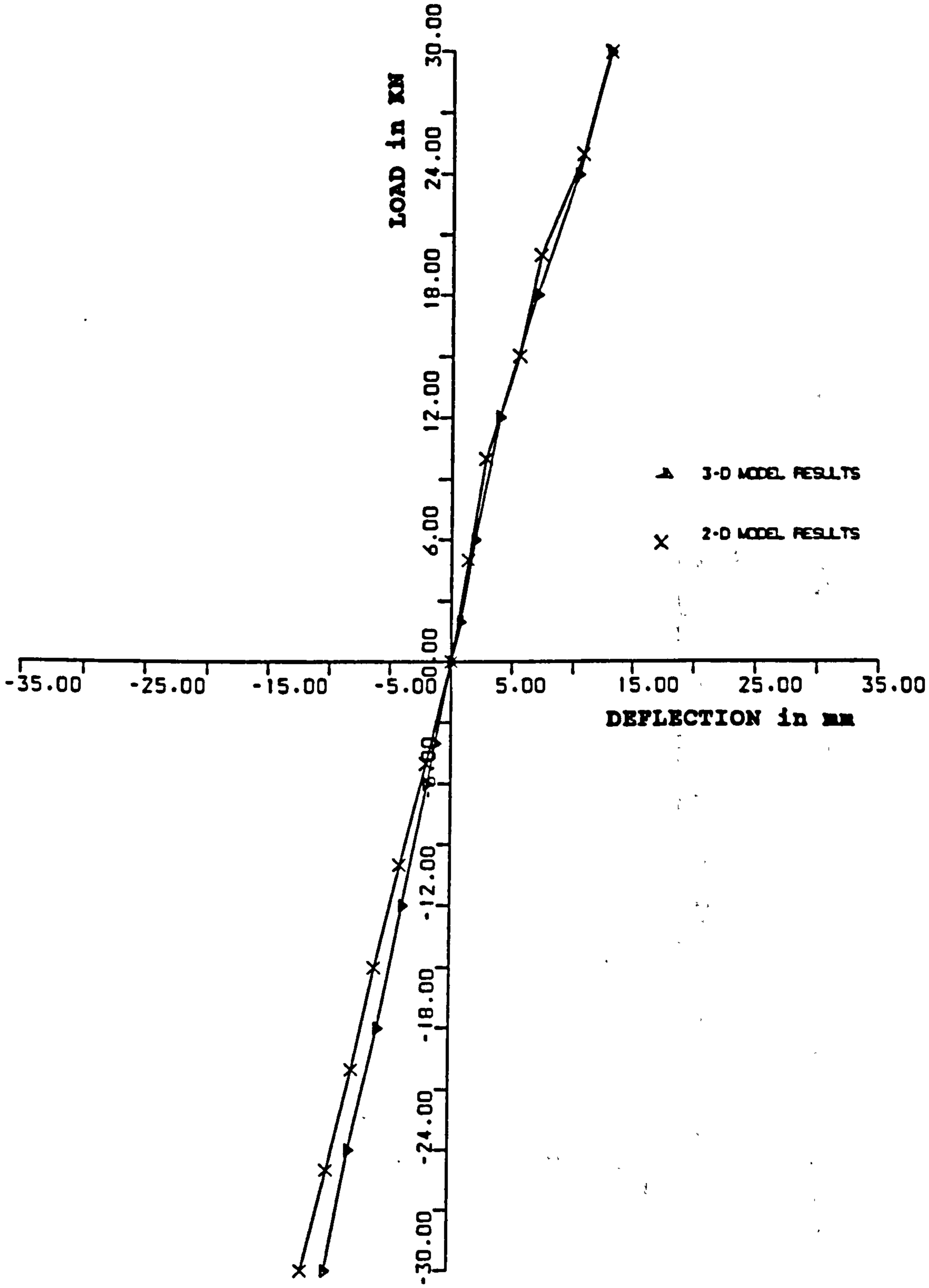

FIGURE 9.9: LOAD-DEFLECTION CURVE, COMPOSITE FRAME WITH WELDED SEAT CLEAT, 3-D & 2-D NUMERICAL RESULTS

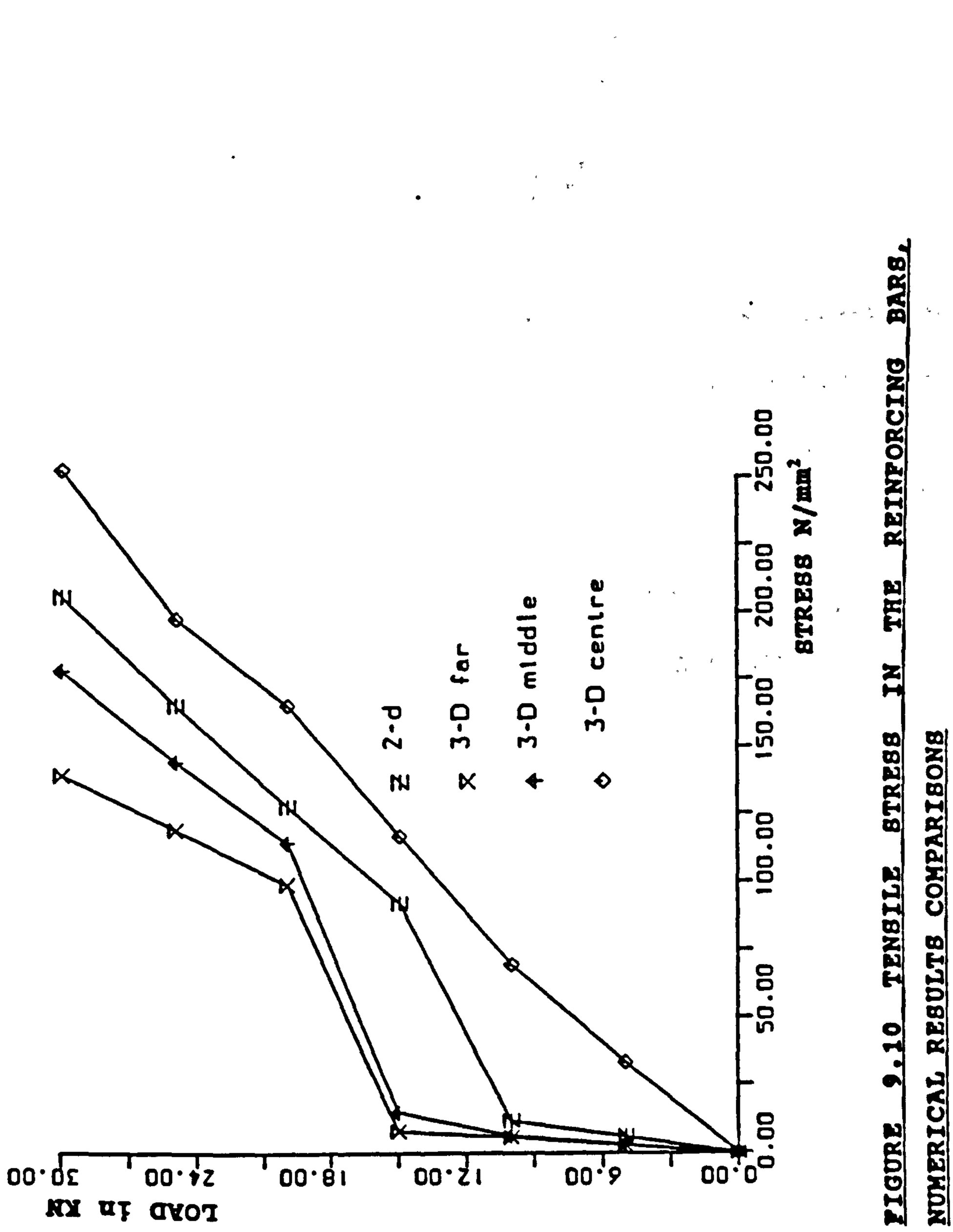

FIGURE 9.10 TENSILE STRESS IN THE REINFORCING BARS, NUMERICAL RESULTS COMPARISONS

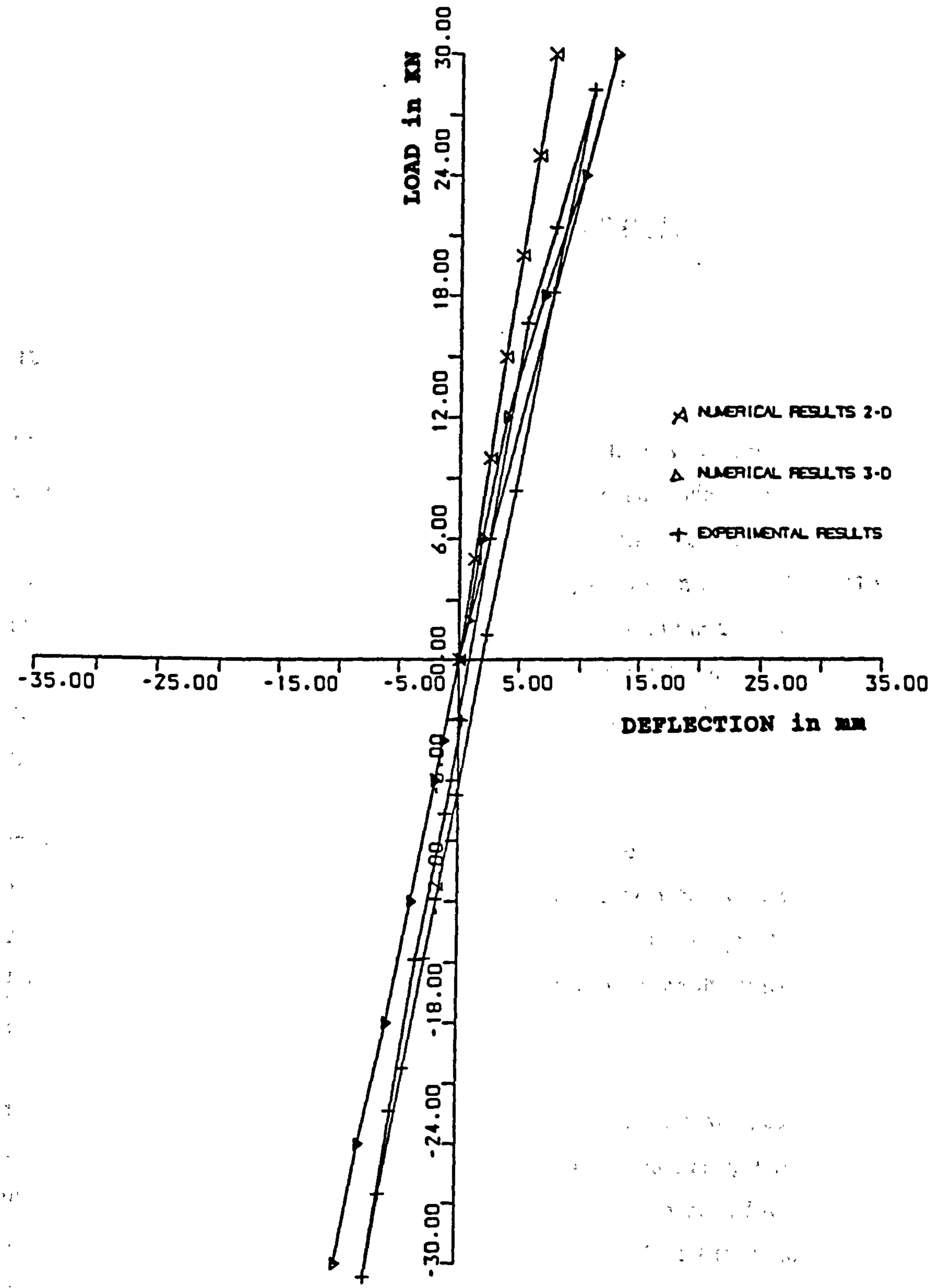

FIGURE 9.11: LOAD-DEFLECTION CURVES, COMPOSITE FRAME WITH WELDED SEAT CLEAT, EXPERIMENTAL AND NUMERICAL RESULTS

CHAPTER TEN

CONCLUSION AND FUTURE WORK

10.1 Introduction

The use of semi-rigid connections in the design of steel frames supporting composite floors with profiled steel decking can provide substantial savings in material and erection costs over the pinned connection design method. It also avoids the intrusion of wind bracing into the useful space within the building. The study reported in the preceding chapters was undertaken, with the aims of achieving a better understanding of the behaviour of semi-rigid composite connections resisting wind loads, and of quantifying the degree of rigidity achieved.

The complex interactions of the various parameters involved in connection formation and the high cost associated with the experimental work, created the need for a numerical simulation. The analysis of the connection subject to wind loads has been carried out using the finite element method using the numerical package ANSYS.

Using the finite element method, two-dimensional models were developed to predict the behaviour of the frame when resisting opening and closing moments. They also provided complete information up to the maximum expected wind load. The models were nonlinear due to the nature of concrete and steel materials. The geometry and material properties used as input data were based on the current practice of composite construction.

A three-dimensional model was also developed to check the accuracy of the 2-D models. Results of ¬ shaped sub-frame (Model One) were compared with those of the 3-D model. The comparison indicated a very good agreement between the results. The verification was needed to increase the degree of confidence in the 2-D numerical predictions.

An experimental study was then carried out. The study was primarily concerned with the overall behaviour of the frame so that results could be applied to real buildings. The localised stress analysis was also justified, and from the results can be drawn clear indications of good construction detailing at the joint to maximise resistance to lateral loads.

The scope of the research was limited to cleated beam to column connections. In these connections the welding process is carried out on the columns only, which minimizes the fabrication cost.

10.2 The Numerical Study

It was found to be practically impossible to model every detail of the structure to achieve total resemblance between the finite element model and the actual structure. As far as the overall behaviour of the model was concerned, it was feasible to adopt a finite element model which approximated the geometry in the actual structure. This was clear in modelling the profiled steel sheet together with the concrete layer contained in it by a concrete layer which had reduced material properties.

Modelling of the partial shear connection has been carried out using a novel system of spar and gap elements. Each shear connector was connected by two spar elements which represent the traction effect. Two closed gap elements were connected to each shear connector to prevent separation and penetration.

The numerical stability of the model was ensured by using a set of suitable boundary conditions and by avoiding sharp variation of the structure's stiffness by following a gradual change in the slab width.

In the four configurations studied, the assumption of the presence of points of contraflexure at mid-height of columns and mid-span of beams was used. Gravity loads were assumed to have no effect on the lateral displacements.

Based on the numerical study, the following conclusions can be deduced:

(1) The semi-rigid composite frame (including concrete slab, steel beams and columns, seat and web cleats) modelled the actual structure very accurately.

(2) The two-dimensional analysis proved to have the ability to represent the actual overall behaviour of composite connections. This was concluded from the good agreement between numerical and experimental results.

(3) The technique of using condensed material properties to represent a set of elements in one element, which was adopted in the three dimensional model, seems to be successful in reducing the number of elements and getting good results as far as the overall behaviour of the model is concerned.

(4) Use of finite element software major packages offers a powerful tool to study complicated engineering problems. A good understanding of the nature of the problem, the geometrical and material properties of different constituents and how to represent these within the programme capabilities is essential to get correct predictions.

(5) The lateral deflection of the frame is critically dependant on the physical gaps between the bolts and their holes. The sensitivity of the model to the presence and size of this gap was proved. With a bolt-hole clearance of

2mm, the lateral sway of the frame was five times that of the frame without any clearance.

(6) Although the connection undertaken proved to have significant lateral stability and strength, it could not limit deflections sufficiently for the full wind load, without some modifications. This was clear from the load-deflection relationship for the frame with typical geometry and assembly details used in current construction.

(7) The connection with initially closed bolt-hole clearance is the stiffest, while that with initially open gaps possess the least stiffness. Even with closed bolt gaps, the standard connection analysed does not have sufficient stiffness to resist the full wind load with the deflection kept within the specified value of 1/300 of the inter storey height.

(8) It was concluded that when end gaps are initially closed, or in the absence of the construction tolerance which could be achieved practically by a packing plate, the connection possesses high early stiffness. It has the highest stiffness if bolt-hole gaps are also closed.

(9) Corner bracing proved to have a very beneficial effect in increasing the stiffness of such connections. It reduces the lateral deflection of the structure and makes the load-deflection curve of it a linear one. The effect of the bracing is achieved regardless of the bolt-hole clearance or the construction tolerance. The major disadvantage of this option is that it is practically difficult and thus expensive.

(10) In the case of a closing moment, the concrete slab is in the tensile stressed zone while in opening moment it resists compression. Use of more reinforcing bars in the slab showed that after the closure of bolt gaps, increased reinforcement area increased the stiffness of the connection.

(11) The frame with the deep beam of section 305×102×28kg/m proved to be laterally stiffer than that with the shallow one of section 250×102×25kg/m. The lateral sway of the frame can be resolved into two components: the first is the deflection of the column as a cantilever, the second is dependent on the angle of rotation (Φ) which is proportional to the second moment of area of the composite beam.

(12) A stiffener plate may be welded to the seat cleat. With this plate, the lever arm of the moment increases to be the distance between the reinforcing bars and the resultant of the forces transmitted by the seat cleat and the stiffener plate. For this reason, the stiffener plate increases the lateral stiffness of the joint.

(13) As an option for increasing the lateral stiffness of the connection, the seat cleat was replaced in one of the numerical models by a larger, heavier one. The lateral stiffness of the joint increased with the use of the deeper angle. In case of opening moment, the tensile force produced from the bending moment is transmitted to the column through the horizontal plate of the cleat angle. An increase of the area of this plate increases the moment capacity of the connection. For a closing moment, the compressive force passes down the seat cleat stiffener into the column web.

(14) With the use of a heavier seat cleat and additional reinforcing bars, wind loads can be resisted by the semi-rigid connections of the frame providing that slip of bolts is prevented somehow.

(15) The complex influences of the various parameters involved in connection formation and the difficulties associated with the experimental work, showed the necessity of the numerical simulation using the finite element method.

(16) Designers are strongly advised to pay more attention to the detailing of the steel part of composite connections and not to leave it to the contractor. With a simple modification, composite beam-column connections can withstand significant amount of wind, or limited horizontal components of earthquake loads.

10.3 The Experimental Study

Based on the experimental results, the following conclusions can be deduced:

(1) As expected, the lateral stiffness of the connection was greatly affected by the movement of the seat cleat relative to the steel beam. This is, in turn, dependant on the relative movement of the seat cleat bolts inside bolt holes. With two bearing bolts, this movement was maximum and consequently, the lateral stiffness of the frame was minimum. When the seat cleat was welded to the steel beam, the relative movement was very limited and the lateral stiffness was greatly increased. Unfortunately, this option is associated with some practical on-site difficulties.

(2) There was no significant increase in the lateral stiffness of the decked frame over the bare steel one. This is because of the orientation of the ribs, which was perpendicular to the steel beam.

(3) Use of High Strength Friction Grip bolts is accompanied by some practical difficulties regarding torque control and bolt inspection. These bolts also showed readiness to slip earlier than expected when the prying moment was reversed.

(4) HSFG bolts should be used in the case of load reversals only with reduced load carrying capacity. The author recommends a reduction to 0.85 of their initially designed capacity. The need for this reduction is clear from the slippage of the bolts at a lower load when the load was reversed.

(5) During the test, neither buckling nor yielding of any part of the steel sections was recognised other than in small areas within bolt holes until sufficient bearing area was established.

(6) None of the welds, including site welds failed during testing of the frame.

(7) No yield of the reinforcing bars occurred.

(8) As a result of having low concrete compressive strength, the results may represent the lower bound of the stiffness offered by such connections in real buildings.

(9) Without any modification, the connection has the ability to resist wind loads in 3 story building when exposed to a design wind speed of 50m/second in Scotland.

(10) With a welded seat cleat the frame can withstand the full wind loads on a five story building without the use of any wind bracing.

(11) With 4 HSFG bolts, a typical frame can resist wind loads in a 5 story building.

(12) The connection studied in this research is the cleated one. More rigid steel details are expected to offer higher lateral stiffness. An example of is the end plate connection which is expected to have the ability to resist wind loads in the same range as the welded seat cleat result without any modification. This is concluded from both the experimental and numerical results which showed that the absence of bolt slip would have led to a stiff joint.

(13) A composite beam-column connection with an end plate steel connection, in which relative motion between the end of the steel beam and the column is

minimized, is capable of resisting wind loads on a five storey building. An additional reinforcement may be needed as described in the experimental part.

(14) To provide sufficient anchorage length to the additional reinforcing bars, two inverted bars may be used to transmit the loads to the column. The shape used in the experimental work is suggested.

(15) Throughout the tests, neither concrete crushing nor excessive tensile cracks were observed. It is therefore concluded that in the range of wind loads safe participation of the concrete slab is expected.

(16) The range of stiffness results obtained from this research is as follows:
With two 8.8 bearing bolts, 1.0KN/mm or 616.2KN.m/rad.
With 2 HSFG bolts 1.5KN/mm or 924 KN.m/rad
With 6 HSFG bolts 2KN/mm or 1232KN.m/rad.
With a welded seat cleat 3.52KN/mm or 2168KN.m/rad.
This range should encompass all likely stiffnesses for other commercial steel joints types.

<u>Design Guide</u>

The following table is given as a guide for the designers. The range of wind loads given covers the three values for the south, midland and scotland areas of Britain. The wind loads are based on a 4m storey height and 6m between transverse steel frames. Wind loads could be calculated for other areas following the same procedure.

The figures quoted in the table are for the critical bottom storey of the building. Lateral load is reduced on the upper storeys and a reduced resistance may be appropriate.

The presence of a core (shaft) around the stair case may be employed to resist a significant amount of lateral loads. Cladding and partitions are also additional sources for lateral stiffness. These lateral load resistances should be calculated in the normal way.

Table 10.1 Design Recommendations

Basic wind speed m/s	No. of storeys	Total wind load on the frame kN	Load/ ¬ sub-frame kN	Design recommendations	Sub-frame resistance Kn
38m/sec Southern areas	3	36.58	9.145	Unmodified frame with 2x8.8 bearing bolts. No additional reinforcement is required.	10.2
	4	49.48	12.37	2 HSFG bolts and 2T16 additional reinforcement.	12.5
	5	62.4	15.6	4 HSFG bolts to be used with the seat cleat. An additional reinforcement of 2T16.	17.0
44m/sec Midlands	3	49.05	12.26	2 HSFG bolts and 2T16 additional reinforcement.	12.5
	4	66.35	16.58	4 HSFG bolts to fix the seat cleat. An additional reinforcement of 2T16.	17.0
	5	83.6	20.9	6 HSFG bolts to fix the seat cleat. An additional reinforcement of 2T16.	21.0
50m/sec Scotland	3	63.34	15.83	4 HSFG bolts to be used with the seat cleat. An additional reinforcement of 2T16.	17.0
	4	85.685	21.42	6 HSFG bolts to fix the seat cleat. An additional reinforcement of 2T16.	21
	5	108.03	27.0	Welded seat cleat together with an additional reinforcement of 2T16.	30.0

10.4 Suggestions for Future Work

The proposed extent of the continuation of this study can be summarised as follows:

(a) Numerical Modelling

(1) To reduce the number of full scale tests, the models already developed may be used to carry out a systematic survey on the parameters affecting the behaviour of the joints. This may be achieved by changing one or more of the associated material and geometrical properties.

(2) Also it should be possible to study the performance of a typical building using combinations of the basic sub-frames. This may include preparing a model representing the first storey of the building. The full-height of the columns may be included and the boundary conditions may be chosen to represent the foundations of the frame. A certain amount of fixity can be assumed instead of the hinge previously used at the column to beam joint.

(3) Studying the behaviour of composite frames subject to dynamic loading. This may be carried out both numerically and experimentally.

(4) Study of the earthquake effects on similar buildings. This effect may be dealt with in a similar way with loads increased to represent those associated with an earthquake. Increasing the rigidity of an existing frame to withstand earthquakes may also be studied.

(b) Experimental

(1) More experimental work on a similar frame sub-assembly with the change of the concrete compressive strength, different percentages of reinforcement, different orientations and types of decking.

(2) Studying the behaviour of a composite frame with less shear connection subject to wind loading numerically and experimentally.

(3) Testing of other composite connections with steel details which avoid the problem of bolt slip.

(4) Site investigation of the yactual behaviour of a similar frame over a certain period of time. This may employ simple on-site instrumentation.

(5) Loading of a typical frame with a heavy truck or a tank. The applied load should be the expected maximum wind load. Measurement of the lateral sway of the frame can then be compared with the predicted and allowable values.

(6) Development of suitable equipment for spot welding of plates with thickness up to 20mm, which is suitable for similar problems, is a good subject for a future research. Understanding welding techniques and metallurgy of steel is essential. As an alternative, a self-drilling self-tapping equipment which is capable of penetrating such thicknesses may be a good solution.

REFERENCES

1. JOHNSON, R.P., "Composite Structures of Steel and Concrete", Vol.1, Beams, Columns, Frames and Applications in Building, 1971.

2. WRIGHT, H.D., EVANS, H.R., and HARDING, P.W., "The Use of Profiled Steel Sheeting in Floor Construction", J. Construct. Steel Research, 1987, pp.279-295.

3. EVANS, H.R. and WRIGHT, H.D., "Steel-Concrete Composite Flooring Deck Structures", Steel-concrete Composite Structures, Stability and Strength, ed. R. NARAYANAN, Elsevier Applied Science.

4. LEON, R.T., "Semi-rigid Composite Construction", J. Construct. Steel Research, Vol.15, 1990, pp.99-120.

5. ZANDONINI, R., "Semi-rigid Composite Joints", Structural Connections: Stability and Strength, ed. R. NARAYANAN, Elsevier Applied Science, 1989, pp.63-120.

6. LEON, R.T., AMMERMAN, D.J., "Semi-rigid Composite Connections for Gravity Loads", American Institute of Steel Construction, First Quarter, 1990, pp.1-11.

7. COOKE, G.M.E., LAWSON, R.M. and NEWMAN, G.M., "Fire Resistance of Composite Deck Slabs", The Structural Engineer, Vol.66, No.16, 16 August 1988, pp.253-261.

8. ECHETA, C.B., " Semi-rigid Connections between Concrete Filled Steel Columns and Composite Beams", Ph.D. Thesis, University of London, 1982.

9. LAWSON, R.M., "Composite Beams and Slabs with Profiled Steel Sheeting", CIRIA Report No.99, 1983.

10. WRIGHT, H.D. and FRANCIS, R.W., "Tests on Composite Beams with Low Levels of Shear Connection", The Structural Engineer, Vol.68, No.15, 7 August 1990.

11. DAVIES, J.M. and FISHER, J., "The Diaphragm Action of Composite Slabs", Proc Instn. Civ. Engnrs, Vol.67, No.2, 1979, PP.891-906.

12. OEHLERS, D.J. and PARK, S.M., "Shear Connectors in Composite Beams with Longitudinally Cracked Slabs", Journal of Structural Engineering, Vol.118, No.8, August, 1992.

13. DANIELS, B.J. and CRISINEL, M., "Composite Slab Behaviour and Strength Analysis. Part I: Calculation Procedure", Journal of Structural

Engineering, Vol.119, No.1, January, 1993.

14. DAVISON, J.B., LAM. D. and NETHERCOT, D.A., "Semi-rigid Action of Composite Joints", The Structural Engineer, Vol.68, No.24, 18 Dec. 1990.

15. BS 5950: Structural Use of Steelwork in Building: Part 4, Code of Practice for Design of floors with Profiled Steel Sheeting, British Standards Institution, London, 1982.

16. JONES, S.W., KIRBY, P.A. and NETHERCOT, D.A., "The Analysis of Frames with Semi-rigid Connections- A State-of-the-art Report", Journal of Constructional Steel Research, Vol.3, No.2, 1983.

17. DANIELS, J.H. and FISHER, J.W., "Static Behaviour of Continuous Composite Beams", Fritz Engineering Laboratory Report No.324/2, Lehigh University of Research, 1967.

18. JOLLY, C.K. and LAWSON, R.M., "End Anchorage in Composite Slabs: an Increased Loadcarrying Capacity", The Structural Engineer, Vol.70, No.11, 2 June 1992.

19. JOHNSON, R.P., "Continuous Composite Beams for Buildings", Report of JABSE-ECCS Symposium, Steel in Buildings, Luxembourg, pp.195-202.

20. XIAO, Y., CHOO, B.S., and NETHERCOT, D.A., "Design of Semi-Rigid Composite Beam-Column Connections", Building Research Establishment Report (unpublished).

21. STARK, J.W.B. and BIJLAARD, F.S.K., "Structural Properties of Connections in Steel Frames", Connections in Steel Structures, Behaviour, strength & design, ed. by Bjorhoved, R., Brozzetti, J. and Colson, A.

22. ANDERSON, D., BIJLAARD, F., NETHERCOT, D.A. and ZANDONINI, R., "Analysis and Design of Steel Frames with Semi-rigid Connections", IABSE Survey No.s-39/87, 1987.

23. ANDERSON, D., "Design Of Multi-storey Steel Frames to Sway Deflection Limitations", Steel Framed Structures, stability and strength ed. by R. NARAYANAN.

24. CUNNINGHAM, R., "Some Aspects of Semi-rigid Connections in Structural Steel Work", The Structural Engineer, Vol.68, No.5, 1990, pp.85-92.

25. BJORHOVDE, R., COLSON, A. and BROZZETTI, J., "Classification System for Beam-to-column Connections", Journal of Structural Engineering, Vol.116, No.11, November, 1990.

26. AMMERMAN, D.J., and LEON, R.T., "Behaviour of Semi-Rigid Composite Connections", American Institute of Steel construction, Second Quarter, 1987, pp.53-61.

27. NETHERCOT, D.A. and ZANDONINI, R., "Methods of Prediction of Joint Behaviour: Beam-to-Column Connections", Structural Connections: Stability and Strength, ed. R. NARAYANAN, Elsevier Applied Science publishers, London, pp.22-62.

28. LEON, R.T., "Behaviour and Design of Semi-Rigid Composite Frames", American Institute of Steel Construction, pp.699-705.

29. BEAULIEU, D. and PICARD, A., "Finite Element Modelling of Connections", Connections in Steel Structures, Behaviour, strength & design, ed. by Bjorhoved *et al.*

30. CHEN, W.F., and KISHI, N., "Semi-rigid Steel Beam to Column Connections: Database and Modelling", ASCE, Journal of Structural Engineering, Vol.115, No.1, January 1989, pp.105-119.

31. MAXWELL, S.M. JENKINS, W.M. and HOWLETT, J.H., "A Theoretical Approach to the Analysis of Connection Behaviour", Joints in Structural Steelwork, ed. by J. H. HOWLETT, W. M. JENKINS and R. STAINSBY.

32. LIPSON, S.L. and HAGUE, M.I., "Elasto-plastic Analysis of Single-angle Bolted-welded Connections using the Finite Element Method", Computers and Structures, Vol.9, 1978, pp.533-45.

33. RICHARD, R.M., GILLETT, P.E., KRIEGH, J.D., and LEWIS, B.A., "The Analysis and Design of Single Plate Framing Connections", Engng J., Amer. Inst. Steel Constr., Vol.17, 1980, pp.38-52.

34. ZANDONINI, R. and ZANON, P., "Experimental Analysis of End Plate Connections", Connections in Steel Structures: Behaviour, strength & Design, ed. R. Bjorhovde *et al.*, London, 1988, pp.44-51.

35. PATEL, K.V. and CHEN, W.F., "Analysis of Fully bolted moment connection using NONSAP, Computers and Structures, Vol.21, No.3, pp.505-511.

36. PUHALI, R., SMOTLAK, I. and ZANDONINI, R., "Semi-rigid Composite Action: Experimental Analysis and a Suitable Model", J. Constr. Steel Research, Vol.15, 1990, pp.121-151.

37. ANSYS, Engineering Analysis System User's Manual, Vols. 1 and 2, Version 4.4a, Swanson Analysis System Inc., Houston, Pennsylvania,

U.S.A., 1991.

38. SIBAI, W.A. and FREY, F., "Numerical Simulation of the Behaviour up to Collapse of two Welded Unstiffened One-side Flange Connections", Connections in Steel Structures, Behaviour, strength & design, ed. by Bjorhoved *et al.*

39. VAN DALEN, K. and GODOY, H., "Strength and Rotational Behaviour of Composite Beam-Column Connections", Canadian Journal of Civil Engineering, Vol.9, No.2, 1982, pp.313-322.

40. LIN, J.J., FAFARD, M., BEAULIEU, D. and MASSICOTTE, B., "Nonlinear Analysis of Composite Bridges by the Finite Element Method", Computers and Structures, Vol.40, No.5, 1991, ed. Chief Harold Liebowitz, programme press, Oxford.

41. LEON, R.T., AMMERMAN, D.J., LIN, J., and McCAULEY, R.D., "Semi-rigid Composite Steel Frames", American Institute of Steel Construction, Fourth Quarter, 1987, pp.147-155.

42. LEON, R.T., "Semi-rigid Composite Steel Frames", A.S.C.E., Apr-May 1987, pp.1-29.

43. AMMERMAN, D.J., "Behaviour and Design of Frames with Semi-Rigid Composite Connections", Ph.D. thesis, University of Minnesota, 1989.

44. XIAO, Y. NETHERCOT, D.N. and CHOO, B.S., "Moment resistance of Composite Connections in Steel and Concrete", Constructional Steel Design, ed. by DOWLING, HARDING, BJORHOVDE, and MARTINEZ-ROMERO, pp.331-343, Elsevier Applied Science, London, 1992.

45. PARSA, A., "Finite Element Modelling of Stress-Concentrations in Reinforced Concrete Offshore Structures", Ph.D. Thesis, Civil Engineering Department, University of Southampton, 1990.

46. POGGI, C. and ZANDONINI, R., "Behaviour and Strength of Steel Frames with Semi-rigid Connections", ASCE Convention, October 1985.

47. LAW, C.L.C., " Planar NO-sway Frames with Semi-rigid Beam-to-column Joints", Ph.D. Thesis, University of Warwick, 1983.

48. STEEL DESIGNERS' MANUAL, Fourth Edition, Constructional Steel Research and Development Organization.

49. BS 3692, "Specification for ISO Metric Precision Hexagon Bolts, Screws and Nuts", British Standards Institution, London, 1967.

50. BS 5400, Steel, Concrete and Composite Bridges, Part 4, Code of Practice for Design of Concrete Bridges, British Standards Institution, London, 1984.

51. BS 8110, The Structural Use of Concrete, Part 1, Code of Practice for Design, British Standards Institution, London, 1985.

52. EL-SHIHY, A.M., "Unwelded Shear Connectors in Composite Steel and Concrete Structures", Ph.D. Theses, University of Southampton, 1986.

53. BS 639, 1976, Covered Electrodes for the Manual Metal-Arc Welding of Carbon and Carbon Manganese Steels, British Standards Institution, London, 1976.

54. NELSON, T.R.W., Weld-Through Deck Application and UK Design Data Manual, 1983.

55. BSI CP3, Chapter V, Part 2, 1972, Code of Basic data for the Design of Buildings, Chapter V: Loading, Part 2: Wind Loads.

56. BS 6399 Loading for Buildings, Part 2: Wind Loading.

57. BS 5950 Structural Use of Steelwork in Building, Part 1, Code of Practice for Design in Simple and Continuous Construction, Hot Rolled Sections, British Institution standards, London, 1985.

APPENDIX I

WIND LOAD CALCULATIONS

Wind loading on buildings can be calculated according to BS6399: Part 2 [55,56]. The basic wind speed appropriate to the location of the building is selected and reduced to a design wind speed. This reduction is carried out using factors which take into consideration topography, shelter from surrounding buildings, height above ground level, building size and period of exposure.

The design wind speed is used to evaluate the dynamic pressure, q kN/m^2. Due to building and roof shape, openings in walls, etc., pressures and suction both external and internal arises. The coefficient of external pressure (C_{pe}) and that of internal pressure (C_{pi}) may be used to calculate the force on any element.

Force on any structural element $=(C_{pe}-C_{pi})\times q \times$area of element

Wind load calculations for design purposes are based on three assumptions [48]. These assumptions are:

(i) Vertical loads have a negligible effect on horizontal displacements.

(ii) A point of contraflexure exists at the mid-height of each column (except in the bottom storey), and at the mid-span of each beam.

(iii) The total horizontal shear is divided between the bays in proportion to their relative stiffness.

These assumptions render a frame statically determinate, except in the bottom storey, and enable each storey to be considered in isolation.

(1) The basic wind speed V is determined according to the district, ranging between 38m/sec in London area and 56m/sec in the North of Scotland. The value of 50m/sec which is considered herein lies within these two extremes and is an upper bound for all but the Scottish highlands.

(2) The design wind speed $V_s = V \times S_1 \times S_2 \times S_3$

where

S_1 topographic factor.
S_2 Ground roughness, building size and height above ground factor.
S_3 is a factor based on statistical concepts (building life factor).

Taking ground roughness category (3) and building size Class (B), the value of S_2 can be obtained from table (3). Taking the whole size of the building = 20 m then:

S_1 = 1
S_2 = 0.83 for the 1st. three stories
S_2 = 0.90 for the 4th. and 5th. stories.
S_3 = 1

$V_s = 50 \times 0.83 = 41.5$m/sec, where $S_2 = 0.83$
$V_s = 50 \times 0.90 = 45.0$m/sec, where $S_2 = 0.90$

The dynamic pressure of wind q can be calculated from the formula:

$$q = 0.613 V_s^2$$

$$q_1 = 0.613 \times (41.5)^2 = 1055.74 N/m^2$$

$$q_2 = 0.613 \times (45.0)^2 = 1241.325 N/m^2$$

The force coefficient is taken equal to 1. The maximum shear force due to wind takes place at the most lower connection. The area considered of the first 3 stories measured from the mid-height of the first floor, A_1 is calculated as follows:

$$A_1 = (3 \times 4 - 2) \times 6 = 60 m^2$$

And the area for the to two stories is A_2 where:

$$A_2=(2\times4-2)\times6=36m^2$$

$$F_1=1\times1055.74\times60\times10^{-3}=63.34kN$$

$$F_2=1\times1241.325\times36\times10^{-3}=44.69kN$$

$$F_{total}=F_1+F_2=108.03kN$$

Assuming that the middle sub-frame (┼ or ┬ shaped) has as twice as much stiffness as the corner ones (┐ shaped), and that opening and closing joint stiffness are equal.

Lateral force per ┐ shaped sub-frame due to wind =108.03/4=27kN.

The limiting value of L/300 of the building height, which is given in reference [48] was considered. The maximum lateral sway at this level should not exceed the value of H/300 where H is the storey height.

Assuming that the storey height =4000mm, maximum deflection should not exceed 4000/300=13.33mm.

In the numerical model, the column height was 2000mm, consequently, maximum lateral deflection should not exceed the value of 2000/300=6.66mm. In reference no. this value is 0.5% of the height which in this case is 0.5×2000/100=10.0mm.

Wind Loads on the Steel Frame

The worst case will occur when the three steel beams are subject to wind. In this case the area exposed to wind is $0.300\times3\times6=5.4m^2$

The area of exposure from the steel columns $=3\times0.256\times4=3.072m^2$

Total area $=5.400+3.072=8.472m^2$

Wind speed <50m/sec.

The coefficient of dynamic pressure k=0.613

$S_1=1$

S_2: (group 3, class A) = 0.95, 0.894 and 0.82 respectively.

The critical section is at the point of contraflexure of the third storey.

$S_3=0.77$ (construction stage)

$V_s=50\times1\times0.95\times0.77=36.57$m/sec.

Dynamic pressure $q=k(V_s)^2=0.613\times(36.57)^2=0.82$kN/m^2

wind loads are calculated bearing in mind that no more than three stories would be left without concreting as follows:

Roof=[(3.07/2)+5.4]×0.82=5.68kN

5th. storey=(3.07+5.4)×.613×(50×0.77×0.894)^2=6.14kN

4th. storey=(3.07+5.4)×0.613×(50×0.77×0.82)^2=5.17kN

P_{total}=5.68+6.14+5.17=16.99kN

Force/Joint=16.99/4=4.24kN

Which is the wind load on a bare steel ⊣ shaped Sub-frame.

<u>Wind Load on the Decked Frame</u>

In this case, the exposed area is the area of the roof exposed to wind together with that of the columns. This can be calculated as follow:

$A_{decking}=6\times[7+8]=90$m^2

$A_{columns}=3\times0.256\times4=3.072$m^2

$A_{total}=90.0+3.072=93.072$m^2

Total wind load=0.82×93.072=76.3kN

Wind load/joint=76.3/4=19.1kN

APPENDIX II

CONCRETE SLAB EFFECTIVE WIDTH

When the structure is subject to closing moment, the effective width of the concrete slab is assumed to follow a parabolic curve. In fact this curve is composed of two parabolas with a point of contraflexure at $x=0.35L_{effective}$, where $L_{effective}$ is the effective span of the beam which equals 7000mm or 8000mm in the two beam spans respectively.

The well-established parabolic distribution of the effective width along a beam was modified by the author and the resulting general formula for the assumed slab effective width along the composite beam is:

$$Z = \left[ax^2 + c \right]_0^f + \left[b(x-h)^2 + d \right]_f^h + \left[e(x-h)^2 + d \right]_h^i + \left[-e\,(x-g)^2 + c \right]_i^g + \left[c \right]_g^{2l}$$

where

$$a = \frac{\left[B_b + 2(D_s) - \frac{L_e}{4} \right]}{\left[2(0.35L_e)^2 \right]} = -1.1562E^{-4}$$

$$b = \frac{\left[\frac{L_e}{4} - B_b - 2(D_c)\right]}{\left[2(\frac{D_c}{2} - 0.15L_e)^2\right]} = 8.19943E^{-4}$$

$$c = \frac{L_e}{4} = \frac{7000}{4} = 1750\ mm$$

$$d = 102 + 2(D_s) = 102 + 2 \times 130 = 362\ mm$$

$$e = \frac{[(\frac{L_e}{4} - B_b - 2D_s)]}{[2\,(\frac{D_c}{2})^2]} = 0.041065$$

$$f = 0.35\ L_e = 0.35\ x\ 7000 = 2450\ mm$$

$$g = \frac{(L_e + D_c)}{2} = \frac{(7000 + 260)}{2} = 3630\ mm$$

$$h = \frac{(L_e - D_c)}{2} = \frac{(7000 - 260)}{2} = 3370\ mm$$

where

i = $L_e/2$=3500mm
L_e = effective span of the composite beam =7000mm
B_b = flange breadth of the steel beam =102mm
D_s = slab overall thickness =130mm
D_c = depth of steel column section =260mm

APPENDIX III

ANALYTICAL VERIFICATION

In this appendix, an attempt is made to analyze the composite frame as a rigid one. It was possible to find the displacement and the angle of rotation of the joint directly from the analysis computations provided. Longitudinal strains of members were ignored which allowed deflections to be measured at right angles to the original position of the members.

The lateral displacement is composed of two components [48]:

$$d_{total}=d_{\Theta}+d_{h}$$

$$d_{\Theta}=H.\Theta,\ \Theta=ML/3EI_{beam} \qquad \text{radians}$$

$$d_{h}=pH^{3}/3EI_{column}$$

where

L = Beam span
H = Column height
I_{beam} = Second moment of area of the composite beam
I_{column} = Second moment of area of the steel column
M = Applied moment $=P.H$

The moment of inertia of the composite beam was calculated considering the frame with the steel beam 305×102×28 UB and the steel column of 254×254×73 UC and a modular ratio of 10 together with the following material properties:

E_{steel} $=2.05\times10^{5}N/mm^{2}$

$E_{concrete}$ $=2.05\times10^{4}N/mm^{2}$

L $=3500mm$

H $=2000mm$

At a lateral load of 30kN, $M=2\times30=60kN.m$

Θ $=M.L/3EI_{beam}$

d_Θ $=H.\Theta$

d_h $=P.H^3/3EI_{column}$

d_{total} $=d_\Theta+d_h$

Comparing the deflection calculated using the previous formula with the numerical results for the same frame analyzed as a semi-rigid one, it was found that the semi-rigid composite frame has a lateral stiffness which is very close to that of a rigid frame.

Sub-frame moment(M) $=30\times2=60kN.m$

Θ $=[60\times3.5\times e9]/3\times2.37e8\times2.05e5=1.440e\text{-}3rad.$

d_Θ $=2000\times1.440e\text{-}3=2.88mm$

d_h $=[30\times(2000)^3]/3\times2.05e5\times1.136e8=3.435$

d_{total} $=2.88+3.435=6.3152mm$

<u>Analysis of the Test Piece</u>

With the test piece geometry:

L $=3434mm$

H $=2045mm$

Θ $=\{[30\times2045\times3434e9]/3\}\times2.37e8\times2.05e5=1.4454e\text{-}3rad.$

d_Θ $=2045\times1.4454e\text{-}3=2.955mm$

d_h $=[30\times(2045)^3]/[3\times2.05e5\times1.136e8]=3.672mm$

d_{total} $=2.955+3.672=6.627mm$

% change due to geometrical difference between assumed and actual geometries

$=\{[6.627\text{-}6.3152]/6.3152\}\times100=4.93\%$

APPENDIX IV

LISTING OF INPUT DATA FILE

In this appendix, one of the input data files which have been used in ANSYS pre-processing mode for the modelling of the ¬ shaped sub-frame is listed. Comments notified by c*, are used to explain the function of a number of certain statements whenever necessary. The commands here are applied for version 4.4A of ANSYS. The model listed here is the 3-D model. Similar files were prepared for the four basic configurations, for the test specimen, and for every stiffened sub-frame in opening and closing directions. The total number of basic models was 10 excluding the stiffened connections and any supporting verifications.

```
/PREP7
/TITLE,3-D MODEL
C****          BEAM NODES
N,1,0,0,0
N,2,0,8.9,0
N,6,0,300,0
FILL,2,6
N,7,0,308.9,0
NGEN,2,7,1,7,1,0,0,3.05
NGEN,2,7,8,9,1,0,0,3.05
NGEN,2,7,13,14,1,0,0,3.05
N,27,0,308.9,0
N,28,0,359.9,0
N,29,403.9,0
N,30,0,438.9,0
NGEN,3,5,27,30,1,0,0,150
NGEN,17,50,1,40,1,150,,
NGEN,2,50,801,840,1,50,,
NGEN,14,50,851,890,1,50,,,
NGEN,9,50,1501,1540,1,25,,
NGEN,6,50,1901,1940,1,26.6,,,
NGEN,6,50,2151,2190,1,25.4,,,
C**********          COLUMN NODES
N,3000,3306,-1736.1,0
N,3001,3320.2,-1736.1,0
N,3009,3545.8,-1736.1,0
FILL,3001,3009
N,3010,3560,-1736.1,0
```

```
NGEN,2,11,3000,3010,1,,,4.3
N,3022,3306,-1736.1,16.57
N,3023,3320.2,-1736.1,16.57
N,3024,3545.8,-1736.1,16.57
N,3025,3560,-1736.1,16.57
NGEN,8,50,3000,3025,1,0,150,0
NGEN,2,50,3350,3375,1,0,116.1,0
NGEN,8,50,3400,3430,1,0,50,0
NGEN,9,50,3750,3775,1,0,25,0
NGEN,2,50,4150,4175,1,,20,
NGEN,2,50,4200,4225,1,,8.9,
NGEN,5,50,4250,4275,1,,72.775,
NGEN,2,50,4450,4475,1,,8.9,
NGEN,2,50,4500,4575,1,,51,
NGEN,2,50,4550,4575,1,,44,
NGEN,2,50,4600,4625,1,,35
C*******                    ELEMENT GENERATION
C*******                    COLUMN
ET,1,45,1,,,,
EX,1,2.05E5                 C**YOUNG'S MODULUS FOR STEEL
NUXY,1,0.25                 C**POSSIONS'S RATIO
R,1,
TYPE,1 $MAT,1  $REAL,1
E,3000,3001,3051,3050,3011,3012,3062,3061
EGEN,10,1,-1
EGEN,33,50,1,10,1
C*******                    CONDENSED STEEL ELEMENTS
EX,2,2.05E6
NUXY,2,0.25
TYPE,1 $MAT,2  $REAL,1
E,3011,3012,3062,3061,3022,3023,3073,3072
EGEN,33,50,-1
E,3020,3021,3071,3070,3024,3025,3075,3074
EGEN,33,50,-1
C********                   STEEL BEAM
TYPE,1 $MAT,1  $REAL,1
E,1,51,52,2,8,58,59,9
EGEN,6,1,-1
EGEN,38,50,397,402,1
C********                   CONDENSED ELEMENTS
EX,3,3.424508E6
NUXY,3,0.25
TYPE,1 $MAT,3  $REAL,1
E,8,58,59,9,15,65,66,16
EGEN,2,5,-1
EGEN,38,50,625,626,1
C********                   CONCRETE ELEMENTS
ET,4,65,1,,,,
```

```
NUXY,4,0.2
EX,4,1.818E4
R,4,
KNL,1
NLSIZE,102
NL,4,13,17
NL,4,14,3.5E-4,8E-4,1.45E-3,2E-3,2.9E-3
NL,4,19,0,6.366,12.73,19.1,22.92,30.0
NL,4,25,100,6.366,12.73,19.1,22.92,30.0
NL,4,55,0.5,0.5
NL,4,61,1,1
NL,4,67,1.85,1.85
NL,4,73,30.0,30.0
TYPE,4 $MAT,4  $REAL,4
E,27,77,78,28,32,82,83,33
EGEN,3,1,-1
EGEN,48,50,701,703,1
C**********                CONDENSED CONCRETE ELEMENTS
EX,5,9.09E4
NUXY,5,0.2
R,5,
KNL,1
NLSIZE,102
NL,5,13,17
NL,5,14,3.5E-4,8E-4,1.45E-3,2E-3,2.9E-3
NL,5,19,0,31.83,63.65,95.5,114.6,150.0
NL,5,25,200,31.83,63.65,95.5,114.6,150.0
NL,5,55,0.5,0.5
NL,5,61,1,1
NL,5,67,9.25,9.25
NL,5,73,150,150
TYPE,4 $MAT,5  $REAL,5
E,32,82,83,33,37,87,88,38
EGEN,3,1,-1
EGEN,48,50,845,847,1
C**********                SHEAR STUDS
ET,6,3
EX,6,2.05E5
NUXY,6,0.25
R,6,283.38,6397.1,19,0.0
TYPE,6 $MAT,6  $REAL,6
E,77,78
E,78,79
EGEN,16,50,989,990,1
EGEN,5,150,1019,1020,1
EGEN,2,200,1027,1028,1
C**********                INTERFACE ELEMENTS BETWEEN
STEEL&CONCRETE
```

```
ET,7,12,0,,1,,,
R,7,0,7.8E6,,1,
MU,7,0.0
KNL,1
TYPE,7 $MAT,7  $REAL,7
E,77,57
EGEN,16,50,-1
EGEN,5,150,-1
EGEN,2,200,-1
E,57,77
EGEN,16,50,-1
EGEN,5,150,-1
EGEN,2,200,-1
E,2177,4505
E,4505,2177
C********** TIE ELEMENTS
ET,8,1
EX,8,6.12E6
NUXY,8,0.25
R,8,1,0
KNL,1
NL,8,13,17
NL,8,14,4.17E-3,8.33E-3,0.0166,0.025,0.033
NL,8,19,0,2.55E4,3.5E4,4.35E4,4.5E4,4.5E4
NL,8,25,100,2.55E4,3.5E4,4.35E4,4.5E4,4.5E4
C**********
TYPE,8 $MAT,8  $REAL,8
E,77,107
EGEN,15,50,-1
E,827,957
EGEN,4,150,-1
E,57,127EGEN,15,50,-1
E,977,807
EGEN,4,150,-1
E,1627,1407
E,1427,1607
E,1627,1907
C********** REINFORCING BARS
ET,9,8
EX,9,2.05E5
NUXY,9,0.25
R,9,14.476
TYPE,9 $MAT,9  $REAL,9
E,29,79
EGEN,48,50,-1
R,10,86.85
TYPE,9 $MAT,9  $REAL,10
E,34,84
```

```
EGEN,48,50,-1
R,11,72.375
TYPE,9 $MAT,9  $REAL,11
E,39,89
EGEN,48,50,-1
C**********          ADDITIONAL REINFORCING BARS 1T16
R,12,201.06,
TYPE,9 $MAT,9  $REAL,12
E,679,729
EGEN,29,50,-1
E,2129,4605
C***************TRANSVERSE REINFORCING BARS
ET,10,8
R,13,28.95
EX,10,2.05E5
NUXY,10,0.25
TYPE,10 $MAT,10  $REAL,13
E,29,34
EGEN,17,50,-1
EGEN,5,150,-1
EGEN,2,200,-1
EGEN,3,300,-1
R,14,144.75
TYPE,10 $MAT,10  $REAL,14
E,34,39
EGEN,17,50,-1
EGEN,5,150,-1
EGEN,2,200,-1
EGEN,3,300,-1
C**********          CONDENSED SHEAR STUDS
R,15,1700.28,3.83826E4,19,0.0
TYPE,6 $MAT,6  $REAL,15
E,2177,2178
E,2178,2179
ET,11,1
EX,11,1.836E7
NUXY,11,0.25
R,16,1,0
KNL,1
NL,11,13,17
NL,11,14,4.17E-3,8.33E-3,0.0166,0.025,0.033
NL,11,19,0,7.65E4,1.05E5,1.305E5,1.35E5,1.35
NL,11,25,100,7.65E4,1.05E5,1.305E5,1.35E5,1.35
TYPE,11 $MAT,11  $REAL,16
E,2177,4500
E,2177,4510
C******* 2 WEB CLEAT BOLTS M16
R,17,200.96,0.0
```

```
TYPE,9 $MAT,9  $REAL,17
E,1754,4350
E,1755,4400
C**********                    SEAT CLEAT
R,18,960,7031,15,0.0
TYPE,6 $MAT,1  $REAL,18
E,1701,4200
C**********                    STIFFENER PLATE
ET,12,42,1,0,3,,,,
R,19,10
TYPE,12 $MAT,1  $REAL,19
E,1701,3900,3950,3950
E,1701,3950,4000,4000
E,1701,4000,4050,4050
E,1701,4050,4100,4100
E,1701,4100,4150,4150
E,1701,4150,4200,4200
C*********                     BOUNDARY CONDITIONS
NRSEL,,0
D,ALL,UZ,0
NALL
NRSEL,NODE,3005
NASEL,NODE,3016
D,ALL,UY,0
D,ALL,UX,0
NALL
NRSEL,X,0
NRSEL,Y,308.9
D,ALL,UY,0
NALL
WSORT,X,3000,0,0
ITER,-30,0,30
F,7,FX,500
F,21,FX,500
AFWRIT
FINISH
/INP,27
```

APPENDIX V

STRESS-STRAIN CURVE OF CONCRETE AS USED IN ANSYS

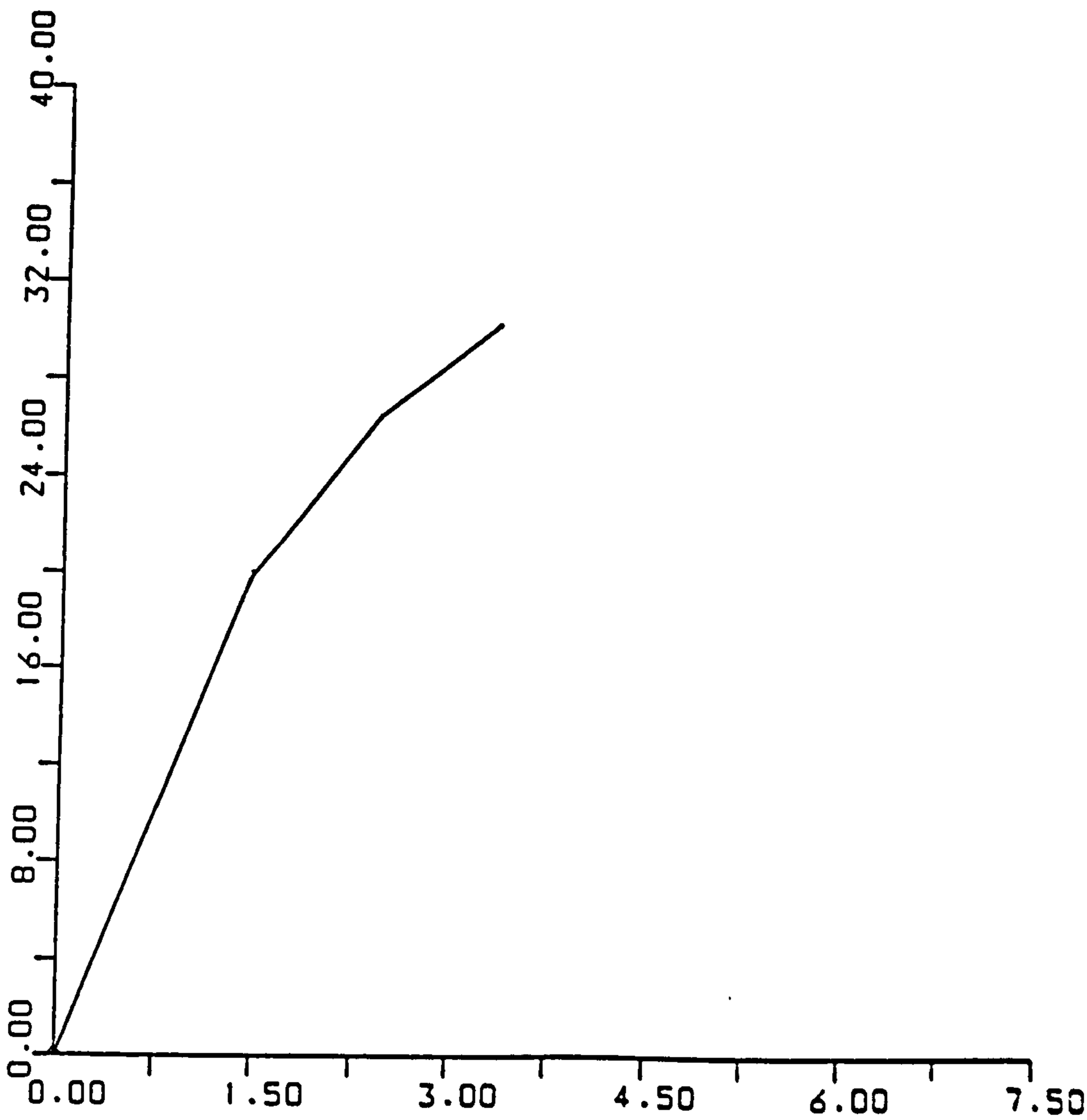

STRESS-STRAIN CURVE FOR CONCRETE IN ANSYS INPUT DATA